frontiers | Research Topics

Presentations at the MELiSSA conference – current and future ways to closed life support systems

2022

Edited by
Cyprien Verseux, Jean-Pierre Paul de Vera and Luigi Gennaro Izzo

Published in
Frontiers in Astronomy and Space Sciences
Frontiers in Plant Science

FRONTIERS EBOOK COPYRIGHT STATEMENT

The copyright in the text of individual articles in this ebook is the property of their respective authors or their respective institutions or funders. The copyright in graphics and images within each article may be subject to copyright of other parties. In both cases this is subject to a license granted to Frontiers.

The compilation of articles constituting this ebook is the property of Frontiers.

Each article within this ebook, and the ebook itself, are published under the most recent version of the Creative Commons CC-BY licence. The version current at the date of publication of this ebook is CC-BY 4.0. If the CC-BY licence is updated, the licence granted by Frontiers is automatically updated to the new version.

When exercising any right under the CC-BY licence, Frontiers must be attributed as the original publisher of the article or ebook, as applicable.

Authors have the responsibility of ensuring that any graphics or other materials which are the property of others may be included in the CC-BY licence, but this should be checked before relying on the CC-BY licence to reproduce those materials. Any copyright notices relating to those materials must be complied with.

Copyright and source acknowledgement notices may not be removed and must be displayed in any copy, derivative work or partial copy which includes the elements in question.

All copyright, and all rights therein, are protected by national and international copyright laws. The above represents a summary only. For further information please read Frontiers' Conditions for Website Use and Copyright Statement, and the applicable CC-BY licence.

ISSN 1664-8714
ISBN 978-2-8325-4634-5
DOI 10.3389/978-2-8325-4634-5

About Frontiers

Frontiers is more than just an open access publisher of scholarly articles: it is a pioneering approach to the world of academia, radically improving the way scholarly research is managed. The grand vision of Frontiers is a world where all people have an equal opportunity to seek, share and generate knowledge. Frontiers provides immediate and permanent online open access to all its publications, but this alone is not enough to realize our grand goals.

Frontiers journal series

The Frontiers journal series is a multi-tier and interdisciplinary set of open-access, online journals, promising a paradigm shift from the current review, selection and dissemination processes in academic publishing. All Frontiers journals are driven by researchers for researchers; therefore, they constitute a service to the scholarly community. At the same time, the *Frontiers journal series* operates on a revolutionary invention, the tiered publishing system, initially addressing specific communities of scholars, and gradually climbing up to broader public understanding, thus serving the interests of the lay society, too.

Dedication to quality

Each Frontiers article is a landmark of the highest quality, thanks to genuinely collaborative interactions between authors and review editors, who include some of the world's best academicians. Research must be certified by peers before entering a stream of knowledge that may eventually reach the public - and shape society; therefore, Frontiers only applies the most rigorous and unbiased reviews. Frontiers revolutionizes research publishing by freely delivering the most outstanding research, evaluated with no bias from both the academic and social point of view. By applying the most advanced information technologies, Frontiers is catapulting scholarly publishing into a new generation.

What are Frontiers Research Topics?

Frontiers Research Topics are very popular trademarks of the *Frontiers journals series*: they are collections of at least ten articles, all centered on a particular subject. With their unique mix of varied contributions from Original Research to Review Articles, Frontiers Research Topics unify the most influential researchers, the latest key findings and historical advances in a hot research area.

Find out more on how to host your own Frontiers Research Topic or contribute to one as an author by contacting the Frontiers editorial office: frontiersin.org/about/contact

Presentations at the 2022 MELiSSA conference – current and future ways to closed life support systems

Topic editors

Cyprien Verseux — University of Bremen, Germany

Jean-Pierre Paul de Vera — German Aerospace Center (DLR), Germany

Luigi Gennaro Izzo — University of Naples Federico II, Italy

Citation

Verseux, C., de Vera, J.-P. P., Izzo, L. G., eds. (2024). *Presentations at the 2022 MELiSSA conference – current and future ways to closed life support systems*. Lausanne: Frontiers Media SA. doi: 10.3389/978-2-8325-4634-5

Table of contents

frontiers | Frontiers in Astronomy and Space Sciences

TYPE Editorial
PUBLISHED 08 March 2024
DOI 10.3389/fspas.2024.1394073

Check for updates

OPEN ACCESS

EDITED AND REVIEWED BY
Alberto Fairén,
Spanish National Research Council (CSIC), Spain

*CORRESPONDENCE
Luigi Gennaro Izzo,
luigigennaro.izzo@unina.it

RECEIVED 29 February 2024
ACCEPTED 04 March 2024
PUBLISHED 08 March 2024

CITATION
Izzo LG, de Vera J-PP and Verseux C (2024), Editorial: Presentations at the 2022 MELiSSA conference—current and future ways to closed life support systems.
Front. Astron. Space Sci. 11:1394073.
doi: 10.3389/fspas.2024.1394073

COPYRIGHT
© 2024 Izzo, de Vera and Verseux. This is an open-access article distributed under the terms of the Creative Commons Attribution License (CC BY). The use, distribution or reproduction in other forums is permitted, provided the original author(s) and the copyright owner(s) are credited and that the original publication in this journal is cited, in accordance with accepted academic practice. No use, distribution or reproduction is permitted which does not comply with these terms.

Editorial: Presentations at the 2022 MELiSSA conference—current and future ways to closed life support systems

Luigi Gennaro Izzo[1]*, Jean-Pierre Paul de Vera[2] and Cyprien Verseux[3]

[1]Department of Agricultural Sciences, University of Naples Federico II, Portici, Italy, [2]Microgravity User Support Center (MUSC), German Aerospace Center (DLR), Cologne, Germany, [3]Center of Applied Space Technology and Microgravity (ZARM), University of Bremen, Bremen, Germany

KEYWORDS

bioregenerative life support systems (BLSSs), micro-ecological life support system alternative (MELiSSA), long-term crewed missions, food production and waste management, air revitalization, modelling and control, circular economy, terrestrial applications

Editorial on the Research Topic
Presentations at the 2022 MELiSSA conference—current and future ways to closed life support systems

Long-duration crewed missions, as foreseen to the Moon and Mars, will require sustainable life support systems. Some functions, such as carbon cycling, will require biology. In 1989, ESA's MELiSSA project was consequently initiated to generate knowledge on bioregenerative life support systems (BLSSs). At the core of this project was a concept where a loop of processes produce food, water, oxygen, and other resources while recycling waste. Over the following three decades, the MELiSSA community have used a progressive approach to refine, characterize, model, and control that loop. Beside laying the foundation for a system that could support long-term crewed missions, this undertaking has led to sustainable applications on Earth.

At the 2022 edition of the MELiSSA Conference (held in Toulouse, France), experts discussed recent achievements and future directions in BLSSs with a focus on circular economy–for space and Earth. Participants were invited to report on their key findings in the present Research Topic. Here we give an overview of the published contributions.

Among the central functions of BLSSs are air revitalization and food production. Both can be performed by photosynthetic organisms. Most often, these are plants; consistently, four contributions were about them. Schiefloe et al. investigated the possibility of using waste streams, including human urine, as fertilizer. They cultivated lettuce with various NH_4^+-to-total N ratios, as well as elevated concentrations of Na^+ and Cl^-, and obtained result which underline the importance of nutrient solution composition, particularly the ratio of ammonium to nitrate, when optimizing biomass production.

Kitaya et al. investigated the effects of fish density on the productivity of lettuce plants and loach fish, as well as on nitrogen usage efficiency, in an aquaponic system. They also

showed that plant growth was not affected when replacing a fraction of the fertilizer with loach excreta, suggesting that the latter could be used to supplement chemical fertilizers.

Plant production requires seeds; and the transportation of large amounts of seeds from Earth would harm the sustainability of long-duration missions. Iovane et al. consequently studied the capacity of plants to reproduce beyond Earth. More specifically, they tested the effects of microgravity (simulated using a clinostat) on the directional growth of pollen tubes in *Solanum lycopersicum* and *Brassica rapa*. They observed significant changes in the growth patterns, tube length and tortuosity of pollen tubes, as well as in pollen germination.

Supplementing the astronauts' diet with bioactive compounds may help them cope with stress and, more broadly, increase their physical and mental health. The cultivation of microgreens in space is therefore the subject of increasing focus. Amitrano et al. investigated the importance of optimizing environmental factors, such as light intensity and vapor pressure deficit, to enhance their growth and nutritional properties. They also emphasized the potential microgreens have for food production in space habitats, underlining their suitability for cultivation in limited volumes, and suggest that species-specific cultivation strategies may help improve growth and nutritional benefits.

Plants are not the only photosynthetic organisms under study in BLSSs: others are microorganisms. The MELiSSA loop, for instance, includes the cyanobacterium *Limnospira indica*. Two studies in the Research Topic deal with this organism. Tallec et al. addressed the need for an automated process for harvesting its biomass and recycling its culture medium. They developed the BioHarvest demonstration unit, which consists of three subsystems: a photobioreactor, a biomass harvesting unit (BHU) and a medium filtration unit based. Despite biomass accumulation on the filter of the BHU, which can limit productivity, their results are promising. Fahrion et al. aimed at optimizing culture conditions for the propagation of *Limnospira indica* in space. They reported that, among various tested combinations, rather low light intensities (36–80 µmol photons m^{-2} s^{-1}) combined with moderate temperatures (30°C–34°C) were most favorable in terms of biomass production and pigment composition. Perozeni et al. demonstrated the successful heterologous expression of zeolin–a recombinant protein with a balanced amino acid profile–in another photosynthetic microorganism: the eukaryotic microalgae *Chlamydomonas reinhardtii*. This achievement may be a step toward microalgae which are metabolically engineered to better meet the crew's dietary requirements.

Not all microorganisms of relevance to life support are confined to dedicated compartments. Doré and Ortega Ugalde highlighted the impact–positive or negative–the microbiome can have on health and emphasize the benefits that its understanding can bring, not only for medical applications but also for enhancing the sustainability of life support systems. They also pointed out the limited number of studies, as well as their sample size and diversity, which have focused on astronauts' microbiome. Another concern pertaining to microbiomes is the contamination of crewed compartments. Lemelle et al. presented insights from the MATISS campaigns, in which the surface contamination rates of the Columbus module, in the International Space Station, were documented over months. They revealed low levels of biocontamination, which they attributed to the effectiveness of long-term air purification systems, and suggested that surface contamination is roughly proportional to the number of astronauts.

When designing BLSSs, creating individual compartments is only one of the challenges. Another is their integration. A stoichiometric model proposed by Vermeulen et al. offers a framework for analyzing nutrient cycling and resource utilization in a conceptually closed, MELiSSA-inspired BLSSs. The authors described a remarkable level of closure–with 12 out of the 14 included compounds showing zero losses, and the continuous provision of 100% of the food and oxygen needs–when balancing the scale of the different compartments.

Overall, the presentations at the 2022 MELiSSA Conference–only a small fraction of which led to articles in this Research Topic–showed that researchers of the MELiSSA community are making significant steps towards sustainable life support systems–as well as inspiring and developing terrestrial applications.

Author contributions

LI: Conceptualization, Writing–original draft, Writing–review and editing. J-PdV: Conceptualization, Writing–review and editing. CV: Conceptualization, Writing–review and editing.

Funding

The author(s) declare that no financial support was received for the research, authorship, and/or publication of this article.

Conflict of interest

The authors declare that the research was conducted in the absence of any commercial or financial relationships that could be construed as a potential conflict of interest.

The author(s) declared that they were an editorial board member of Frontiers, at the time of submission. This had no impact on the peer review process and the final decision.

Publisher's note

All claims expressed in this article are solely those of the authors and do not necessarily represent those of their affiliated organizations, or those of the publisher, the editors and the reviewers. Any product that may be evaluated in this article, or claim that may be made by its manufacturer, is not guaranteed or endorsed by the publisher.

frontiers | Frontiers in Astronomy and Space Sciences

TYPE Original Research
PUBLISHED 27 April 2023
DOI 10.3389/fspas.2023.1178332

Check for updates

OPEN ACCESS

EDITED BY
Cyprien Verseux,
University of Bremen, Germany

REVIEWED BY
Alessandro Concas,
University of Cagliari, Italy
Gisela Detrell,
University of Stuttgart, Germany

*CORRESPONDENCE
Natalie Leys,
natalie.leys@sckcen.be

RECEIVED 02 March 2023
ACCEPTED 17 April 2023
PUBLISHED 27 April 2023

CITATION
Fahrion J, Dussap CG and Leys N (2023), Assessment of batch culture conditions for cyanobacterial propagation for a bioreactor in space.
Front. Astron. Space Sci. 10:1178332.
doi: 10.3389/fspas.2023.1178332

COPYRIGHT
© 2023 Fahrion, Dussap and Leys. This is an open-access article distributed under the terms of the Creative Commons Attribution License (CC BY). The use, distribution or reproduction in other forums is permitted, provided the original author(s) and the copyright owner(s) are credited and that the original publication in this journal is cited, in accordance with accepted academic practice. No use, distribution or reproduction is permitted which does not comply with these terms.

Assessment of batch culture conditions for cyanobacterial propagation for a bioreactor in space

Jana Fahrion[1,2], Claude Gilles Dussap[2] and Natalie Leys[1]*

[1]Microbiology Unit, Belgian Nuclear Research Center SCK CEN, Mol, Belgium, [2]Université Clermont Auvergne, CNRS, Clermont Auvergne INP, Institut Pascal, Clermont-Ferrand France, France

One important point in human space exploration is the reliable air, water and food production for the space crew, less dependent from cargo supply. Bioregenerative life support systems aim to overcome this challenge. The life support program MELiSSA of the European Space Agency uses the cyanobacterium *Limnospira indica* for air revitalization and food production. In the Space flight experiments ArtEMISS-B and -C, *L. indica* is tested on the International Space Station. In this study we elucidate which conditions are most favorable for cell propagation from inoculum to a full culture in space to enable a high final biomass concentration, with high pigment composition for an efficient bioprocess. We found that lower light intensities (36–75 µmol photons m^{-2} s^{-1}) show higher maximum biomass densities and higher pigment contents than cultures grown above 100 µmol photons m^{-2} s^{-1}. 36 µmol photons m^{-2} s^{-1} resulted in maximum biomass concentrations of 3.36 ± 0.15 g L^{-1} (23 °C), while cultures grown at 140 µmol photons m^{-2} s^{-1} only achieved concentrations of 0.82 ± 0.10 g L^{-1} (25°C) (–75.8%). Colder temperatures (21°C–25°C) showed a negative effect on the pigment content. At 36 µmol photons m^{-2} s^{-1}, a temperature of 30°C gave a phycocyanin concentration of 0.122 ± 0.014 g g DW^{-1} and 23°C resulted in 0.030 ± 0.003 g g DW^{-1} (–75.4%). In conclusion, a low light intensity (36–80 µmol photons m^{-2} s^{-1}) in combination with warm temperature (30°C–34°C) is optimal to obtain cultures with high pigment contents and high biomass concentrations in a batch culture.

KEYWORDS

space exploration, bioregenerative life support systems, microalgae, batch cultures, air revitalization, cyanobacteria, space microbiology

1 Introduction

Edible cyanobacteria are promising organisms for life support systems in space. The MELiSSA loop, a life support system initiated by the European Space Agency (ESA) in 1988 (Lasseur et al., 2010) aims to recycle the wastes of space travelers (e.g., feces, urine and CO_2) to produce new edible biomass, potable water and oxygen (O_2) for space craft crews. The IVa compartment of MELiSSA aims at biological air revitalization and food production via a photobioreactor (PBR) containing photosynthetic, blue-green pigmented cyanobacterium *L. indica* PCC8005 (Poughon et al., 2020). *Limnospira indica* PCC8005 was formerly classified as part of the *Arthrospira* genus (Nowicka-Krawczyk et al., 2019). In a commercial context, *L. indica* is one of the strains sold under the name spirulina. Spirulina as a product has already been consumed by humans in equatorial Africa and Mexico for a long time (Ciferri, 1983;

Barnett et al., 2005). Nowadays, the food industry sells spirulina as a supplement and so-called superfood because of its high protein and antioxidant content (Prasanna et al., 2010; Ma et al., 2019). The edible cyanobacterium *Limnospira indica*, likewise other species that are sold under the term Spirulina, contains protein of high quality, minerals, vitamins as well as pigments (Farag et al., 2015; Furmaniak et al., 2017). Benefits of the use of *L. indica* as a food source for space travelers include its high radiation resistance (up to 6,400 Gy, gamma-rays) (Badri et al., 2015; Yadav et al., 2019; Yadav et al., 2021) and its high content of bioactive compounds with health beneficial effects (e.g., anti-inflammatory effects) (Wu et al., 2016; Segers et al., 2022). An overview of the benefits of Spirulina for Space applications has recently been published (Fais et al., 2022a).

Before bioreactors for life support systems can be made operational in space, it is of utmost importance to understand the bioprocesses thoroughly, allowing predictive modelling and reliable processes and reactor control. Especially in the future, when the MELiSSA loop is used to supply the crew of a space craft, parameters to detect changes in culture health must be available to avert failure of the system. In the ArtEMISS B and -C precursor Space flight experiments, *L. indica* is cultivated in 4 parallel photobioreactors designed for microgravity conditions and controlled by light-limiting conditions, meaning that the light intensity is the parameter by which the production of oxygen and biomass is controlled. The start-up of the bioreactor in space includes a revival of the dormant inoculum (in dark and cold) and propagation in batch mode, in axenic conditions and under continuous illumination. The oxygen and biomass productivity in PBRs is strongly dependent on the geometry of the culturing flask, the light intensity and the efficient oxygen removal (Cornet and Dussap, 2009). Therefore, depending on the experimental set-up, varying biomass and oxygen productivities are reported in literature. For example, Farges et al. (2009) reported a biomass productivity of 0.077 g L^{-1} d^{-1} for 33 µmol photons m^{-2} s^{-1} in an 1.2 L bench scale membrane bioreactor; while Garcia-Gragera et al. (2021) obtained already a maximum biomass productivity of 0.58 g L^{-1} d^{-1} for 932 µmol photons m^{-2} s^{-1} and a maximum oxygen productivity of 1.19 mmol L^{-1} h^{-1} in the larger intensified 90 L cylindrical airlift bioreactor at the MELiSSA pilot plant in Barcelona. In the ArtEMISS project, mini-sized PBRs which are adapted to spaceflight conditions are used. These PBRs are flat cylindrical reactors, equipped with 1 side illumination by LEDs, and work with a small liquid volume (60 mL) and relatively low light flux (45–80 µmol photons m^{-2} s^{-1}, 33 °C). Low light intensities are used to accommodate for more difficult gas liquid separation under microgravity in space and to prevent oxygen bubble formation in the liquid. Gas release from liquid is challenging under microgravity, as the buoyancy force is absent and it is fully depending on diffusion and technically forced convection over the membrane (Antar et al., 2006). Additionally, low light intensities promote slower growth and allow longer exposure to Space (e.g., cosmic radiation, microgravity) while demanding low amounts of feed resources. The CO_2 feed as growth limiting factor is excluded in this ArtC pilot experiment as it is not extracted from the cabin air, but provided in abundance as dissolved bicarbonate in the liquid medium feed. The challenges of CO_2 gas to liquid transfer from cabin air in microgravity in space, will be address in a next ISS flight experiment of the MELiSSA team, called BIORAT, using a different flight hardware design including a gas exchange module and also a biomass harvesting module (Lasseur, 2008).

In the ArtEMISS B space flight experiment (ArtB) on the ISS in 2017, 4 consecutive repeated-batch cultures (90% harvest) were grown inside the PBRs at 35 µmol photons m^{-2} s^{-1} for 4 weeks. This experiment was the first one to allow online recording and transmission of the oxygen and biomass production rate on board the International Space station (ISS). It could be shown that the developed predictive model for bioprocess and bioreactor control via light limitation was still applicable for cultures in Space (Poughon et al., 2020). A follow-up experiment operating the bioreactor with continuous feeding and different light intensities between 45 and 80 µmol photons m^{-2} s^{-1} to grow *L. indica* PCC8005 in turbidostatic modus is scheduled to fly to the ISS in 2023 (ArtC) (Lasseur and Mergeay, 2021). Therefore, in ArtC the scalability of the bioprocess in response to increasing light intensities will be assessed.

Not only the biomass and oxygen production are of high importance for the use of *L. indica* in life support systems, but also the biomass composition and the resulting nutritive value. Cyanobacteria have large protein pigment complexes, called phycobilisomes, that function as photon harvesting antenna on their membranes. To secure a stable nutritive value (e.g., protein, glycogen and pigment content), growth conditions like medium composition, light intensity, temperature and culture density need to be defined and monitored carefully.

It is known that temperature and light conditions have an impact on revival and oxygen and biomass production kinetics and biomass composition (Moore et al., 1995; Ravelonandro et al., 2008; Garcia-Gragera et al., 2021). Our study focusses on conditions relevant for PBR systems for space applications like moderate temperatures between 21°C and 34°C and low light intensities (i.e. 36, 45, 75 and 140 µmol photons m^{-2} s^{-1}) which cause a light limiting growth and are usually used to secure stable and slow growth in space environments. Additionally, to a detailed growth analysis, we assessed the pigment and glycogen contents to get an overview of the nutritive value. The detailed understanding of the adaptions of the cultures and their mechanisms is important to secure a reliable photobioreactor and to find solutions for heating or light problems that might come up in future life support systems. Therefore, the goal of this study was to provide ground reference values for several important parameters of specifically selected strain P3 of *L. indica* PCC8005 to use as comparison in future MELiSSA experiments such as ArtEMISS C. We present data on the impact of different factors such as light flux intensity, in combination with low and high temperature, on the growth, photosynthetic activity and molecular composition of *L. indica* PCC8005 for application in space. The combination of low light and warm temperature are not common conditions used in Earth cultures or bioreactors but aimed for in space, and an in-depth growth analysis of this space relevant strain is essential to assess the validity of the currently available general data for this specific strain.

2 Materials and methods

2.1 Bacterial strain and culture conditions

In our laboratory collection we obtained multiple morphotypes of *L. indica* strain PCC8005 over the years of continuous cultivation

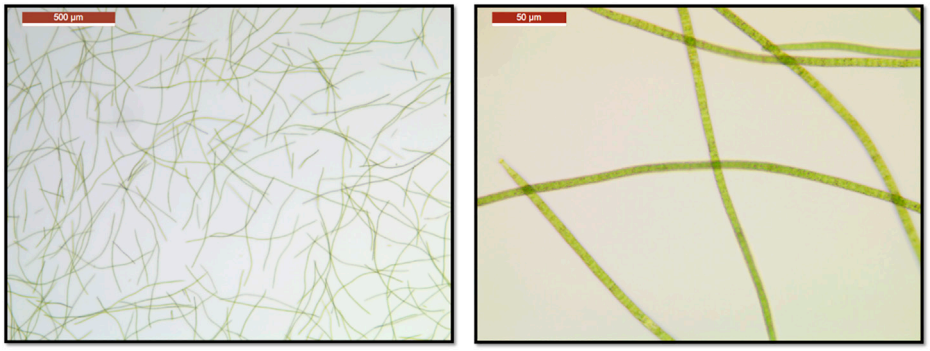

FIGURE 1
Light Microscopy pictures of *Limnospira indica* PCC8005 P3 at two different magnifications (left: ×50, right: 400X) showing long (in average ~700 µm; up to 1.5 mm) and straight trichomes.

in an incubator in continuous shaking and stable illumination (~35 µmol photons m^{-2} s^{-1}, 24/7) and temperature (~30°C). The morphotypes differ in, for example, morphology, floating/sedimentation behavior, growth rate, and radiation resistance (Yadav et al., 2019). The culture that was used in the present study is called P3, and forms long (~700 µm on average, up to 1.5 mm), thin (~6 µm) and straight trichomes (Figure 1). This strain was chosen as a good candidate for the use in Space PBRs because its straight shape makes it well-adapted to low light and in addition, it does not easily clump or form biofilms on the gas PTFE membrane under the selected test conditions, and it is easy to keep in a well homogenized suspension by shaking or stirring, and easy to harvest by filtration or centrifugation as it does not float but sediments.

The cyanobacterium *Limnospira indica* strain PCC8005 subculture P3 was grown in Zarrouk's medium as modified by Cogne et al. (2003) (pH = 9,5). Depending on the experiment, different temperatures (23°C ± 2°C, 25°C ± 2°C, 30°C ± 2°C, 32 ± 2 and 34°C ± 2°C) (Binder incubators) and several light flux intensities (36 ± 2, 45 ± 2, 75 ± 5 and 140 ± 10 µmol photons m^{-2} s^{-1}) were used. The cultures were constantly (24h/day) illuminated with full PAR emitting light sources (LEDs and halogen lamps) in all experiments. The constant illumination, in contrast to the usage of a day/night cycle, was used because it allows continuous oxygen production, which is the final aim in the ArtC Space flight experiment and the final MELiSSA system tailored to the astronaut as oxygen consumers. The chosen cyanobacterial strain is also fully efficient in photosynthetic biomass production in continuous light, and does not need any darkness to do so. All cultures were grown in regular Erlenmeyer flasks (250 and 150 mL) equipped with a cotton plug and aluminum foil to avoid evaporation while allowing gas exchange by diffusion. In each experiment, 250 mL Erlenmeyer flasks filled with 150 mL medium (gas/liquid ratio of 0.66) or 150 mL Erlenmeyer flasks filled with 65 mL medium (gas/liquid ratio of 1.30) were used. The medium contains dissolved bicarbonate as carbon source, as will be the case in the ArtC flight experiment. In both cases, the cultures were inoculated with 5% v/v or 10% v/v (depending on the OD_{770nm} of the parent culture) and 95% v/v and 90% v/v Zarrouk medium as modified by Cogne et al. (2003), respectively, to target a starting concentration of ca. OD_{770nm}–0.100. The gas phase consists of ambient air. All cultures were shaken at 120 rpm using horizontal orbital Heidolph and Edmund Bühler GmbH shakers. Samples for molecular analysis (pigment and glycogen) were taken at different time points. At each time point, 2 mL of well mixed culture were transferred to a 2 mL Eppendorf tube and centrifuged at 10,000 g for 15 min (Eppendorf Centrifuge 5804 R) at room temperature (21°C ± 1°C). Afterwards, the cell-free supernatant was discarded and the tubes were centrifuged at 10,000 g for 5 min. The remaining supernatant was discarded and the pellets were flash-frozen in liquid nitrogen and stored at −80°C (PHCbi TwinGuard freezers) until further analysis.

2.2 Overview of the tested culture conditions

In order to find and describe the adaptions in behavior of *L. indica* PCC8005 P3 to different growth conditions, several experiments were conducted. In ArtEMiSS C the following growth conditions will be used: *L. indica* strain PCC8005 subculture P3 at 45–55-70–80 µmol photons m^{-2} s^{-1}, 33°C ± 1°C, homogenous culture (800–1,000 rpm with magnetic stirrer in the bioreactor hardware), in Zarrouk's medium (as modified by Cogne et al. (2003)). The conditions used in the present study imitate the nominal ArtEMISS B and C conditions and add some off-nominal conditions, like lower temperatures (23, 25, 30°C) and higher light intensity [140 µmol photons m^{-2} s^{-1} (µmol photons = µE)] as additional controls. All test were performed with normal Earth gravity, without irradiation, and ambient air as headspace, in the shaken Erlenmeyer set-up describe in Section 2.1.

2.3 Optical density and pH measurements

The cell concentration in the culture was monitored as optical density (OD), via absorbance spectrometry at different wavelengths. The values for optical density (OD) were obtained using a NANOCOLOR® UV/VIS II spectrophotometer (MACHEREY-NAGEL). The OD was measured by absorbance at 468 nm, 630 nm, 750 nm and 770 nm in 1 mL semi-micro cuvettes

(greiner BIO-ONE). These wavelengths were adapted from the ArtEMISS B space flight conditions. The 468 nm wavelength is used to estimate the chlorophyll a content because chlorophyll pigments have an absorption peak at this wavelength (Guidi et al., 2017). The same accounts for phycocyanin/allophycocyanin at the wavelength 630 nm (Zhang and Chen, 1999). The two remaining wavelengths 750 nm and 770 nm are used to measure the amount of cells in the culture (Akimoto et al., 2012). In this study, the OD measurements at 468, 630, and 750 nm were measured daily as a quality control of the cultures (data not shown). The OD measurements at 770 nm were used to assess the biomass production (see section 2.4).

A KCl pH electrode (InLab®, Mettler Toledo) was used to determine the pH values of the culture medium. As we are working in high pH conditions, we verified the working range of the pH electrode by preparing several NaOH solutions of strictly defined pH values and were able to show that the electrode measures correctly up to a pH of 13.

2.4 Biomass concentration analysis

In order to estimate the biomass concentration in the cultures, the dry weight (g DW L^{-1}) to OD 770 nm ratio was determined by putting 2 mL of cultures grown under different conditions (25°C–30°C, 36–75 µmol photons m^{-2} s^{-1}) on pre-weighed membrane disc filters (water wettable PTFE, Pall Laboratory, pore size 45 µm, ⌀ 25 mm) using a vacuum pump. The filters were dried for a minimum of 48 h at 60°C and weighed again. The cultures were sampled and measured in triplicates (technical replicates). In total, 4 cultures were used per tested condition (biological replicates), therefore 12 samples were used to obtain one point in the dry weight curves that were used to determine the correlation factor between OD_{770nm} values and DW biomass values. The OD_{770nm} to dry weight ratio which was obtained during the experiments discussed in this study was found to be stable over different conditions:

$$y = 1.0462x + 0.3003 \quad (1)$$

Eq. 1 shows the OD_{770nm} to dry weight ratio, where x is the OD_{770nm} absorbance and y is the dry weight in g L^{-1}. This ratio was used to calculate the biomass concentration (X, g L^{-1}), the specific growth rate (μ_{max}, d^{-1}) and the average biomass productivity (P_{av}, g L^{-1} d^{-1}). Exponential, linear and stationary phase were defined by regression using Excel 2016. The maximum growth rate μ_{max} was obtained by using a logarithmic conversion and linear regression of the exponential phase (approximately the first 3–4 days of growth). The average biomass productivity P_{av} represents the slope of the linear regression of the linear growth phase, starting at the endpoint of the exponential phase and ending at the point of highest biomass concentration. Additionally, the time until the stationary phase is reached (T_{stat}, d) was determined using the peaks of the growth curves (accuracy ±0.5 days).

2.5 Quantum yield measurements

The photosynthetic capacity and efficiency of the cultures was determined by measuring the effective quantum yield (QY) of PSII. The QY of PSII is determined by pulse amplitude modulated (PAM) fluorimetry (Schreiber et al., 1995; Aguirre-von-Wobeser et al., 2000; Schuurmans et al., 2015). The QY ($\Delta F/F_m'$) is defined as shown in Equation (2).

$$QY = \frac{F_m' - F_t'}{F_m'} \quad (2)$$

F_m' is the maximal fluorescence in light adaptation and F_t' is the current fluorescence. The quantum yield (QY) was measured using an AquaPen-C AP 110-C from Photon System Instruments (PSI) with a flash pulse of 30% (900 µmol photons m^{-2} s^{-1}, 630 nm) and a super pulse of 70% (2,100 µmol photons m^{-2} s^{-1}, 630 nm), according to the fixed values in the AquaPen-C manual. The device directly calculates the $\Delta F/F_m'$ ratio and gives the QY value as output. In theory, the QY has to be between 0 and 1, with 1 meaning 100% of the photons are used for photosynthesis. In practice, the measured values for healthy cyanobacteria usually lie between 0.3 and 0.6 (Gao et al., 2007; Masojídek et al., 2010; Allahverdiyeva et al., 2013; Schuurmans et al., 2015).

2.5.1 Pigment analysis

The phycobilisomes of *L. indica* contain the light harvesting pigments phycocyanin and allophycocyanin (Johnson et al., 1988) which transfer the energy further to the photosystems II and I (PSII and PSI) reaction centers. The PSII and PSI contain the pigment chlorophyll a (Chl a), which acts as the primary electron donor in the electron transport chain (Rakhimberdieva et al., 2001; Raven et al., 2005). Other chlorophyll pigments, such as chlorophyll b, c or d, are not abundant in *L. indica* (Averina et al., 2019; Milia et al., 2022). The protocol for pigment analysis used was slightly adapted from Badri et al. (2015) and allows to measure the concentrations of allophycocyanin, phycocyanin and chlorophyll with a spectrophotometer. Briefly, the frozen cell pellets of 2 ml of culture were suspended in 1 mL of 0.05 M Na_2HPO_4 at pH 7. Then, 5 cycles of freezing in liquid N_2 and thawing at 37 °C in a water bath were performed to crack the cells. Then, 100 µL lysozyme (100 mg/ml) were added and the tubes were incubated for 30 min at 37°C. The tubes were centrifuged at 13,000 g for 10 min and the supernatant was measured with a NANOCOLOR® UV/VIS II spectrophotometer for absorbance at 615 nm and 652 nm, to determine the concentrations of antenna pigments in the extract. The extraction of chlorophyll was performed on the remaining pellet of the phycobilliprotein extraction. Firstly, the pellets were washed three times using 0.05 M Na_2HPO_4 at pH 7. Then, 1 mL of 100% methanol was used to extract the organic soluble pigment chlorophyll. Three cycles of ultra-sonication (30 kHz, 10 s, amplitude 30%, 1 pulse per second, Hielscher Ultrasound Technology, UP50H) were performed to fully extract and dissolve the chlorophyll pigments. Centrifugation at 4°C for 10 min at 13,000 g was performed, and the supernatant was measured at 665 nm using a NANOCOLOR® UV/VIS II spectrophotometer (MACHEREY-NAGEL) and semi-micro cuvettes (Greiner BIO-ONE) to determine the chlorophyll concentration in the extract. To calculate the pigment concentration in the original culture, i.e., pigment weight (mg) per mL, conversion Eqs. 3–5 as published in Bennett and Lawrence (1973) were used:

$$Phycocyanin\left(\frac{mg}{mL}\right) = \frac{OD_{615nm} - 0,474\,OD_{652nm}}{5,34} \quad (3)$$

$$Allophycocyanin\left(\frac{mg}{mL}\right) = \frac{OD_{652nm} - 0,208\,OD_{615nm}}{5,09} \quad (4)$$

$$Chlorophyll\left(\frac{mg}{mL}\right) = \frac{OD_{665nm}}{74,5} \quad (5)$$

The results obtained from these equations were normalized using the biomass concentrations [g L^{-1}] to obtain pigment concentrations in g g DW^{-1}. Typically, phycocyanin and allophycocyanin constitute 15%–20% of the dry weight in *Arthrospira* when cultured in photobioreactors (Chaiklahan et al., 2012; Lee et al., 2016; Chaiklahan et al., 2022).

2.6 Glycogen analysis

The glycogen extraction protocol was adapted from Phélippé et al. (2019). In short, the thawed pellet of 2 ml of culture was suspended in 1 mL 100% methanol and incubated at 45°C for 45 min in a heating block (550 rpm). The suspension was then centrifuged at room temperature for 10 min at 12,000 g and the supernatant was discarded. The pellet containing the glycogen was resuspended in 200 µl of 30% KOH solution. Now the suspension was incubated at 90°C in a heating block for 30 min (550 rpm). The suspension was cooled down to room temperature and 600 µl pre-chilled (4°C) 100% ethanol was added to precipitate the glycogen. The samples were stored at −20°C for 1 h. Afterwards, the samples were centrifuged at room temperature for 5 min at 12,000 g and the supernatant was discarded. The pellet was washed 2 times with 600 µl pre-chilled (4°C) 100% ethanol. Then, the pellet was dried at 60°C in a heating block for 10 min to evaporate the ethanol (open lid). The dried pellet was resuspended in 100 µl 100 mM sodium acetate buffer + 5 mM calcium chloride at pH 4.5. 20 µl of amyloglucosidase enzyme solution (3300 U/ml) was added (Total Starch Assay, Megazyme) and the suspension was incubated at 60°C in a heating block (550 rpm) for 15 min (enzymatic hydrolysis of glycogen into glucose). Then, the samples were split into two aliquots of 50 µL and 800 µL hexokinase (GlucoseAssayReagent, G3293, Sigma-Aldrich) was added to one of the aliquots. This suspension was incubated at room temperature for 15 min. The sample blank consisted of the other 50 µL aliquot and 800 µL ddH_2O and the reagent blank was made using 50 µL ddH_2O and 800 µL hexokinase solution. A calibration curve was created using pure glycogen from algae (Megazyme) in MilliQ as a standard. The absorbance (A_{340}) of the blanks and samples was measured with the NANOCOLOR® UV/VIS II spectrophotometer (MACHEREY-NAGEL) at λ = 340 nm using semi-micro cuvettes (greiner BIO-ONE). The glycogen content was determined using the standard curve. Based on literature, glycogen content varies extremely depending on the culturing conditions.

Phélippé et al. (2019) compared the data of several publications using *Arthrospira platensis* in PBRs in batch mode and found that the glycogen content lies between ~5% and 65% g g DW^{-1} depending on the growth conditions.

2.7 Statistical analysis

In order to obtain the specific growth rate during exponential phase (μ_{max}) and the corresponding 95% confidence intervals (CI), the values of biomass concentrations of the exponential phase were converted using the natural logarithm followed by linear regression of the experiment time *versus* ln [biomass concentration (g/L)] (Excel 2016 data analysis tool pack). Statistically significant differences were defined by comparing the mean μ_{max} values of one condition with the CIs of all other conditions. The average biomass productivity during linear phase (P_{av}) and the corresponding 95% CIs were obtained by linear regression [biomass concentration (g/L) = P_{av} x + c] of the biomass concentration data of the linear phase.

The results of X_{max}, max. pH, QY, max. pigment concentrations and %wt of Glycogen were evaluated using One-way ANOVA followed by multi-comparisons by Tukey test at a probability level of $p < 0.05$ using Graphpad Prism 9. The error bars on the figures correspond to standard deviations (SD), from the calculated mean values.

3 Results

3.1 Impact of light and temperature on the biomass production

Firstly, the impact of different temperatures (23°C, 25°C, 30°C, 32 °C and 34°C) and low light conditions (36, 45, 75 and 140 µmol photons m^{-2} s^{-1}) on the biomass production, was tested. The maximum growth rate (μ_{max}), average biomass productivity (P_{av}), maximum biomass concentration (X_{max}) and the time of active proliferation (T_{stat}) were determined for each condition. The maximum biomass concentration (X_{max}, g L^{-1}) is defined as the highest biomass concentration in a growth curve and is therefore also the point before reaching stationary phase. The cultures grown at the highest light intensity of 140 µmol photons m^{-2} s^{-1} grew the fastest in the first days of culturing without light limitation, and thus showed the highest μ_{max} values for this exponential growth phase. The light intensity and temperature both have a clear effect on the growth of the cultures. Suboptimal cold growth temperature (lower than 30°C) has mainly an impact at higher light intensity (75 or 140 µmol photons m^{-2} s^{-1}) (Figure 2). At the contrary, colder temperature is beneficial under low light conditions, and allows a longer batch duration and a higher final biomass concentration (Tables 3 and 4).

It can be seen that the lower light intensities reached a higher maximum biomass before reaching the death phase. Additionally, the higher the light intensity, the faster the stationary phase is reached. Thus, the cultures with the highest growth rates during the exponential phase, have the lowest maximum biomass concentrations. For example, the cultures grown at 140 µmol photons m^{-2} s^{-1} and 25°C only grew for 3 days while the cultures grown at 45 µmol photons m^{-2} s^{-1} and 25°C grew for 16 days.

P_{av} showed only slight differences between the conditions. Nonetheless, for example, the two lowest light intensities in combination with 30°C–32 °C resulted in significantly higher average productivities during linear growth compared to most of the other conditions (Tables 1–4). It should be mentioned here that P_{av} could not be calculated for all conditions, as the linear growth

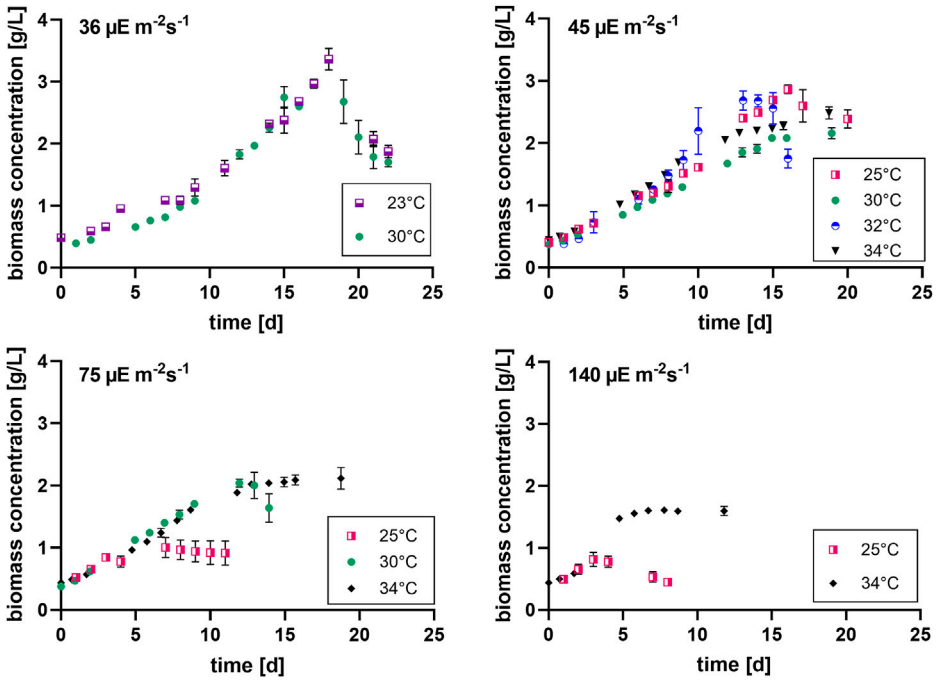

FIGURE 2
Biomass concentration curves at different light intensities (36, 45, 75 and 140 µmol photons m^{-2} s^{-1}) [µE = µmol photons], with n = four to eight, all values are presented as mean ± SD (Tables 3 and 4).

TABLE 1 Overview of the maximum specific growth rates (μ_{max}) for biomass concentration X (DW) in the different growth conditions. The maximum growth rate reflects only the first 3–4 days of growth, where an exponential growth was shown by using a logarithmic scale and linear regression, the values are shown as mean ± CI(95%) of four to eight cultures. Different letters (a-l) indicate significant differences ($p < 0,05$).

μ_{max} [d^{-1}] (°C)	36 µmol photons m^{-2} s^{-1}	45 µmol photons m^{-2} s^{-1}	75 µmol photons m^{-2} s^{-1}	140 µmol photons m^{-2} s^{-1}
23	0.16 ± 0.02^{a}	-	-	-
25	-	0.19 ± 0.01^{c}	0.24 ± 0.03^{g}	0.25 ± 0.08^{cdfghi}
30	0.13 ± 0.01^{b}	0.17 ± 0.01^{ad}	0.22 ± 0.01^{eh}	-
32	-	0.21 ± 0.03^{ce}	-	-
34	-	0.18 ± 0.01^{f}	0.17 ± 0.01^{af}	0.26 ± 0.02^{i}

TABLE 2 Overview of the average biomass productivity in the different growth conditions. P_{av} is the slope of the linear regression in the linear growth phase, the values are shown as mean ± CI(95%) of four to eight cultures.

P_{av} [g L^{-1} d^{-1}] (°C)	36 µmol photons m^{-2} s^{-1}	45 µmol photons m^{-2} s^{-1}	75 µmol photons m^{-2} s^{-1}	140 µmol photons m^{-2} s^{-1}
23	0.20 ± 0.01^{a}	-	-	-
25	-	0.18 ± 0.01^{c}	*	*
30	0.23 ± 0.02^{b}	0.13 ± 0.01^{d}	0.13 ± 0.01^{d}	-
32	-	0.25 ± 0.04^{b}	-	-
34	-	0.14 ± 0.01^{e}	0.13 ± 0.01^{d}	*

*Linear growth phase too short for analysis.
Different letters (a-e) indicate significant differences ($p < 0,05$).

phase only consisted of one or even zero time points at 75 and 140 µmol photons m^{-2} s^{-1} in combination with 25°C and 25°C and 34°C, respectively.

In summary, the higher the light intensity, the shorter the production phase (the lower the max. biomass concentration) and the faster the cultures reach stationary phase.

TABLE 3 Maximum biomass concentration (X_{max}) obtained at the end of the batch under the different conditions. The values are shown as mean ± SD of four to eight cultures.

Max. Biomass conc. X_{max} [g L^{-1}] (°C)	36 µmol photons m^{-2} s^{-1}	45 µmol photons m^{-2} s^{-1}	75 µmol photons m^{-2} s^{-1}	140 µmol photons m^{-2} s^{-1}
23	3.36 ± 0.15^{a}	-	-	-
25	-	2.86 ± 0.07^{b}	1.00 ± 0.14^{e}	0.82 ± 0.10^{e}
30	2.75 ± 0.18^{bc}	2.14 ± 0.08^{d}	2.04 ± 0.07^{d}	-
32	-	2.68 ± 0.15^{bc}	-	-
34	-	2.49 ± 0.10^{c}	2.12 ± 0.17^{d}	1.61 ± 0.01^{f}

Different letters (a-f) indicate significant differences (One-way ANOVA followed by Tukey test, $p < 0,05$).

TABLE 4 Duration of active proliferation [time until stationary phase is reached T_{stat} (d)].

T_{stat} [d] (°C)	36 µmol photons m^{-2} s^{-1}	45 µmol photons m^{-2} s^{-1}	75 µmol photons m^{-2} s^{-1}	140 µmol photons m^{-2} s^{-1}
23	18	-	-	-
25	-	16	7	3
30	15	16	12	-
32	-	13	-	-
34	-	13	13	6

3.2 Impact of light and temperature on culture pH

The pH was shown to be a good and easy parameter to monitor biomass production for *Limnospira indica* PCC8005 when dissolved bicarbonate is used as the carbon source in batch modus. The pH of the overall culture medium goes up when biomass is produced, because bicarbonate is consumed from the medium and converted inside the cells, in the carboxyzomes, to CO_2 and OH^- ions, in the process of photosynthesis (Miller and Colman, 1980; Poughon et al., 2020). These OH^- ions are released into the growth medium, causing the pH to rise. Figure 3 shows that the lower light intensities in combination with lower temperatures result in higher end pH values of the batch cultures, which matches the higher final biomass concentrations as reported in the previous section. The two lowest light intensities (36 and 45 µmol photons m^{-2} s^{-1}) reach pH values above 11.5 in all tested temperature conditions (Table 5). Higher light intensities, especially in combination with cold temperature, restrain growth and pH increase. For example, 34°C in combination with 140 µmol photons m^{-2} s^{-1} reaches the stationary phase before reaching pH 11.5, the same light at 25°C even stopped before reaching pH values over 10.

Table 5 shows the maximum pH values of the different cultures. Light intensity as well as temperature show a significant effect. The two lowest light conditions combined with 30°C and 32°C respectively, show the highest maximum pH, which is the same trend as we see for the average biomass productivity (Table 2).

3.3 Impact of low light on photosynthetic efficiency (QY) under different temperature regimes

The quantum yield was assessed in several growth conditions. All chosen time points were in the exponential and linear growth phase of the cultures to obtain reliable mean values (stationary phase not included).

Empirical observation revealed that the QY data is a good indicator of photosynthetic efficiency as it declines very rapidly when the cultures reach stationary phase, before any changes in OD or DW can be observed. For example, the cultures grown at 75 µmol photons m^{-2} s^{-1} and 30°C were on their biomass peak on day 12, but the QY value dropped already to 0.35 (previous data point was 0,45) on that day. The cultures grown at 45 µmol photons m^{-2} s^{-1} and 30°C showed the same effect on day 19 (biomass peak but QY dropped from 0.50 to 0.26). Table 6 shows that the QY of all tested conditions is in a range between 0,40 and 0,50. Nevertheless, significant differences were found for several conditions. For example, the QY in conditions of low light flux (36 µmol photons m^{-2} s^{-1}) in combination with high temperature (34°C) was significantly lower than the QY for lower temperature (25°C, 45 µmol photons m^{-2} s^{-1}) and for higher light (34°C, 75 µmol photons m^{-2} s^{-1}) conditions.

3.4 Impact of low light on pigment content, under different temperature regimes

During most growth experiments, samples for pigment extractions were taken. The extractions covered three different photosynthetic pigments, phycocyanin, allophycocyanin and chlorophyll. Figure 4 shows the phycocyanin content during the culturing time. The phycocyanin content per g DW drops drastically when the cultures reach the stationary phase. Tables 7–9 show the maximum pigment contents. In all three pigments, the impact of light and temperature shows a similar pattern. The lower light conditions (36 and 45 µmol photons m^{-2} s^{-1}) in combination with higher temperatures (30°C–34°C) show the highest pigment contents. Under warm temperature (30°C–34°C), small

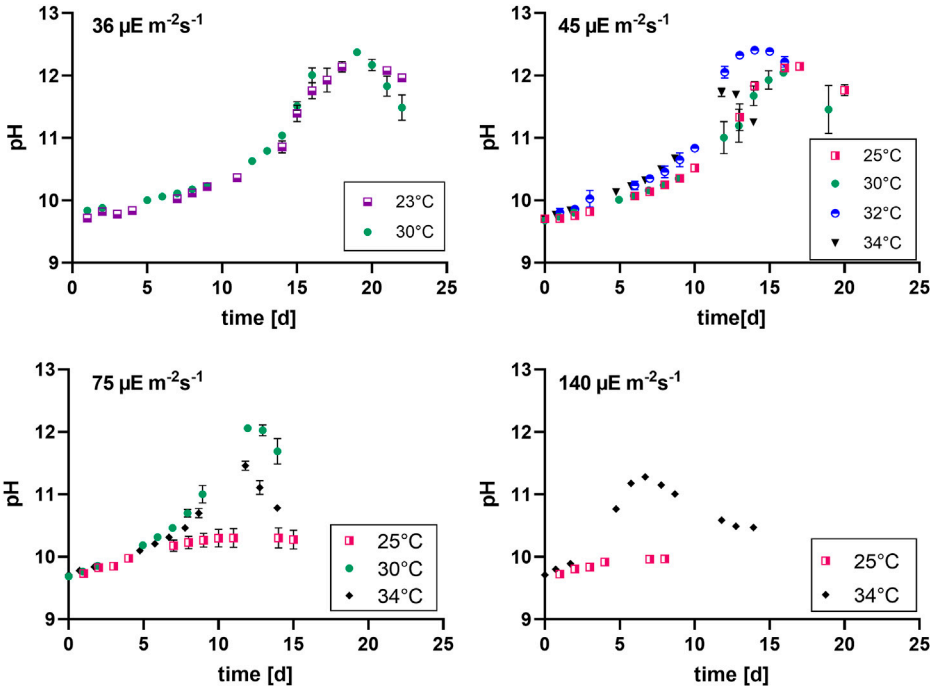

FIGURE 3
pH evolution at different light intensities (36, 45, 75 and 140 µmol photons m^{-2} s^{-1}), *n* = four to eight, all values are presented as mean ± SD.

TABLE 5 Maximum pH values under different conditions, the values are shown as mean ± SD of four to eight cultures.

Max. pH (°C)	36 µmol photons m^{-2} s^{-1}	45 µmol photons m^{-2} s^{-1}	75 µmol photons m^{-2} s^{-1}	140 µmol photons m^{-2} s^{-1}
23	12.14 ± 0.07^{a}	-	-	-
25	-	12.15 ± 0.05^{a}	10.30 ± 0.13^{d}	9.97 ± 0.03^{f}
30	12.38 ± 0.04^{b}	12.05 ± 0.04^{a}	12.06 ± 0.04^{a}	-
32	-	12.40 ± 0.03^{b}	-	-
34	-	11.70 ± 0.03^{c}	11.46 ± 0.08^{e}	11.27 ± 0.04^{g}

Different letters (a-g) indicate significant differences (One-way ANOVA followed by Tukey test, $p < 0{,}05$).

TABLE 6 QY of the cultures grown under different conditions, the values are shown as mean ± SD of four to eight cultures.

QY (°C)	36 µmol photons m^{-2} s^{-1}	45 µmol photons m^{-2} s^{-1}	75 µmol photons m^{-2} s^{-1}	140 µmol photons m^{-2} s^{-1}
23	0.45 ± 0.05^{abcg}	-	-	-
25	-	0.46 ± 0.04^{aj}	0.42 ± 0.07^{cdjk}	0.48 ± 0.02^{aceik}
30	-	0.43 ± 0.04^{cfgj}	0.44 ± 0.02^{ach}	-
34	0.40 ± 0.02^{bdefh}	0.41 ± 0.03^{bc}	0.48 ± 0.01^{ai}	0.42 ± 0.06^{bc}

Different letters (a-k) indicate significant differences (One-way ANOVA followed by Tukey test, $p < 0{,}05$).

variations in light intensities below 100 µmol photons m^{-2} s^{-1} (36, 45 and 75 µmol photons m^{-2} s^{-1}) do not have a significant impact on the antenna pigment concentrations (0.130 ± 0.009 g phycocyanin per g DW for 45 µmol photons m^{-2} s^{-1} at 34°C, vs 0.129 ± 0.008 g phycocyanin per g DW for 75 µmol photons m^{-2} s^{-1} at 34°C), only a light intensity of 140 µmol photons m^{-2} s^{-1} (34°C) induced a significantly lower pigment concentration (0.051 ± 0.017 g phycocyanin per g DW). Lower temperatures also caused significantly lower antenna pigment (phycocyanin and allophycocyanin) and chlorophyll concentrations. For example, a temperature of 30°C in combination with 36 µmol photons m^{-2} s^{-1} gave a phycocyanin concentration of 0.122 ±

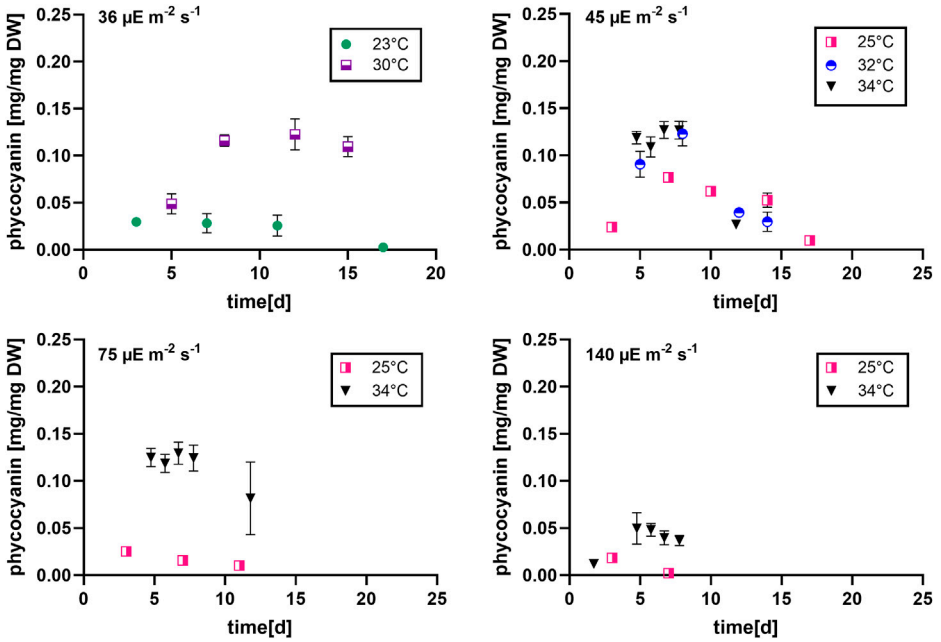

FIGURE 4
Phycocyanin content at different light intensities (36, 45, 75 and 140 µmol photons m^{-2} s^{-1}) over the culturing time, *n* = four to eight, all values are presented as mean ± SD.

TABLE 7 Maximum phycocyanin content. The values are shown as mean ± SD of four to eight cultures.

Max. Phycocyanin [g g DW^{-1}] (°C)	36 µmol photons m^{-2} s^{-1}	45 µmol photons m^{-2} s^{-1}	75 µmol photons m^{-2} s^{-1}	140 µmol photons m^{-2} s^{-1}
23	0.030 ± 0.003^{ad}	-	-	-
25	-	0.077 ± 0.004^{c}	0.025 ± 0.004^{d}	0.018 ± 0.004^{d}
30	0.122 ± 0.014^{b}	-	-	-
32	-	0.123 ± 0.013^{b}	-	-
34	-	0.130 ± 0.009^{b}	0.129 ± 0.008^{b}	0.051 ± 0.017^{a}

Different letters (a-d) indicate significant differences (One-way ANOVA followed by Tukey test, $p < 0,05$).

0.014 g g DW^{-1} and at 23°C, only 0.030 ± 0.003 g g DW^{-1} (−75,4%) could be achieved.

3.5 Impact of low light on glycogen content under different temperature conditions

The total glycogen content was determined in different growth conditions. Figure 5 shows the corresponding results. The glycogen content was found to be below 40% for all conditions, nonetheless, significant differences were found between the different temperature conditions. Cultures grown under the two lower light intensities did not reach values above 10% (g g DW^{-1}). The two highest light intensities of 75 and 140 µmol photons m^{-2} s^{-1} show a strong difference between the temperature conditions; i.e., suboptimal colder temperature (25°C) induced higher glycogen concentrations.

4 Discussion

4.1 Biomass production

The average biomass productivity of the linear growth phase (P_{av}) of *L. indica* under different temperatures and light intensities showed a remarkable significant increase under two conditons (36 µmol photons m^{-2} s^{-1} with 30°C and 45 µmol photons m^{-2} s^{-1} with 32°C), while the maximum growth rate (μ_{max}), culturing time (T_{stat}) and the max. biomass concentration (X_{max}) showed very strong differences between most culture conditions. Therefore it can be argued that in the first few days of culturing (during exponential phase without light limitation), the cells are proliferating at different rates but reach more similar productivities after this first phase. The reason for this are the light limiting conditions which are becoming more similar over time due to an increased growth rate at the higher light fluxes and higher temperatures at the beginning, *versus* slower

TABLE 8 Maximum allophycocyanin content, the values are shown as mean ± SD of four to eight cultures.

Max. Allophycocyanin [g g DW^{-1}] (°C)	36 µmol photons m^{-2} s^{-1}	45 µmol photons m^{-2} s^{-1}	75 µmol photons m^{-2} s^{-1}	140 µmol photons m^{-2} s^{-1}
23	0.017 ± 0.004^{ad}	-	-	-
25	-	0.029 ± 0.002^{c}	0.010 ± 0.001^{ae}	0.006 ± 0.001^{e}
30	0.042 ± 0.007^{b}	-	-	-
32	-	0.040 ± 0.004^{b}	-	-
34	-	0.039 ± 0.002^{b}	0.038 ± 0.003^{b}	0.022 ± 0.003^{cd}

Different letters (a-e) indicate significant differences (One-way ANOVA followed by Tukey test, $p < 0,05$).

TABLE 9 Maximum chlorophyll content, the values are shown as mean ± SD of four to eight cultures.

Max. Chlorophyll [g g DW^{-1}] (°C)	36 µmol photons m^{-2} s^{-1}	45 µmol photons m^{-2} s^{-1}	75 µmol photons m^{-2} s^{-1}	140 µmol photons m^{-2} s^{-1}
23	0.012 ± 0.001^{a}	-	-	-
25	-	0.020 ± 0.001^{bc}	0.007 ± 0.001^{e}	0.004 ± 0.001^{e}
30	0.020 ± 0.002^{b}	-	-	-
32	-	0.020 ± 0.002^{bc}	-	-
34	-	0.024 ± 0.000^{d}	0.024 ± 0.002^{d}	0.017 ± 0.001^{bc}

Different letters (a-f) indicate significant differences (One-way ANOVA followed by Tukey test, $p < 0,05$).

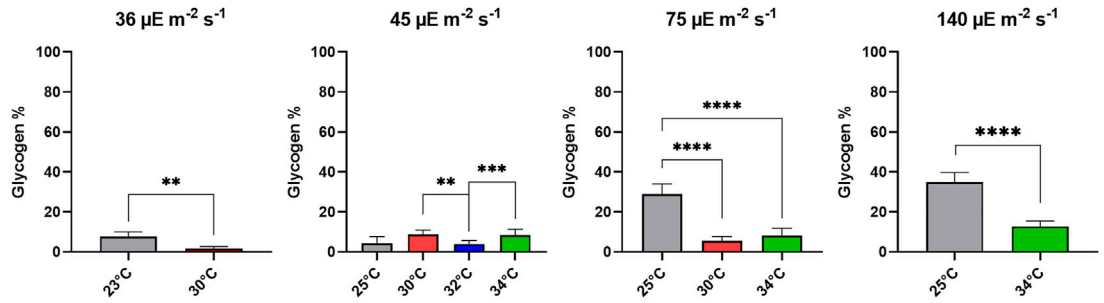

FIGURE 5
Glycogen content (wt%) of *Limnospira indica* cultures under different light intensities and temperatures, the values are shown as mean ± SD, statistics using one-way ANOVA followed by Tukey test, * = $p < 0,05$; ** = $p < 0,01$; *** = $p < 0.001$ and **** = $p < 00,001$.

biomass accumulation under lower light fluxes, resulting in similar light conditions in both cases. For the high light fluxes, no P_{av} could be obtained because the linear phase was too short, thus, statements can only be made for the lower light fluxes between 35 and 75 µmol photons m^{-2} s^{-1}.

The *Limnospira indica* PCC8005 P3 strain used in these experiments has adapted to a constant lower light environment at warm temperatur during the long cultivation time in our incubators in our laboratories. In our facilities, this strain is kept at 25–35 µmol photons m^{-2} s^{-1} and at 30°C. Thus, the strain is not acclimated to higher light conditions anymore and experiences photoinhibition when suddenly exposed to higher light conditions. Photoinhibition is a complex process occuring in all photosynthetic organisms under stressfull high light conditions. Photoinhibition occurs when the amount of absorbed photons produces more electrons than can be used in the Calvin cycle (Chojnacka and Noworyta, 2004). This causes an increase in reactive oxygen species (ROS) and therefore triggers several defence, detox and repair mechanisms in the cells, for example, the production of certain antioxidants. In case of strong photoinhibition, the amount of ROS inside the cell causes too much oxidative damage to the cell structures and leads to death of the photosynthetic organism (Scandalios, 2005; Erickson et al., 2015; Maltsev et al., 2021). It was also shown previously, that the

H_2O_2 concentration increases inside cyanobacterial cells when different environmental stresses like high light fluxes or phosphorus depletion are applied (Asaeda et al., 2022). Muhetaer et al. (2020) suggest that the production of H_2O_2 by the photosytem is the main reason for the reduced growth under high light in the cyanobacterial species *Pseudanabaena galeata* and *Microcystis aeruginosa*. They additionally showed that a longer exposure to unpreferable light conditions increases the negative effect on the growth of the cultures. In our study, the higher light conditions reached much lower maximum biomass concentrations, which supports the assumption that high light is inhibiting the growth after a few days, most likely due to an accumulation of reactive oxygen species.

The optimal light conditions are different not only for different species but also for different strains. The original habitat of the cyanobacteria impacts their light and temperature optima and therefore the adaptation of different species and strains to low or high light differs strongly (Moore et al., 1995; Vonshak and Tomaselli, 2000). Bautista and Laroche (2021) suggest that the differing responses of strains to light stress could have a genotypic origin which controls the turnover rate of the protein D1, a component of PS II. They mention additionally, that cultures can adapt to higher light intensities when exposed to such conditions for a longer period. In our current follow-up studies, we investigate possibilities to adapt the strain to different light flux intensities.

It is therefore not suprising that the values of optimal light intensities and the corresponding biomass productivities and biomass concentrations are varying strongly in literature. Maltsev et al. (2021) found in their study that the optimal light intensity for the growth of various microalgae lies between 26 and 400 µmol photons m^{-2} s^{-1}. Several studies found high biomass productivities under high light conditions, for example, a light intensity of 2,300 µmol photons m^{-2} s^{-1} (~29°C) caused a very high biomass production of 0.67 g L^{-1} d^{-1} in a photobioreactor with *Arthrospira platensis* BP in a semi-continuous mode at an OD_{560nm} of 0.6 in the studies of Chaiklahan et al. (2022). Further; Garcia-Gragera et al. (2021) reports a maximum biomass productivity of 0.58 g L^{-1} d^{-1} and a max. biomass concentration of 1.65 g L^{-1} for 932 µmol photons m^{-2} s^{-1} in experiments performed at the MELiSSA pilot plant; Deamici et al. (2022) used 120 µmol photons m^{-2} s^{-1} in a batch set-up using a photobioreactor, and found an average biomass productivity of 0.11 ± 0.01 g L^{-1} d^{-1}, a max. biomass concentration of 1.52 ± 0.01 g L^{-1}, and a μ_{max} of 0.55 ± 0.01 d^{-1}. In the ArtEMISS B space flight, at 35 µmol photons m^{-2} s^{-1} and 33 °C; Poughon et al. (2020) found a maximum biomass productivity of ~0.12 g L^{-1} d^{-1}, while Farges et al. (2009) reports a biomass productivity of 0.077 g L^{-1} d^{-1} for 33 µmol photons m^{-2} s^{-1} in an 1.2 L membrane bioreactor; Ravelonandro et al. (2008) performed experiments on a *Spirulina platensis* strain in modified Zarrouk medium and showed that very low intensities of green light at 1,200 lux (~16 µmol photons m^{-2} s^{-1}, ~30°C) reached a productivity of 0.18 g L^{-1} d^{-1}, a maximum growth rate of 0.624 d^{-1} and a maximum biomass concentration of 0.26 g L^{-1}. In another study, different species of red algae were shown to have higher growth rates under low irradiances (65 vs 300 µmol photons m^{-2} s^{-1}). Additionally, it could be shown that the temperature optima for some of the red algae species changed depending on the light intensity. The combination of low temperature with high light showed the slowest growth (Zucchi and Necchi, 2001), similar to our results on *L. indica* PCC8005. For multiple other photosynthetic organisms, like aquatic and land plants, it was already shown in the 1980s that lower temperatures increase the stress of photoinhibition caused by high light conditions (Powles, 1984).

Therefore it can be concluded that even though a lot of variability is found in the reported literature values, our results lie in the same range and the maximum biomass concentration (3.36 ± 0.15 g L^{-1} at 36 µmol photons m^{-2} s^{-1} and 23°C) is even higher than the reported values.

It is important to keep in mind that several factors influence the light conditions inside a culture. For example, a high biomass density in a culture causes shading effects which impact the light availability and therefore also the biomass production (Poughon et al., 2020; Garcia-Gragera et al., 2021; Chaiklahan et al., 2022), therefore not only the light intensity but also the availability of light plays an important role. Additionally, the wavelength composition of the light influences the performance of a cyanobacterial culture. Several studies have been performed on the use of different wavelengths (Ravelonandro et al., 2008; Bland and Angenent, 2016).

In our experiments, the temperature was shown to have a significant but smaller impact on the biomass production under low light conditions (<100 µmol photons m^{-2} s^{-1}) but was shown to have a high impact on other parameters such as pigment production. Thus, the smaller influence of temperature on biomass productivity was also shown in other reported studies. De Oliveira et al. (1999) found that only small changes in growth kinetics (*Spirulina maxima* and *Spirulina platensis*) are detectable when the temperature is changed. Only temperatures that are outside of the optimal range showed a big impact in their study.

4.2 pH

It is remarkable that all except three conditions reached pH values above 11.5. The pH increases due to the bicarbonate uptake of *L. indica* and the resulting OH^- release (Poughon et al., 2020). These high pH values shift the bicarbonate to carbonate species equilibrium and causes a HCO_3^- scarcity. The fact that many of the cultures continue their growth above pH 11 suggest that this strain is exceptionally well equipped for high pH values and low bicarbonate abundance. Many cyanobacteria have developed the ability to take up HCO_3^- due to the limited availability of CO_2 in marine and fresh waters (Smith and Ferry, 2000). When a cyanobacterium is able to grow at pH values higher than 10, it uses active HCO_3^- transport inside the cell because at pH > 10, very limited and decreasing amounts of CO_2 are present. Bicarbonate is less available above pH values of 10.3, because at this pH, the bicarbonate HCO_3^- concentration in the medium is lower than carbonate CO_3^{2-} concentration, which become the more abundant species (Deamici et al., 2022). Thus, the high pH values which have been measured under low light conditions probably can be explained by an exceptionally efficient HCO_3^- uptake of the *L. indica PCC8005* P3 strain.

Banares-Espana et al. (2006) have shown that different strains of the cyanobacterium *M. aeruginosa* have different pH compensation points, meaning they have different capacities to use HCO_3^- as a carbon source. These results support our hypothesis that the P3 strain might have developed a high HCO_3^- affinity and is therefore able to survive even above pH values of 11.5.

The higher light intensities do not show high pH values before the stationary phase. Therefore a carbon limitation is unlikely for these conditions. As explained in the previous section, photoinhibition causing lethal ROS doses is a likely explanation for the early death of the cultures. An additional possible explanation could be a nitrogen depletion due to limitation in the nitrogen assembly machinery (see discussion section glycogen).

The pH values were in line with the biomass productions and therefore this parameter can be used under varying conditions to monitor the growth status of the cultures. Additionally, the pH of the surrounding medium influences the biomass and pigment production of *A. platensis* (Gomont). Ismaiel et al. (2016) showed that the highest biomass for the Gomont strain could be obtained at pH 9.0. The highest chlorophyll and phycocyanin production were obtained at pH 8.5. Thus, the decreasing phycocyanin content at the end of the culturing time could be a pH induced effect (Figure 4).

4.3 Quantum yield

The QY of all tested cultures was between 0.40 and 0.50. Nevertheless, the statistical analysis revealed significant difference between several conditions. The highest QY values were obtained for cultures grown under higher light intensities (140 µmol photons m^{-2} s^{-1} with 25°C and 75 µmol photons m^{-2} s^{-1} with 34°C). This shows that the QY increases slightly under increasing light intensities. We could not find a direct correlation between the pigment content and the QY (see Table 6 vs; Tables 7–9). The combinations of (1) low temperature with low light, and (2) high temperature with high light seem to promote a high QY. According to Schuurmans et al. (2015) is it important to use the QY only as a qualitative value and it should not be compared in between species or even strains. Thus, the small differences between the QY values observed in this study should also be interpreted with caution. In summary, all cultures showed QY values between 0.40 and 0.50 and therefore it can be concluded that the photosynthetic performance was similar in the different conditions.

4.4 Pigments

A high pigment content (phycocyanin, allophycocyanin and chlorophyll) goes hand in hand with a high protein and antioxidant nutritive value of *L. indica* and accordingly it was one of our goals to find suitable conditions.

As mentioned, literature research revealed that phycocyanin and allophycocyanin constitute between 15% and 20% of the dry weight in *Arthrospira* when cultured in PBRs (Chaiklahan et al., 2012; Lee et al., 2016; Chaiklahan et al., 2022) which aligns with the values we obtained for the combinations of low light and high temperature (Table 7, 8). Several parameters have an influence on the pigment content. For example, not only the light intensity but also the wavelength composition has an impact on the phycocyanin production (Fekrat et al., 2022). The halogen lamps and LEDs which we used emit the full photosynthetic active irradiation in all experiments, thus, an impact of this parameter is unlikely in this study.

Other studies have shown that in several species of red algae, the pigment content changed significantly with the culturing temperature and for some species, the amount of phycobilliprotein increased when the light intensity was decreased (Zucchi and Necchi, 2001). Our results show a similar trend when 140 mol photons m^{-2} s^{-1} is compared to the lower light intensities. Deamici et al. (2022) obtained a chlorophyll content of 1.11 ± 0.15 mg g DW^{-1} (~0.001 g g DW^{-1}, in *L. indica* PCC8005) which is much lower than the values presented in this study. Garcia-Gragera et al. (2021) found a phycobilliprotein content between 0.037 and 0.125 g g DW^{-1} and a chlorophyll content between 0.007 and 0.018 g g DW^{-1} (also in *L. indica* PCC8005), which is very similar to our results (0.018 and 0.130 g g DW^{-1} for phycocyanin and 0.004—0.024 g g DW^{-1} for chlorophyll).

Karemore et al. (2020) confirmed that the temperature does not only play a role in the general biomass production but also impacts the pigment content in a semi-continuous PBR culture of *A. platensis*. A constant high temperature of 35°C caused a higher phycocyanin content in their study and the percentage of phycocyanin per dry weight decreased over the culturing time. In this study, cultures grown under higher temperatures were also shown to have an increased pigment content (phycocyanin, allophycocyanin and chlorophyll a) and therefore, these conditions are preferably used in regard to the nutritive value of *L. indica*. Temperature and light intensity both have a strong impact on the pigment contents and neither low temperature nor high light were shown to be favorable of this parameter in our experiments.

4.5 Glycogen

In *L. indica* PCC8005, 82% of the total carbohydrates were found to be glycogen (Bermudez and Paulina, 2022). Not only *Limnospira* but many cyanobacteria store glycogen as a carbon stock. The built-up of these stocks can be used as an electron sink (Damrow et al., 2016). Literature results revealed that high light intensity stress and nitrogen depletion play major roles in the metabolism of carbohydrates (Phélippé et al., 2019). For example, it was shown that cyanobacteria mutants which can not produce glycogen can not survive nitrogen starvation and also bleach faster at high light intensities (Carrieri et al., 2012; Hickman et al., 2013; Cano et al., 2018). In *Synechocystis* sp. PCC 6803, the glycogen metabolism was shown to be an important energy buffering system and glycogen accumulation is a direct result of high energy charges (Cano et al., 2018). The cyanobacteria *Merismopedia tenuissima* and *Oscillatoria rubescens* where shown to be more efficient at incorporating HCO_3^- into low molecular weight compounds under lower light conditions (20 vs > 90 µmol photons m^{-2} s^{-1}) and *M. tenuissima* produced less polysaccharides and more proteins under low light conditions (Konopka and Schnur, 1980), which is a similar trend than what we observed. Sakamoto and Bryant (1997) found that lower temperatures can cause the same effects as nitrogen depletion, causing an increase in glycogen accumulation. Sakamoto and Bryant (1997) found that *Synechococcus* sp. *PCC 7002* grown at 15°C under 50 and 250 µmol photons m^{-2} s^{-1} showed an increase in glycogen content when nitrate was used as the nitrogen source. Additionally, cultures grown at the same temperature but with urea as the sole nitrogen

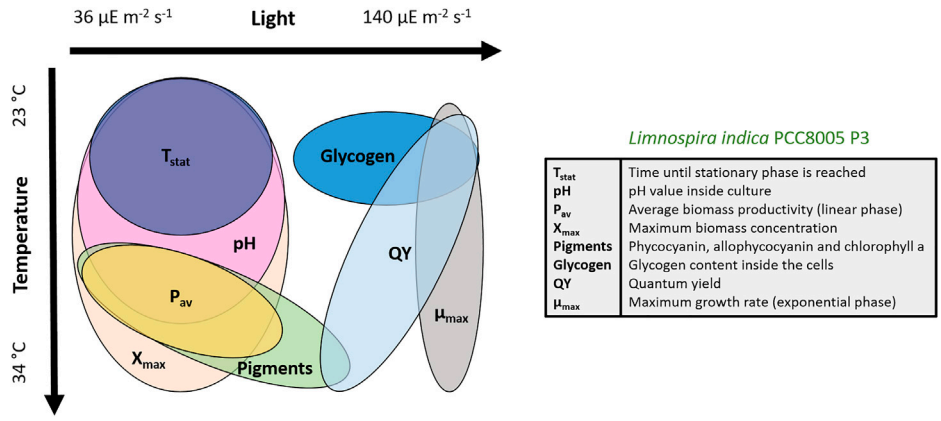

FIGURE 6
Qualitative overview of the impact of light and temperature on *Limnospira indica* PCC8005 P3. The maxima of each parameter are illustrated.

source, the glycogen accumulation could only be observed at the higher light intensity. Thus, it has been concluded that the cold growth conditions cause a nitrogen depletion effect. In a follow-up study (Sakamoto and Bryant, 1999), they found proof that the inactivation of nitrate/nitrite transporters is the main reason for limited growth under low temperatures. Additionally, Sakamoto and Bryant (1997) have shown that the high light, low temperature condition causes a decrease in phycobilliprotein, similar to the results obtained in the present study, and that this decrease in pigment content can be counteracted by using a different nitrogen source as urea.

The whole intracellular composition of *L. indica* changes depending on the growth conditions. For example, the light intensity has an impact on the ratio of extracellular polymeric substances (EPS) to intracellular glycogen. Phélippé et al. (2019) showed a decrease in the EPS/glycogen ratio from 3.1 at 100 µmol photons m^{-2} s^{-1} to 0.6 at 1,200 µmol photons m^{-2} s^{-1}, due to the fact that at higher light intensity the glycogen content increases to a larger extend than the EPS in the cells. They additionally compared the data of several publications using *A. platensis* in PBRs in batch mode and found that the glycogen content is varying severely (~5%–65% g g DW^{-1}) depending on the growth conditions which were used. For example, high salinity, nitrogen depletion and high light intensity have a strong impact on the glycogen production and the light intensity was found to be the most crucial. Only the high light intensities at lower temp produced more then 10% glycogen in our study. In summary, the high light conditions cause a high electron abundance in the cell, but the anabolic protein production pathways cannot follow the high flux of electrons under low temperatures and therefore electons are used to reduce CO_2 and stock the carbon in a reduced form as glycogen.

Deamici et al. (2022) found a carbohydrate content of 14.01 ± 1.84 g g DW^{-1} at 120 µmol photons m^{-2} s^{-1} which is similar to our glycogen value of 12.71 ± 2.58 at 140 µmol photons m^{-2} s^{-1} (34°C). Changes in glycogen content have an impact on the sedimentation behavior of the culture (Deschoenmaeker et al., 2017). Sedimentation (due to glycogen) and aggregation (due to EPS) are especially important for PBR operation in gravity environments like on Earth, as an increase in sedimentation velocity may cause mixing problems that result in not evenly distributed light and nutrients in the culture and problems with optical biomass measurements (Poughon et al., 2020; Fais et al., 2022b).

5 Conclusion

This study was one of the steps to determine the most optimal propagation conditions in a space bioreactor of the future life support system organism *Limnospira indica* and helps us to avert problems during upcoming space flight experiments. In order to complete the picture, we are currently investigating the impact of chronic low-dose irradiation and simulated microgravity on the *L. indica* cultures. The corresponding results will be presented in follow-up studies.

Figure 6 shows the peaks of the different parameters and how they overlap. Our main goals were a high pigment content, high QY, high maximum biomass concentration and low glycogen content. The graphical illustration shows that a higher temperature (30°C or above) in combination with low light (35—75 µmol photons m^{-2} s^{-1}) is most optimal to reach these goals and propagate a healthy batch culture.

Data availability statement

The raw data supporting the conclusions of this article will be made available by the authors, without undue reservation.

Author contributions

JF and NL designed the experimental set-ups, JF performed the experiments in the laboratory and wrote the first draft, NL and CD contributed to reviewing and editing. All authors contributed to the article and approved the submitted version.

Funding

This work was funded via the SCK CEN PHD Grant of JF, which is part of the ArtEMISS project funded by Belspo and ESA via the PRODEX program. The ArtEMISS project is part of the MELiSSA program of ESA.

Acknowledgments

This study was sponsored via the ESA ARTEMISS prodex contract and is part of the MELiSSA program of ESA, in the context of a PhD program of SCKCEN. The authors would like to thank Gabriele Ellena and Ilse Coninx for their help in the laboratory.

Conflict of interest

The authors declare that the research was conducted in the absence of any commercial or financial relationships that could be construed as a potential conflict of interest.

Publisher's note

All claims expressed in this article are solely those of the authors and do not necessarily represent those of their affiliated organizations, or those of the publisher, the editors and the reviewers. Any product that may be evaluated in this article, or claim that may be made by its manufacturer, is not guaranteed or endorsed by the publisher.

References

Aguirre-von-Wobeser, E., Figueroa, F. L., Cabello-Pasini, A., and Cabello-Pasini, A. (2000). Effect of UV radiation on photoinhibition of marine macrophytes in culture systems. *J. Appl. Phycol.* 12, 159–168. doi:10.1023/a:1008198404529

Akimoto, S., Yokono, M., Hamada, F., Teshigahara, A., Aikawa, S., and Kondo, A. (2012). Adaptation of light-harvesting systems of Arthrospira platensis to light conditions, probed by time-resolved fluorescence spectroscopy. *Biochimica Biophysica Acta (BBA)-Bioenergetics* 1817, 1483–1489. doi:10.1016/j.bbabio.2012.01.006

Allahverdiyeva, Y., Mustila, H., Ermakova, M., Bersanini, L., Richaud, P., Ajlani, G., et al. (2013). Flavodiiron proteins Flv1 and Flv3 enable cyanobacterial growth and photosynthesis under fluctuating light. *Proc. Natl. Acad. Sci.* 110, 4111–4116. doi:10.1073/pnas.1221194110

Antar, B., Reiss, D., and Lehman, D. (2006). "Gas-liquid separation strategies in microgravity environment," in 45th AIAA Aerospace Sciences Meeting and Exhibit, Reno, Nevada, 08 January 2007 - 11 January 2007, 950.

Asaeda, T., Rahman, M., and Abeynayaka, H. D. L. (2022). Hydrogen peroxide can be a plausible biomarker in cyanobacterial bloom treatment. *Sci. Rep.* 12, 1–11. doi:10.1038/s41598-021-02978-6

Averina, S. G., Velichko, N. V., Pinevich, A. A., Senatskaya, E. V., and Pinevich, A. V. (2019). Non-a chlorophylls in cyanobacteria. *Photosynthetica* 57, 1109–1118. doi:10.32615/ps.2019.130

Badri, H., Monsieurs, P., Coninx, I., Wattiez, R., and Leys, N. (2015). Molecular investigation of the radiation resistance of edible cyanobacterium*Arthrospira*sp. PCC 8005. *Microbiologyopen* 4, 187–207. doi:10.1002/mbo3.229

Banares-Espana, E., López-Rodas, V., Salgado, C., Costas, E., and Flores-Moya, A. (2006). Inter-strain variability in the photosynthetic use of inorganic carbon, exemplified by the pH compensation point, in the cyanobacterium Microcystis aeruginosa. *Aquat. Bot.* 85, 159–162. doi:10.1016/j.aquabot.2006.03.009

Barnett, M., Bhadouria, P., and Bisen, P. (2005). Arthrospira platensis: Brief history and description. *Curr. Pharm. Biotechnol.* 6, 373–379. doi:10.2174/138920105774370607

Bautista, E. G., and Laroche, C. (2021). Arthrospira platensis as a feasible feedstock for bioethanol production. *Appl. Sci.* 11, 6756. doi:10.3390/app11156756

Bennett, A., and Lawrence, B. (1973). Complementary chromatic adaptation in a filamentous blue-green alga. *J. Cell. Biol.* 58, 419–435. doi:10.1083/jcb.58.2.419

Bermudez, C., and Paulina, S. (2022). The cyanobacterium Limnospira: Carbohydrates production, photosynthetic activity, and biomass harvesting.

Bland, E., and Angenent, L. T. (2016). Pigment-targeted light wavelength and intensity promotes efficient photoautotrophic growth of Cyanobacteria. *Bioresour. Technol.* 216, 579–586. doi:10.1016/j.biortech.2016.05.116

Cano, M., Holland, S. C., Artier, J., Burnap, R. L., Ghirardi, M., Morgan, J. A., et al. (2018). Glycogen synthesis and metabolite overflow contribute to energy balancing in cyanobacteria. *Cell. Rep.* 23, 667–672. doi:10.1016/j.celrep.2018.03.083

Carrieri, D., Paddock, T., Pin-Ching, M., Seibert, M., and Yu, J. (2012). Photo-catalytic conversion of carbon dioxide to organic acids by a recombinant cyanobacterium incapable of glycogen storage. *Energy and Environ. Sci.* 5, 9457–9461. doi:10.1039/c2ee23181f

Chaiklahan, R., Chirasuwan, N., and Bunnag, B. (2012). Stability of phycocyanin extracted from Spirulina sp.: Influence of temperature, pH and preservatives. *Process Biochem.* 47, 659–664. doi:10.1016/j.procbio.2012.01.010

Chaiklahan, R., Chirasuwan, N., Srinorasing, T., Attasat, S., Nopharatana, A., and Bunnag, B. (2022). Enhanced biomass and phycocyanin production of Arthrospira (Spirulina) platensis by a cultivation management strategy: Light intensity and cell concentration. *Bioresour. Technol.* 343, 126077. doi:10.1016/j.biortech.2021.126077

Chojnacka, K., and Noworyta, A. (2004). Evaluation of Spirulina sp. growth in photoautotrophic, heterotrophic and mixotrophic cultures. *Enzyme Microb. Technol.* 34, 461–465. doi:10.1016/j.enzmictec.2003.12.002

Ciferri, O. (1983). 'Spirulina, the edible microorganism. *Microbiol. Rev.* 47, 551–578. doi:10.1128/mr.47.4.551-578.1983

Cogne, G., Lehmann, B., Dussap, C. G., and Gros, J. B. (2003). 'Uptake of macrominerals and trace elements by the cyanobacterium spirulina platensis (Arthrospira platensis PCC 8005) under photoautotrophic conditions: Culture medium optimization. *Biotechnol. Bioeng.* 81, 588–593. doi:10.1002/bit.10504

Cornet, J. F., and Dussap, C. G. (2009). A simple and reliable formula for assessment of maximum volumetric productivities in photobioreactors. *Biotechnol. Prog.* 25, 424–435. Wiley InterScience. doi:10.1002/btpr.138

Damrow, R., Maldener, I., and Zilliges, Y. (2016). The multiple functions of common microbial carbon polymers, glycogen and PHB, during stress responses in the non-diazotrophic cyanobacterium Synechocystis sp. PCC 6803. *Front. Microbiol.* 7, 966. doi:10.3389/fmicb.2016.00966

De Oliveira, M. A. C. L., Monteiro, M. P. C., Robbs, P. G., and Leite, S. G. F. (1999). 'Growth and chemical composition of Spirulina maxima and Spirulina platensis biomass at different temperatures. *Aquac. Int.* 7, 261–275. doi:10.1023/a:1009233230706

Deamici, K. M., Greque de Morais, M., Oliveira dos Santos, L., Gros, F., Vieira Costa, J. A., and Laroche, C. (2022). Magnetic field action on Limnospira indica PCC8005 cultures: Enhancement of biomass yield and protein content. *Appl. Sci.* 12, 1533. doi:10.3390/app12031533

Deschoenmaeker, F., Bayon-Vicente, G., Sachdeva, N., Depraetere, O., Cabrera Pino, J. C., Leroy, B., et al. (2017). Impact of different nitrogen sources on the growth of Arthrospira sp. PCC 8005 under batch and continuous cultivation - a biochemical, transcriptomic and proteomic profile. *Bioresour. Technol.* 237, 78–88. doi:10.1016/j.biortech.2017.03.145

Erickson, E., Wakao, S., and Niyogi, K. K. (2015). 'Light stress and photoprotection in Chlamydomonas reinhardtii. *Plant J.* 82, 449–465. doi:10.1111/tpj.12825

Fais, G., Manca, A., Bolognesi, F., Borselli, M., Concas, A., Busutti, M., et al. (2022a). Wide range applications of spirulina: From Earth to space missions. *Mar. Drugs* 20, 299. doi:10.3390/md20050299

Fais, G., Manca, A., Concas, A., Pantaleo, A., and Cao, G. (2022b). 'A novel process to grow edible microalgae on Mars by exploiting *in situ*-available resources: Experimental investigation. *Acta Astronaut.* 201, 454–463. doi:10.1016/j.actaastro.2022.09.058

Farag, M. R., Alagawany, M., Abd El-Hac, M. E., and Dhama, K. (2015). 'Nutritional and healthical aspects of spirulina (Arthrospira) for poultry, animals and human. *Int. J. Pharmacol.* 12, 36–51. doi:10.3923/ijp.2016.36.51

Farges, B., Laroche, C., Cornet, J.-F., and Dussap, C.-G. (2009). Spectral kinetic modeling and long-term behavior assessment of Arthrospira platensis growth in photobioreactor under red (620 nm) light illumination. *Biotechnol. Prog.* 25, 151–162. Wiley InterScience. doi:10.1002/btpr.95

Fekrat, F., Shahbazi, M., Amin Hejazi, M., and Nami, B. (2022). Optimization of light conditions by affecting the growth and production of C-Phycocyanin in Spirulina platensis microalgae. *J. plant process Funct.* 11, 79–94.

Furmaniak, M. A., Misztak, A. E., Franczuk, M. D., Wilmotte, A., Waleron, M., and Waleron, K. F. (2017). 'Edible cyanobacterial genus Arthrospira: Actual state of the art in cultivation methods, genetics, and application in medicine. *Front. Microbiol.* 8, 2541. doi:10.3389/fmicb.2017.02541

Gao, K., Yu, H., and Brown, M. T. (2007). 'Solar PAR and UV radiation affects the physiology and morphology of the cyanobacterium Anabaena sp. PCC 7120. *J. Photochem. Photobiol. B Biol.* 89, 117–124. doi:10.1016/j.jphotobiol.2007.09.006

Garcia-Gragera, D., Peiro, E., Arnau, C., Cornet, J-F., Dussap, C-G., and Godia, F. (2021). Dynamics of long-term continuous culture of Limnospira indica in an air-lift photobioreactor. *Microb. Biotechnol.* 15, 931–948. doi:10.1111/1751-7915.13882

Guidi, L., Tattini, M., and Landi, M. (2017). "How does chloroplast protect chlorophyll against excessive light," in *Chlorophyll* (London: Intech), 21.

Hickman, J. W., Kotovic, K. M., Miller, C., Paul, W., Kaiser, B., Jurista, T., et al. (2013). 'Glycogen synthesis is a required component of the nitrogen stress response in Synechococcus elongatus PCC 7942. *Algal Res.* 2, 98–106. doi:10.1016/j.algal.2013.01.008

Ismaiel, M. M., El-Ayouty, Y. M., and Piercey-Normore, M. (2016). Role of pH on antioxidants production by Spirulina (Arthrospira) platensis. *Braz. J. Microbiol.* 47, 298–304. doi:10.1016/j.bjm.2016.01.003

Johnson, T. R., Haynes, J. I., 2nd, Wealand, J. L., Yarbrough, L. R., and Hirschberg, R. (1988). Structure and regulation of genes encoding phycocyanin and allophycocyanin from Anabaena variabilis ATCC 29413. *J. Bacteriol.* 170, 1858–1865. doi:10.1128/jb.170.4.1858-1865.1988

Karemore, A., Yuan, Y., Porubsky, W., and Chance, R. (2020). Biomass and pigment production for Arthrospira platensis via semi-continuous cultivation in photobioreactors: Temperature effects. *Biotechnol. Bioeng.* 117, 3081–3093. doi:10.1002/bit.27480

Konopka, A., and Schnur, M. (1980). 'Effect of light intensity on macromolecular synthesis in cyanobacteria. *Microb. Ecol.* 6, 291–301. doi:10.1007/bf02010492

Lasseur, C., Brunet, J., de Weever, H., Dixon, M., Dussap, C. G., Gódia, F., et al. (2010). MELiSSA: The European project of closed life support system. *Gravitational Space Biol.* 23 (2), 3.

Lasseur, C. (2008). "Melissa: The European project of a closed life support system," in 37th COSPAR Scientific Assembly, Montreal, Canada, 13-20 July 2008, 1706.

Lasseur, C., and Mergeay, M. (2021). Current and future ways to closed life support systems: Virtual MELiSSA conference. *Ecol. Eng. Environ. Prot.* 1, 75–85.

Lee, S-H., Lee, J. E., Kim, Y., and Lee, S. Y. (2016). The production of high purity phycocyanin by Spirulina platensis using light-emitting diodes based two-stage cultivation. *Appl. Biochem. Biotechnol.* 178, 382–395. doi:10.1007/s12010-015-1879-5

Ma, Z., Ahmed, F., Yuan, B., and Zhang, W. (2019). 'Fresh living Arthrospira as dietary supplements: Current status and challenges. *Trends Food Sci. Technol.* 88, 439–444. doi:10.1016/j.tifs.2019.04.010

Maltsev, Y., Maltseva, K., Kulikovskiy, M., and Maltseva, S. (2021). 'Influence of light conditions on microalgae growth and content of lipids, carotenoids, and fatty acid composition. *Biology* 10, 1060. doi:10.3390/biology10101060

Masojídek, J., Vonshak, A., and Torzillo, G. (2010). "'Chlorophyll fluorescence applications in microalgal mass cultures," in *Chlorophyll a fluorescence in aquatic sciences: Methods and applications* (Berlin: Springer).

Milia, M., Corrias, F., Addis, P., Zitelli, G. C., Cicchi, B., Torzillo, G., et al. (2022). Influence of different light sources on the biochemical composition of Arthrospira spp. grown in model systems. *Foods* 11, 399. doi:10.3390/foods11030399

Miller, A. G., and Colman, B. (1980). Evidence for HCO3–transport by the blue-green alga (cyanobacterium) Coccochloris peniocystis'. *Plant physiology*. 65, 397–402.

Moore, L. R., Goericke, R., and Chisholm, S. W. (1995). Comparative physiology of Synechococcus and prochlorococcus: Influence of light and temperature on growth, pigments, fluorescence and absorptive properties. *Mar. Ecol. Prog. Ser.* 116, 259–275. doi:10.3354/meps116259

Muhetaer, G., Asaeda, T., Jayasanka, S. M., Baniya, M. B., Helayaye, D. L. A., Rashid, M. H., et al. (2020). Effects of light intensity and exposure period on the growth and stress responses of two cyanobacteria species: Pseudanabaena galeata and Microcystis aeruginosa. *Water* 12, 407. doi:10.3390/w12020407

Nowicka-Krawczyk, P., Muhlsteinova, R., and Hauer, T. (2019). Detailed characterization of the Arthrospira type species separating commercially grown taxa into the new genus Limnospira (Cyanobacteria). *Sci. Rep.* 9, 694. doi:10.1038/s41598-018-36831-0

Phélippé, M., Gonçalves, O., Thouand, G., Cogne, G., and Laroche, C. (2019). Characterization of the polysaccharides chemical diversity of the cyanobacteria Arthrospira platensis. *Algal Res.* 38, 101426. doi:10.1016/j.algal.2019.101426

Poughon, L., Laroche, C., Creuly, C., Dussap, C. G., Paille, C., Lasseur, C., et al. (2020). Limnospira indica PCC8005 growth in photobioreactor: Model and simulation of the ISS and ground experiments. *Life Sci. Space Res. (Amst)* 25, 53–65. doi:10.1016/j.lssr.2020.03.002

Powles, S. B. (1984). 'Photoinhibition of photosynthesis induced by visible light. *Annu. Rev. plant physiology* 35, 15–44. doi:10.1146/annurev.pp.35.060184.000311

Prasanna, R., Sood, A., Jaiswal, P., Nayak, S., Gupta, V., Chaudhary, V., et al. (2010). Rediscovering cyanobacteria as valuable sources of bioactive compounds (Review). *Appl. Biochem. Microbiol.* 46, 119–134. doi:10.1134/s0003683810020018

Rakhimberdieva, M. G., Boichenko, V. A., Karapetyan, N. V., and Stadnichuk, I. N. (2001). Interaction of phycobilisomes with photosystem II dimers and photosystem I monomers and trimers in the cyanobacterium Spirulina platensis. *Biochemistry* 40, 15780–15788. doi:10.1021/bi010009t

Ravelonandro, P. H., Ratianarivo, D. H., Joannis-Cassan, C., Isambert, A., and Raherimandimby, M. (2008). 'Influence of light quality and intensity in the cultivation of Spirulina platensis from Toliara (Madagascar) in a closed system. *J. Chem. Technol. Biotechnol.* 83, 842–848. doi:10.1002/jctb.1878

Raven, P. H., Evert, R. F., and Eichhorn, S. E. (2005). Photosynthesis, light, and life. *Biol. plants* 7, 119.

Sakamoto, T., and Bryant, D. A. (1997). Growth at low temperature causes nitrogen limitation in the cyanobacterium Synechococcus sp. PCC 7002. *Archives Microbiol.* 169, 10–19. doi:10.1007/s002030050535

Sakamoto, T., and Bryant, D. A. (1999). Nitrate transport and not photoinhibition limits growth of the freshwater cyanobacterium Synechococcus species PCC 6301 at low temperature. *Plant physiol.* 119, 785–794. doi:10.1104/pp.119.2.785

Scandalios, J. G. (2005). 'Oxidative stress: Molecular perception and transduction of signals triggering antioxidant gene defenses. *Braz. J. Med. Biol. Res.* 38, 995–1014. doi:10.1590/s0100-879x2005000700003

Schreiber, U., Endo, T., Mi, H., and Asada, K. (1995). 'Quenching analysis of chlorophyll fluorescence by the saturation pulse method: Particular aspects relating to the study of eukaryotic algae and cyanobacteria. *Plant Cell. Physiology* 36, 873–882. doi:10.1093/oxfordjournals.pcp.a078833

Schuurmans, R. M., van Alphen, P., Schuurmans, J. M., Matthijs, H. C. P., and Hellingwerf, K. J. (2015). 'Comparison of the photosynthetic yield of cyanobacteria and green algae: Different methods give different answers. *PLoS One* 10, e0139061. doi:10.1371/journal.pone.0139061

Segers, C., Mysara, M., Coolkens, A., Baatout, S., Leys, N., Lebeer, S., et al. (2022). 'Limnospira indica PCC 8005 or lacticaseibacillus rhamnosus GG dietary supplementation modulate the gut microbiome in mice. *Appl. Microbiol.* 2, 636–650. doi:10.3390/applmicrobiol2030049

Smith, K. S., and Ferry, J. G. (2000). Prokaryotic carbonic anhydrases. *FEMS Microbiol. Rev.* 24, 335–366. doi:10.1111/j.1574-6976.2000.tb00546.x

Vonshak, A., and Tomaselli, L. (2000). "'Arthrospira (spirulina): Systematics and ecophysioIogy," in *The ecology of cyanobacteria* (Berlin: Springer).

Wu, Q., Liu, L., Miron, A., Klímová, B., Wan, D., and Kuča, K. (2016). 'The antioxidant, immunomodulatory, and anti-inflammatory activities of spirulina: An overview. *Archives Toxicol.* 90, 1817–1840. doi:10.1007/s00204-016-1744-5

Yadav, A., Maertens, L., Meese, T., Van Nieuwerburgh, F., Mysara, M., Leys, N., et al. (2021). Genetic responses of metabolically active Limnospira indica strain PCC 8005 exposed to γ-radiation during its lifecycle. *Microorganisms* 9, 1626. doi:10.3390/microorganisms9081626

Yadav, A., Monsieurs, P., Misztak, A., Waleron, K., Leys, N., Cuypers, A., et al. (2019). 'Helical and linear morphotypes of Arthrospira sp. PCC 8005 display genomic differences and respond differently to 60Co gamma irradiation. *Eur. J. Phycol.* 55, 129–146. doi:10.1080/09670262.2019.1675763

Zhang, Y-M., and Chen, F. (1999). 'A simple method for efficient separation and purification of c-phycocyanin and allophycocyanin from Spirulina platensis. *Biotechnol. Tech.* 13, 601–603. doi:10.1023/a:1008914405302

Zucchi, M., and Necchi, O., Jr. (2001). Effects of temperature, irradiance and photoperiod on growth and pigment content in some freshwater red algae in culture. *Phycol. Res.* 49, 103–114. doi:10.1111/j.1440-1835.2001.tb00240.x

frontiers | Frontiers in Plant Science

TYPE Original Research
PUBLISHED 09 May 2023
DOI 10.3389/fpls.2023.1184064

Check for updates

OPEN ACCESS

EDITED BY
Cyprien Verseux,
University of Bremen, Germany

REVIEWED BY
Pannaga Pavan Jutur,
International Centre for Genetic Engineering and Biotechnology, India
Edmundo Lozoya-Gloria,
Unidad Irapuato (CINVESTAV), Mexico

*CORRESPONDENCE
Matteo Ballottari
matteo.ballottari@univr.it

RECEIVED 10 March 2023
ACCEPTED 17 April 2023
PUBLISHED 09 May 2023

CITATION
Perozeni F, Pivato M, Angelini M, Maricchiolo E, Pompa A and Ballottari M (2023) Towards microalga-based superfoods: heterologous expression of zeolin in *Chlamydomonas reinhardtii*. *Front. Plant Sci.* 14:1184064. doi: 10.3389/fpls.2023.1184064

COPYRIGHT
© 2023 Perozeni, Pivato, Angelini, Maricchiolo, Pompa and Ballottari. This is an open-access article distributed under the terms of the Creative Commons Attribution License (CC BY). The use, distribution or reproduction in other forums is permitted, provided the original author(s) and the copyright owner(s) are credited and that the original publication in this journal is cited, in accordance with accepted academic practice. No use, distribution or reproduction is permitted which does not comply with these terms.

Towards microalga-based superfoods: heterologous expression of zeolin in *Chlamydomonas reinhardtii*

Federico Perozeni[1], Matteo Pivato[1], Margherita Angelini[1], Elisa Maricchiolo[2], Andrea Pompa[2] and Matteo Ballottari[1]*

[1]Dipartimento di Biotecnologie, Università degli Studi di Verona, Verona, Italy, [2]Dipartimento di Scienze Biomolecolari, Università degli Studi di Urbino, Urbino, Italy

Microalgae are unicellular photosynthetic organisms that can be grown in artificial systems to capture CO_2, release oxygen, use nitrogen- and phosphorus-rich wastes, and produce biomass and bioproducts of interest including edible biomass for space exploration. In the present study, we report a metabolic engineering strategy for the green alga *Chlamydomonas reinhardtii* to produce high-value proteins for nutritional purposes. *Chlamydomonas reinhardtii* is a species approved by the U.S. Food and Drug Administration (FDA) for human consumption, and its consumption has been reported to improve gastrointestinal health in both murine models and humans. By utilizing the biotechnological tools available for this green alga, we introduced a synthetic gene encoding a chimeric protein, zeolin, obtained by merging the γ-zein and phaseolin proteins, in the algal genome. Zein and phaseolin are major seed storage proteins of maize (*Zea mays*) and bean (*Phaseolus vulgaris*) that accumulate in the endoplasmic reticulum (ER) and storage vacuoles, respectively. Seed storage proteins have unbalanced amino acid content, and for this reason, need to be complemented with each other in the diet. The chimeric recombinant zeolin protein represents an amino acid storage strategy with a balanced amino acid profile. Zeolin protein was thus efficiently expressed in *Chlamydomonas reinhardtii*; thus, we obtained strains that accumulate this recombinant protein in the endoplasmic reticulum, reaching a concentration up to 5.5 fg $cell^{-1}$, or secrete it in the growth medium, with a titer value up to 82 µg/L, enabling the production of microalga-based super-food.

KEYWORDS

***Chlamydomonas*, protein expression, synthetic biology, microalgae, zein, phaseolin**

1 Introduction

Food production is one of the key challenges faced in supporting life in extra-terrestrial environments for space exploration. Several constraints are present when planning food production in spacecraft or in enclosed environments under harsh conditions, such as limited water and oxygen on the Moon or Mars, cosmic radiation, requirements for

nutrient recovery from wastes, and limited spaces. With increasing population, food demands, and desire for healthier lifestyles, alternative sources of functional foods are important for space exploration and terrestrial applications. In this context, photosynthetic microalgae cultivation could be an interesting opportunity because of their reduced water footprint compared to crops and the possibility of growing in different environmental conditions using wastewater as a nitrogen and phosphorous source. The presence of carbon concentration mechanisms in microalgae and the absence of non-photosynthetic tissue, as in the case of vascular plants, allow microalgae to efficiently assimilate CO_2, releasing oxygen as a byproduct of the photosynthetic process (Onyeaka et al., 2021). Moreover, the biomass produced by microalgae has considerable nutritional value and contains relatively high concentrations of proteins, polyunsaturated fatty acids, polysaccharides, pigments, vitamins, minerals, phenolic compounds and sterols (Camacho et al., 2019). Microalgae biomass has also been reported to be enriched in copper and iron, potentially matching 21% and 11% of the Required Daily Allowance (RDA) for these metals (Koyande et al., 2019). Therefore, microalgae could be considered to enhance CO_2 sequestration, recover nutrients from waste, and produce edible biomass, with several species already approved as novel foods by the European Food Safety Association (EFSA) and the U.S. Food and Drug Administration (FDA) (Torres-Tiji et al., 2020; Mendes et al., 2022).

The green alga *Chlamydomonas reinhardtii* is a model organism for microalgae and is one of the most used species for laboratory research purposes (fundamental and applied research) because it has fast growth, does not require expensive supplements or an elaborate system for cultivation, is capable of sexual reproduction, and is easily engineered by genetic manipulation of nuclear, chloroplast, and mitochondrial genomes. The rapid advancements in recombinant protein production in this host suggest that in the near future, it could have an important role in the production of compounds of interest for the pharmaceutical and nutraceutical industries (Masi et al., 2023). In addition, it has recently received the Generally Recognized As Safe (GRAS) certification from the FDA for food applications. Recently, *C. reinhardtii* was reported having a positive effect for gastrointestinal function when used as functional food ingredient in both murine and human models (Fields et al., 2020). Metabolic engineering approaches have been proposed to improve carbon storage in lipids; however, little effort has been made to improve carbon storage in proteins in *C. reinhardtii*.

Seed storage proteins accumulate at high levels in seeds as nitrogen, carbon, and sulfur reserves and are then used during seed germination. They do not have any enzymatic function and accumulate in the protein bodies (Krishnan and Coe, 2001). Seed storage proteins of legumes and cereals are two major sources of proteins for humans. From a nutritional perspective, they complement each other: the storage proteins from legumes are poor in sulfur amino acids, and those from cereals are poor in lysine and tryptophan. Among the different storage proteins, phaseolins and zeins have been extensively studied as the main seed storage proteins in legumes and cereals, respectively (Suárez-Martínez et al., 2016; Khan et al., 2019). Phaseolin, a glycoprotein belonging to the 7S vicilin class, is the major seed storage protein in the common bean. Each phaseolin polypeptide is cotranslationally glycosylated in the endoplasmic reticulum (ER) lumen (De La Fuente et al., 2012). being a trimeric high-mannose glycosylated protein of approximately 150 kDa, containing almost identical monomers with a molecular mass ranging from 45 to 51 kDa and isoelectric points of 5.6 to 5.8 (Sathe, 2016). Maize endosperm zein protein belongs to the prolamin family, which are the most abundant type of proteins stored in cereal seeds such as wheat, maize, sorghum, rice, and barley. Zein are divided into four subfamilies based on their solubility and amino acid composition: α (22 and 19 kDa), β (15-kDa), γ (50 kDa, 27 kDa, and 16 kDa), and δ (18 kDa and 10 kDa) zeins (Holding, 2014), and these proteins are found in protein bodies (PBs) inside the endoplasmic reticulum (ER) (Lending and Larkins, 1989), accounting for more than 60% of the total stored proteins in the endosperm of maize kernels (Llop-Tous et al., 2010; Holding, 2014; Khan et al., 2019). Numerous studies have suggested that the packaging of zein and non-zein proteins into PBs has a peculiar role in maize endosperm development, influencing kernel properties (e.g., texture, functionality, and protein quality) (Guo et al., 2013; Holding, 2014). Due to reciprocal limitations in terms of amino acid composition, phaseolin and γ-zein proteins were fused together to create a new recombinant protein, zeolin, characterized by a balanced amino acid content. The chimeric zeolin protein contained the entire phaseolin sequence, including the signal peptide, followed by the unstructured 15 amino acid linker $(GGGGS)_3$ and 89 amino acids of mature γ-zein (27 kDa), starting from the fifth residue after the γ-zein signal peptide. The total number of amino acids was 525, including 24 residues of the N-terminal phaseolin signal peptide (Mainieri et al., 2004). When expressed in *Nicotiana tabacum* leaves, zeolin successfully accumulated, forming PBs in the ER (Mainieri et al., 2004). Zeolin is insoluble in the absence of reducing agents, whereas, phaseolin can be easily solubilized in the absence of reducing agents. This suggests that the protein interactions are different. Insolubility is also caused by disulfide bonds, a characteristic of γ-zein (Vitale et al., 1982) which are transferred to zeolin. It was also observed that zein has a dominant effect on phaseolin intracellular traffic: the zein fragment prevents zeolin from being delivered to the vacuole and ER retention can be conferred to another protein by γ-zein domains (Holding, 2014).

In this study, heterologous expression of zeolin was obtained in the green alga *C. reinhardtii* which could play an integral role in paving the way for the production of a microalgal superfood source. Zeolin gene, previously expressed in tobacco leaves (Mainieri et al., 2004), was here completely redesigned in order to optimize its expression in *C. reinhardtii*. Four different vectors were designed to express and accumulate the targeted or retained protein of interest in the endoplasmic reticulum of *C. reinhardtii*. The different expression vectors were characterized for having specific sequences at N and/or C terminus to achieve ER localization of zeolin: phaseolin or BIP signal peptide was used to target the protein inside the ER, while HDEL sequence was added as an ER retention sequence.

2 Materials and methods

2.1 Algal strains and culture conditions

C. reinhardtii UVM4 (UV-mediated mutant 4) (Neupert et al., 2009) strain was used as the background for all the transformations. Algal cells were cultivated under mixotrophic conditions using Tris-acetate-phosphate (TAP) (Kropat et al., 2011)in shaker flasks at 25°C and 100–150 µmol photons m^{-2} s^{-1} of continuous white light, unless otherwise stated. Cultivation on solidified agar plates was performed under the same conditions.

2.2 Construction of transformation vectors, transformation, and mutant screening

The zeolin-expressing vectors for *C. reinhardtii* transformation were prepared as follows. Starting from the amino acid sequence of zeolin (Supplementary Figure S1), the nucleotide sequence was optimized in silico, considering *C. reinhardtii* codon usage using Optimizer online tool (Puigbò et al., 2007). The mVenus (YFP) fluorescent coding sequence was added at the C-terminus of zeolin as an expression reporter for the selection of expression lines. A GSG-linker was also added between zeolin and YFP to allow the correct folding of the two proteins. To enhance protein expression and accumulation, RuBisCO introns were added to the coding sequence. Three *rbcs2* intron 1 copies were inserted into the zeolin sequence, and *rbcs2* intron 2 was added to the mVenus sequence according to the protocol designed by Baier et al. (Baier et al., 2018b). The optimized synthetic zeolin sequence is shown in Supplementary Figure S2. Additional peptides were then added at the N- or C-terminus to drive intracellular localization of zeolin: N terminus of the *C. reinhardtii* BiP1 protein (A8I7T8, herein named BiP) was used to drive ER localization, while HDEL ER retention sequence was added at the C-terminus (Rasala et al., 2014) as reported in the schematic diagram of the different vectors used in Figure 1.

The synthesized nucleotide sequence (Thermo Scientific, USA) was BamHI-BglII cloned into a pOpt2 modified vector. This vector was modified from the original pOpt2 (Lauersen et al., 2015) containing a 10x H-tag instead of S-tag. Conversely, BIP sequence was amplified with specific primer from pCM0-056 vector included in MocloToolkit (Crozet et al., 2018) and NdeI-BamHI cloned into pOpt2_Zeolin_YFP_Paro vector while the HDEL sequence was inserted into pOpt2_Zeolin_YFP_Paro and pOpt2_BIP_Zeo lin_YFP_Paro by amplification of YFP with overhang primers and subsequent BglII-EcoRI cloning.

The different vectors were then used to transform the microalga *C. reinhardtii*; the UVM4 mutant strain, previously selected for efficient heterologous protein transformation, was adopted as the background (Neupert et al., 2009). Stable nuclear transformation was performed by glass beads agitation as previously described (Kindle, 1990). Transformants were selected on TAP agar plates supplied with 12 µg/mL of paromomycin for 6–7 days at a light intensity of 200 µmol photons m^{-2} s^{-1}. Antibiotic-resistant colonies were cultivated in 96–well microtiter plates at a light intensity of 200 µmol photons m^{-2} s^{-1} until they were sufficiently dense. YFP fluorescence was measured using an Infinite PRO 200 plate reader (TECAN, Switzerland) with excitation at 509 ± 4.5 nm and emission at 540 ± 10 nm. Signals were normalized to 720 nm absorbance (cell scattering) to determine the highest expressing lines (Pivato et al., 2021).

2.3 Total protein extraction, SDS-PAGE, and western blotting

Total cells, exhaust growth media, and purified proteins were separated using SDS-PAGE (Laemmli, 1970). Separated proteins were stained using Coomassie Brilliant Blue solution or analyzed by immunodetection using an anti-GFP (Green Fluorescent Protein) antibody (Agrisera, Sweden). Protein accumulation over time in cells or supernatants was assessed by loading the same number of

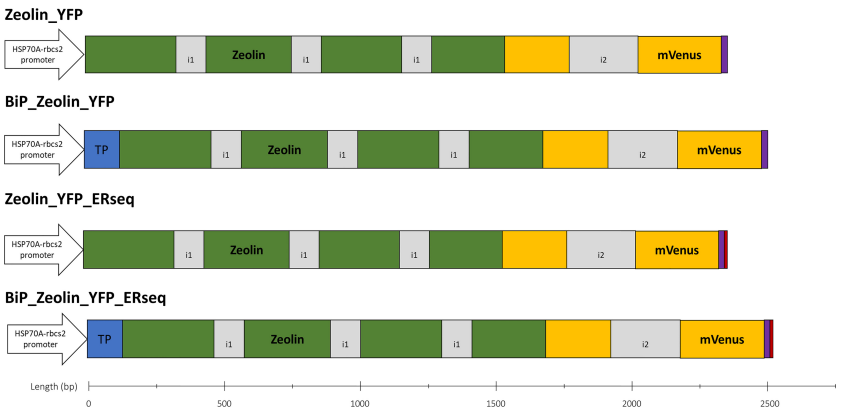

FIGURE 1
Zeolin expression vectors. Schematic overview of all expression vectors used in this work. All expression cassettes use the HSP70A-Rbcs2 hybrid promoter (containing *rbcs2* intron 1 and its 5′ UTR), and coding sequence are in frame with mVenus (YFP) sequence to generate a fusion protein. BIP1 target peptide (blue) directs proteins into ER. HDEL sequence (red) is used to retain proteins into ER. All proteins expressed carry a 10x H-tag at the C-terminus (purple). Intron 1 (i1) and 2 (i2) of *rbcs2* are depicted in grey color.

cells and the equivalent volume of growth medium obtained after centrifugation to remove cells followed by concentration using membrane spin columns (GE Healthcare, USA). The cell density was measured using Countess 3 (Thermo Scientific, USA). Protein quantification was performed by densitometric analysis using ImageLab software and recombinant YFP produced in *E.coli* as standard.

2.4 Zeolin purification

Zeolin_YFP was purified from BIP_Zeolin_YFP expressing lines, exploiting the presence of the H-tag at the C-terminus of the recombinant protein. After 4 days of cultivation, 1 L of culture was subjected to centrifugation to remove the cells, and the resulting supernatant containing secreted Zeolin_YFP was loaded onto an H-tag chromatographic affinity column. The elution was performed using 500 mM imidazole.

2.5 Growth analysis

Cell density was measured at 720 nm OD, and total dry biomass was evaluated by overnight lyophilization pellets followed by gravimetric determination as previously reported (Pivato et al., 2021). Cell dimension was measured by software analysis on microscope photos with n>70 (Perozeni et al., 2018). Statistical analysis was performed using a two-tailed t-test and compared with the UVM4.

2.6 Confocal microscopy

The subcellular localization of Zeolin_YFP was examined by confocal microscopy. Images were recorded using a Leica TCS-SP5 inverted confocal microscope (Leica Microsystems, Germany). mVenus (YFP) and chlorophyll were excited at 514 nm, and fluorescence emissions were detected at 522–572 nm and 680–720 nm for YFP and chlorophyll a, respectively as previously reported (Pivato et al., 2021).

3 Results

3.1 Zeolin expression in *Chlamydomonas reinhardtii*

Zeolin expression in *C. reinhardtii* was designed starting from the amino acid sequence previously expressed in tobacco (Mainieri et al., 2004) obtained by fusing T343 phaseolin from *Phaseolus vulgaris* L., including its signal peptide, with an unstructured 15 amino acids linker and 89 amino acids of mature γ-zein from *Zea mays* (Supplementary Figure S1). Zeolin gene for heterologous expression in *C. reinhardtii* was synthetically redesigned by codon optimization and intron spreading to enhance transgene expression, as previously described (Baier et al., 2018b) and reported in detailed in the Materials and Methods section. Previous work demonstrated that the highest zeolin accumulation in tobacco leaves was obtained when the protein accumulated in the ER while chloroplast localization was not efficient; therefore, chloroplast localization was not considered in this study. Instead, ER was targeted for intracellular zeolin localization. The zeolin sequence used in this study included a phaseolin N-terminus signal peptide, which was reported in tobacco to drive protein accumulation in the ER (expression vector Zeolin_YFP). To ensure a higher probability of the protein being targeted into the ER, a vector with an N-terminus signal peptide of the HSP70 molecular chaperone BiP (BiP1) from *C. reinhardtii* (Rasala et al., 2014) was also prepared (expression vector BiP_Zeolin_YFP). Finally, because successful zeolin protein expression in *Nicotiana tabacum* was obtained when zeolin was retained in the ER-forming protein bodies, expression vectors containing an ER retention sequence at the C-terminus of zeolin were obtained using the HDEL sequence previously reported to improve the retention of proteins in this compartment in *C. reinhardtii* (Rasala et al., 2014). HDEL sequences were added at the C-terminus of zeolin either in presence (BiP_Zeolin_YFP_Erseq expression vector) or absence (Zeolin_YFP_Erseq expression vector) of BiP signal sequence at N-terminus. A scheme of the different vectors adopted in this study is shown in Figure 1. The different vectors were then used to transform the microalga *C. reinhardtii*; the UVM4 mutant strain, previously selected for efficient heterologous protein transformation, was adopted as the background (Neupert et al., 2009).

Putative transformant lines with the highest YFP fluorescence (at least 2-fold compared to the average YFP fluorescence emission of the screened lines) were then selected and investigated by western blotting (Figure 2). As reported in Figure 2 and Supplementary Figures S3–S5, positive signals at ~80 kDa were identified for all the expression vectors used (Table 1). Considering the expected molecular weight of ~85.5 kDa for the mature zeolin-YFP protein, the slightly lower molecular weight observed could be related to additional proteolysis of the protein. The lines with the

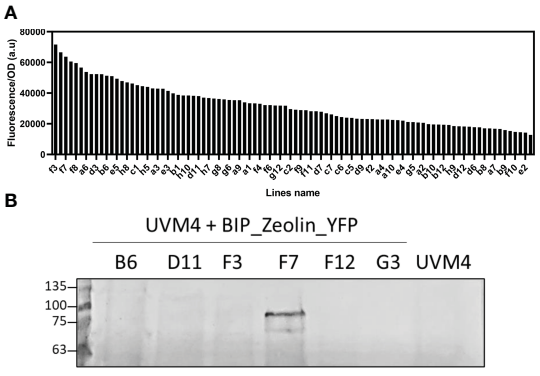

FIGURE 2
Fluorescence screening and Western blot analysis. **(A)** Fluorescence screening on putative BIP_Zeolin_YFP expressing lines (excitation: 509 ± 4.5 nm; emission: 540 ± 10 nm). **(B)** Western blot against YFP on putative BIP_Zeolin_YFP expressing lines (expected MW 85.5 kDa).

TABLE 1 Numbers of lines screened by YFP fluorescence and western blotting.

Expression vector	Transformant screened	YFP positive lines	Lines selected (YFP fluorescence)	Zeolin-YFP expressing lines (western blot)
Zeolin_YFP	192	45	8	5
BiP_Zeolin_YFP	96	39	6	1
Zeolin_YFP_ERseq_	192	20	5	5
BiP_Zeolin_YFP_ERseq	168	83	5	1

'YFP positive lines' refers to the transformant lines with an increase in YFP fluorescence of at least two-fold after normalization to the cell scattering at 720 nm, compared to the average of the 20 lines with the lowest YFP fluorescence emission per 720-nm cell scattering. The lines selected after YFP screening are those whose YFP fluorescence showed an increase of at least 3-fold compared to the average of the 20 lines with the lowest YFP fluorescence emission per 720-nm cell scattering.

strongest accumulation of zeolin-YFP complex (D2.2 for Zeolin_YFP, F7 for BiP_Zeolin_YFP, E9.1, Zeolin_YFP_ER and B5.1 for BiP_Zeolin_YFP_ER, respectively) were then used for the following analysis.

3.2 Zeolin localization

The presence of YFP fused to zeolin allowed the investigation of the zeolin-YFP complex localization by confocal microscopy (Figure 3). In the case of cells transformed with the Zeolin_YFP vector, the YFP signal was measured around the nucleus and did not overlap with the chlorophyll fluorescence signal (second column), which can be reconducted to ER localization according to literature (Rasala et al., 2014). The same behavior was observed in BiP_Zeolin_YFP-expressing lines, demonstrating that either phaseolin or BiP N-terminus signal peptides drive zeolin translation in the ER. In the case of Zeolin_YFP_ERseq, where the ER retention sequence HDEL was added at the C-terminus of the zeolin-YFP complex, the YFP fluorescence signal was again detected as a net around the nucleus, consisting of ER localization and excluding nucleus, cytosol, or chloroplast localization. However, in some cases, the zeolin-YFP complex in Zeolin_YFP_ERseq transformant lines was found to be located in defined spherical structures with extremely high fluorescence, which can be reconducted to protein bodies, and the formation of protein bodies was reported in tobacco leaves to significantly increase the intracellular accumulation of zeolin (Mainieri et al., 2004). The variability observed in terms of protein body formation in Zeolin_YFP_ ERseq-expressing cells could be related to a different level of expression, with protein body formation where zeolin-YFP expression reached a certain level. Finally, the addition of both the BIP target peptide and the HDEL retention sequence gives confocal microscopy a hybrid picture. Proteins are both located in filaments around the nucleus but also in high-fluorescence circular bodies.

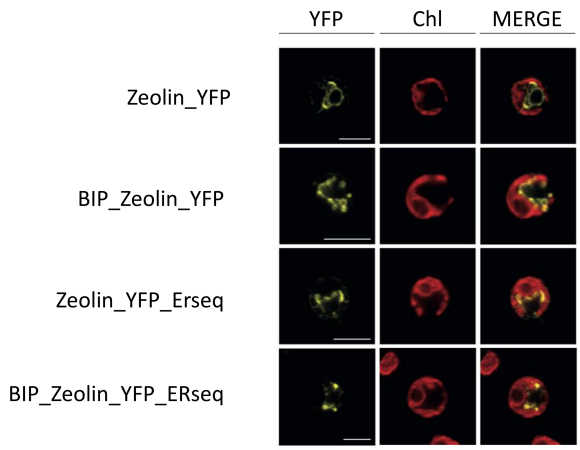

FIGURE 3
Zeolin localization. Analysis of endogenous (first line) or additional (lines 2–5) Zeolin_YFP target peptide. YFP fluorescence (YFP), chlorophyll autofluorescence (Chl), and merger of these two channels are shown. Excitation for YFP was 514 nm and 633 nm for chlorophylls. Emission was detected at 522–572 nm for YFP and 670–690 nm for chlorophylls. Scale bar represents 5 µm.

3.3 Zeolin influence on cell growth

The influence of zeolin-YFP expression on cell growth and biomass productivity was analyzed by cultivating the transformed lines in mixotrophic conditions under high (500 µmol $m^{-s}s^{-1}$) or low light (80 µmol $m^{-s}s^{-1}$) conditions. Cell scattering at 720 nm was used to follow the growth kinetics of the zeolin-expressing lines and their background UVM4. As shown in Figure 4, similar growth kinetics were observed for cells grown under low or high light conditions. Under either low or high light conditions, a slightly reduced growth could be observed for zeolin-expressing lines compared to UVM4 on the first days of cultivation, but on the second day under low light or on the third day under high light, no significant difference could be observed between transformed lines and UVM4. The cell areas of the different lines grown at 80 or 500 µmol $m^{-s}s^{-1}$ were then measured. Similar values between the different genotypes were retrieved and investigated for cells grown under high or low light. Biomass dry weight was also measured at the end of the growth curves, as shown in Figure 4 Under high light conditions, increased biomass production was observed compared to low light conditions, likely a consequence of the increased light energy available. Under both low and high light conditions, the dry weights of the different zeolin-expressing lines were similar to those of UVM4, except for the Zeolin_YFP_ERseq transformant line, which was characterized by a slightly reduced dry weight compared to its background under both light conditions. Interestingly, the Zeolin_YFP_ERseq vector was the best condition for inducing zeolin accumulation in protein bodies, which could potentially have a minor negative effect on cell growth.

10.3389/fpls.2023.1184064

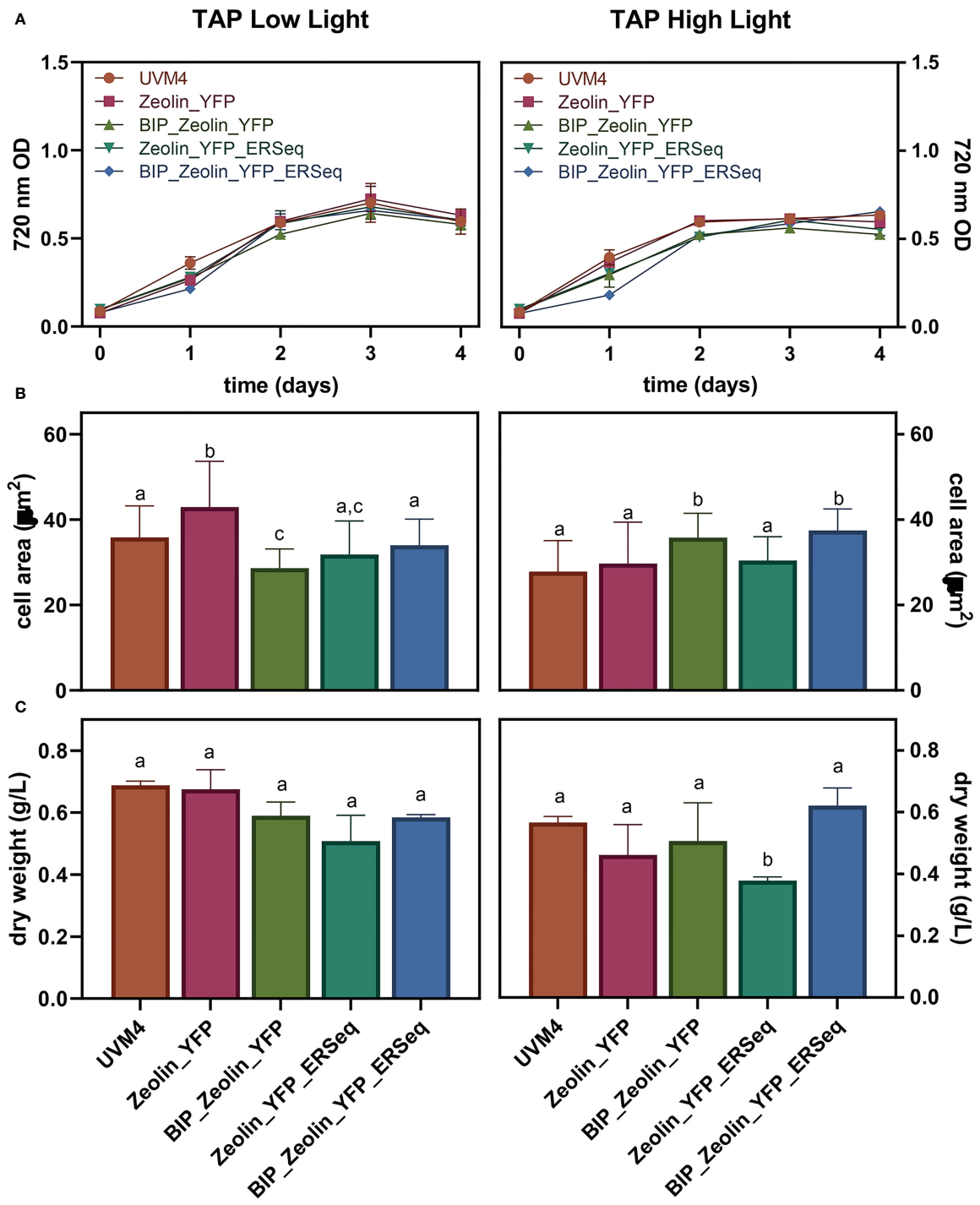

FIGURE 4
Expressing lines growth performance. Growth test was conducted in mixotrophy (TAP) in low (80 µmol photons m-2 s-2) or high (500 µmol photons m-2 s-2) light. 720 nm optical density **(A)**, cell dimensions **(B)** as well as dry biomass **(C)** were evaluated. The significantly different values ($P < 0.05$) in panels B and C are indicated with different letters. For cell areas **(B)** n=70 while for dry weight values **(C)** n=3.

3.4 Zeolin is retained in ER only in the presence of HDEL sequence

Zeolin is retained in the ER of plant leaves. In the case of *C. reinhardtii*, proteins targeted to the ER were reported to be secreted in several locations and loaded in vesicles targeted to the plasma membrane. To monitor zeolin secretion in the expressing lines, western blot analysis of cells and growth media was performed at different times of cultivation. UVM4 and zeolin-expressing lines were cultivated for up to 4 d in TAP medium at 200 µmol $m^{-s}s^{-1}$. At different cultivation times, cells were harvested by centrifugation, and pellets and supernatants were separately analyzed by western blotting using α-GFP antibody recognizing the zeolin-YFP complex. In the case of UVM4, no YFP bands were detected in

cells or in the exhausted growth medium during the four days of sampling, as expected (Supplementary Figure S6). In contrast, as shown in Figure 5, for the Zeolin_YFP transformed line, a double band at ~80 kDa was detected in cells harvested after 1 d of cultivation, which strongly decreased in the following days of cultivation, accompanied by an increase in the zeolin-YFP signal at higher molecular weight (~140 kDa) appearing in the supernatant, suggesting a possible secretion in dimeric form (see below for further details). The observation of a double band of the zeolin-YFP complex suggests the presence of partial protein degradation, as previously observed in the case of zeolin expressed in tobacco leaves (Mainieri et al., 2004), whereas the appearance of a clear band in the supernatants suggests zeolin-YFP protein secretion. Similar results were obtained for BiP_Zeolin_YFP, where most of the zeolin-YFP complexes were present in the supernatant after 3 or 4 d of cultivation. Completely different results were obtained in the case of Zeolin_YFP_ERseq transformant lines; in this case, YFP positive signals as a double band at ~80 kDa were observed only in cells for all four days of cultivation, while no zeolin-YFP could be detected in the growth medium. This result suggests that zeolin-YFP was successfully retained inside the cell and was not secreted in the presence of the HDEL sequence. In the case of the BIP_Zeolin_YFP_ERseq line, where both BiP and HDEL sequences were added to the N- and C-termini of the zeolin-YFP complex, a double band was detected at 80 kDa in the pellet samples, with the strongest protein signal observed on the second day in the pellet, whereas in the supernatant, a clear band appeared only on the fourth day. These results suggest that in the presence of both the BiP signal peptide and HDEL ER retention signal, the secretion of the protein is present yet delayed compared to when the HDEL sequence is absent (Zeolin_YFP and BiP_Zeolin_YFP). A possible explanation could be that the double signal peptide (the one contained in the zeolin sequence and the extra one from Bip) delays the folding of the protein, which is therefore retained in the ER for longer periods before being secreted, resulting in an intermediate phenotype compared to the case in which only one of the two sequences was added to the zeolin-YFP complex.

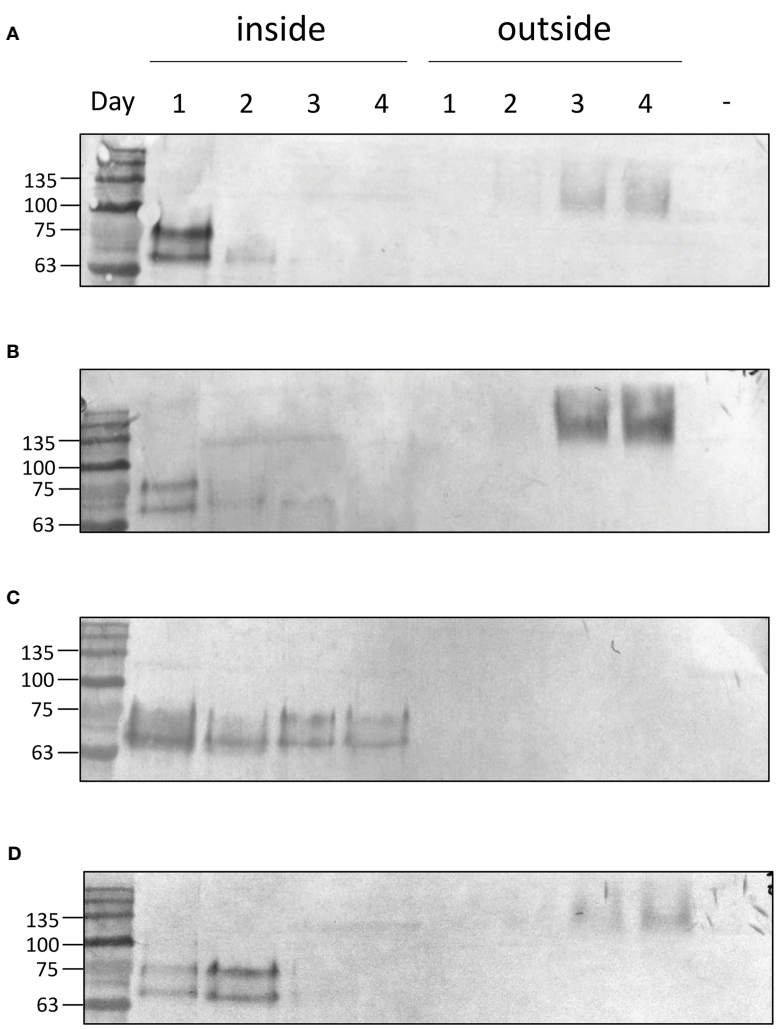

FIGURE 5
Zeolin accumulation and distribution. Western blot analysis showing protein accumulation at different days of cultivation in expressing lines either in the cell (inside) or secreted in the supernatant (outside). Data are referred to Zeolin_YFP **(A)**, BIP_Zeolin_YFP **(B)**, Zeolin_YFP_Erseq **(C)** and BIP_Zeolin_YFP_Erseq **(D)**. The negative control is marked with **(-)** and is represented by UVM4 supernatant at day 4.

The zeolin-YFP complex secreted in the expression lines Zeolin_YFP, BiP_Zeoin_YFP, and BIP_Zeolin_YFP_ERseq was detected at a higher molecular weight than the zeolin-YFP complex retained in the cells (Figure 5). The higher molecular weight of the secreted protein can be caused by a post-translational modification (i.e., N-glycosylation, as in phaseolin) or by interference in the electrophoretic pathway, caused by the salts contained in the growth medium or by the formation of complex aggregates in the secreted proteins. Another possibility is that the protein forms a dimer once it reaches the extracellular space, which would explain the molecular weight of approximately 150 kDa, which is exactly double the weight of the protein found inside the cells. To investigate the latter hypothesis, the secreted zeolin_YFP was purified from the growth medium by affinity chromatography owing to the presence of a His tag at the C-terminus. The purified zeolin-YFP was studied by western blot analysis. As shown in Supplementary Figure S7, a band of approximately 150 kDa was detected with the YFP antibody; these data are consistent with what was previously observed in western blot analysis of the supernatant. To clarify the nature of the 150 kDa band, western blot analysis was repeated by incubating the purified Zeolin-YFP complex at 100°C for 5 min to interrupt possible states of aggregation. Heat treatment resulted in a decrease in the molecular weight of the protein, while the intensity of the band remained the same, possibly indicating that the higher apparent molecular weight migration was due to the formation of zeolin-YFP dimers.

The quantification of the zeolin accumulated in the cells or secreted into the medium is reported in Figure 6 and was calculated using isolated YFP as a standard. The maximum zeolin accumulation per cell was observed in the Zeolin_YFP_ERseq expressing line after two days of cultivation. The reduced content on the fourth day suggested that zeolin protein bodies accumulated in the Zeolin_YFP_ Erseq-expressing line were partially degraded and/or their biosynthesis was reduced during cell cultivation. Finally, the total protein content in the different zeolin-expressing lines was analyzed, as reported in Table 2. Similar total protein content was measured in all the different zeolin-expressing lines compared to the UVM4 background, even though a slight increase in the total protein fraction per cell could be observed in the case of Zeolin_YFP_Erseq compared to Zeolin_YFP and BiP_Zeoin_YFP transformant lines.

4 Discussion

Seed storage proteins in legumes and cereals are the two main sources of protein for human nutrition. However, seed storage proteins from legumes are poor in sulfur amino acids, whereas cereal proteins are poor in Lysine and Tryptophan. Zeolin, the chimeric protein obtained by fusing phaseolin and zein, was proposed as a possible solution to provide a complete and balanced amino acid nutrition profile (Mainieri et al., 2004). In this study, we obtained heterologous expression of zeolin in the model organism for the green alga *C. reinhardtii*, which can be considered a novel sustainable protein source, with its ability to use light energy to assimilate CO_2 and inorganic nutrients into edible biomass without competing for land and water with other food crops. Moreover, the high photosynthetic efficiency of microalgae and their lower water footprint compared to crops make these organisms potential candidates to support life during space exploration as food and oxygen providers. The protein content of microalgae is species-related, but typically is very high, ranging from 30 to 60% of the total dry matter (Wang et al., 2021). The goal of this study was to further modify the protein content by introducing a storage protein with balanced amino acids, which could potentially accumulate in protein bodies. Zeolin localization in the ER was targeted because this compartment is a suitable organelle for protein accumulation, and previous studies in tobacco have shown that zeolin reaches a high concentration in the ER-forming inclusion body.

Zeolin_YFP-expressing lines were stable and showed protein accumulation in the ER at the initial stage of cultivation, whereas zeolin-YFP secretion was observed in the mid-exponential and saturation phases. These results demonstrate that the N-terminus phaseolin signal peptide is recognized as an entry signal to the secretory pathway in *C. reinhardtii*. The secretion of zeolin-YFP further support the transient ER localization of the protein, being the translation in the ER required for the secretion of heterologous proteins in *C. reinhardtii* (Lauersen et al., 2013; Rasala et al., 2014; Baier et al., 2018a; Molino et al., 2018). Zeolin-YFP secretion is likely at the base of some discrepancy observed between YFP screening and western blot analysis of transformant lines (Figure 2; Supplementary Figures S3–5) because the cells were not synchronized for this screening procedure. In *Nicotiana tabacum*, zeolin forms protein bodies in the ER; however, considering that the two hosts have two different cell structures, it is reasonable that the mechanism is not conserved. The secretion of zeolin-YFP in the engineered strains described herein demonstrates that the mechanism of ER retention is different in zeolin-expressing tobacco leaves and *C. reinhardtii* cells. Alternatively, it is possible that YFP at the C-terminus of the recombinant zeolin-YFP complex negatively affects ER retention and protein body formation. HDEL addition at the C-terminus led to retention of the protein inside the ER. Even if we cannot exclude the possibility that a fraction of zeolin may be confined in the cytosol, interfering with ER import. ER retention mediated by the HDEL sequence caused the formation of protein bodies, which were clearly visible by confocal microscopy. As previously suggested, zeolin protein bodies are likely too large to be packed in vesicles entering the secretion pathway (Mainieri et al., 2004). The simultaneous addition of the BiP signal peptide at the N-terminus and HDEL at the C-terminus led to an intermediate phenotype, with most zeolin-YFP retained in the cells even after two days of cultivation, whereas at the saturation phase (days 3 and 4), the chimeric protein was essentially secreted. According to these results, the presence of the BIP transit peptide strongly improved the ER localization of zeolin-YFP and its delivery in the secretion pathway, while the HDEL sequence at the C-terminus increased its retention in the ER. It is important to note that in plants, both KDEL and HDEL ER retention signals also promote protein delivery into the vacuole (Gomord et al., 1997): In the case of *C. reinhardtii*, HDEL sequence was reported to induce ER retention,

10.3389/fpls.2023.1184064

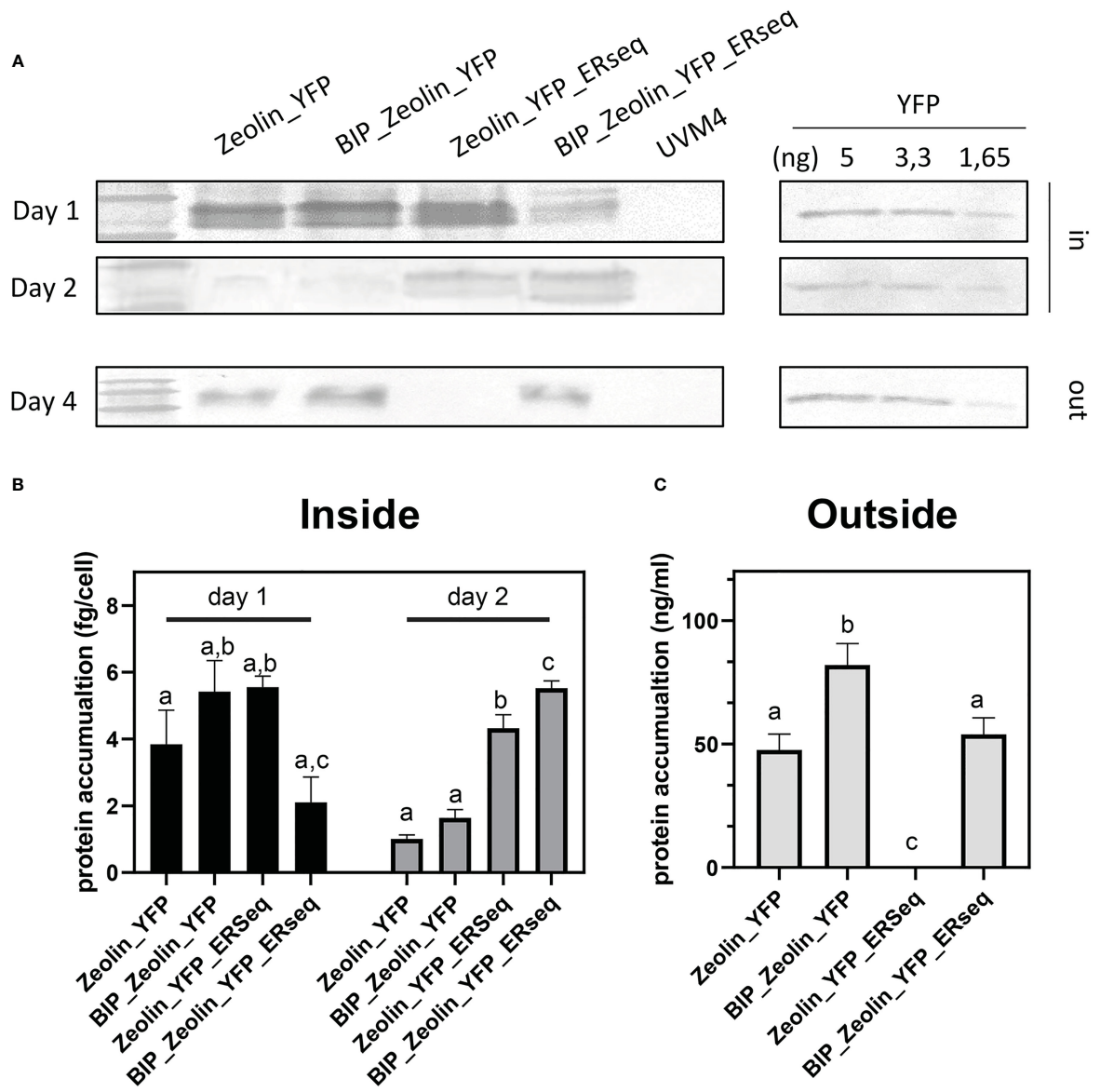

FIGURE 6
Zeolin quantification. **(A)** Quantitative western blot of Zeolin accumulating lines both for cell (inside) and supernatant (outside). YFP used as standard is shown with the loaded amount. **(B)** Zeolin quantification inside cell for zeolin expressing lines at day 1 and 2. **(C)** Zeolin quantification into supernatant (outside) for zeolin expressing lines at day 4. Results represent mean values and standard deviation from biological triplicates (n = 3). The significantly differences ($P < 0.05$) between different genotype at the same time point and same localization (inside or outside the cells) are indicated with different letters.

TABLE 2 Protein content per dry weight of zeolin-YFP expressing lines.

	UVM4	Zeolin_YFP	BiP_Zeolin_YFP	Zeolin_YFP_ERseq_	BiP_Zeolin_YFP_ERseq
% protein/total weight	30.9 ± 4.7 ^{a,b}	23.8 ± 2.8 ^{b}	24.5 ± 2.0 ^{b}	35.9 ± 6.1 ^{a,c}	29.1 ± 1.1 ^{a,c}

Total protein content in the different zeolin-expressing lines measured using micro BCA assay kit (Thermo Fisher). The significantly different values ($P< 0.05$) are indicated with different letters.

but we cannot exclude that zeolin-YFP with the HDEL sequence at the C-terminus might be partially delivered to other hydrolytic compartments in *C. reinhardtii* cells. The slightly reduced biomass accumulation observed in Zeolin_YFP_ERseq expressing lines raises the question of a possible negative effect on growth due to protein body formation in the ER, which might induce the onset of protein degradation pathways.

The Zeolin_YFP retained in the cell was detected by SDS-PAGE as a double band at ~80kDa. The expected molecular weight of the mature zeolin-YFP complex is 85.5 kDa: the lower apparent

molecular weight observed may be due to partial proteolysis of the protein. It is interesting to note that when retained in the cell, the protein was detected as a double band, as reported by Mainieri et. al., probably referring to the presence of two different proteolytic products. The secreted zeolin-YFP chimeric protein was detected at a higher molecular weight (~140 kDa) due to the presence of protein aggregates (dimers) that can be dissolved upon thermal treatment (Supplementary Figure S7). The nature of zein can explain its higher molecular weight; zein appears as a heterologous zein mix (disulfide-linked aggregates), in which γ-zein is the starting point and is essential for protein body formation. Moreover, post-translational modifications are likely to occur, probably glycosylation, considering that in beans, phaseolin monomers are N-glycosylated and transported from the ER and Golgi complex to the protein storage vacuoles.

Zeolin production yield by engineered strains was quite low, reaching values of ~6 fg/cell when retained in the ER, whereas a concentration of ~82 μg/L was obtained when zeolin-YFP was secreted. Several reasons can explain why the production is low. A negative effect could be related to the presence of YFP and His tags and the C-terminus; it is well known that different tags could have different impacts on protein expression in both prokaryotic and eukaryotic cells (Baier et al., 2018a; Koppl et al., 2022). Moreover, we cannot exclude the possibility that the protein could accumulate and degrade without forming protein bodies. It is important to note that zeolin retention in the ER is facilitated by the formation of Cys-bound in its C-terminus region. In our zeolin-YFP chimeric protein, the C-terminus contains YFP, a 27-kDa protein with a well-defined secondary structure that can interfere with the formation of Cys bonds and thus, ER retention. A strategy to fully exploit the zeolin potential is represented by the expression of zeolite alone, without any fluorophore. With the exception of the zeolin-YFP variant presenting the HDEL sequence at the C-terminus, the recombinant chimeric protein was secreted, excluding possible feedback inhibition due to protein accumulation. A further possible explanation could be the correlation between zeolin-YFP production and acetate availability (carbon source in TAP medium), indicating that depletion of the carbon source in the first two days causes a decrease in zeolin-YFP biosynthesis. To study this hypothesis and test C level as a limiting factor, further experiments must be performed under autotrophy conditions (CO_2 as a C source) or constant acetate supplementation. In addition to the random nature of gene insertion, expression is affected by the position effect; thus, by screening a large number of lines, it is possible to obtain lines with higher accumulation. Moreover, insertion of multiple gene copies could have a positive effect on protein accumulation. Finally, we cannot exclude the possibility that other growth conditions may have different effects on protein production and accumulation.

In conclusion, we obtained heterologous expression of a chimeric seed storage protein in a model organism for green alga, *C. reinhardtii*. Using the ER retention sequence HDEL, it was possible to induce zeolin accumulation as protein bodies in the ER, even with low expression efficiency. It is interesting to note that *C. reinhardtii* has already been recognized as safe for human consumption by the FDA, and previous work has demonstrated the possibility of inducing the accumulation of other compounds important for human nutrition, such as antioxidants or omega-3 fatty acids (Nguyen et al., 2013). With the objective of obtaining a sustainable superfood with a high nutritional profile and the ability to convert CO_2 and inorganic nutrients into edible biomass, zeolin expression in *C. reinhardtii* combined with metabolic engineering represents a possible solution.

Data availability statement

The original contributions presented in the study are included in the article/Supplementary Material. Further inquiries can be directed to the corresponding author.

Author contributions

MB and AP conceived of the study. MB and AP supervised experiments. FP and MA performed or contributed to all experiments reported herein. MP performed confocal microscopy analysis. MB, FP, and AP wrote the manuscript with contributions from all authors. All authors discussed the results, contributed to data interpretation, and commented on the manuscript. All authors contributed to the article and approved the submitted version.

Funding

This research was funded by CARIVERONA FOUNDATION (Grant No. 2019.0419.2019) to MB, by the Italian Ministry of University and Research (MUR, Grant PON Ricerca e Innovazione, Progetti-Progetti DM 1062) to FP, and by the Department of Biomolecular Sciences " food safety" University of Urbino Carlo Bo (Grant DISB_POMPA_PROG_ SIC_ALIMENTARE).

Conflict of interest

The authors declare that the research was conducted in the absence of any commercial or financial relationships that could be construed as a potential conflict of interest.

Publisher's note

All claims expressed in this article are solely those of the authors and do not necessarily represent those of their affiliated organizations, or those of the publisher, the editors and the reviewers. Any product that may be evaluated in this article, or claim that may be made by its manufacturer, is not guaranteed or endorsed by the publisher.

Supplementary material

The Supplementary Material for this article can be found online at: https://www.frontiersin.org/articles/10.3389/fpls.2023.1184064/full#supplementary-material

References

Baier, T., Kros, D., Feiner, R. C., Lauersen, K. J., Muller, K. M., and Kruse, O. (2018a). Engineered fusion proteins for efficient protein secretion and purification of a human growth factor from the green microalga chlamydomonas reinhardtii. *ACS Synth Biol.* 7 (11), 2547–2557. doi: 10.1021/acssynbio.8b00226

Baier, T., Wichmann, J., Kruse, O., and Lauersen, K. J. (2018b). Intron-containing algal transgenes mediate efficient recombinant gene expression in the green microalga chlamydomonas reinhardtii. *Nucleic Acids Res.* 46 (13), 6909–6919. doi: 10.1093/nar/gky532

Camacho, F., Macedo, A., and Malcata, F. (2019). Potential industrial applications and commercialization of microalgae in the functional food and feed industries: a short review. *Mar. Drugs* 17 (6). doi: 10.3390/md17060312

Crozet, P., Navarro, F. J., Willmund, F., Mehrshahi, P., Bakowski, K., Lauersen, K. J., et al. (2018). Birth of a photosynthetic chassis: a MoClo toolkit enabling synthetic biology in the microalga chlamydomonas reinhardtii. *ACS Synthetic Biol.* 7 (9), 2074–2086. doi: 10.1021/acssynbio.8b00251

De La Fuente, M. D., López-Pedrouso, M., Alonso, J., Santalla, M., De Ron, A. M., Álvarez, G., et al. (2012). In-depth characterization of the phaseolin protein diversity of common bean (Phaseolus vulgaris l.) based on two-dimensional electrophoresis and mass spectrometry. *Food Technol. Biotechnol.* 50 (3), 315–325. doi: 10.3390/su11195443

Fields, F. J., Lejzerowicz, F., Schroeder, D., Ngoi, S. M., Tran, M., McDonald, D., et al. (2020). Effects of the microalgae chlamydomonas on gastrointestinal health. *J. Funct. Foods* 65, 103738. doi: 10.1016/j.jff.2019.103738

Gomord, V., Denmat, L. A., Fitchette-Lainé, A. C., Satiat-Jeunemaitre, B., Hawes, C., and Faye, L. (1997). The c-terminal HDEL sequence is sufficient for retention of secretory proteins in the endoplasmic reticulum (ER) but promotes vacuolar targeting of proteins that escape the ER. *Plant J.* 11 (2), 313–325. doi: 10.1046/j.1365-313x.1997.11020313.x

Guo, X., Yuan, L., Chen, H., Sato, S. J., Clemente, T. E., and Holding, D. R. (2013). Nonredundant function of zeins and their correct stoichiometric ratio drive protein body formation in maize endosperm. *Plant Physiol.* 162 (3), 1359–1369. doi: 10.1104/pp.113.218941

Holding, D. R. (2014). Recent advances in the study of prolamin storage protein organization and function. *Front. Plant Sci.* 5. doi: 10.3389/fpls.2014.00276

Khan, N. U., Sheteiwy, M., Lihua, N., Khan, M. M. U., and Han, Z. (2019). An update on the maize zein-gene family in the post-genomics era. *Food Production Process. Nutr.* 1 (1), 13. doi: 10.1186/s43014-019-0012-5

Kindle, K. L. (1990). High-frequency nuclear transformation of chlamydomonas reinhardtii. *Proc. Natl. Acad. Sci. U.S.A.* 87 (3), 1228–1232. doi: 10.1073/pnas.87.3.1228

Koppl, C., Lingg, N., Fischer, A., Kross, C., Loibl, J., Buchinger, W., et al. (2022). Fusion tag design influences soluble recombinant protein production in escherichia coli. *Int. J. Mol. Sci.* 23 (14). doi: 10.3390/ijms23147678

Koyande, A. K., Chew, K. W., Rambabu, K., Tao, Y., Chu, D.-T., and Show, P.-L. (2019). Microalgae: a potential alternative to health supplementation for humans. *Food Sci. Hum. Wellness* 8 (1), 16–24. doi: 10.1016/j.fshw.2019.03.001

Krishnan, H. B., and Coe, E. H. (2001). "Seed storage proteins," in *Encyclopedia of genetics*. Eds. S. Brenner and J. H. Miller (New York: Academic Press).

Kropat, J., Hong-Hermesdorf, A., Casero, D., Ent, P., Castruita, M., Pellegrini, M., et al. (2011). A revised mineral nutrient supplement increases biomass and growth rate in chlamydomonas reinhardtii. *Plant J.* 66 (5), 770–780. doi: 10.1111/j.1365-313X.2011.04537.x

Laemmli, U. K. (1970). Cleavage of structural proteins during the assembly of the head of bacteriophage T4. *Nature* 227 (5259), 680–685. doi: 10.1038/227680a0

Lauersen, K. J., Berger, H., Mussgnug, J. H., and Kruse, O. (2013). Efficient recombinant protein production and secretion from nuclear transgenes in chlamydomonas reinhardtii. *J. Biotechnol.* 167 (2), 101–110. doi: 10.1016/j.jbiotec.2012.10.010

Lauersen, K. J., Kruse, O., and Mussgnug, J. H. (2015). Targeted expression of nuclear transgenes in chlamydomonas reinhardtii with a versatile, modular vector toolkit. *Appl. Microbiol. Biotechnol.* 99 (8), 3491–3503. doi: 10.1007/s00253-014-6354-7

Lending, C. R., and Larkins, B. A. (1989). Changes in the zein composition of protein bodies during maize endosperm development. *Plant Cell* 1 (10), 1011–1023. doi: 10.1105/tpc.1.10.1011

Llop-Tous, I., Madurga, S., Giralt, E., Marzabal, P., Torrent, M., and Ludevid, M. D. (2010). Relevant elements of a maize gamma-zein domain involved in protein body biogenesis. *J. Biol. Chem.* 285 (46), 35633–35644. doi: 10.1074/jbc.M110.116285

Mainieri, D., Rossi, M., Archinti, M., Bellucci, M., De Marchis, F., Vavassori, S., et al. (2004). Zeolin. a new recombinant storage protein constructed using maize gamma-zein and bean phaseolin. *Plant Physiol.* 136 (3), 3447–3456. doi: 10.1104/pp.104.046409

Masi, A., Leonelli, F., Scognamiglio, V., Gasperuzzo, G., Antonacci, A., and Terzidis, M. A. (2023). Chlamydomonas reinhardtii: a factory of nutraceutical and food supplements for human health. *Molecules* 28 (3), 1185. doi: 10.3390/molecules28031185

Mendes, M. C., Navalho, S., Ferreira, A., Paulino, C., Figueiredo, D., Silva, D., et al. (2022). Algae as food in Europe: an overview of species diversity and their application. *Foods* 11 (13), 1871. doi: 10.3390/foods11131871

Molino, J. V. D., de Carvalho, J. C. M., and Mayfield, S. P. (2018). Comparison of secretory signal peptides for heterologous protein expression in microalgae: expanding the secretion portfolio for chlamydomonas reinhardtii. *PloS One* 13 (2), e0192433. doi: 10.1371/journal.pone.0192433

Neupert, J., Karcher, D., and Bock, R. (2009). Generation of chlamydomonas strains that efficiently express nuclear transgenes. *Plant J.* 57 (6), 1140–1150. doi: 10.1111/j.1365-313X.2008.03746.x

Nguyen, H. M., Cuiné, S., Beyly-Adriano, A., Légeret, B., Billon, E., Auroy, P., et al. (2013). The green microalga chlamydomonas reinhardtii has a single ω-3 fatty acid desaturase that localizes to the chloroplast and impacts both plastidic and extraplastidic membrane lipids. *Plant Physiol.* 163 (2), 914–928. doi: 10.1104/pp.113.223941

Onyeaka, H., Miri, T., Obileke, K., Hart, A., Anumudu, C., and Al-Sharify, Z. T. (2021). Minimizing carbon footprint *via* microalgae as a biological capture. *Carbon Capture Sci. Technol.* 1, 100007. doi: 10.1016/j.ccst.2021.100007

Perozeni, F., Stella, G. R., and Ballottari, M. (2018). LHCSR expression under HSP70/RBCS2 promoter as a strategy to increase productivity in microalgae. *Int. J. Mol. Sci.* 19 (1). doi: 10.3390/ijms19010155

Pivato, M., Perozeni, F., Licausi, F., Cazzaniga, S., and Ballottari, M. (2021). Heterologous expression of cyanobacterial orange carotenoid protein (OCP2) as a soluble carrier of ketocarotenoids in chlamydomonas reinhardtii. *Algal Res.* 55, 102255. doi: 10.1016/j.algal.2021.102255

Puigbò, P., Guzmán, E., Romeu, A., and Garcia-Vallvé, S. (2007). OPTIMIZER: a web server for optimizing the codon usage of DNA sequences. *Nucleic Acids Res.* 35 (suppl_2), W126–W131. doi: 10.1093/nar/gkm219

Rasala, B. A., Chao, S.-S., Pier, M., Barrera, D. J., and Mayfield, S. P. (2014). Enhanced genetic tools for engineering multigene traits into green algae. *PloS One* 9 (4), e94028. doi: 10.1371/journal.pone.0094028

Sathe, S. K. (2016). "Beans, overview," in *Reference module in food science* (Elsevier). doi: 10.1016/B978-0-08-100596-5.00033-0

Suárez-Martínez, S. E., Ferríz-Martínez, R. A., Campos-Vega, R., Elton-Puente, J. E., de la Torre Carbot, K., and García-Gasca, T. (2016). Bean seeds: leading nutraceutical source for human health. *CyTA - J. Food* 14, 131–137. doi: 10.1080/19476337.2015.1063548

Torres-Tiji, Y., Fields, F. J., and Mayfield, S. P. (2020). Microalgae as a future food source. *Biotechnol. Adv.* 41, 107536. doi: 10.1016/j.biotechadv.2020.107536

Vitale, A., Smaniotto, E., Longhi, R., and Galante, E. (1982). Reduced soluble proteins associated with maize endosperm protein bodies. *J. Exp. Bot.* 33 (3), 439–448. doi: 10.1093/jxb/33.3.439

Wang, Y., Tibbetts, S. M., and McGinn, P. J. (2021). Microalgae as sources of high-quality protein for human food and protein supplements. *Foods* 10 (12). doi: 10.3390/foods10123002

frontiers | Frontiers in Plant Science

TYPE Original Research
PUBLISHED 02 June 2023
DOI 10.3389/fpls.2023.1186967

Check for updates

OPEN ACCESS

EDITED BY
Maurice Bosch,
Aberystwyth University, United Kingdom

REVIEWED BY
Ioannis-Dimosthenis S. Adamakis,
National and Kapodistrian University of Athens, Greece
Sarah E. Wyatt,
Ohio University, United States

*CORRESPONDENCE
Maurizio Iovane
maurizio.iovane@unina.it
Luigi Gennaro Izzo
luigigennaro.izzo@unina.it

RECEIVED 15 March 2023
ACCEPTED 09 May 2023
PUBLISHED 02 June 2023

CITATION
Iovane M, Izzo LG, Romano LE and Aronne G (2023) Simulated microgravity affects directional growth of pollen tubes in candidate space crops. *Front. Plant Sci.* 14:1186967. doi: 10.3389/fpls.2023.1186967

COPYRIGHT
© 2023 Iovane, Izzo, Romano and Aronne. This is an open-access article distributed under the terms of the Creative Commons Attribution License (CC BY). The use, distribution or reproduction in other forums is permitted, provided the original author(s) and the copyright owner(s) are credited and that the original publication in this journal is cited, in accordance with accepted academic practice. No use, distribution or reproduction is permitted which does not comply with these terms.

Simulated microgravity affects directional growth of pollen tubes in candidate space crops

Maurizio Iovane*, Luigi Gennaro Izzo*, Leone Ermes Romano and Giovanna Aronne

Department of Agricultural Sciences, University of Naples Federico II, Portici, Italy

Background: Long-term space missions will necessarily require producing viable seeds to be used for plant cultivation over time under altered gravity conditions. Pollen is known to play a key role in determining seed and fruit production over seed-to-seed cycles, but very few studies have evaluated pollen functionality under altered gravity.

Methods: We performed ground-based experiments to test how simulated microgravity can affect the directional growth of pollen tubes as a potential bottleneck in seed and fruit sets. The effect of clinorotation was assessed in the pollen of *Solanum lycopersicum* L. cv. 'Micro-Tom' and *Brassica rapa* L. var. *silvestris*, both eligible for cultivation in space. Pollen tube length and tortuosity were compared under 1*g* and simulated microgravity with a uniaxial clinostat.

Results: The main results highlighted that simulated microgravity significantly increased pollen tube length and tortuosity compared to 1*g* conditions. Further, clinorotation prompted a differential effect on pollen germination between *S. lycopersicum* and *B. rapa*. A more in-depth analysis evaluating the effect of gravity on the directional growth of pollen tubes excluded gravitropic responses as responsible for the tube tip position reached after germination.

Discussion: This research provides new insights into how altered gravity can interfere with plant reproduction and, in particular, microgametophyte functionality. Our findings represent a basis for further studies aimed at understanding the effect of real microgravity on plant reproduction and developing countermeasures to ensure seed-to-seed cultivation in long-term space missions and achieve self-sufficiency in food supplies from Earth.

KEYWORDS

simulated microgravity, pollen tube, pollen germination, clinostat, space crops, Micro-Tom, *Brassica rapa*, seed-to-seed

1 Introduction

Future space exploration requires plant-based bioregenerative life support systems (BLSS) to produce edible biomass and oxygen, recycle water, absorb carbon dioxide, and support astronauts' psychological health (Kordyum and Hasenstein, 2021). Indeed, plants are essential components of BLSS, and for decades, many experiments with plants have been performed to test the feasibility of plant cultivation in space (e.g., Zabel et al., 2016; De Pascale et al., 2021; Romano and Aronne, 2021).

Early efforts to cultivate plants for extended periods in microgravity resulted in reduced growth and complications in the transition to the reproductive stage (Kordyum et al., 1983; Kuang et al., 1995). In 1982, *Arabidopsis thaliana* became the first plant species to flower in space and produce seeds (Merkies and Laurinavichyus, 1983). However, only half of the seeds were viable and germinated in developing plants without growth defects (Salisbury, 1999). Environmental constraints such as low ventilation and high ethylene concentrations have been considered the main causes of interrupted or reduced reproductive success in many early experiments in space (De Micco et al., 2013). Recently, the advancement of plant growth systems has led to numerous successful seed sets in space and to a seed-to-seed-to-seed cycle of *A. thaliana* that was achieved entirely on the International Space Station (Link et al., 2014).

Overall, plant biology research in space indicates that real and simulated microgravity do not prevent plant reproduction, but they can affect the quality of embryos and the development of seedlings (Kuang et al., 2000b; Musgrave et al., 2000; Link et al., 2014; Izzo et al., 2022). Various alterations in seeds produced in space include delayed embryonic development, modification of storage reserves, delayed starch use in cotyledons, and decreased cell number in cotyledons (Kuang et al., 2000a; Kuang et al., 2000b; Musgrave et al., 2005). Currently, the identification of mechanisms by which space factors can affect plant reproduction is becoming increasingly critical for plant cultivation in future human settlements on the Moon and Mars (Kordyum et al., 2020). Indeed, the completion of the seed-to-seed cycle in the BLSSs is essential to producing viable seeds to be used for plant cultivation over time independently of Earth's supply.

Within the plant reproductive cycle, viable and germinable pollen is needed to trigger the double fertilization responsible for seed formation. Indeed, both pollen viability and germination are positively correlated with fruit and seed set (Paupière et al., 2017; Herrera et al., 2018). Therefore, possible effects of space factors on successful seed production can be addressed by defects in pollen viability and germinability. Previous experiments showed that most *Arabidopsis* and *Brassica* pollen grains produced under microgravity conditions were viable (Kuang et al., 1996; Kuang et al., 2000b). Nevertheless, this is not enough to fulfill the reproductive cycle. Once formed, viable pollen needs to be transferred to the stigma, posing some challenges in microgravity, especially for self-incompatible species that require cross-pollination to succeed in seed production (Kuang et al., 2000a). Furthermore, once it arrives on the stigma surface, pollen must germinate and guide its pollen tube across the ovary into the ovule to trigger double fertilization and seed formation. In the alternation between sporophyte (diploid) and gametophyte (haploid) generation in sexual plant reproduction, pollen represents the male gametophyte and is therefore an independent organism with a very short lifespan whose survival is essential to achieve the full completion of the plant reproductive cycle (Pacini and Dolferus, 2019).

Pollen is very sensitive to environmental factors that could affect pollen tube development. The earliest stage of pollen development was revealed to be the most sensitive to temperature changes, with a drastic reduction of pollen germination caused by high temperatures during microsporogenesis (Iovane and Aronne, 2021). Moreover, pollen germination is strongly influenced by relative humidity and its combination with temperature conditions (Güçlü and Koyuncu, 2017; Aronne et al., 2021). Indeed, a drastic loss in pollen viability occurs when pollen is exposed to a combination of high humidity and high temperature, whereas this does not happen when pollen is exposed to the same temperatures but lower humidity levels (Iovane et al., 2022a). Additionally, the possibility of plants growing and reproducing in space will depend on their capability to accomplish both sporophyte and gametophyte generations under altered microgravity conditions. In this scenario, investigations into how simulated microgravity can affect pollen germination and tube growth might provide useful insights into space-related issues in plant reproduction.

Among the instruments used to simulate microgravity, clinostats are meant to reduce the effect of constant gravity acceleration on Earth, and they have been largely used to perform ground-based experiments on the effects of simulated microgravity on plant growth and development (Dedolph and Dipert, 1971; Kiss et al., 2019). Even if clinostats do not reproduce weightlessness, ground-based research in simulated microgravity provides useful understandings to predict plant responses in real microgravity (Kiss et al., 2019). Although plants are known to be extremely sensitive to gravity (Muthert et al., 2020; Sathasivam et al., 2021), gravitropism in pollen tubes has not yet been assessed. To date, the microgametophyte (pollen) tube path towards the ovary is known to be guided exclusively by chemotropic stimuli due to specialized pistil tissues (Kandasamy et al., 1994), whereas the possible co-existence with pollen gravitropism has been generally overlooked.

To date, a few studies have shown that simulated microgravity affects several aspects of pollen tube development, such as alterations in sperm cell migration and callose plug formation (De Micco et al., 2005; De Micco et al., 2006), but gravitropism in pollen tubes has not yet been assessed. Previous studies were performed under *in vitro* conditions where the absence of a Ca2+ gradient allowed isolation of the effect of simulated microgravity. Thus, to test the hypothesis that chemotropism always coexists with gravitropism in germinating pollen, *in vitro* conditions would be ideal to reveal the effect of altered gravity in orientating pollen tubes. In the framework of future space missions with seed-to-seed crop cycles, it is crucial to study how altered gravity could interfere with pollen germination and tube directional growth to achieve fertilization.

Among candidate space crops, *Solanum lycopersicum* L. cv. 'Micro-Tom' and *Brassica rapa* L. are two promising crops for

cultivation on board spacecrafts, mainly for their compact size and short life cycle (Musgrave et al., 2005; Matsukura et al., 2008; Shikata and Ezura, 2016; Burgner et al., 2020). 'Micro-Tom' is a macro-thermal fruity crop that has already achieved a seed-to-seed cycle under simulated microgravity, even though fruit setting was almost halved under clinorotation (Colla et al., 2007). *B. rapa* is a micro-thermal leafy crop that has already been grown from seed to seed under microgravity conditions on the Mir space station in 1997; however, seeds and siliques formed from the second generation of plants on board resulted in compromise (Musgrave et al., 2005). *Brassica* spp. are close relatives of *A. thaliana*, and there is substantial homology between their nuclear genomes (Tatematsu et al., 2004). Particularly, the pollen of *B. rapa* L. var. *sylvestris* has already been investigated for aberrant callose plug deposition during tube development under simulated microgravity (De Micco et al., 2006).

Research on possible gravitropic responses of pollen is needed to have a better understanding of how altered gravity can limit seed and fruit production over repeated seed-to-seed cycles in candidate space crops. In this context, our study is the first to perform *in vitro* pollen germination on a clinostat to isolate the effect of simulated microgravity and unravel the possible gravitropism of the pollen tube. Specifically, our aim was to compare the effect of simulated microgravity and Earth gravity on pollen tube orientation in *S. lycopersicum* L. cv. 'Micro-Tom' and *Brassica rapa* L var. *sylvestris* as potential bottlenecks in regular seed and fruit development for cultivation in space.

2 Material and methods

2.1 Plant material

The effect of simulated microgravity on pollen germination and tube orientation was assessed in *S. lycopersicum* L. cv. 'Micro-Tom' and *B. rapa* L var. *sylvestris*, both recognized as candidate space crops. 'Micro-Tom' and *Brassica* plants were grown from seeds to flower in two different growth chambers. In 'Micro-Tom' plants, a photosynthetic photon flux density (PPFD) of 400 ± 15 µmol m^{-2} s^{-1} was provided by white LEDs in a 16 h d^{-1} photoperiod. Relative humidity was kept at 70 ± 5% and the air temperature was set at 22 ± 0.5°C both reported as the optimum for tomatoes (Sato et al., 2001; Matsuda et al., 2014). As for *Brassica* plants, the PPFD from white LEDs was 250 ± 10 µmol m^{-2} s^{-1} in a 12 h d^{-1} photoperiod. Relative humidity and air temperature were kept at 70 ± 5% and 18 ± 0.5°C, respectively. PPFD was measured during each treatment using a spectroradiometer (SS-110; Apogee Instruments Inc., Logan, UT).

2.2 Pollen sampling and viability measurement

Pollen was collected from flowers sampled shortly before anthesis to prevent possible pollen damage once exposed to the external environment. More specifically, undehisced anthers were detached from 200 flower buds per species, distributed in two different Petri dishes, and left to dehisce in a closed container filled with dry silica gel. This method sped up pollen release from anthers and allowed for the production of one bulk sample of pollen per species within a few hours of flower sampling (Iovane et al., 2022b).

Before clinorotation, the pollen viability of the bulk samples was assessed through the diaminobenzidine (DAB) reaction (Dafni, 1992) to ensure that the pollen used for the experiment was of high quality. We evaluated pollen viability on five pollen samples per species taken from the respective bulk. Each pollen sample was spread into a 10 µl droplet of water previously placed on a slide. One droplet of 10 µl of DAB reagent was added to each pollen sample, and slides were gently warmed on a heating plate and mounted. Pollen grains were scored as viable when stained dark/brown and as not viable when they remained faint/colorless. Each slide mounting a single pollen sample was photographed under a light microscope, and pollen viability was scored through image analyses on six photos per slide. The viability percentage was measured by counting at least 100 pollen grains per photo on a total of 30 photos per species (two species × five slides × six photos).

2.3 Pollen germination and gravity treatments

To test the effect of simulated microgravity on pollen germination, Petri dishes with germinating pollen were split between a control (1g) and a clinostat treatment (cl). In the control treatment, pollen germinated on agar germination medium inside Petri dishes vertically positioned according to the 1g gravity vector. Simulated microgravity treatment was performed on a uniaxial clinostat consisting of two metallic supports and two rotating dishes joined by a rigid shaft. Petri dishes with germinating pollen were fixed on the rotating shaft at a specific distance from the rotating axis to obtain ineffective centrifuge acceleration on pollen, according to a spin velocity of the rigid shaft set at two revolutions per minute. *In vitro* pollen germination was tested using two different agar media optimized for 'Micro-Tom' and *B. rapa* (Sato et al., 1998; Karapanos et al., 2010). In more detail, pollen from the bulk samples was placed in 10 Petri dishes per species lined with an agar medium made of 0.9% agar and 15% sucrose (w/v) for 'Micro-Tom' pollen and 0.9% agar and 20% sucrose (w/v) for *B. rapa*.

2.4 Microscopy and image analysis of germinating pollen

The effect of clinorotation on pollen germination and tube development in agar media was assessed through image analyses comparing pollen germinability, tube length, and tortuosity index between control (1g) and clinostat (simulated microgravity) treatments. Image analysis of germinating pollen was performed with ImageJ v1.53 software on photos taken with a digital camera (EOS 60D, Canon) mounted on a light microscope (Olympus® BX-60). Each photo was taken keeping track of the Petri dish

orientation with respect to the direction of the gravity vector. Germinating pollen was photographed after 24 and 48 h, and germination scoring was performed through image analyses on 400 photos (two species × two gravity treatments × five Petri dishes × two germination times × 10 photos). Germination percentages were assessed by considering as germinated grains those with a pollen tube longer than the grain diameter. Pollen tube length (L) was assessed on 600 pollen tubes and scored on 200 photos tracing the whole length of the pollen tube from the exine apertures to the pollen tube tip. On the same photos, the pollen tortuosity index was measured to estimate bending/directionality throughout the pollen tube path (Figure 1). The tortuosity index (T) was calculated using the following equation:

$$T = L/C$$

where L (length) is the total length of the pollen tube and C (chord) is the distance between the pollen exine aperture and the pollen tube tip. The reported tortuosity index can vary from 1 (L = C) to +∞ (L > C). More specifically, tortuosity values close to 1 indicate that the pollen tube developed straight from the exine to the tube tip, whereas increasing tortuosity values indicate an increase in direction changes during elongation of the pollen tube.

Furthermore, to detect a possible gravitropic response of pollen tubes, we investigated the direction of tube elongation in the control and clinostat treatments. For this purpose, we divided the images of each germinated pollen grain into four quadrants with respect to the direction of the gravity vector, scored the direction of 300 pollen tubes inside the agar medium, and calculated the percentage of pollen tube tips reaching each quadrant (Figure 2).

We hypothesized that the expected frequencies of pollen tube tip location would be equally distributed across the Petri dish containing the germination medium (25% in each quadrant). In the case of $P < 0.05$, the observed frequencies would differ from those expected, therefore showing a preferential growth direction of pollen tube tips. Specifically, in the control treatment, a positive or negative gravitropic response would result if pollen tube tips were preferentially located in quadrants I or III, respectively.

2.5 Data analysis

Data were analyzed with IBM® SPSS Statistics. Shapiro–Wilk's test and Levene's test were respectively used to assess the normality and homogeneity of the variances of the datasets. Differences in pollen germination, tube length, and tortuosity between ground and clinostat treatments were tested using ANOVA ($P < 0.05$) and the Brown–Forsythe robust test for equality of means. The observed and expected frequencies of pollen tube tip location in the different

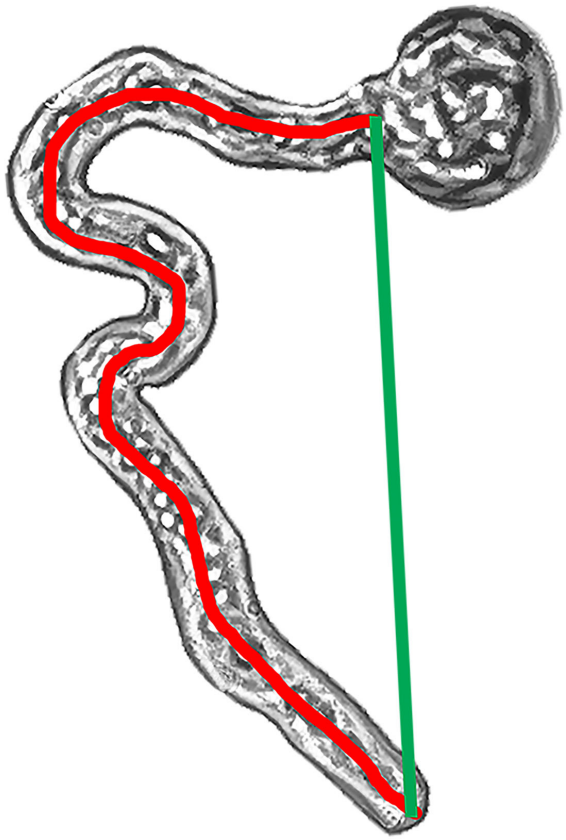

FIGURE 1
Tortuosity index calculated as L/C—length/chord through image analyses on pollen grains germinated in agar medium. Pollen tube length (L—red line) was traced throughout the whole length of the pollen tube. The pollen tube chord (C—green line) was traced as the straight line between the pollen exine aperture and the tube tip.

10.3389/fpls.2023.1186967

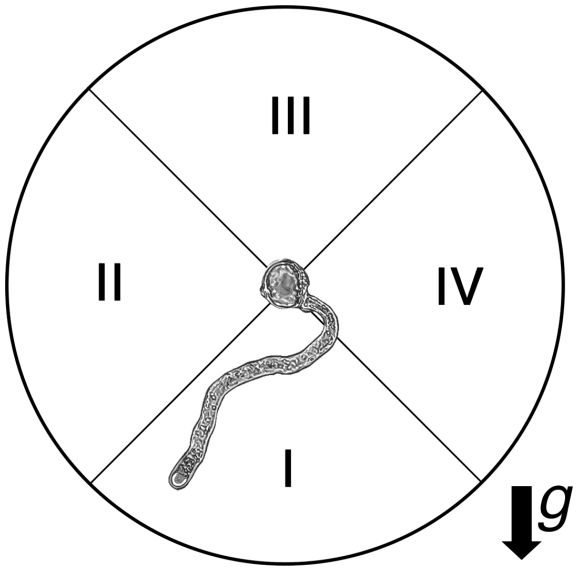

FIGURE 2
Evaluation of pollen tube tip location with respect to gravity vector (*g*) under 1*g* and clinorotation treatments through image analyses.

quadrants under control and simulated microgravity treatments were compared through a Chi-square test.

3 Results

The DAB test for pollen viability showed that pollen was well formed and functional in both species. Moreover, the viability of all pollen samples taken from the bulk of each species was high and uniform, ranging between 87%–91% in 'Micro-Tom' and 86%–94% in *B. rapa*, and no significant differences were detected among pollen samples intra-species (Figure 3).

Data on pollen germination showed clear differences between control and clinostat treatments (Figure 4). More specifically, the two-way ANOVA showed a significant (P <0.05) effect of germination time, gravity, and their interaction. The two species reacted differently to gravity since simulated microgravity reduced pollen germination in 'Micro-Tom' but increased pollen germination in *B. rapa* compared to the control condition. However, in both species, simulated microgravity significantly increased pollen germination when prolonging pollen incubation from 24 to 48 h, whereas no differences in pollen germination were found between 24 and 48 h of incubation under the 1*g* condition.

Thereafter, the pairwise comparison of pollen tube length between control and clinostat treatments highlighted a similar response in 'Micro-Tom' and *B. rapa*. Despite the great difference in tube length, pollen of both species developed longer tubes in simulated microgravity than in control conditions (Figure 5). Considering pollen tube length and pollen germination data, results highlighted that simulated microgravity promoted pollen tube length in both species despite reducing the germination rate in *B. rapa*.

As far as pollen tube path in germinated grains, a first visual overview of pollen tubes showed a clear difference between control and clinostat treatments, especially in 'Micro-Tom' (Figure 6). More in detail, control pollen developed straighter tubes compared to the simulated microgravity condition, in which tube tips changed their direction more frequently throughout the pollen tube path. The straightness/curviness of pollen tube paths was compared between control and clinostat by measuring the tortuosity index in 300 pollen tubes per species. Results showed that simulated microgravity significantly increased pollen tube tortuosity compared to control. Moreover, ANOVA reported that the difference in tortuosity between control and simulated microgravity was more significant in 'Micro-Tom' (P <0.001, Figure 7A) than in *B. rapa* (P <0.05, Figure 7B), which is also highlighted in the box plots showing the distribution of tortuosity values in the two gravity treatments (Figure 7). Indeed, in 'Micro-Tom,' most of the values of the tortuosity index are distributed consistently around the median in the control treatment, whereas a much wider distribution with increasing tortuosity values results in the clinostat treatment. Differently, the tortuosity index of *B. rapa* pollen tubes were similarly distributed around the median both in control and in simulated microgravity, but still had significantly higher values in the clinostat treatment.

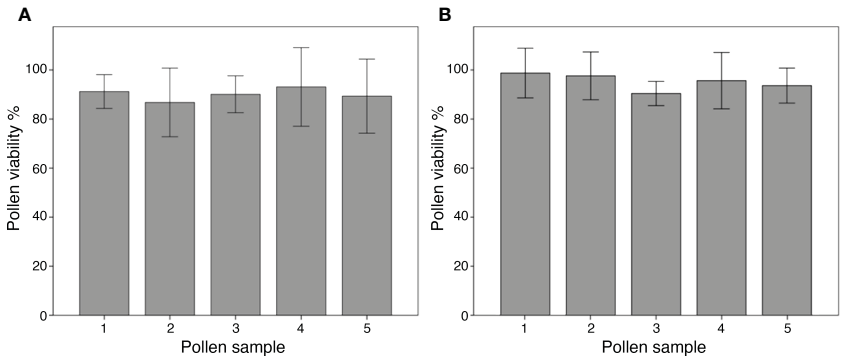

FIGURE 3
Viability of bulk pollen from flowers of 'Micro-Tom' **(A)** and *Brassica rapa* **(B)**. Each bar shows the pollen viability of a single pollen sample from the bulk, expressed as the mean of the viability percentage scored on six photos per sample. ANOVA reported no significant differences intra-species among pollen samples (P <0.05). Bars represent ± SE.

10.3389/fpls.2023.1186967

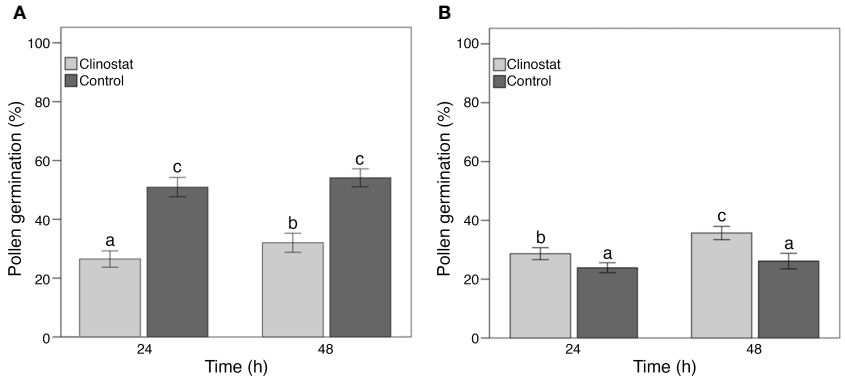

FIGURE 4
Germination of bulk pollen samples from flowers of 'Micro-Tom' **(A)** and *Brassica rapa* **(B)**. Pollen germination was scored after 24 and 48 h both in clinostat (simulated microgravity) and control (1g) conditions. Each bar shows the mean pollen germination percentage scored on 50 photos. Significant differences intra-species are reported with different letters ($P < 0.05$). Bars represent ± SE.

Finally, the evaluation of possible gravitropic responses in pollen tubes showed no preferential distribution of pollen tube tips across the Petri dishes, both in control and simulated microgravity treatments (Figure 8). Specifically, we analyzed data assuming no gravitropic response of pollen tubes of 'Micro-Tom' and *B. rapa*, therefore hypothesizing an equal distribution (25% in each quadrant) of tube tips across the Petri dish in both control and simulated microgravity. The Chi-square test revealed no significant differences between observed and expected frequencies of pollen tube tips in the four quadrants, independently of the gravity treatments and the species tested (Table S1, $P < 0.05$). Therefore, we confirmed the null hypothesis that the orientation of pollen tubes of 'Micro-Tom' and *B. rapa* was not subjected to gravitropic responses.

4 Discussion

Results on initial pollen viability revealed that growing conditions were optimally set to avoid any interference of abiotic factors with reproductive features. Indeed, pollen samples of both species reported viability over 80%, and no significant differences intraspecies between pollen samples proved high uniformity in pollen grains taken from the same bulk (Figure 3). Therefore, the two bulk pollen samples (one bulk per species) represented a proper starting point to perform further analyses and compare results intra- and inter-species concerning further pollen traits under simulated microgravity conditions.

The viability of pollen grains is not sufficient to predict pollen's capability to elongate a pollen tube and achieve fertilization (Dafni et al., 2005; Pacini and Dolferus, 2019). Our results also demonstrated that pollen with high viability can germinate under simulated microgravity with a significantly different ratio according to the species tested (Figure 4). Considering this, pollen germination rate may be applied as an inclusion criterion in ranking space crops for seed-to-seed cultivation in space (Aronne et al., 2020). Both pollen viability and germination are strongly correlated with fruit and seed set (Paupière et al., 2017; Herrera et al., 2018) and are therefore essential to ensuring repeated seed-to-seed cycles on board a spacecraft.

Since most plant breeding research has been conducted through the sporophyte, the influence of the gametophytic phase, including pollen tube development, has been generally overlooked. However, the possibility of applying gametophytic selection in plant breeding

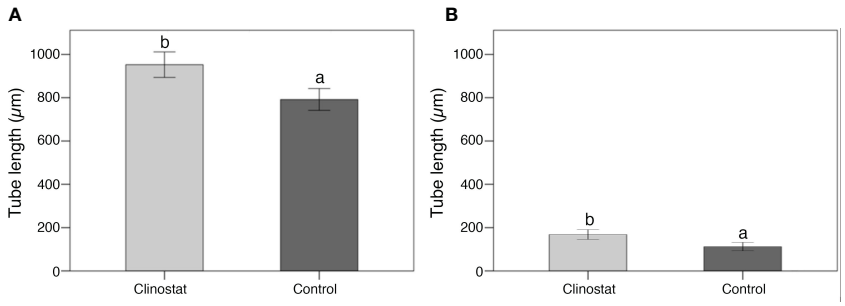

FIGURE 5
Pollen tube length in clinostat (simulated microgravity) and control (1g) treatments in 'Micro-Tom' **(A)** and *Brassica rapa* **(B)** (300 pollen tubes per species). Each bar shows the mean of 150 pollen tube lengths scored on 50 photos. Significant differences intra-species are reported with different letters ($P < 0.05$). Bars represent ± SE.

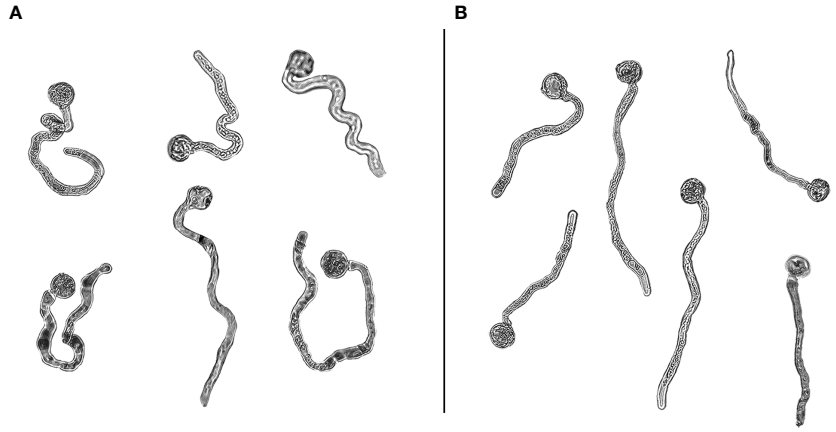

FIGURE 6
'Micro-Tom' pollen grains germinated in simulated microgravity **(A)** and in control **(B)** treatments.

programs on Earth had already been supported by Hormaza and Herrero (1992), who highlighted the overlap in the genetic expression between the sporophyte and the gametophyte in relation to different abiotic stresses (Mulcahy, 1984; Ottaviano and Mulcahy, 1989; Ottaviano et al., 1990). Therefore, the selection of space candidate species and cultivars with the highest germination rate of pollen developed under altered gravity conditions can be considered a potential application of gametophytic selection in a space environment. Since it can be performed in a small environment and over a short period, this breeding procedure could be conducted by astronauts with the aim of screening and selecting species and cultivars that best adapt to real microgravity (De Micco et al., 2013).

To date, research has shown that simulated microgravity affects several aspects of pollen tube development (De Micco et al., 2005; De Micco et al., 2006), but how the gravity vector could affect pollen tube movements is still unknown. Despite this study proving a clear effect of simulated microgravity on the tortuosity of pollen tube movements (Figure 6), our results excluded gravitropism as a pollen tube response affecting the final position of tube tips in the germination medium (Figure 8).

How clinorotation affect the tortuosity of pollen tubes might be addressed by the key role of the cytoskeleton in coordinating vesicle trafficking responsible for pollen tube elongation (Sack, 1991). More specifically, clinorotation may have altered the production of metabolites related to pollen tube development, such as starch and callose, involved in the same ultrastructural changes occurring in the actin cytoskeleton of pollen tubes during the self-incompatibility reactions (De Micco et al., 2006; Cai and Del Duca, 2019). Indeed, the actin filaments located in the sub-apical portion of elongating pollen tubes are reported to be involved in the vesicle trafficking responsible for the formation and maintenance of the tube apex (Vidali et al., 2009; Qin and Yang, 2011; Hepler and Winship, 2014; Fu, 2015). Actin filaments of the cytoskeleton have a crucial role in tube development and growth direction, but how altered gravity can regulate the directionality of pollen tubes remains to be determined (Cheung et al., 2010).

To date, the microgametophyte (pollen) tube path towards the ovary is known to be mainly driven by chemotropic stimuli related to the Ca2+ gradient throughout the style (Kandasamy et al., 1994; Kim et al., 2019), whereas the possible co-existence with pollen gravitropism has been generally overlooked. Despite *in vitro*

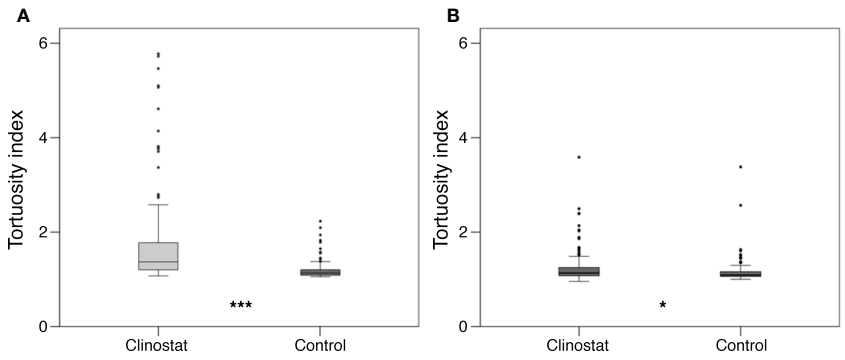

FIGURE 7
Pollen tube tortuosity of 'Micro-Tom' **(A)** and *Brassica rapa* **(B)** (300 pollen tubes per species) in clinostat (simulated microgravity) and control (1*g*) treatments. Each boxplot shows the values of 150 pollen tubes (***P <0.001; *P <0.05).

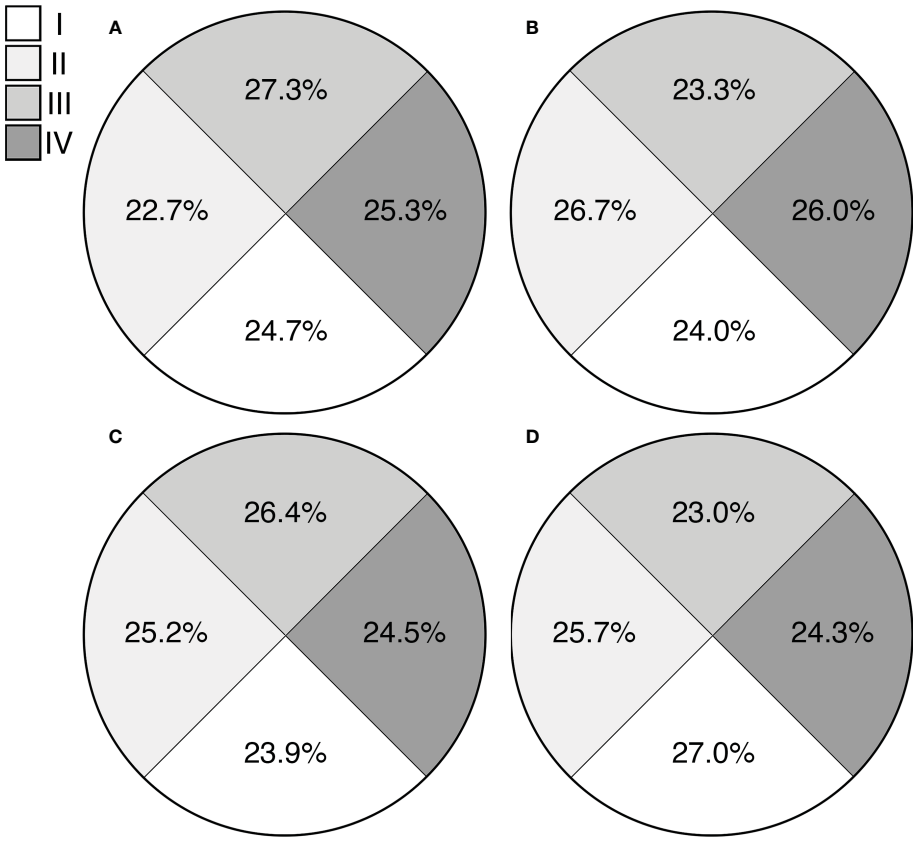

FIGURE 8
Evaluation of tube tip orientation of 'Micro-Tom' in simulated microgravity **(A)** and control **(B)** treatments and of *Brassica rapa* in simulated microgravity **(C)** and control **(D)** treatments. Percentage values indicate the observed frequencies of pollen tube tips reaching each quadrant.

conditions being assumed to mimic the natural state of pollen during pollen tube elongation, functional differences with *in vivo* or in *semi-vivo* conditions might occur. For instance, pollen tubes elongate faster, tubes live longer, and sperm cells (in bicellular species) form sooner and more reliably *in vivo* than *in vitro* (Kakani et al., 2005; Shi et al., 2018). Pollen tube growth *in vivo* involves interactions with pistil tissues, especially at critical stages such as tube reorientation and the cessation of growth. Thus, considering the role of chemotropism in the directional growth of pollen tubes, we performed the experiment *in vitro* to isolate the effect of the gravity vector on pollen tube directionality and exclude interferences related to chemotropic stimuli occurring *in vivo*.

Overall, our analyses investigating male gametophyte functionality in simulated microgravity suggested that pollen germination and tube directional growth are affected by changes in gravity and highlighted different responses between 'Micro-Tom' and *B. rapa*. To date, research has never considered gravitropism as a driver for pollen tube movement. Our *in vitro* germination tests represented the best first approach to exclude possible chemotropic interferences and isolate the effect of the altered gravity vector on the directional growth of pollen tubes.

Even though our results excluded gravitropism in pollen tubes, further tests are necessary to confirm our results in real microgravity conditions and in other candidate space crops. In conclusion, a better understanding of how gravity can interfere with plant reproduction is needed to ensure seed and fruit production over repeated seed-to-seed-to-seed cycles, and it is a first step towards self-sufficiency from Earth supplies in long-term space missions.

Data availability statement

The raw data supporting the conclusions of this article will be made available by the authors, without undue reservation.

Author contributions

MI: Conceptualization, methodology, investigation, visualization, and writing—original draft preparation. LI: Investigation, visualization, and writing—review & editing. LR: Writing—review & editing. GA: Conceptualization, methodology, writing—review & editing, and funding acquisition. All authors listed have made a substantial, direct, and intellectual contribution to the work and approved it for publication.

Funding

This research has been financially supported by the project *In-situ* REsource Bio-Utilization for life Support system (ReBUS), unique project code (CUP) F74I16000000005 financed by the Italian Space Agency.

Conflict of interest

The authors declare that the research was conducted in the absence of any commercial or financial relationships that could be construed as a potential conflict of interest.

Publisher's note

All claims expressed in this article are solely those of the authors and do not necessarily represent those of their affiliated organizations, or those of the publisher, the editors and the reviewers. Any product that may be evaluated in this article, or claim that may be made by its manufacturer, is not guaranteed or endorsed by the publisher.

Supplementary material

The Supplementary Material for this article can be found online at: https://www.frontiersin.org/articles/10.3389/fpls.2023.1186967/full#supplementary-material

References

Aronne, G., Iovane, M., and Strumia, S. (2021). Temperature and humidity affect pollen viability and may trigger distyly disruption in threatened species. *Ann. D. Bot.* 11, 77–82. doi: 10.13133/2239-3129/17157

Aronne, G., Romano, L. E., and Izzo, L. G. (2020). Subsequent inclusion/exclusion criteria to select the best species for an experiment performed on the ISS in a refurbished hardware. *Life Sci. Space Res.* 27, 19–26. doi: 10.1016/j.lssr.2020.07.002

Burgner, S. E., Nemali, K., Massa, G. D., Wheeler, R. M., Morrow, R. C., and Mitchell, C. A. (2020). Growth and photosynthetic responses of Chinese cabbage (Brassica rapa l. cv. Tokyo bekana) to continuously elevated carbon dioxide in a simulated space station "Veggie" crop-production environment. *Life Sci. Space Res.* 27, 83–88. doi: 10.1016/j.lssr.2020.07.007

Cai, G., and Del Duca, S. (2019). Pollen tube and plant reproduction. *Int. J. Mol. Sci.* 20 (3), 531. doi: 10.3390/ijms20030531

Cheung, A. Y., Niroomand, S., Zou, Y., and Wu, H. M. (2010). A transmembrane formin nucleates subapical actin assembly and controls tip-focused growth in pollen tubes. *Proc. Natl. Acad. Sci.* 107 (37), 16390–16395. doi: 10.1073/pnas.1008527107

Colla, G., Rouphael, Y., Cardarelli, M., Mazzucato, A., and Olimpieri, I. (2007). Growth, yield and reproduction of dwarf tomato grown under simulated microgravity conditions. *Plant Biosyst.* 141, 75–81. doi: 10.1080/11263500601153735

Dafni, A. (1992). *Pollination ecology: a practical approach* (Oxford, UK: Oxford University Press).

Dafni, A., Kevan, P. G., and Husband, B. C. (2005). *Practical pollination biology*. (Cambridge: Enviroquest Ltd).

Dedolph, R. R., and Dipert, M. H. (1971). The physical basis of gravity stimulus nullification by clinostat rotation. *Plant Physiol.* 47 (6), 756–764. doi: 10.1104/pp.47.6.756

De Micco, V., Aronne, G., and De Pascale, S. (2005). Effect of simulated microgravity on seedling development and vascular differentiation of soy. *Acta Astronautica* 58 (3), 139–148. doi: 10.1016/j.actaastro.2005.06.002

De Micco, V., Pascale, S., Paradiso, R., and Aronne, G. (2013). Microgravity effects on different stages of higher plant life cycle and completion of the seed-to-seed cycle. *Plant Biol. J.* 16, 31–38. doi: 10.1111/plb.12098

De Micco, V., Scala, M., and Aronne, G. (2006). Effects of simulated microgravity on male gametophyte of prunus, pyrus, and *Brassica* species. *Protoplasma* 228, 121–126. doi: 10.1007/s00709-006-0161-7

De Pascale, S., Arena, C., Aronne, G., De Micco, V., Pannico, A., Paradiso, R., et al. (2021). Biology and crop production in space environments: challenges and opportunities. *Life Sci. Sp. Res.* 29, 30–37. doi: 10.1016/j.lssr.2021.02.005

Fu, Y. (2015). The cytoskeleton in the pollen tube. *Curr. Opin. Plant Biol.* 28, 111–119. doi: 10.1016/j.pbi.2015.10.004

Güçlü, F., and Koyuncu, F. (2017). Effects of relative humidity on *in vitro* pollen germination and tube growth in sweet cherries (Prunus avium l.). *Sci. Pap. Ser. B Hortic.* 61, 15–19.

Hepler, P. K., and Winship, L. J. (2014). The pollen tube clear zone: clues to the mechanism of polarized growth. *J. Integr. Plant Biol.* 57, 79–92. doi: 10.1111/jipb.12315

Herrera, S., Lora, J., Hormaza, J. I., Herrero, M., and Rodrigo, J. (2018). Optimizing production in the new generation of apricot cultivars: self-incompatibility, s-RNase allele identification, and incompatibility group assignment. *Front. Plant Sci.* 9. doi: 10.3389/fpls.2018.00527

Hormaza, J. I., and Herrero, M. Pollen selection. *Theor. Appl. Genet.* (1992) 83 (6-7), 663–672. doi: 10.1007/BF00226682

Iovane, M., and Aronne, G. (2021). High temperatures during microsporogenesis fatally shorten pollen lifespan. *Plant Reprod.* 35, 9–17. doi: 10.1007/s00497-021-00425-0

Iovane, M., Cirillo, A., Izzo, L. G., Di Vaio, C., and Aronne, G. (2022a). High temperature and humidity affect pollen viability and longevity in olea europaea l. *Agronomy* 12, 1–12. doi: 10.3390/agronomy12010001

Iovane, M., Izzo, L. G., Cirillo, A., Romano, L. E., Di Vaio, C., and Aronne, G. (2022b). Flowering and pollen resilience to high temperature of apricot cultivars. *Scientia Hortic.* 304, 111261. doi: 10.1016/j.scienta.2022.111261

Izzo, L. G., Romano, L. E., Muthert, L. W. F., Iovane, M., Capozzi, F., Manzano, A., et al. (2022). Interaction of gravitropism and phototropism in roots of *Brassica oleracea.* environ. *Exp. Bot.* 193, 104700. doi: 10.1016/j.envexpbot.2021.104700

Kakani, V. G., Reddy, K. R., Koti, S., Wallace, T. P., Prasad, P. V. V., Reddy, V. R., et al. (2005). Differences in *in vitro* pollen germination and pollen tube growth of cotton cultivars in response to high temperature. *Ann. Bot.* 96 (1), 59–67. doi: 10.1093/aob/mci149

Kandasamy, M. K., Nasrallah, J. B., and Nashrallah, M. E. (1994). Pollen-pistil interactions and developmental regulation of pollen tube growth in *Arabidopsis*. *Development* 120, 3405–3418. doi: 10.1242/dev.120.12.3405

Karapanos, I. C., Akoumianakis, K. A., Olympios, C. M., and Passam, H. C. (2010). Tomato pollen respiration in relation to *in vitro* germination and pollen tube growth under favourable and stress-inducing temperatures. *Sex Plant Reprod.* 23, 219–224. doi: 10.1007/s00497-009-0132-1

Kim, Y. J., Zhang, D., and Jung, K. H. (2019). Molecular basis of pollen germination in cereals. *Trends Plant Sci.* 24 (12), 1126–1136. doi: 10.1016/j.tplants.2019.08.005

Kiss, J. Z., Wolverton, C., Wyatt, S. E., Hasenstein, K. H., and van Loon, J. J. W. A. (2019). Comparison of microgravity analogs to spaceflight in studies of plant growth and development. *Front. Plant Sci.* 10, 1577. doi: 10.3389/fpls.2019.01577

Kordyum, E., and Hasenstein, K. H. (2021). Plant biology for space exploration – building on the past, preparing for the future. *Life Sci. Sp. Res.* 29, 1–7. doi: 10.1016/j.lssr.2021.01.003

Kordyum, E., Hedukha, O., Artemeko, O., and Ivanenko, G. (2020). Seed and vegetative propagation of plants in microgravity 7 (5), 500–507. doi: 10.15982/j.issn.2096-9287.2020.20191113001

Kordyum, E. L., Sytnik, K. M., and Chernyaeva, I. I. (1983). Peculiarities of genital organ formation in *Arabidopsis thaliana* (L) heynh. under spaceflight conditions. *Adv. Space Res.* 3 (9), 247–250. doi: 10.1016/0273-1177(83)90064-9

Kuang, A., Musgrave, M. E., and Matthews, S. W. (1996). Modification of reproductive development in *Arabidopsis thaliana* under spaceflight conditions. *Planta* 198, 588–594. doi: 10.1007/BF00262646

Kuang, A., Musgrave, M. E., Matthews, S. W., Cummins, D. B., and Tucker, S. C. (1995). Pollen and ovule development in *Arabidopsis thaliana* under spaceflight conditions. *Am. J. Bot.* 82 (5), 585–595. doi: 10.1002/j.1537-2197.1995.tb11503.x

Kuang, A., Popova, A., Xiao, Y., and Musgrave, M. E. (2000a). Pollination and embryo development in *Brassica rapa* l. @ in microgravity. *Int. J. Plant Sci.* 161, 203–211. doi: 10.1086/314254

Kuang, A., Xiao, Y., McClure, G., and Musgrave, M. E. (2000b). Influence of microgravity on ultrastructure and storage reserves in seeds of *Brassica rapa* l. *Ann. Bot.* 85, 851–859. doi: 10.1006/anbo.2000.1153

Link, B. M., Busse, J. S., and Stankovic, B. (2014). Seed-to-seed-to-seed growth and development of *Arabidopsis* in microgravity. *Astrobiology* 14, 866–875. doi: 10.1089/ast.2014.1184

Matsuda, R., Ozawa, N., and Fujiwara, K. (2014). Leaf photosynthesis, plant growth, and carbohydrate accumulation of tomato under different photoperiods and diurnal temperature differences. *Sci. Hortic.* 170, 150–158. doi: 10.1016/j.scienta.2014.03.014

Matsukura, C., Aoki, K., Fukuda, N., Mizoguchi, T., Asamizu, E., Saito, T., et al. (2008). Comprehensive resources for tomato functional genomics based on the miniature model tomato micro-tom. *Curr. Genomics* 9 (7), 436–443. doi: 10.2174/138920208786241225

Merkies, A. I., and Laurinavichyus, R. S. (1983). Complete cycle of individual development of *Arabidopsis* thaliana haynh plants at salyut orbital station. *Doklady Akademii Nauk SSSR* 271 (2), 509–512.

Mulcahy, D. L. (1984). "Manipulation of gametophytic populations," in *Efficiency in plant breeding: proceedings 10th congress on eucarpia*. Eds. W. Lan-gel, A. C. Zeven and N. G. Hogenboom (Wageningen, the Netherlands: Pudoc, Wageningen), p 167–p 175.

Musgrave, M. E., Kuang, A., Tuominen, L. K., Levine, L. H., and Morrow, R. C. (2005). Seed storage reserves and glucosinolates in *Brassica rapa* l. grown on the international space station. *J. Am. Soc Hortic. Sci.* 130, 848–856. doi: 10.21273/jashs.130.6.848

Musgrave, M. E., Kuang, A., Xiao, Y., Stout, S. C., Bingham, G. E., Briarty, L. G., et al. (2000). Gravity independence of seed-to-seed cycling in *Brassica rapa*. *Planta* 210 (3), 400–406. doi: 10.1007/PL00008148

Muthert, L. W. F., Izzo, L. G., van Zanten, M., and Aronne, G. (2020). Root tropisms: investigations on earth and in space to unravel plant growth direction. *Front. Plant Sci.* 10, 1807. doi: 10.3389/fpls.2019.01807

Ottaviano, E., and Mulcahy, D. L. (1989). Genetics of angiosperm pollen. *Adv. Genet.* 26, 1–64. doi: 10.1016/S0065-2660(08)60222-9

Ottaviano, E., Sari-Gorla, M., and Mulcahy, D. L. (1990). "Pollen selection: efficiency and monitoring," in *Isozymes: structure, function, and use in biology and medicine*. Eds. Z. I. Ogita and C. L. Market (New York: Wiley-Liss), p 575–p 588.

Pacini, E., and Dolferus, R. (2019). Pollen developmental arrest: maintaining pollen fertility in a world with a changing climate. *Front. Plant Sci.* 10. doi: 10.3389/fpls.2019.00679

Paupière, M. J., van Haperen, P., Rieu, I., Visser, R. G. F., Tikunov, Y. M., and Bovy, A. G. (2017). Screening for pollen tolerance to high temperatures in tomato. *Euphytica* 213, 230. doi: 10.1007/s10681-017-1927-z

Qin, Y., and Yang, Z. (2011). Rapid tip growth: insights from pollen tubes. *Seminars Cell & Development. biol.* 22 (8), 816–824. doi: 10.1016/j.semcdb.2011.06.004

Romano, L. E., and Aronne, G. (2021). The world smallest plants (Wolffia sp.) as potential species for bioregenerative life support systems in space. *Plants* 10 (9), 1896. doi: 10.3390/plants10091896

Sack, F. D. (1991). Plant gravity sensing. *Int. Rev. Cytol* 127, 193–252. doi: 10.1016/S0074-7696(08)60695-6

Salisbury, F. B. (1999). "Chapter 5 growing crops for space explorers on the moon, Mars, or in space," in *Advances in space biology and medicine*. Ed. S. L. Bontinc (Stamford, Connecticut: Elsevier), 131–162.

Sathasivam, M., Hosamani, R., K Swamy, B., and Kumaran G, S. (2021). Plant responses to real and simulated microgravity. *Life Sci. Sp. Res* 28, 74–86. doi: 10.1016/j.lssr.2020.10.001

Sato, S., Katoh, N., Iwai, S., and Hagimori, M. (1998). Establishment of reliable methods of *in vitro* pollen germination and pollen preservation of *Brassica rapa* (syn. *B. campestris*). *Euphytica* 103, 29–33. doi: 10.1023/A:1018381417657

Sato, S., Peet, M. M., and Gardner, R. G. (2001). Formation of parthenocarpic fruit, undeveloped flowers and aborted flowers in tomato under moderately elevated temperatures. *Sci. Hortic.* 90, 243–254. doi: 10.1016/S0304-4238(00)00262-4

Shi, W., Li, X., Schmidt, R. C., Struik, P. C., Yin, X., and Jagadish, S. K. (2018). Pollen germination and *in vivo* fertilization in response to high-temperature during flowering in hybrid and inbred rice. *Plant Cell Environ.* 41 (6), 1287–1297. doi: 10.1111/pce.13146

Shikata, M., and Ezura, H. (2016). Micro-tom tomato as an alternative plant model system: mutant collection and efficient transformation. *Plant Signal Transduction: Methods Protoc.* 1363, 47–55. doi: 10.1007/978-1-4939-3115-6_5

Tatematsu, K., Kumagai, S., Muto, H., Sato, A., Watahiki, M. K., Harper, R. M., et al. (2004). Massugu2 encodes Aux/IAA19, an auxin-regulated protein that functions together with the transcriptional activator NPH4/ARF7 to regulate differential growth responses of hypocotyl and formation of lateral roots in *Arabidopsis thaliana*. *Plant Cell* 16, 379–393. doi: 10.1105/tpc.018630

Vidali, L., Rounds, C. M., Hepler, P. K., and Bezanilla, M. (2009). Lifeact-mEGFP reveals a dynamic apical f-actin network in tip growing plant cells. *PloS One* 4 (5), e5744. doi: 10.1371/journal.pone.0005744

Zabel, P., Bamsey, M., Schubert, D., and Tajmar, M. (2016). Review and analysis of over 40 years of space plant growth systems. *Life Sci. Sp. Res.* 10, 1–16. doi: 10.1016/j.lssr.2016.06.004

frontiers | Frontiers in Plant Science

TYPE Original Research
PUBLISHED 19 July 2023
DOI 10.3389/fpls.2023.1190945

Check for updates

OPEN ACCESS

EDITED BY
Jean-Pierre Paul de Vera,
German Aerospace Center (DLR), Germany

REVIEWED BY
Andrzej Kalisz,
University of Agriculture in Krakow, Poland
Antonio Ferrante,
University of Milan, Italy

*CORRESPONDENCE
Chiara Amitrano
chiara.amitrano@unina.it
Stefania De Pascale
depascal@unina.it

†These authors have contributed equally to this work and share first authorship

RECEIVED 21 March 2023
ACCEPTED 29 June 2023
PUBLISHED 19 July 2023

CITATION
Amitrano C, Paglialunga G, Battistelli A, De Micco V, Del Bianco M, Liuzzi G, Moscatello S, Paradiso R, Proietti S, Rouphael Y and De Pascale S (2023) Defining growth requirements of microgreens in space cultivation via biomass production, morpho-anatomical and nutritional traits analysis. *Front. Plant Sci.* 14:1190945. doi: 10.3389/fpls.2023.1190945

COPYRIGHT
© 2023 Amitrano, Paglialunga, Battistelli, De Micco, Del Bianco, Liuzzi, Moscatello, Paradiso, Proietti, Rouphael and De Pascale. This is an open-access article distributed under the terms of the Creative Commons Attribution License (CC BY). The use, distribution or reproduction in other forums is permitted, provided the original author(s) and the copyright owner(s) are credited and that the original publication in this journal is cited, in accordance with accepted academic practice. No use, distribution or reproduction is permitted which does not comply with these terms.

Defining growth requirements of microgreens in space cultivation via biomass production, morpho-anatomical and nutritional traits analysis

Chiara Amitrano[1*†], Gabriele Paglialunga[2†], Alberto Battistelli[2], Veronica De Micco[1], Marta Del Bianco[3], Greta Liuzzi[1], Stefano Moscatello[2], Roberta Paradiso[1], Simona Proietti[2], Youssef Rouphael[1] and Stefania De Pascale[1*]

[1]Department of Agricultural Sciences, University of Naples Federico II, Portici, Naples, Italy, [2]Research Institute on Terrestrial Ecosystems (IRET), National Research Council of Italy (CNR), Porano, Terni, Italy, [3]Italian Space Agency, Rome, Italy

During long-term manned missions to the Moon or Mars, the integration of astronauts' diet with fresh food rich in functional compounds, like microgreens, could strengthen their physiological defenses against the oxidative stress induced by the exposure to space factors. Therefore, the development of targeted cultivation practices for microgreens in space is mandatory, since the cultivation in small, closed facilities may alter plant anatomy, physiology, and resource utilization with species-specific responses. Here, the combined effect of two vapor pressure deficit levels (VPD: 0.14 and 1.71 kPa) and two light intensities (150 and 300 μmol photons m^{-2} s^{-1} PPFD) on two species for microgreen production (*Brassica oleracea* var. *capitata* f. *sabauda* 'Vertus' and *Raphanus raphanistrum* subsp. *sativus* 'Saxa'), was tested on biomass production per square meter, morpho-anatomical development, nutritional and nutraceutical properties. Microgreens were grown in fully controlled conditions under air temperature of 18/24°C, on coconut fiber mats, RGB light spectrum and 12 h photoperiod, till they reached the stage of first true leaves. At this stage microgreens were samples, for growth and morpho-anatomical analyses, and to investigate the biochemical composition in terms of ascorbic acid, phenols, anthocyanin, carotenoids, carbohydrates, as well as of anti-nutritional compounds, such as nitrate, sulfate, and phosphate. Major differences in growth were mostly driven by the species with 'Saxa' always presenting the highest fresh and dry weight as well as the highest elongation; however light intensity and VPDs influenced the anatomical development of microgreens, and the accumulation of ascorbic acid, carbohydrates, nitrate, and phosphate. Both 'Saxa' and 'Vertus' at low VPD (LV) and 150 PPFD increased the tissue thickness and synthetized high β-carotene and photosynthetic pigments. Moreover, 'Vertus' LV 150, produced the highest content of ascorbate, fundamental for nutritional properties in space environment. The differences among the treatments and their interaction suggested a relevant difference in resource use efficiency. In the light of the above, microgreens can be considered

suitable for cultivation in limited-volume growth modules directly onboard, provided that all the environmental factors are combined and modulated according to the species requirements to enhance their growth and biomass production, and to achieve specific nutritional traits.

KEYWORDS

anatomics, antioxidants, bioregenerative life support systems (BLSSs), *Brassica oleracea* var. *capitata* f. *sabauda*, light intensity, morpho-anatomical traits, *Raphanus raphanistrum* subsp. sativus, vapor pressure deficit (VPD)

1 Introduction

The human settlement on Moon, Mars, or other celestial bodies as well as long-term living on transit space vehicles, are among the greatest challenges for mankind. However, to fulfill these purposes, many obstacles still need to be overcome, like the production of high nutritional food directly in space (Carillo et al., 2020; De Micco et al., 2021a; De Micco et al., 2021b). Indeed, one of the main constrains impacting the feasibility of long-term space missions is related to the huge mass and volume occupied by prepackaged, shelf-stable food, and to the unfeasibility of resupplying from Earth during manned interplanetary missions, lasting more than six months (Wheeler, 2003; Perchonok et al., 2012). Thus, a bio-regenerative system based on crop plants to produce food while emitting oxygen, absorbing carbon dioxide, and recycling gray water, will be a great asset to future space exploration (Poulet et al., 2016).

Growing plants in space requires the knowledge of their species-specific responses not only to the typical space constraints, such as altered gravity and ionizing radiation, but also to all the environmental factors that normally modulate plant performance on Earth. Environmental and cultivation factors (e.g., VPD, light intensity and quality, temperature, water availability, substrate), can alter plant growth and metabolic processes depending on the ontogenetic stage, and can have unexpected effects when acting in the confined environment and limited volume, typical of the space facilities (Amitrano et al., 2020a; De Micco et al., 2021a; De Pascale et al., 2021). Hence, in the upcoming years, to allow plant-based *in-situ* food production in space it would be mandatory to define the best ontogenetic specific environmental variable baselines and develop agronomical procedures to ensure an efficient food production, to meet the dietary needs of the crew members.

Microgreens are suitable for cultivation as food supplements because of their small size, low demand for photon flux, short cultivation cycle, high harvest index, and high nutritional potential (Kyriacou et al., 2017; El-Nakhel et al., 2021). Since the space environment poses significant risks to human health, primarily due to oxidative stress induced by ionizing radiation and microgravity (McPhee and Charles, 2009), microgreens consumption represents a valuable nutritional strategy to mitigate health risks during space travels (Kyriacou et al., 2017; Johnson, 2019; Teng et al., 2023). The extensive research on health promoting phytochemicals including vitamins, carotenoids, flavonoids and glucosinolates, has demonstrated the antioxidant potential of these compounds (Balsano and Alisi, 2009). Several works investigated the nutrition contribution of microgreens demonstrating that the daily intake of different nutraceuticals can be partially or fully obtained through microgreens supplementation (Ghoora et al., 2020; Renna et al., 2020).

Although microgreens are young plantlets, harvested at the most till the second true leaf stage, several studies demonstrated that the modulation of environmental and agronomic parameters influenced their response in terms of yield and phytochemical content (Samuolienė et al., 2013; Di Gioia et al., 2017; Lobiuc et al., 2017; Kyriacou et al., 2020).

Light is the source of energy for plant growth, and it is pivotal to many processes during plant life. In protected cultivation, the setting of an optimal light intensity is fundamental considering that light requirement may change among species and varieties (Poulet et al., 2014). A proper light modulation is also important for system design and efficiency in facilities dedicated to plant production under fully controlled environmental conditions, like vertical farming (Zabel et al., 2020; Kobayashi et al., 2022; Paglialunga et al., 2022). In the last decades, literature about plant-light interaction in controlled environment increased considerably, also by virtue of space related studies, after the invention of Light Emitting Diode (LED) technology (Avercheva et al., 2016; D'Aquino et al., 2022; Paradiso and Proietti, 2022). The modulation of light intensity can have positive effects on plants nutraceutical values (Proietti et al., 2013; Proietti et al., 2023), even when the intensity is high and could be perceived by plants as stress, inducing them to synthetize antioxidant compounds to mitigate

Abbreviations: LV, low VPD; HV, High VPD; VPD, Vapor Pressure Deficit; PPFD, Photosynthetic Photon Flux Density; ML, Microgreens Length; FW, Fresh Weight; DW, Dry Weight; DM, Dry Matter Percentage; LV, Low Vapor Pressure Deficit; HV, High Vapor Pressure Deficit; PT, Palisade Thickness; ST, Spongy Parenchyma Thickness; TT, Total Thickness; IS, Intercellular Spaces; LET, Leaf Epidermal Thickness,DHAs; Dehydroascorbic Acid; AsA, Ascorbic Acid; TAsA, Total Ascorbic Acid; TAcy, Total Anthocyanins; TPoly, Total Phenolic Content; Neo, Neoxanthin; Vio, Violaxanthin; Lut, Lutein, Chl, Chlorophyll; β-Car, β-Carotene; TSolub, Total Soluble Non-Structural Carbohydrates; TNsc, Total Non-structural Carbohydrates.

ROS (reactive oxygen species) formation (Pattison et al., 2018; Modarelli et al., 2022). Excess of light can also affect the photosystems' efficiency and inducing photo-inhibition mechanisms, other than causing the formation of a peculiar plant structure and changing the profiles and ratios of photosynthetic pigments (De Micco et al., 2023). It was recently demonstrated that it is possible to improve the antioxidant profile in several microgreen species by modulating the photoperiod, light intensity, and wavelength (Liu et al., 2022; Tantharapornrerk et al., 2023). Therefore, light modulation can be a powerful tool to control performances and quality of microgreens grown in space also considering interactions with other environmental variables.

Among environmental control needs, VPD regulation is one of the utmost challenges to face in indoor agriculture due to its dynamic interaction with crops in the soil-plant-atmosphere *continuum* (Leonardi et al., 2000; Amitrano et al., 2021a; Amitrano et al., 2021b). Recent studies clearly indicate that VPD impacts all physiological and biochemical processes related to transpiration, also affecting the morpho-anatomical development of crops in terms of leaf lamina tissues organization, stomatal and veins dimensions and densities, which in turn modify crops physiology in terms of gas-exchange and water use (Zhang et al., 2019; Amitrano et al., 2022). The influence of VPD on crops' nutraceutical compounds has been way less studied compared to other environmental factors, but some research has agreed that high VPD levels (1.7 - 3 kPa) enhanced the bioactive value of some crops (tomato, cucumber, lettuce), increasing their ascorbic acid, β-carotene and polyphenolic content (Davey et al., 2000; Rosales et al., 2006; Bisbis et al., 2018). However, to the best of our knowledge, there is no information about the effect of different VPDs on microgreens production and nutritional potential nor on the combined effects on these parameters exerted by concomitant variations in light intensity and VPD.

Light and VPD are key aspects of the environmental control in Biorigenerative Life Support Systems (BLSSs) being crucial determinants of gas-exchange in leaves and particularly of transpiration. Moreover, the condensation of transpired water, driven by VPD and light conditions, is among the most demanding processes in controlled environment systems in terms on hardware and energy requirements, being even more difficult to control in space environment (Zabel et al., 2022). Moreover, as reported by Amitrano et al., 2020b on mung bean sprouts, both VPD and light have proven to change biomass allocation, antioxidant production, and morpho-functional traits already at the very early stage of development (e.g. germinated seeds, sprouts).

In this experiment, we cultivated two species (*Brassica oleracea* var. *capitata* f. *sabauda* 'Vertus' and *Raphanus raphanistrum* subsp. *sativus* 'Saxa') for microgreen production testing the combined effect of two vapor pressure deficits (VPD: 0.14 and 1.71 kPa) and two light intensities (150 and 300 µmol photons m^{-2} s^{-1}). We analyzed microgreen morpho-anatomical development and biomass production to have an overview of their resource use-efficiency and growth. The innovative approach of the experiment is the strategy aiming to define system baselines, with an experimental protocol including interaction between light and VPD, with the target of achieving the nutritional quality expected for each species. To do so, we analyzed the nutritional and nutraceutical potential, in terms of ascorbic acid, phenols, anthocyanin, carotenoids, and carbohydrates, as well as the content of anti-nutritional compounds such as nitrate, sulfate and phosphate. Our results may contribute to the definition of the scientific requirements for the design of a flight apparatus for microgreen production in space.

2 Materials and methods

2.1 Plant material and experimental design

Two microgreen cultivars belonging to two different species were used: i) cabbage, *Brassica oleracea* var. *capitata* f. *sabauda* 'Vertus' and ii) radish, *Raphanus raphanistrum* subsp. *sativus* 'Saxa'. For simplicity through the text and tables 'Saxa' and 'Vertus' will be indicated as species. The two species were previously selected in the first step of this project (please refer to paragraph 7: funding), through a rigorous selection process based on algorithms and cultivation trials (Izzo et al., 2023 Frontiers, under review) following the same approach reported in Aronne et al., 2020. Seeds were purchased from a local provider and experiments were run at the Department of Agricultural Sciences of the University of Naples Federico II (Naples, IT), in two consecutive cycles. Both cycles were conducted in a two-shelves growth chamber (KBP-6395F, Termaks, Bergen, Norway), equipped with a LED lighting panel (K5 Series XL750, Kind LED, Santa Rosa, CA, USA), with an emission wavelength in a range of 400-700 nm (Figure 1). The two cultivation cycles were identical in terms of light intensity, quality, photoperiod and air temperature, except for the VPD levels. The first cycle was performed under a VPD of 0.14 kPa (defined as Low VPD, LV) and the second under a VPD of 1.71 kPa (defined as High VPD, HV) at ambient CO_2. The two VPDs were achieved keeping air temperature (T) at 24 ± 1°C during the day and 18 ± 2°C during the night and changing the RH accordingly. Both T and RH% were monitored inside the chamber using mini-sensors (Testo 174H, Testo, Germany), equipped with a data-logger collecting data every 15 minutes.7 g of seeds for 'Saxa' and 6 g for 'Vertus' were sown on coconut fiber mats into plastic trays (width 14 cm x lenght 19 cm x depht 6 cm), and fertigated with a quarter-strength modified Hoagland solution (in mM: 2.0 nitrate, 0.25 sulfur, 0.20 phosphorus, 0.62 potassium, 0.75 calcium, 0.17 magnesium, 0.25 ammonium; in µM: 20 iron, 9 manganese, 0.3 copper, 1.6 zinc, 20 boron, 0.3 molybdenum), with an electrical conductivity (EC) of 0.4 ± 0.1 dSm^{-1}, and a pH of 6 ± 0.2. Two light intensities were set in the two chamber shelves, the first of 300 µmol m^{-2} s^{-1} photosynthetic photon flux density (PPFD) and the second of 150 µmol m^{-2} s^{-1}, with a red (R), green (G), blue (B) spectrum of R45: G10: B45 (in % of the total emission), and a 12 h photoperiod.

Each treatment was replicated in 6 trays and daily rotation of the trays ensured a homogenous exposure to light and humidity. Microgreens were harvested at the appearance of the first two true leaves by cutting at the substrate level. Specifically, cultivation lasted 10 days in cabbage and 11 days in radish. At harvest, biometrical analyses were performed, and a sub-sample of 6 microgreens was stored in a fixative solution for anatomical analyses, while a second

FIGURE 1
Different views **(A, B)** of the climatic growth chamber used for the two experiments on *Brassica oleracea* var. *capitata* f *sabauda* 'Vertus' and radish, *Raphanus raphanistrum* subsp. *sativus* 'Saxa' microgreens under Low VPD (LV) and High VPD (HV), at two light intensities (150 and 300 µmol photons m^{-2} s^{-1}).

sub-sample of 10 g was rapidly frozen, lyophilized and stored at −80°C for biochemical analyses.

2.2 Colorimetric and biometric measurements

Just before harvesting, the color properties of the microgreen canopy were measured in three different positions of each tray by means of an 8 mm-aperture Minolta CR-400 Chroma Meter (Minolta Camera Co. Ltd., Osaka, Japan). The meter was calibrated with a standard white plate before measurements. Leaf chromaticity was performed following the *Commission Internationale de l'Eclairage* and expressed as: greenness (a*), yellowness (b*) and lightness (L*), used to calculate chroma (Chroma = (a*2+b*2)1/2) and Hue angle (H° = arctan (b*/a*).

After cutting, the whole harvested material was weighed to determine the fresh weight, expressed in kg m^{-2}, 10 microgreens per tray were used to measure the microgreen length (ML). The dry weight (DW), expressed as g m^{-2}, was obtained after drying the remaining material in a forced-air oven at 65°C until constant weight. Dry matter content (DM%) was also calculated and expressed as a percentage of fresh weight.

2.3 Plant anatomical investigation

For the anatomical investigation each microgreen leaf stored in the F.A.A. fixative solution (40% formaldehyde, glacial acetic acid, 50% ethanol, 5:5:90 by volume) was dissected to keep a portion of the median region of the lamina (about 5x5 mm), which was dehydrated in an ethanol series (from 50 to 95%), then embedded in the JB4 acrylic resin (Polysciences, USA). Thin cross sections (5 µm thick) were cut using a rotary microtome (pfm medical, Bio-optical, Germany) and mounted on a microscope slide, then stained with 0.025% toluidine blue (Feder and O'brien, 1968) and analyzed using a transmitted light microscope (BX51, Olympus, Germany) equipped with a digital camera (Olympus EP50, Olympus, Germany). Digital images were collected and analyzed through the Olympus cellSens 3.2 software, and thickness was measured in: i) the upper epidermis (UET), ii) the lower epidermis (LET), iii) the palisade parenchyma (PT), iv) the spongy parenchyma (ST), and v) the total leaf lamina (TLT) and expressed in µm. Moreover, the intercellular spaces (IS) were measured as the percentage of the area occupied by space among cells over a given surface of parenchyma. All the measurements were taken in 3 positions along the lamina, avoiding veins and damaged areas if present.

2.4 Ascorbate, anthocyanins and polyphenols content

For ascorbic acid (AsA) determination, 10 mg of freeze-dried powder were extracted using 2 mL of 3% metaphosphoric acid (MPA) in a glass-glass homogenizer at 4°C. The extract was then centrifuged at 16,000 g for 5 min at 4°C, then the supernatant was recovered and filtered through 0.2 µm PPII nylon filters (Whatman) before the quantification of AsA. For Dehydro-ascorbate (DHAs) quantification DHA in the filtered extract was reduced to AsA with the reducing agent Tris (2-carboxyethyl) phosphine (TCEP). 5 mmol L^{-1} TCEP was added in the filtered extract, which was then incubated for 30 min at 25°C under continuous shaking. After incubation the samples were injected into HPLC for the quantification of Total Ascorbic Acid (TAsA). The DHAs content was calculated as the difference between TAsA and AsA. The chromatographic quantification of ascorbic acid was performed as described by Chebrolu et al. (2012). Ascorbic acid content was determined using an HPLC U3000 system (Dionex™ ICS-5000;

Thermo Fisher Scientific, Waltham, MA, United States). Separation was achieved using a Luna C18(2) (Phenomenex, Bologna, Italy) column with an isocratic mobile phase consisting of 0.010 mol L^{-1} of KH_2PO_4 pH 2.8. After a chromatographic run of 15 min (flow rate 0.7 mL min^{-1}), AsA peak was detected at 254 nm using a UV/VIS detector (ThermoScientific ™ Dionex). Peaks processing was performed with the software Chromeleon 7.2 (ThermoScientific™ Dionex), and the quantifications were elaborated against the calibration curve of ascorbic acid standard (Supelco®, 595 N Harrison Rd, Bellefonte, PA 16823, USA).

Determination of Total Anthocyanins (TAcy) content was achieved by the extraction of 10 mg powder from freeze-dried material in 2 mL of 1% HCl in methanol for 1 hour at 65°C. The extract was clarified by centrifugation at 16,000 g for 5 min. The supernatant was then recovered, and the total anthocyanins content was determined spectrophotometrically, measuring the absorbance at 530 and 657 nm in order to correct the chlorophyll degradation products. The concentration was expressed as cyanidin-3-glucoside equivalent by using an extinction coefficient of 30,000 mol^{-1} cm^{-1}. Total phenolic content (TPoly) was determined following Usenik et al. (2008). Extraction was conducted with 10 mg of the freeze-dried powder in 2 mL of 100% methanol. Supernatant was recovered after centrifugation at 16,000 g for 5 min and used to measure spectrophotometrically the absorbance at 765 nm. TPoly was then calculated by relating the absorbance of each sample with the calibration curve of gallic acid (Supelco®, 595 N Harrison Rd, Bellefonte, PA 16823, USA).

2.5 Photosynthetic pigments and carbohydrates content

For pigment determinations, 10 mg of freeze-dried microgreen powder was extracted in a glass-glass homogenizer, with 2 mL 100% acetone at 4°C, under dark conditions. The extracts were centrifuged at 16,000 g for 5 min at 4°C and filtered through a 0.2 µm nylon PPII syringe disposable filter; 15 µl of the filtered extract were used to assay the concentration of neoxanthin (Neo), violaxanthin (Vio), luteine (Lut), β-carotene (β-car), chlorophyll a and b (Chl a+b), using a HPLC U3000 system (Dionex™ ICS-5000; Thermo Fisher Scientific, Waltham, MA, United States), equipped with a Luna C18(2) (Phenomenex, Bologna, Italy) analytical column (5 µm, 250 mm × 4.6 mm) and a related guard column (Phenomenex, Bologna, Italy), maintained at 30°C. The separation run lasted 22 min at a flow rate of 1 mL min^{-1}. From 0 to 4 min, the mobile phase was composed of solution A: 1.75% water, 1.75% methanol, 1.75% dichloromethane, and 94.75% acetonitrile; from 4.1 to 18 min the mobile phase was composed of solution B: 50% acetonitrile and 50% diethyl acetate. Final re-equilibration of 4 min was conducted with solution A. The autosampler temperature was set at 4°C, the UV detector wavelength was 440 nm, and the concentration of all the pigments was quantified against standard curves (Supelco®, 595 N Harrison Rd, Bellefonte, PA 16823, USA) as reported in Žnidarčič et al. (2011).

The extraction of total non-structural carbohydrates (TNsc) was conducted using 10 mg of the freeze-dried powder material in 1 mL of 80% ethanol at 80°C for 45 min, under continuous shaking. The extract was centrifuged at 16,000 g for 5 min, then soluble sugars (glucose, fructose, and sucrose) were recovered in the supernatant and starch in the pellet. The measurement of total soluble sugars (TSolub) was performed by spectrophotometric coupled enzymatic assay as described by Scartazza et al. (2017). The sugar assays were performed in dual-wavelength mode (340-405 nm) in an Elisa plate reader (Spectrostar Nano, BMG Labtech, Germany). After separation, the supernatant containing soluble sugars, was immediately analyzed for soluble sugar content, or stored at −20°C until analysis. The pellet was washed four times with a 50 mM Na Acetate buffer (pH 4.5), suspended in 1 mL of the same buffer and autoclaved at 120°C for 45 min to solubilize the starch. After autoclaving, the pellets were incubated at 50°C for 1 h with amyloglucosidase (70 U) and α-amylase (4U) for the complete starch hydrolysis. The determination of starch was conducted by measuring the glucose, produced by the hydrolysis, as described before for the soluble sugars content.

2.6 Anions analysis

The extraction of inorganic anions (nitrate, sulfate, and phosphate) was achieved using 10 mg freeze-dried powder in water at 80°C for 45 min, under continuous shaking. After the extraction, the sample was centrifuged at 16,000 g for 5 min and the supernatant was recovered and filtrated using a 0.2 µm nylon PPII syringe filter, before the injection in a ion chromatography system (DionexTM ICS-5000; Thermo Fisher Scientific, Waltham, MA, United States), equipped with a conductivity detector, an analytical IonPac AS11-HC column (4 × 250mm) (Thermo Fisher Scientific) and a related guard column and IonPac Anion Trap Column $(ATC)^{-1}$ (Thermo Fisher Scientific). The chromatographic system was coupled with an ERSTM 500 Electrolytically Regenerated Suppressor, (DionexTM ICS- 5000; Thermo Fisher Scientific) to suppress unwanted ionic interference in the analysis. The runs were carried out at a temperature of 30°C and a flow rate of 1 mL min^{-1}. A sodium hydroxide stepped gradient was used as the mobile phase as in Proietti et al. (2019). The electrical signal was integrated into micro-Siemens (µS). The eluents and the inorganic anion standard solutions were prepared using HPLC-grade reagents (Merck KGaA, Darmstadt, Germany). The chromatographic system control, data acquisition and processing were performed by the software Chromeleon 7.2 (ThermoScientific™ Dionex).

2.7 Statistical analyses

To test the influence of the three independent factors, i) Species, ii) VPD, iii) Light intensity, on the dependent variables, a three-way analysis of variance (ANOVA) was performed using the IBM SPSS Statistics software (SPSS, Chicago, IL, USA). When the interactions were significant, a one-way ANOVA was performed, separating the values according to Tukey test with a p value ≤ 0.05. Moreover, a multivariate analysis was performed as principal component analysis (PCA) on all the calculated traits (biometric, anatomical,

and biochemical traits), using the software Past3 (Natural History Museum, University of Oslo, Norway). Variables used as input for multivariate analysis were standardized to zero mean and unit variance.

3 Results

3.1 Growth analysis

The main factors of this investigation (species, VPD and light) had a significant effect, alone and in interaction, on microgreen growth depending on the specific parameter (Table 1, Figure 2). Particularly, the species alone elicited a significant effect ($p \leq 0.001$) on the fresh weight (FW), dry weight (DW) and microgreen length (ML), always showing higher values in 'Saxa' compared to 'Vertus'. Differently, the VPD had a significant effect ($p \leq 0.001$) only on ML where at lowest values (LV) corresponded a higher elongation. Light elicited significant effects ($p \leq 0.01$) on DW and DM%, with increments of both parameters at 300 PPFD, and on ML ($p \leq 0.001$) with decreases in elongation at 300 PPFD. The interaction among the three factors (SxVxL) showed a significance of $p \leq 0.01$ for DW and ML, but it was non-significant for FW and DM%.

Concerning the DW (Figure 2B), highest values were found in S LV 300 and S HV 300, in turn higher than S LV 150 and S HV 150, followed by V HV 150 and 300; lowest values were observed in V LV 150 and 300. For the ML (Figure 2D), highest values were found in S LV 150 and 300 and S HV 150, followed by V LV 150 and V HV 150, which were in turn higher than S HV 300 and V LV 300; lowest values were found in V HV 300.

3.2 Colorimetry analysis

Table 2 shows the results from colorimetry analysis. Here, the effect of the species alone was significant for all the parameters analyzed ($p \leq 0.001$), except for the Hue, always showing higher values in 'Saxa' compared to 'Vertus'. Differently, the VPD had significant effects only on brightness (b*) ($p \leq 0.05$) with increments in the parameter at HV and on Hue angle ($p \leq 0.001$) with decreases in the parameter at HV. The light intensity was significant for b*, chroma and Hue ($p \leq 0.001$), and lightness (L*) ($p \leq 0.01$). The highest light intensity (300 PPFD) determined higher values of b*, L* and chroma but lower Hue. Here, the interaction SxVxL was significant, only for the Hue value ($p \leq 0.001$) which showed higher values in S HV 150 and V LV 150, followed by S LV at both 150 and 300, which were in turn higher than V HV 150 and V LV 300. Lowest values were found in S HV 300 and V HV 300.

3.3 Anatomical analysis

All the treatments allowed the formation of an ordinary mesophyll structure (Figure 3), however there were significant differences in the parameters analyzed among treatments (Table 3). The main factors had a significant effect, alone and in interaction, depending on the specific parameter. The Species elicited significant differences except for the lower epidermis thickness (LET), always with higher values in 'Saxa' but with a different degree of significance: p value ≤0.001 for palisade thickness (PT), spongy thickness (ST), and intercellular space percentage (IS), and $p \leq 0.01$ for the upper epidermis thickness (UET) and total

TABLE 1 Analysis of variance and means comparison for growth-related traits of Fresh Weight (FW), Dry Weight (DW), Dry Matter Content (DM) and microgreen length (ML) of 'Saxa' and 'Vertus' microgreens grown under Low VPD (LV) and High VPD (HV), under two light intensities: 150 and 300 PPFD (μmol photons m^{-2} s^{-1}).

	FW (kg m^{-2})	DW (g m^{-2})	DM (%)	ML (cm)
Species				
Saxa (S)	1.36 ± 0.43a	124 ± 13.5a	8.62 ± 0.73	5.62 ± 1.03a
Vertus (V)	1.09 ± 0.11b	91.4 ± 15.6b	8.67 ± 0.82	4.86 ± 0.69b
VPD				
Low (LV)	1.08 ± 0.32	102 ± 24.4	8.38 ± 0.58	5.53 ± 0.83a
High (HV)	1.07 ± 0.29	113 ± 18.8	8.32 ± 1.04	4.93 ± 0.98b
Light				
300 PPFD	1.35 ± 0.26	113 ± 24.2a	8.71 ± 0.50a	4.82 ± 0.86b
150 PPFD	1.32 ± 0.37	102 ± 18.6b	7.98 ± 0.95b	5.66 ± 0.85a
Significance				
Species	***	***	NS	***
VPD	NS	NS	NS	***
Light	NS	**	**	***
SxVxL	NS	**	*	**

NS, *, **, *** stands for non-significant or significant at $p \leq 0.05$, $p \leq 0.01$, $p \leq 0.001$. Different letters correspond to significant differences according to Tukey test.

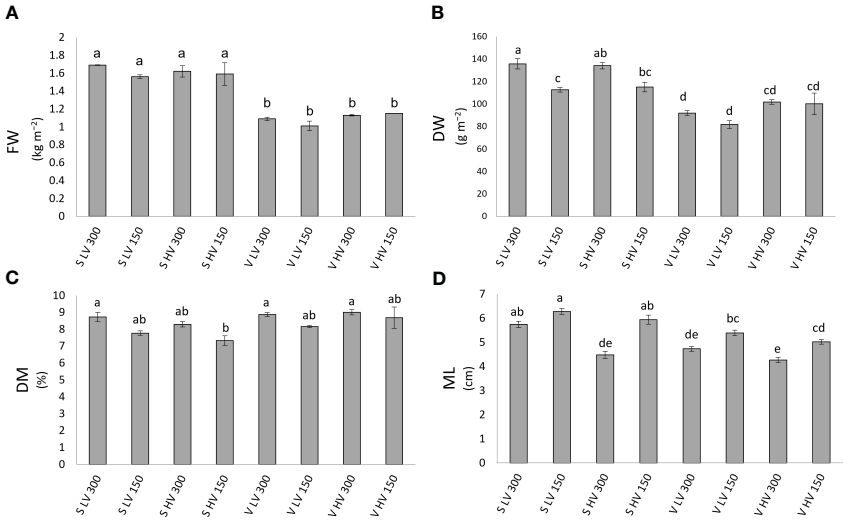

FIGURE 2
Fresh weight (FW, **(A)**, dry weight (DW, **(B)**, dry matter content (DM%, **(C)** and microgreens length (ML, **(D)**, of 'Saxa' and 'Vertus' microgreens grown under Low VPD (LV) and High VPD (HV) at the two light intensities (150 and 300 µmol photons m^{-2} s^{-1}). All data are expressed as mean ± standard errors. Different letters correspond to statistically significant differences according to Tukey test ($p \leq 0.05$).

lamina thickness (TLT). The VPD significantly influenced PT ($p \leq 0.01$), ST ($p \leq 0.05$), TLT ($p \leq 0.001$) with increments at LV and IS ($p \leq 0.001$) with reduction at LV. Differently, light intensity significantly influenced PT ($p \leq 0.01$) with increments at 300 PPFD and TLT ($p \leq 0.01$), ST, and IS ($p \leq 0.001$) with increments at 150 PPFD.

The interaction among the main factors (SxVxL) significantly influenced all parameters except for LET, with UET and PT ($p \leq 0.05$), ST and IS ($p \leq 0.01$) and TLT ($p \leq 0.001$). 'Saxa' developed thicker leaves with more intercellular spaces. Overall, microgreens at LV resulted thicker with less IS% compared to HV and microgreens at 150 PPFD enhanced their total thickness, the thickness of the spongy parenchyma and IS % compared to microgreens grown at 300 PPFD, which however had a thicker palisade tissue.

3.4 Ascorbate, anthocyanins and phenolic content

The effect of the three main factors (species, light intensity and VPD) alone and in interaction on dehydroascorbic acid (DHAs), ascorbic acid (Asa), total ascorbic acid (TAsA), total anthocyanins (TAcy), and total phenolic content (TPoly) are reported in Table 4. 'Vertus' microgreens showed significantly higher values than 'Saxa' for all variables except for TAcy. The effect of VPD was significant only in DHAs and AsA. The LV treatment increased the content of DHAs and decreased that of AsA. The two light intensity levels differentially modulated the accumulation of AsA ($p \leq 0.01$) and Tot AsA ($p \leq 0.001$), always with higher content at 300 PPFD than at 150 PPFD.

The interaction among the main factors (SxVxL) only influenced the DHAs content, determining the highest value in 'Vertus' under 300 PPFD and Low VPD (V LV 300) ($p \leq 0.05$). The TAcy content was not significantly influenced by any of the experimental factors.

3.5 Photosynthetic pigment and carbohydrates content

The pigments accumulation was mainly driven by the species, determining significant differences between 'Saxa' and 'Vertus'. Indeed, 'Vertus' has a higher content of neoxanthin ($p \leq 0.05$), lutein ($p \leq 0.01$), chlorophylls a+b ($p \leq 0.05$) and β-carotene ($p \leq 0.01$) compared to 'Saxa' (Table 5). A different level of accumulation of pigments was found for neoxanthin ($p \leq 0.001$), lutein ($p \leq 0.05$) and β-carotene ($p \leq 0.05$) in response to the VPD, with a higher content of these compounds at LV. Conversely, the different light intensities as well as the interaction among factors did not determine significant variations for any of the pigments analyzed. Concerning the starch, total soluble non-structural carbohydrates (TSolub), and total non-structural carbohydrates (TNsc) higher values were found in 'Vertus' microgreens ($p \leq 0.001$) (Table 5). The VPD was statistically significant only in starch ($p \leq 0.05$), with higher values under LV, while the light intensity resulted significant in all the parameters ($p \leq 0.001$), always with increments at 300 PPFD. The three factors interaction resulted to influence only the accumulation of starch ($p \leq 0.01$), that was two-fold higher in the combination V HV 300 compared to V LV 300 and over 10 times greater compared to the averages values of the other experimental conditions.

3.6 Anions content

The anions analysis revealed that the two species differently accumulated nitrate, sulfate, and phosphate (Table 6), with 'Saxa'

10.3389/fpls.2023.1190945

TABLE 2 Analysis of variance and means comparison for colorimetry-related traits of greenness (a*), yellowness (b*), lightness (L*), Chroma and Hue angle of 'Saxa' and 'Vertus' microgreens grown under Low VPD (LV) and High VPD (HV) at the two light intensities (150 and 300 µmol photons m^{-2} s^{-1}).

	a*	b*	L*	Chroma	Hue
Species					
Saxa (S)	-13.3 ± 1.24a	20.68 ± 2.34a	36.6 ± 5.07a	24.6 ± 2.53a	123± 1.85
Vertus (V)	-11.7 ± 0.86b	18.25 ± 1.73b	34.5 ± 3.55b	21.7 ± 1.83b	123 ± 1.67
VPD					
Low (LV)	-12.3 ± 1.37	18.97 ± 2.46b	35.4 ± 4.76	22.7 ± 2.75	123 ± 1.56a
High (HV)	-12.4 ± 1.24	19.73 ± 2.12a	35.3 ± 3.89	23.4 ± 2.34	122 ± 1.87b
Light					
300 PPFD	-12.5 ± 1.43	20.15 ± 2.01a	36.2 ± 4.36a	23.7 ± 2.21a	122 ± 1.62b
150 PPFD	-12.3 ± 1.14	19.30 ± 2.35b	34.7 ± 4.33b	22.4 ± 2.73b	123 ± 1.53a
Interaction					
S LV 300	-13.5 ± 0.14	20.9 ± 0.35	38.7 ± 0.56	24.9 ± 0.36	123 ± 0.29ab
S LV 150	-13.2 ± 0.27	20.2 ± 0.47	35.0 ± 1.09	24.2 ± 0.53	123 ± 0.26ab
S HV 300	-13.1 ± 0.13	21.5 ± 0.29	37.8 ± 0.69	25.2 ± 0.29	121 ± 0.27d
S HV 150	-13.5 ± 0.22	20.1 ± 0.37	35.1 ± 0.71	24.3 ± 0.41	124 ± 0.26a
V LV 300	-11.8 ± 0.14	18.9 ± 0.25	34.3 ± 0.74	22.3 ± 0.28	122 ± 0.20cd
V LV 150	-11.6 ± 0.16	17.4 ± 0.26	34.7 ± 0.57	20.9 ± 0.30	124 ± 0.19a
V HV 300	-11.7 ± 0.13	19.4 ± 0.23	34.3 ± 0.55	22.6 ± 0.25	121 ± 0.22d
V HV 150	-11.6 ± 0.12	18.1 ± 0.27	34.3 ± 0.45	21.5 ± 0.27	123 ± 0.28bc
Significance					
Species	***	***	***	***	NS
VPD	NS	*	NS	NS	***
Light	NS	***	**	***	***
SxVxL	NS	NS	NS	NS	***

NS, *, **, *** stands for non-significant or significant at $p \leq 0.05$, $p \leq 0.01$, $p \leq 0.001$. Different letters correspond to significant differences according to Tukey test.

reaching a content of nitrate ($p \leq 0.001$) and phosphate ($p \leq 0.01$) about two-fold higher compared to 'Vertus'. On the other hand, 'Vertus' accumulated more sulfate ($p \leq 0.001$). The effect of VPD resulted statistically significant only for the accumulation of nitrate ($p \leq 0.05$) where the LV led to 52% increment compared to HV. Differently, the light intensity alone was never significant as well as the interaction among factors.

3.7 Principal component analysis

The PCA scatter plot reported in Figure 4 shows that the first two components explained a 97.6% of the total variance, with PC1 explaining most of the total variance (94.8%) and PC2 the remaining 2.8%. The first component (PC1) was highly positively correlated with all the variables, except for DW, FW and PT. It is interesting to notice that the scatter plot clearly separated the two species into separated groups; however, both 'Saxa' and 'Vertus' microgreens at LV and 150 PPFD differently separated creating other two sub-groups.

4 Discussion

So far, different species and cultivars have been tested as possible candidates for food production in space according to some specific requirements, including their nutritional values, resource-use efficiency and suitability to grow in a closed controlled environment (De Pascale et al., 2021). Therefore, it is fundamental to investigate the interaction among environmental variables on microgreens growth, development, and phytochemical production.

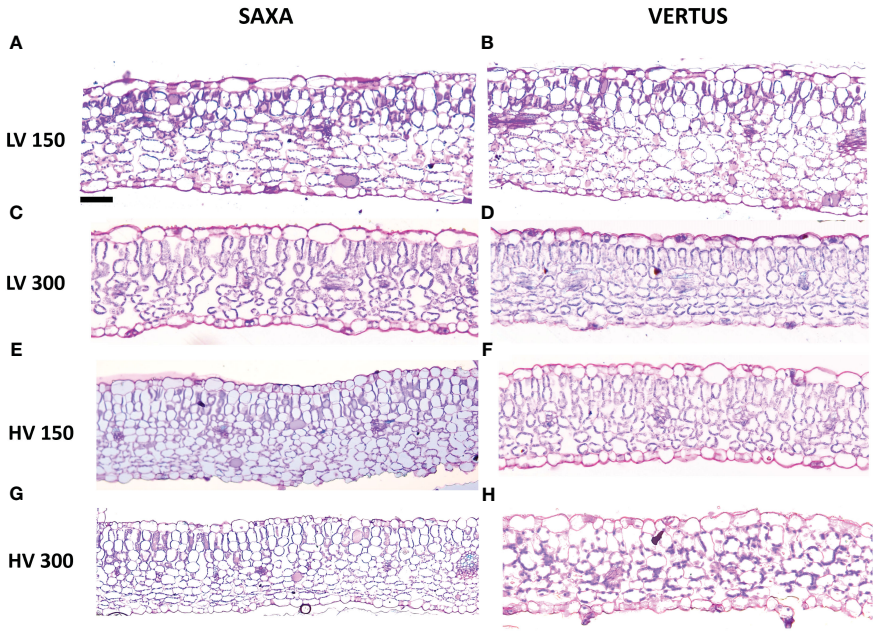

FIGURE 3
Light microscopy views of leaf lamina cross sections randomly chosen among the many shots of 'Saxa' **(A, C, E, G)** and 'Vertus' **(B, D, F, H)** microgreens under low VPD (LV, **(A–D)** and high VPD (HV, **(E–H)** at the two light intensities (150 PPFD, **(A, B, E, F)** and 300 PPFD, **(C, D, G, H)**. Images are at the same magnification, scale bar = 50μm.

4.1 Species-related differences

In the present study, the two species tested, *B. oleracea* 'Vertus' and *R. raphanistrum* 'Saxa', although both belonging to the Brassicaceae family, showed a very different growth, morpho-anatomical development, and bioactive compounds level. 'Saxa', which was harvested first (10 days after sowing vs. 11 for 'Vertus'), reached the highest fresh and dry weight as well as the highest elongation (Table 1, Figure 2). This could be explained by the anatomical analysis (Table 3), which highlighted a thicker mesophyll in 'Saxa' compared to 'Vertus', due to a higher palisade and spongy thickness and also due to a higher percentage of intercellular spaces. Leaf anatomical structure has a fundamental relationship with the plant photosynthetic performance, and usually a thicker and more dense tissue facilitates the transfer of gas and water among mesophyll cells (Amitrano et al., 2022). Moreover, palisade cells are also known to concentrate more chloroplasts compared to spongy cells (Nguyen et al., 2019), so one would expect 'Saxa' to have a higher photosynthetic pigment content. In our study, however, the content of both chlorophylls and carotenoids, as well as neoxanthin and lutein, was higher in 'Vertus' (Table 5). This is probably ascribed to the reduced palisade thickness of 'Vertus' leaves, which may force the plant to synthesize more pigments in order to intercept more light, thus increasing the photosynthetic efficiency. 'Vertus' also presented the highest content of dehydroascorbate, ascorbate and polyphenols compared to 'Saxa' (Table 2). Species-specific differences can play a significant role in determining the content of ascorbate in different plants (Davey et al., 2000). Ascorbate (or vitamin C) is a well-known antioxidant and radical scavenger and is an essential dietary nutrient in humans. Its role in human body involves the enhancement of the immune system (Crucian et al., 2018), prevention of bone density loss (Weber, 1999) and a function as a cofactor in the biosynthesis of collagen, carnitine, and neurotransmitters (Naidu, 2003). Recently, vitamin C has also been reported to have a role as radioprotector (Cai et al., 2001; Yamamoto et al., 2010; Mortazavi et al., 2015), thus in a space mission context, can help neutralizing free radicals and protecting cells from damage induced by ionizing radiation (Gómez et al., 2021). Another difference between the two species concerned the accumulation of minerals (Table 6). 'Saxa' was found to be a higher accumulator of nitrates and phosphate, while 'Vertus' accumulated more sulfate. It is noteworthy that the nitrate content in both plant species was well below the maximum levels allowed in food products by the European Commission regulation No 1258/2011. Therefore, the accumulation of these compounds for the two microgreen species under the above-reported growing conditions does not represent a health concern (Amitrano et al., 2021c).

4.2 Light intensity influence on microgreen development and phytochemical content

Different studies have shown that light intensity has a significant impact on the antioxidant potential of microgreens in terms of anthocyanins and polyphenols content, usually with increments in light corresponding to increments in the phytochemical profile (Samuolienė et al., 2013; Craver et al., 2017). Here we found that

TABLE 3 Analysis of variance and means comparison for anatomical-related traits of Upper Epidermis Thickness (UET), Palisade parenchyma Thickness (PT), Spongy parenchyma Thickness (ST), Lower Epidermis Thickness (LET), Total Lamina Thickness (TLT) and the percentage of Intercellular Spaces (IS) of 'Saxa' and 'Vertus' microgreens grown under Low VPD (LV) and High VPD (HV) at the two light intensities (150 and 300 µmol photons m^{-2} s^{-1}).

	UET (µm)	PT (µm)	ST (µm)	LET (µm)	TLT (µm)	IS (%)
Species						
Saxa (S)	23.1 ± 5.14a	110 ± 23.4a	187 ± 55.2a	20.2 ± 5.40	340 ± 63.4a	37.6 ± 0.71a
Vertus (V)	21.1 ± 5.12b	97.3 ± 20.0b	157 ± 36.8b	19.8 ± 4.30	295 ± 41.5b	28.4 ± 0.62b
VPD						
Low (LV)	22.2 ± 5.11	107 ± 23.6a	180 ± 61.1a	20.6 ± 5.56a	331 ± 66.1a	30.4 ± 1.14b
High (HV)	22.1 ± 5.32	101 ± 21.5b	165 ± 34.8b	19.5 ± 4.15b	308 ± 48.4b	35.8 ± 1.12a
Light						
300 PPFD	22.2 ± 5.76	120 ± 25.3a	150 ± 36.8b	19.8 ± 5.48	209 ± 10.7b	21.6 ± 0.53b
150 PPFD	22.1 ± 4.76	100 ± 19.8b	190 ± 51.4a	20.2 ± 4.39	301 ± 53.8a	41.3 ± 0.53a
Interaction						
S LV 300	24.3 ± 1.09a	120 ± 4.01a	162 ± 5.58b	21.5 ± 1.41	328 ± 8.67b	24.4 ± 0.18f
S LV 150	21.1 ± 0.67ab	107 ± 3.83abc	243 ± 11.2a	19.8 ± 0.90	391 ± 12.5a	43.8 ± 0.32b
S HV 300	22.8 ± 0.89a	104 ± 5.61bcd	159 ± 6.32bc	18.9 ± 0.82	305 ± 10.9b	27.5 ± 0.56e
S HV 150	24.4 ± 0.91a	111 ± 2.41abc	172 ± 3.11b	20.6 ± 0.69	199 ± 3.93c	49.6 ± 0.13a
V LV 300	22.8 ± 1.19a	118 ± 3.21ab	128 ± 4.13c	21.2 ± 0.88	291 ± 5.67bc	14.4 ± 0.18h
V LV 150	20.9 ± 0.77ab	84.5 ± 2.44e	166 ± 4.23b	20.1 ± 0.90	292 ± 5.36bc	34.5 ± 0.22d
V HV 300	18.1 ± 0.92b	90.6 ± 3.48de	150 ± 10.2bc	17.8 ± 0.91	277 ± 12.9bc	19.5 ± 0.15g
V HV 150	21.9 ± 0.75ab	95.5 ± 2.65cde	174 ± 5.14b	20.1 ± 0.54	311 ± 5.48b	39.4 ± 0.17c
Significance						
Species	**	***	***	NS	**	***
VPD	NS	**	*	*	***	***
Light	NS	**	***	NS	**	***
SxVxL	*	*	**	NS	***	**

NS, *, **, *** stands for non-significant or significant at $p \leq 0.05$, $p \leq 0.01$, $p \leq 0.001$. Different letters correspond to significant differences according to Tukey test.

the highest light intensity (300 PPFD) was associated with a higher ascorbate content (Table 4), consistently with previous research demonstrating a progressive ascorbate accumulation in microgreens, proportionally to the light level (Jones-Baumgardt et al., 2020). However, in our study we did not find a significant variation in the content of anthocyanin or polyphenols in microgreen grown under different light irradiances, nor in the carotenoids and other photosynthetic pigment content. Secondary phytochemicals, such as polyphenols and anthocyanins, are highly desirable in astronaut's diet since they have several positive impacts on health, including cardiovascular health, neuroprotective function, diabetes management, anti-inflammatory and anti-cancer activity (Gonçalves et al., 2021) and could help counteract the detrimental effect of space environment (Gómez et al., 2021). Carotenoids are also essential for human nutrition; incorporating carotenoids into the food supply for space missions could have multiple benefits, including antioxidant protection (Palozza and Krinsky, 1992), immune system support (Chew and Park, 2004), and eye health maintenance (Ma et al., 2012). The fact that these compounds (anthocyanins, polyphenols and carotenoids), which are also desirable for nutritional purposes, do not increase with light intensity represents an added value as there is always a trade-off between light intensity and electricity consumption in controlled environment agriculture (Kobayashi et al., 2022), especially in the sight of space outposts oriented towards eliminating or minimizing superfluous wastes (Poulet et al., 2014). Moreover, in our study, microgreens at 150 PPFD grew taller than those at 300 PPFD, probably because of a stretching mechanism, typical of plants grown under low light intensity, which lengthen towards the light source in order to enhance their light harvesting capacity (Colonna et al., 2016).

It is worth noting that the lower light intensity did not impact the total fresh weight of microgreens which was still comparable to that produced at 300 PPFD (Table 1). The dry weight, however, as well as the dry matter content, increased under the high light intensity. This

10.3389/fpls.2023.1190945

TABLE 4 Analysis of variance and means comparison for dehydro-ascorbate (DHAs), ascorbate (AsA), total ascorbate (TAsA), total anthocyanins (TAcy) and total polyphenols (TPoly) content of 'Saxa' and 'Vertus' microgreen grown under Low VPD (LV) and High VPD (HV) at the two light intensities: 150 and 300 PPFD (µmol photons m^{-2} s^{-1}).

	DHAs	AsA	TAsA	TAcy	TPoly
	(mg 100g FW^{-1})	(mg 100g FW^{-1})	(mg 100g FW^{-1})	(mg 100g FW^{-1})	(mg 100g FW^{-1})
Species					
Saxa (S)	16.6 ± 2.13b	13.1 ± 1.81b	29.7 ± 2.48b	6.04 ± 0.66	145 ± 8.57b
Vertus (V)	37.2 ± 2.76a	24.5 ± 3.06a	61.6 ± 2.06a	5.59 ± 0.33	193 ± 8.94a
VPD					
Low (LV)	31.4 ± 3.9a	15.7 ± 2.09b	47.1 ± 4.97	6.46 ± 0.59	172.± 10.26
High (HV)	22.4 ± 3.53b	21.8 ± 3.53a	44.2 ± 5.62	5.21 ± 0.38	166 ± 12.28
Light					
300 PPFD	27.8 ± 3.5a	23.1 ± 3.46a	50.9 ± 5.01a	6.37 ± 0.32	175 ± 10.52
150 PPFD	25.9 ± 4.36a	14.4 ± 1.77b	40.4 ± 5.14b	5.30 ± 0.64	163 ± 11.82
Interaction					
S LV 300	21.7 ± 1.27bc	16.5 ± 5.12	38.3 ± 4.77	6.35 ± 0.26	151 ± 2.2
S LV 150	18.6 ± 5.54c	8.95 ± 2.35	27.6 ± 3.18	7.32 ± 2.45	162 ± 34.2
S HV 300	18.2 ± 1.76c	13.6 ± 1.47	31.8 ± 3.12	6.68 ± 1.08	140 ± 6.28
S HV 150	8.02 ± 3.36c	13.1 ± 4.88	21.2 ± 3.98	4.41 ± 0.12	127 ± 7.45
V LV 300	46.4 ± 3.97a	22.4 ± 3.87	68.7 ± 1.02	6.95 ± 0.73	185 ± 11.6
V LV 150	38.9 ± 4.36ab	14.9 ± 2.03	53.9 ± 4.75	5.23 ± 0.09	190 ± 22.1
V HV 300	25.3 ± 2.92bc	40.0 ± 3.21	64.9 ± 0.21	5.54 ± 0.25	225 ± 5.50
V HV 150	38.3 ± 3.06ab	20.6 ± 0.91	58.8 ± 2.46	4.22 ± 0.06	171 ± 17.5
Significance					
Species	***	***	***	NS	***
VPD	**	*	NS	NS	NS
Light	NS	**	***	NS	NS
S x V x L	*	NS	NS	NS	NS

NS, *, **, *** stands for non-significant or significant at $p \leq 0.05$, $p \leq 0.01$, $p \leq 0.001$. Different letters correspond to significant differences according to Tukey test.

is a common response of plants grown under high irradiance and is also consistent with the enhanced thickness of the palisade tissue under 300 PPFD (Table 3). The increase in palisade tissue thickness goes in parallel with the development of more chloroplasts, thus with increments in the photosynthetic rate (Oguchi et al., 2005). Besides, being the site of photosynthesis, chloroplasts also represent a site for starch storage in the form of grains (Zeiger et al., 2002). Indeed, in our study at 300 PPFD, together with the increments in palisade tissue, the total NSC levels increased (Table 5). The two species showed to be accumulators of soluble carbohydrates, since soluble sugars (glucose, fructose, sucrose) dominated the total non-structural carbohydrate content. Starch was always much lower than soluble sugars, but its content varied more in response to the environmental variables tested. In almost all photosynthetic organisms', starch is one important products of photosynthesis and the storage carbohydrates in leaves, allowing the accumulation of carbon and energy without affecting the osmolyte concentration of the cell. (Malinova et al., 2018). Starch is accumulated in chloroplast during the day and degraded at night to support plant needs, with a complex pathway requiring the coordinated actions of several enzymes (Stettler et al., 2009). Even though we cannot go deeper into the starch kinetics, here, we can hypothesize that, as for other species like *Arabidopsis*, *Lemna*, and mung bean (Yehu et al., 2015; Mengin et al., 2017; Amitrano et al., 2020b), under high irradiance microgreens allocate photosynthates to starch, as a response to an imbalance between photosynthate production and use. This shows that plant metabolism as early as 10-11 days after germination was already fully dominated by photosynthetic production of assimilates, highlighting the importance of the environmental control on gas exchanges as a tool to govern plant performances even in microgreens production.

TABLE 5 Analysis of variance and means comparison for Neoxanthin (Neo), Violaxanthin (Vio), Lutein (Lut), Chlorophylls (Chl a+b), β-caroten (β-car), Starch, total soluble sugars (TSolub), Total Non-Structural carbohydrates (TNsc) content of 'Saxa' and 'Vertus' microgreens grown under Low VPD (LV) and High VPD (HV) at the two light intensities:150 and 300 PPFD (μmol photons m^{-2} s^{-1}).

	Neo	Vio	Lut	Chl a+b	β-Car	Starch	TSolub	TNsc
	(mg 100g FW^{-1})	(mg 100g FW^{-1})	(mg 100g FW^{-1})	(mg 100g FW^{-1})	(mg 100g FW^{-1})	(mg 100g FW^{-1})	(mg 100g FW^{-1})	(mg 100g FW^{-1})
Species								
Saxa (S)	1.40 ± 0.10b	27.5 ± 2.59	4.98 ± 0.35b	64.3 ± 5.26b	3.64 ± 0.25b	54.7 ± 9.28b	463.9 ± 46.7 b	518.6 ± 54.9b
Vertus (V)	1.69 ± 0.134a	22.9 ± 1.61	6.60 ± 0.37a	82.0 ± 5.14a	4.60 ± 0.22a	258 ± 72.3a	1127 ± 70.7a	1386.3 ± 128.9a
VPD								
Low (LV)	1.80 ± 0.12a	27.9 ± 2.54	6.27 ± 0.44a	79.0 ± 6.21	4.44 ± 0.31a	129 ± 35.6a	831.9 ± 111.7	960.8 ± 139.8
High (HV)	1.28 ± 0.83b	22.5 ± 1.55	5.32 ± 0.37b	67.3 ± 4.85	3.80 ± 0.20b	184 ± 76.1b	759.7 ± 120.3	944.0 ± 185.2
Light								
300 PPFD	1.50 ± 0.11	25.2 ± 1.0	5.76 ± 0.39	70.9 ± 4.9	4.05 ± 0.25	271 ± 68.9a	954.6 ± 116.4a	1226.3 ± 174.2a
150 PPFD	1.58 ± 0.14	25.2 ± 3.04	5.82 ± 0.47	75.4 ± 6.54	4.20 ± 0.30	41.6 ± 6.44b	637.0 ± 95.3b	678.7 ± 99.4b
Interaction								
S LV 300	1.49 ± 0.15	25.1 ± 3.25	4.84 ± 0.61	58.1 ± 8.35	3.39 ± 0.33	94.4 ± 4.81c	628.4 ± 46.2	722.8 ± 41.5
S LV 150	1.67 ± 0.32	35.3 ± 9.43	6.12 ± 1.21	81.3 ± 17.91	4.47 ± 0.89	42.8 ± 10.9c	402.1 ± 83.7	444.9 ± 90.7
S HV 300	1.03 ± 0.17	24.6 ± 1.07	4.34 ± 0.03	54.4 ± 1.87	3.14 ± 0.17	64.2 ± 11.4c	533.5 ± 56.6	597.7 ± 67.9
S HV 150	1.4 ± 0.07	24.7 ± 2.62	4.64 ± 0.12	63.3 ± 1.09	3.57 ± 0.1	17.3 ± 4.07c	291.9 ± 54.5	309.2 ± 57.0
V LV 300	1.93 ± 0.05	26.3 ± 1.21	6.65 ± 0.33	82.2 ± 5.03	4.80 ± 0.02	319 ± 53.6b	1355.6 ± 87.79	1674.9 ± 34.4
V LV 150	2.12 ± 0.28	25.0 ± 2.26	7.47 ± 0.8	94.4 ± 9.48	5.11 ± 0.63	59.3 ± 5.65c	941.5 ± 42.1	1000.7 ± 42.6
V HV 300	1.57 ± 0.13	24.7 ± 2.83	7.23 ± 0.29	88.9 ± 2.23	4.85 ± 0.14	608 ± 79.9a	1300.9 ± 52.4	1909.5 ± 45.6
V HV 150	1.13 ± 0.12	15.8 ± 2.81	5.06 ± 0.67	62.6 ± 3.19	3.63 ± 0.24	47.2 ± 16.6c	912.7 ± 128.2	959.9 ± 130.6
Significance								
Species	*	NS	**	*	**	***	***	***
VPD	***	NS	*	NS	*	*	NS	NS
Light	NS	NS	NS	NS	NS	***	***	***
S x V x L	NS	NS	NS	NS	NS	**	NS	NS

NS, *, **, *** stands for non-significant or significant at $p \leq 0.05$, $p \leq 0.01$, $p \leq 0.001$. Different letters correspond to significant differences according to Tukey test.

4.3 VPD levels influence on microgreen development and phytochemical content

The air VPD is the primary factor affecting the transpiration rate of crops in controlled environment, thus affecting plants' photosynthetic rate and the whole development of the leaf lamina (Carins Murphy et al., 2014; Amitrano et al., 2019). It has been demonstrated that plants grown under high VPD levels reduce the photosynthesis and the biomass production and are often characterized by a lower leaf thickness and a reduction of cell enlargement (Aliniaeifard et al., 2014). Our results partially agree with this statement, since HV microgreens did not show significant

10.3389/fpls.2023.1190945

TABLE 6 Analysis of variance and means comparison for nitrate, sulfate, phosphate content of 'Saxa' and 'Vertus' microgreens grown under Low VPD (LV) and High VPD (HV) at the two light intensities (150 and 300 µmol photons m^{-2} s^{-1}).

	Nitrate	Sulfate	Phosphate
	(mg 100g FW^{-1})	(mg 100g FW^{-1})	(mg 100g FW^{-1})
Species			
Saxa (S)	74.9 ± 6.84a	12.4 ± 1.19b	32.7 ± 4.5a
Vertus (V)	36.1 ± 8.74b	23.6 ± 1.31a	17.9 ± 2.13b
VPD			
Low (LV)	66.5 ± 9.96a	18.4 ± 2.38	28.2 ± 5.08
High (HV)	43.7 ± 8.71b	17.6 ± 1.79	22.4 ± 2.74
Light			
300 PPFD	50.3 ± 8.52	19.3 ± 2.1	21.0 ± 2.47
150 PPFD	58.6 ± 10.8	16.8 ± 2.05	29.6 ± 5.04
Interaction			
S LV 300	58.7 ± 8.49abc	11.9 ± 1.48	25.5 ± 5.78
S LV 150	94.6 ± 18.3a	11.3 ± 3.19	48.5 ± 13.2
S HV 300	57.5 ± 2.64abc	14.8 ± 2.85	21.6 ± 3.17
S HV 150	83.5 ± 4.90ab	11.5 ± 2.59	35.4 ± 3.16
V LV 300	66.6 ± 26.1abc	28.2 ± 0.62	17.2 ± 7.78
V LV 150	43.7 ± 10.2abc	22.3 ± 3.16	21.5 ± 2.3
V HV 300	21.3 ± 4.03bc	22.0 ± 2.28	19.8 ± 3.54
V HV 150	12.6 ± 0.48c	22.1 ± 2.81	12.9 ± 0.97
Significance			
Species	***	***	**
VPD	*	NS	NS
Light	NS	NS	NS
S x V x L	*	NS	NS

NS, *, **, *** stands for non-significant or significant at $p \leq 0.05$, $p \leq 0.01$, $p \leq 0.001$. Different letters correspond to significant differences according to Tukey test.

difference in growth in term of fresh and dry weight, only resulting shorter than LV microgreens (Table 1, Figure 2). However, HV microgreens showed a reduced tissue thickness and a higher percentage of intercellular spaces, compared to LV (Table 3). As mentioned before, having more intercellular spaces can represent a disadvantage for HV microgreens, already subjected to an enhanced transpiration due to the dryer air (high VPD). Indeed, the wide presence of intercellular spaces reduces the cell connection, decreasing the velocity of both gas and water flows, thus imposing a high mesophyll resistance (Amitrano et al., 2019). In accordance with our results, in a previous study on *V. radiata* sprouts subjected to different levels of relative humidity, sprouts at low RH (high VPD) evolved morpho-anatomical traits which increased the resistance to water flows and did not allow them to elude water loss and allocate biomass (Amitrano et al., 2020b). Here, HV condition did not negatively impact microgreen biomass accumulation, but the leaf anatomy developed by HV microgreens characterized by a higher resistance of gas and water flows, would probably lower the photosynthetic and hydraulic efficiency in future plant growth phases.

Furthermore, we observed that HV microgreens had a greater content of ascorbate. To our knowledge there is no previous research on the effect of VPD on microgreens. Our results could be compared with findings from Amitrano et al., (2021c) which reported an increase in total ascorbate content in lettuce grown at 1.76 kPa in comparison to 0.69 kPa, due to the mild stress given by the high VPD conditions. Usually, when plants are subjected to mild stresses caused by high temperature, salinity, VPD or drought, they tend to synthesize more antioxidants with scavenger activity, trying to react to the oxidative stress. The production of antioxidants is effective above a threshold depending on the type and intensity of the stress. Exceeded the threshold, plants are not able to react anymore with their biochemical activities and start to perish (Lihavainen et al., 2016).

Here we also found that the high VPD level reduced the content of nitrates in both species. This effect is useful in the sight of

cultivating microgreens for nutritional purposes. Usually, lower content of nitrates is also associated with the qualitative parameters with respect to the yellowish of the leaves, and in particular with enhanced L*, b* and chroma and reduced hue (Navarro et al., 2012). In this study, there were no significant differences between HV and LV microgreens concerning L* and chroma; however, microgreens at HV showed an enhanced yellowness exemplified by the parameter b* and by a reduced chroma. For edible products the analysis of color is an important tool since consumers are easily influenced by the qualitative aspect of vegetables (Jha, 2010). Furthermore, several studies have found an inverse relationship between b* and dry weight, using the b* parameter as a proxy for stress level (Ibraheem et al., 2012; Dodig et al., 2019). LV microgreens with a reduced yellowness in both species achieved a better visual quality, they also maintained high levels of polyphenols, vitamin C and anthocyanins and enhanced the accumulation of pigments such as neoxanthin, lutein and β-carotene, compared to HV (Table 5). These pigments, besides having important nutritional functions, are used as proxies for the photosynthetic performance of the plant. Carotenoids are primarily involved in the protective mechanisms of the photosynthetic apparatus from photo-damages (Demmig-Adams and Adams, 2006). Lutein and neoxanthin are involved in the xanthophyll cycle and ease the distribution of absorbed light energy in the leaf, therefore are correlated with the photosynthetic activity (Wong et al., 2020). Thus, LV microgreens not only grew taller, raising the phytochemical content, but also had a more efficient functioning, demonstrated by the more suitable anatomical structure and the high content of pigments and if such a trend is maintained, probably adult plants may have a greater photosynthetic performance. However, the combination of more environmental factors together, can have synergistic or antagonistic effects on microgreen growth and phytochemical content.

4.4 Microgreens response to microenvironment and general conclusions

The combination of VPD and light intensity influenced the growth, quality, and the morpho–anatomical traits of the two species. As highlighted by the multivariate analysis performed on all the traits analyzed (Figure 4), the genetics had a remarkable effect since 'Saxa' and 'Vertus', at different VPDs and light intensities, separated into two groups mainly driven by the species. However, both microgreens' species separated into two different sub-groups due to the effect of LV and 150 PPFD. 'Saxa' LV 150 was mainly driven by spongy thickness, violaxanthin and sulfate content, while 'Vertus' LV 150 due to the remaining pigments content. Both species grown at LV under 150 PPFD achieved the highest height and fresh weight. Even if they reduced the dry weight compared to microgreens grown under 300 PPFD, they managed to achieve a dry matter content (DM%) comparable to those grown under the highest light intensity (Figure 1). DM%, referred to as tissue density, is a good predictor of resource capture and use (Shipley and Vu, 2002). Tomlins et al. (2012) found in sweet potato correlation between the dry matter content and the carotenoids content, attributed to textural changes: plants with high β-carotene were also more solid and less tender, thus preferred by consumers. Our results agree with this research since both 'Saxa' and 'Vertus' LV 150 increased the tissue thickness and synthetize high β-carotene and photosynthetic pigments (Table 6). Moreover 'Vertus' LV 150, was the one treatment to develop the highest content of ascorbate, as aforementioned fundamental for nutritional properties in space environment.

In conclusion, it is notable that the effects of environmental factors on the development and the antioxidant potential of microgreens can be complex and dependent on multiple factors. Thus, the modulation of environmental parameters during the early morphogenesis represents a valuable tool to adjust the quality of the products and the plant architecture to fulfill specific needs like the production of more compact plants with high phytochemical content to use in controlled environment systems (Demotes-Mainard et al., 2016; Mah et al., 2018).

For these reasons, to allow microgreen cultivation in space as food supplements, the development of space-targeted agro-technologies is mandatory, taking in mind the possible alterations induced by space flight environments. Indeed, the cultivation in closed facilities of limited volume under microgravity may change microgreen resource utilization, likely modifying the nutritional properties of the products, with species-specific responses. In the light of the above, choosing a low VPD together with a low light intensity might be a good strategy to save energy, while developing microgreens with a high phytochemical content, important for nutritional values and as good anatomical traits indicators of high resource use efficiency, useful also if some of these species could be grown as adult plants to be used as bio-regenerators or for seeds production, and not only as microgreens for dietary supplements. Indeed, it must be taken into account that crop systems like microgreens need a high number of seeds, which can represent a significant upload mass influencing mission planning and payload design, especially in short-duration missions (De Micco et al., 2009). The quantity of seeds to be transported depends on the mission duration, the production capacity of the facilities, the number of crew members, and the average daily consumption of microgreens. Therefore, it is a parameter that needs to be considered specifically for each mission case. Thus, having some plants dedicated to seed production can be an added value; however, in our experiment, the quantity used (6-7 g per trays) is capable of producing a fresh biomass of 1.09 and 1.36 kg and considering 50g per meal it is possible to provide an approximate of 20 meals. Thus, 1 kilogram of seeds is sufficient for a 3-month production representing an efficient volume expenditure.

Data availability statement

The raw data supporting the conclusions of this article will be made available by the authors, without undue reservation.

Author contributions

VM, YR, RP, AB, SDP supervision, conceptualization, resources and coordination; SDP, MB funding acquisition, CA and GL run the experiments, the sampling and the biometric and anatomical analysis; GP, SM, SP run the biochemical analysis; CA and GP worked on data curation and on the manuscript preparation; All authors contributed to the article and approved the submitted version.

Funding

This research was conducted in the framework of the project "Systems and technologies for the production of microgreens in the space 'Microgreens x Microgravity' - MICROx2", carried out with the collaboration and the coordination of the Italian Space Agency (ASI). Agreement n. 2021-2-HH.0.

Acknowledgments

The authors wish to thank Dr. Christophe El-Nakhel for his technical support in the laboratory.

Conflict of interest

The authors declare that the research was conducted in the absence of any commercial or financial relationships that could be construed as a potential conflict of interest.

Publisher's note

All claims expressed in this article are solely those of the authors and do not necessarily represent those of their affiliated organizations, or those of the publisher, the editors and the reviewers. Any product that may be evaluated in this article, or claim that may be made by its manufacturer, is not guaranteed or endorsed by the publisher.

References

Aliniaeifard, S., Malcolm Matamoros, P., and Van Meeteren, U. (2014). Stomatal malfunctioning under low VPD conditions: induced by alterations in stomatal morphology and leaf anatomy or in the ABA signaling? *Physiol. Plant* 152, 688–699. doi: 10.1111/ppl.12216

Amitrano, C., Arena, C., Cirillo, V., De Pascale, S., and De Micco, V. (2021a). Leaf morpho-anatomical traits in vigna radiata l. affect plant photosynthetic acclimation to changing vapor pressure deficit. *Env. Exp. Bot.* 186, 104453. doi: 10.1016/j.envexpbot.2021.104453

Amitrano, C., Arena, C., De Pascale, S., and De Micco, V. (2020b). Light and low relative humidity increase antioxidants content in mung bean (*Vigna radiata* l.) sprouts. *Plants.* 9 (9), 1093. doi: 10.3390/plants9091093

Amitrano, C., Arena, C., Rouphael, Y., De Pascale, S., and De Micco, V. (2019). Vapour pressure deficit: the hidden driver behind plant morphofunctional traits in controlled environments. *Ann. Appl. Biol.* 175, 313–325. doi: 10.1111/aab.12544

Amitrano, C., Chirico, G. B., De Pascale, S., Rouphael, Y., and De Micco, V. (2020a). Crop management in controlled environment agriculture (CEA) systems using predictive mathematical models. *Sensors.* 20 (11), 3110. doi: 10.3390/s20113110

Amitrano, C., Junker, A., D'Agostino, N., De Pascale, S., and De Micco, V. (2022). Integration of high-throughput phenotyping with anatomical traits of leaves to help understanding lettuce acclimation to a changing environment. *Planta.* 256 (4), 68. doi: 10.1007/s00425-022-03984-2

Amitrano, C., Rouphael, Y., De Pascale, S., and De Micco, V. (2021c). Modulating vapor pressure deficit in the plant micro-environment may enhance the bioactive value of lettuce. *Horticult.* 7 (2), 32. doi: 10.3390/horticulturae7020032

Amitrano, C., Rouphael, Y., Pannico, A., De Pascale, S., and De Micco, V. (2021b). Reducing the evaporative demand improves photosynthesis and water use efficiency of indoor cultivated lettuce. *Agronomy.* 11 (7), 1396. doi: 10.3390/agronomy11071396

Aronne, G., Romano, L. E., and Izzo, L. G. (2020). Subsequent inclusion/exclusion criteria to select the best species for an experiment performed on the ISS in a refurbished hardware. *Life Sci. Space Res.* 27, 19–26. doi: 10.1016/j.lssr.2020.07.002

Avercheva, O. V., Berkovich, Y. A., Konovalova, I. O., Radchenko, S. G., Lapach, S. N., Bassarskaya, E., et al. (2016). Optimizing LED lighting for space plant growth unit: joint effects of photon flux density, red to white ratios and intermittent light pulses. *Life Sci. Space Res. (Amst).* 11, 29–42. doi: 10.1016/j.lssr.2016.12.001

Balsano, C., and Alisi, A. (2009). Antioxidant effects of natural bioactive compounds. *Curr. Pharm. Des.* 15 (26), 3063–3073. doi: 10.2174/138161209789058084

Bisbis, M. B., Gruda, N., and Blanke, M. (2018). Potential impacts of climate change on vegetable production and product quality–a review. *J. Clean. Prod.* 170, 1602–1620. doi: 10.1016/j.jclepro.2017.09.224

Cai, L., Koropatnick, J., and Cherian, M. G. (2001). Roles of vitamin c in radiation-induced DNA damage in presence and absence of copper. *Chemico-Biological Interact.* 137 (1), 75–88. doi: 10.1016/S0009-2797(01)00210-1

Carillo, P., Morrone, B., Fusco, G. M., De Pascale, S., and Rouphael, Y. (2020). Challenges for a sustainable food production system on board of the international space station: a technical review. *Agronomy.* 10 (5), 687. doi: 10.3390/agronomy10050687

Carins Murphy, M. R., Jordan, G. J., and Brodribb, T. J. (2014). Acclimation to humidity modifies the link between leaf size and the density of veins and stomata. *Plant Cell. Environ.* 37, 124–131. doi: 10.1111/pce.12136

Chebrolu, K. K., Jayaprakasha, G. K., Yoo, K. S., Jifon, J. L., and Patil, B. S. (2012). An improved sample preparation method for quantification of ascorbic acid and dehydroascorbic acid by HPLC. *L.W.T.* 47 (2), 443–449. doi: 10.1016/j.lwt.2012.02.004

Chew, B. P., and Park, J. S. (2004). Carotenoid action on the immune response. *J. Nutr.* 134 (1), 257S–261S. doi: 10.1093/jn/134.1.257S

Colonna, E., Rouphael, Y., Barbieri, G., and De Pascale, S. (2016). Nutritional quality of ten leafy vegetables harvested at two light intensities. *Food Chem.* 199, 702–710. doi: 10.1016/j.foodchem.2015.12.068

Craver, J. K., Gerovac, J. R., Lopez, R. G., and Kopsell, D. A. (2017). Light intensity and light quality from sole-source light-emitting diodes impact phytochemical concentrations within brassica microgreens. *J. Am. Soc Hortic. Sci.* 142 (1), 3–12. doi: 10.21273/JASHS03830-16

Crucian, B. E., Choukèr, A., Simpson, R. J., Mehta, S., Marshall, G., Smith, S. M., et al. (2018). Immune system dysregulation during spaceflight: potential countermeasures for deep space exploration missions. *Front. Immunol.* 9. doi: 10.3389/fimmu.2018.01437

D'Aquino, L., Lanza, B., Gambale, E., Sighicelli, M., Menegoni, P., Modarelli, G. C., et al. (2022). Growth and metabolism of basil grown in a new-concept microcosm under different lighting conditions. *Sci. Hortic* 299, 111035. doi: 10.1016/j.scienta.2022.111035

Davey, M. W., Montagu, M. V., Inze, D., Sanmartin, M., Kanellis, A., Smirnoff, N., et al. (2000). Plant l-ascorbic acid: chemistry, function, metabolism, bioavailability and effects of processing. *J. Sci. Food Agric.* 80 (7), 825–860. doi: 10.1002/(SICI)1097-0010(20000515)80:7<825::AID-JSFA598>3.0.CO;2-6

De Micco, V., Amitrano, C., Balzano, A., Cirillo, C., Izzo, L. G., Vitale, E., et al. (2023). Anthropogenic dusts influence leaf anatomical and eco-physiological traits of black locust (*Robinia pseudoacacia* l.) growing on Vesuvius volcano. *Forests.* 14 (2), 212. doi: 10.3390/f14020212

De Micco, V., Amitrano, C., Vitaglione, P., Ferracane, R., Pugliese, M., and Arena, C. (2021a). Effect of light quality and ionising radiation on morphological and

nutraceutical traits of sprouts for astronauts' diet. *Acta Astronaut.* 185, 188–197. doi: 10.1016/j.actaastro.2021.05.007

De Micco, V., Aronne, G., Colla, G., Fortezza, R., and De Pascale, S. (2009). Agro-biology for bioregenerative life support systems in long-term space missions: general constraints and the Italian efforts. *J. Plant Interact.* 4 (4), 241–252. doi: 10.1080/17429140903161348

De Micco, V., De Francesco, S., Amitrano, C., and Arena, C. (2021b). Comparative analysis of the effect of carbon-and titanium-ions irradiation on morpho-anatomical and biochemical traits of *Dolichos melanophthalmus* dc. seedlings aimed to space exploration. *Plants.* 10 (11), 2272. doi: 10.3390/plants10112272

Demmig-Adams, B., and Adams, W. W. (2006). Photoprotection in an ecological context: the remarkable complexity of thermal energy dissipation. *New Phytol.* 172, 11–21. doi: 10.1111/j.1469-8137.2006.01835.x

Demotes-Mainard, S., Péron, T., Corot, A., Bertheloot, J., Le Gourrierec, J., Pelleschi-Travier, S., et al. (2016). Plant responses to red and far-red lights, applications in horticulture. *Environ. Exp. Bot.* 121, 4–21. doi: 10.1016/j.envexpbot.2015.05.010

De Pascale, S., Arena, C., Aronne, G., De Micco, V., Pannico, A., Paradiso, R., et al. (2021). Biology and crop production in space environments: challenges and opportunities. *Life Sci. Space Res. (Amst).* 29, 30–37. doi: 10.1016/j.lssr.2021.02.005

Di Gioia, F., De Bellis, P., Mininni, C., Santamaria, P., and Serio, F. (2017). Physicochemical, agronomical and microbiological evaluation of alternative growing media for the production of rapini (Brassica rapa l.) microgreens. *J. Sci. Food Agric.* 97 (4), 1212–1219. doi: 10.1002/jsfa.7852

Dodig, D., Božinović, S., Nikolić, A., Zorić, M., Vančetović, J., Ignjatović-Micić, D., et al. (2019). Image-derived traits related to mid-season growth performance of maize under nitrogen and water stress. *Front. Plant Sci.* 10. doi: 10.3389/fpls.2019.00814

El-Nakhel, C., Pannico, A., Graziani, G., Kyriacou, M. C., Gaspari, A., Ritieni, A., et al. (2021). Nutrient supplementation configures the bioactive profile and production characteristics of three brassica l. microgreens species grown in peat-based media. *Agronomy.* 11 (2), 346. doi: 10.3390/agronomy11020346

Feder, N., and O'brien, T. (1968). Plant microtechnique: some principles and new methods. *Am. J. Bot.* 55, 123–142. doi: 10.2307/2440500

Ghoora, M. D., Babu, D. R., and Srividya, N. (2020). Nutrient composition, oxalate content and nutritional ranking of ten culinary microgreens. *J. Food Compost. Anal.* 91, 103495. doi: 10.1016/j.jfca.2020.103495

Gómez, X., Sanon, S., Zambrano, K., Asquel, S., Bassantes, M., Morales, J. E., et al. (2021). Key points for the development of antioxidant cocktails to prevent cellular stress and damage caused by reactive oxygen species (ROS) during manned space missions. *NPJ Microgravity.* 7, 35. doi: 10.1038/s41526-021-00162-8

Gonçalves, A. C., Nunes, A. R., Falcão, A., Alves, G., and Silva, L. R. (2021). Dietary effects of anthocyanins in human health: a comprehensive review. *Pharmaceuticals.* 14 (7), 690. doi: 10.3390/ph14070690

Ibraheem, N. A., Hasan, M. M., Khan, R. Z., and Mishra, P. K. (2012). Understanding color models: a review. *ARPN J. Sci. Technol.* 2 (3), 265–275.

Jha, S. N. (2010). *Nondestructive evaluation of food quality: theory and practices* (Berlin/Heidelberg, Germany: Springer Science and Business media), 17–40. doi: 10.1007/978-3-642-15796-7_2

Johnson, C. M. (2019). "Microgreens for human nutrition in spaceflight," in *Annual meeting of the American society for gravitational and space research.* (Denver, CO: Published o NTRS - NASA Technical Reports Server).

Jones-Baumgardt, C., Ying, Q., Zheng, Y., and Bozzo, G. G. (2020). The growth and morphology of microgreens is associated with modified ascorbate and anthocyanin profiles in response to the intensity of sole-source light-emitting diodes. *Can. J. Plant Sci.* 101 (2), 212–228. doi: 10.1139/cjps-2020-0060

Kobayashi, Y., Kotilainen, T., Carmona-García, G., Leip, A., and Tuomisto, H. L. (2022). Vertical farming: a trade-off between land area need for crops and for renewable energy production. *J. Clean. Prod.* 379, 134507. doi: 10.1016/j.jclepro.2022.134507

Kyriacou, M. C., De Pascale, S., Kyratzis, A., and Rouphael, Y. (2017). Microgreens as a component of space life support systems: a cornucopia of functional food. *Front. Plant Sci.* 1587. doi: 10.3389/fpls.2017.01587

Kyriacou, M. C., El-Nakhel, C., Pannico, A., Graziani, G., Soteriou, G. A., Giordano, M., et al. (2020). Phenolic constitution, phytochemical and macronutrient content in three species of microgreens as modulated by natural fiber and synthetic substrates. *Antioxidants.* 9 (3), 252. doi: 10.3390/antiox9030252

Leonardi, C., Guichard, S., and Bertin, N. (2000). High vapour pressure deficit influences growth, transpiration and quality of tomato. *fruits. Sci. Hortic.* 84 (3-4), 285–296. doi: 10.1016/S0304-4238(99)00127-2

Lihavainen, J., Keinänen, M., Keski-Saari, S., Kontunen-Soppela, S., Sõber, A., and Oksanen, E. (2016). Artificially decreased vapour pressuredeficit in field conditions modifies foliar metabolite profiles in birch and aspen. *J. Exp. Bot.* 67, 4367–4378. doi: 10.1093/jxb/erw219

Liu, Z., Teng, Z., Pearlstein, D. J., Chen, P., Yu, L., Zhou, B., et al. (2022). Effects of different light-emitting diode illuminations on bioactive compounds in ruby streaks mustard microgreens by ultra-high performance liquid chromatography–High-Resolution mass spectrometry. *ACS Food Sci. Technol.* 2 (9), 1483–1494. doi: 10.1021/acsfoodscitech.2c00193

Lobiuc, A., Vasilache, V., Pintilie, O., Stoleru, T., Burducea, M., Oroian, M., et al. (2017). Blue and red LED illumination improves growth and bioactive compounds contents in acyanic and cyanic *Ocimum basilicum* l. microgreens. *Molecules.* 22 (12), 2111. doi: 10.3390/molecules22122111

Ma, L., Dou, H. L., Wu, Y. Q., Huang, Y. M., Huang, Y. B., Xu, X. R., et al. (2012). Lutein and zeaxanthin intake and the risk of age-related macular degeneration: a systematic review and meta-analysis. *B.J.N.* 107 (3), 350–359. doi: 10.1017/S0007114511004260

Mah, J. J., Llewellyn, D., and Zheng, Y. (2018). Morphology and flowering responses of four bedding plant species to a range of red to far red ratios. *HortScience.* 53 (4), 472–478. doi: 10.21273/HORTSCI12714-17

Malinova, I., Qasim, H., Brust, H., and Fettke, J. (2018). Parameters of starch granule genesis in chloroplasts of arabidopsis thaliana. *Front. Plant Sci.* 9. doi: 10.3389/fpls.2018.00761

McPhee, J. C., and Charles, J. B. (2009). *Human health and performance risks of space exploration missions: evidence reviewed by the NASA human research program* Vol. 3405 (Houston, Texas: National Aeronautics and Space Administration, Lyndon B. Johnson Space Center; Washington, DC).

Mengin, V., Pyl, E.-T., Moraes, T. A., Sulpice, R., Krohn, N., Encke, B., et al. (2017). Photosynthate partitioning to starch in arabidopsis thaliana is insensitive to light intensity but sensitive to photoperiod due to a restriction on growth in the light in short photoperiods. *Plant Cell Environ.* 40 (11), 2608-2627. doi: 10.1111/pce.13000

Modarelli, G. C., Paradiso, R., Arena, C., De Pascale, S., and Van Labeke, M. C. (2022). High light intensity from blue-red LEDs enhance photosynthetic performance, plant growth, and optical properties of red lettuce in controlled environment. *Horticulturae.* 8 (2), 114. doi: 10.3390/horticulturae8020114

Mortazavi, S. M. J., Foadi, M., Mozdarani, H., Haghani, M., Mosleh, S. M., Abolghasemi, P., et al. (2015). Future role of vitamin c in radiation mitigation and its possible applications in manned deep space missions: survival study and the measurement of cell viability. Iran. *J. Radiat. Res.* 13 (1), 55–60. doi: 10.7508/ijrr.2015.01.007

Naidu, K. A. (2003). Vitamin c in human health and disease is still a mystery? an overview. *Nutr. J.* 2, 7. doi: 10.1186/1475-2891-2-7

Navarro, A., Elia, A., Conversa, G., Campi, P., and Mastrorilli, M. (2012). Potted mycorrhizal carnation plants and saline stress: growth, quality and nutritional plant responses. *Sci. Hortic.* 140, 131–139. doi: 10.1016/j.scienta.2012.03.016

Nguyen, T., Tran, T., and Nguyen, Q. (2019). Effects of light intensity on the growth, photosynthesis and leaf microstructure of hydroponic cultivated spinach (Spinacia oleracea l.) under a combination of red and blue LEDs in house. *Int. J. Agric. Technol.* 15 (1), 75–90.

Oguchi, R., Hikosaka, K., and Hirose, T. (2005). Leaf anatomy as a constraint for photosynthetic acclimation: differential responses in leaf anatomy to increasing growth irradiance among three deciduous trees. *Plant Cell Environ.* 28 (7), 916–927. doi: 10.1111/j.1365-3040.2005.01344.x

Paglialunga, G., Proietti, S., Cardarelli, M., Moscatello, S., Colla, G., and Battistelli, A. (2022). Chicory taproot production: effects of biostimulants under partial or full controlled environmental conditions. *Agronomy.* 12 (11), 2816. doi: 10.3390/agronomy12112816

Palozza, P., and Krinsky, N. I. (1992). Antioxidant effects of carotenoids in vivo and *in vitro*: an overview. *Meth. Enzymol.* 213, 403–420. doi: 10.1016/0076-6879(92)13142-k

Paradiso, R., and Proietti, S. (2022). Light-quality manipulation to control plant growth and photomorphogenesis in greenhouse horticulture: the state of the art and the opportunities of modern LED systems. *J. Plant Growth Regul.* 41 (2), 742–780. doi: 10.1007/s00344-021-10337-y

Pattison, P. M., Tsao, J. Y., Brainard, G. C., and Bugbee, B. (2018). LEDs For photons, physiology and food. *Nature.* 563 (7732), 493–500. doi: 10.1038/s41586-018-0706-x

Perchonok, M. H., Cooper, M. R., and Catauro, P. M. (2012). Mission to Mars: food production and processing for the final frontier. *Annu. Rev. Food Sci. Technol.* 3, 311–330. doi: 10.1146/annurev-food-022811-101222

Poulet, L., Fontaine, J. P., and Dussap, C. G. (2016). Plant's response to space environment: a comprehensive review including mechanistic modelling for future space gardeners. *Bot. Lett.* 163 (3), 337–347. doi: 10.1080/23818107.2016.1194228

Poulet, L., Massa, G. D., Morrow, R. C., Bourget, C. M., Wheeler, R. M., and Mitchell, C. A. (2014). Significant reduction in energy for plant-growth lighting in space using targeted LED lighting and spectral manipulation. *Life Sci. Space Res.* 2, 43–53. doi: 10.1016/j.lssr.2014.06.002

Proietti, S., Moscatello, S., Giacomelli, G. A., and Battistelli, A. (2013). Influence of the interaction between light intensity and CO2 concentration on productivity and quality of spinach (Spinacia oleracea l.) grown in fully controlled environment. *A.S.R.* 52 (6), 1193–1200. doi: 10.1016/j.asr.2013.06.005

Proietti, S., Moscatello, S., Villani, F., Mecucci, F., Walker, R. P., Famiani, F., et al. (2019). Quality and nutritional compounds of *Prunus cerasus* l. var. austera fruit grown in central Italy. *Hortic. Sci.* 54 (6), 1005–1012. doi: 10.21273/HORTSCI13960-19

Proietti, S., Paradiso, R., Moscatello, S., Saccardo, F., and Battistelli, A. (2023). Light intensity affects the assimilation rate and carbohydrates partitioning in spinach grown in a controlled environment. *Plants* 12 (4), 804. doi: 10.3390/plants12040804

Renna, M., Stellacci, A. M., Corbo, F., and Santamaria, P. (2020). The use of a nutrient quality score is effective to assess the overall nutritional value of three brassica microgreens. *Foods* 9 (9), 1226. doi: 10.3390/foods9091226

Rosales, M. A., Ruiz, J. M., Hernández, J., Soriano, T., Castilla, N., and Romero, L. (2006). Antioxidant content and ascorbate metabolism in cherry tomato exocarp in relation to temperature and solar radiation. *J. Sci. Food Agric.* 86 (10), 1545–1551. doi: 10.1002/jsfa.2546

Samuolienė, G., Brazaitytė, A., Jankauskienė, J., Viršilė, A., Sirtautas, R., Novičkovas, A., et al. (2013). LED irradiance level affects growth and nutritional quality of brassica microgreens. *Cent. Eur. J. Biol.* 8, 1241–1249. doi: 10.2478/s11535-013-0246-1

Scartazza, A., Moscatello, S., Gavrichkova, O., Buia, M. C., Lauteri, M., Battistelli, A., et al. (2017). Carbon and nitrogen allocation strategy in posidonia oceanica is altered by seawater acidification. *Sci. Total Environ.* 607, 954–964. doi: 10.1016/j.scitotenv.2017.06.084

Shipley, B., and Vu, T. T. (2002). Dry matter content as a measure of dry matter concentration in plants and their parts. *New Phytol.* 153 (2), 359–364. doi: 10.1046/j.0028-646X.2001.00320.x

Stettler, M., Eicke, S., Mettler, T., Messerli, G., Hörtensteiner, S., and Zeeman, S. C. (2009). Blocking the metabolism of starch breakdown products in arabidopsis leaves triggers chloroplast degradation. *Mol. Plant* 2 (6), 1233–1246. doi: 10.1093/mp/ssp093

Tantharapornrerk, N., Vichitsoonthonkul, T., Techavuthiporn, C., and Photchanachai, S. (2023). Growth and antioxidant system of Chinese kale microgreens in response to different illumination of light sources. *N.Z.J. Crop Hortic. Sci.* 51 (1), 108–122. doi: 10.1080/01140671.2021.1958876

Teng, Z., Luo, Y., Pearlstein, D. J., Wheeler, R. M., Johnson, C. M., Wang, Q., et al. (2023). Microgreens for home, commercial, and space farming: a comprehensive update of the most recent developments. *Annu. Rev. Food. Sci. Technol.* 14, 539–562. doi: 10.1146/annurev-food-060721-024636

Tomlins, K., Owori, C., Bechoff, A., Menya, G., and Westby, A. (2012). Relationship among the carotenoid content, dry matter content and sensory attributes of sweet potato. *Food Chem.* 131 (1), 14–21. doi: 10.1016/j.foodchem.2011.07.072

Usenik, V., Fabčič, J., and Štampar, F. (2008). Sugars, organic acids, phenolic composition and antioxidant activity of sweet cherry (Prunus avium l.). *Food Chem.* 107 (1), 185–192. doi: 10.1016/j.foodchem.2007.08.004

Weber, (1999). The role of vitamins in the prevention of osteoporosis–a brief status report. *Int. J. Vitam. Nutr. Res.* 69, 194–197. doi: 10.1024/0300-9831.69.3.194

Wheeler, R. M. (2003). Carbon balance in bioregenerative life support systems: effects of system closure, waste management, and crop harvest index. *Adv. Space Res.* 31, 169–175. doi: 10.1016/S0273-1177(02)00742-1

Wong, C. Y. S., D'Odorico, P., Arain, M. A., and Ensminger, I. (2020). Tracking the phenology of photosynthesis using carotenoid-sensitive and near-infrared reflectance vegetation indices in a temperate evergreen and mixed deciduous forest. *New Phytol.* 226 (6), 1682-1695. doi: 10.1111/nph.16479

Yamamoto, T., Kinoshita, M., Shinomiya, N., Hiroi, S., Sugasawa, H., Matsushita, Y., et al. (2010). Pretreatment with ascorbic acid prevents lethal gastrointestinal syndrome in mice receiving a massive amount of radiation. *J. Radiat. Res.* 51 (2), 145–156. doi: 10.1269/jrr.09078

Yehu, Y., Changjiang, Y., Li, Y., Jinshan, Z., Changjiang, S., Yubin, M., et al. (2015). The influence of light intensity and photoperiod on duckweed biomass and starch accumulation for bioethanol production. *Bioresour. Technol.* 187, 84–90. doi: 10.1016/j.biortech.2015.03.097

Zabel, P., Vrakking, V., Zeidler, C., and Schubert, D. (2022). "Energy and power demand of food production in space based on results of the EDEN ISS Antarctic greenhouse," in *51st International Conference on Environmental Systems ICES-2022-87*, (St. Paul, Minnesota: ICES-2022-87 (ICES Annual report)), 10-14 July 2022.

Zabel, P., Zeidler, C., Vrakking, V., Dorn, M., and Schubert, D. (2020). Biomass production of the EDEN ISS space greenhouse in Antarctica during the 2018 experiment phase. *Front. Plant Sci.* 11. doi: 10.3389/fpls.2020.00656

Zeiger, E., Talbott, L. D., Frechilla, S., Srivastava, A., and Zhu, J. (2002). The guard cell chloroplast: a perspective for the twenty-first century. *New Phytol.* 153, 415–424. doi: 10.1046/j.0028-646X.2001.NPH328.doc.x

Zhang, Q., Ficklin, D. L., Manzoni, S., Wang, L., Way, D., Phillips, R. P., et al. (2019). Response of ecosystem intrinsic water use efficiency and gross primary productivity to rising vapor pressure deficit. *Environ. Res. Lett.* 14 (7), 074023. doi: 10.1088/1748-9326/ab2603

Žnidarčič, D., Ban, D., and Šircelj, H. (2011). Carotenoid and chlorophyll composition of commonly consumed leafy vegetables in Mediterranean countries. *Food Chem.* 129 (3), 1164–1168. doi: 10.1016/j.foodchem.2011.05.097

frontiers | Frontiers in Plant Science

TYPE Original Research
PUBLISHED 31 July 2023
DOI 10.3389/fpls.2023.1229476

Check for updates

OPEN ACCESS

EDITED BY
Cyprien Verseux,
University of Bremen, Germany

REVIEWED BY
Roberta Bulgari,
University of Turin, Italy
Byoung Ryong Jeong,
Gyeongsang National University,
Republic of Korea

*CORRESPONDENCE
Mona Schiefloe
mona.schiefloe@ciris.no
Øyvind Mejdell Jakobsen
oyvind.m.jakobsen@ciris.no

†These authors have contributed equally to this work and share first authorship

RECEIVED 26 May 2023
ACCEPTED 13 July 2023
PUBLISHED 31 July 2023

CITATION
Schiefloe M, Jakobsen ØM, Pannico A, Quadri C and Jost A-IK (2023) From urine to food and oxygen: effects of high and low NH_4^+:NO_3^- ratio on lettuce cultivated in a gas-tight hydroponic facility. *Front. Plant Sci.* 14:1229476. doi: 10.3389/fpls.2023.1229476

COPYRIGHT
© 2023 Schiefloe, Jakobsen, Pannico, Quadri and Jost. This is an open-access article distributed under the terms of the Creative Commons Attribution License (CC BY). The use, distribution or reproduction in other forums is permitted, provided the original author(s) and the copyright owner(s) are credited and that the original publication in this journal is cited, in accordance with accepted academic practice. No use, distribution or reproduction is permitted which does not comply with these terms.

From urine to food and oxygen: effects of high and low NH_4^+:NO_3^- ratio on lettuce cultivated in a gas-tight hydroponic facility

Mona Schiefloe[1*†], Øyvind Mejdell Jakobsen[1*†], Antonio Pannico[2], Claudia Quadri[3] and Ann-Iren Kittang Jost[1]

[1]Centre for Interdisciplinary Research in Space (CIRiS), NTNU Social Research, Trondheim, Norway, [2]Department of Agricultural Sciences, University of Naples Federico II, Portici, Italy, [3]EnginSoft Società per Azioni, Bergamo, Italy

In situ production of food, water and oxygen is essential for long-duration human space missions. Higher plants represent a key element in Bioregenerative Life Support Systems (BLSS), where crop cultivation can be based on water and nutrients recovered from waste and wastewater. Human urine exemplifies an important waste stream with potential to provide crops with nitrogen (N) and other nutrients. Dynamic waste composition and treatment processes may result in mineralized fractions with varying ammonium (NH_4^+) to nitrate (NO_3^-) ratios. In this study, lettuce was cultivated in the unique ESA MELiSSA Plant Characterization Unit, an advanced, gas-tight hydroponic research facility offering controlled environment and continuous monitoring of atmospheric gas composition. To evaluate biological and system effects of nutrient solution NH_4^+:NO_3^- ratio, two crop tests were run with different NH_4^+ to total N ratio (NH_4^+:N) and elevated concentrations of Na^+ and Cl^- in line with a urine recycling scenario. Plants cultivated at 0.5 mol·mol^{-1} NH_4^+:N ($HiNH_4^+$) achieved 50% lower shoot biomass compared to those cultivated at 0.1 mol·mol^{-1} NH_4^+:N ($LoNH_4^+$), accompanied by higher shoot dry weight content and lower harvest index. Analyses of projected leaf area over time indicated that the reduced biomass observed at harvest could be attributed to a lower specific growth rate during the close-to-exponential growth phase. The $HiNH_4^+$ crop produced 40% less O_2 over the full cultivation period. However, normalization of the results indicated a marginal increase in O_2 production per time and per projected leaf area for the $HiNH_4^+$ crop during the exponential growth phase, in line with a higher shoot chlorophyll content. Mineral analysis demonstrated that the biomass content of NH_4^+ and NO_3^- varied in line with the nutrient solution composition. The ratio of consumed NH_4^+ to consumed N was higher than the NH_4^+:N ratio of the nutrient solution for both crop tests, resulting in decreasing NH_4^+:N ratios in the nutrient solution over time. The results provide enhanced insight for design of waste processes and crop cultivation to optimize overall BLSS efficiency and hold valuable potential for improved resource utilization also in terrestrial food production systems.

KEYWORDS

ammonium, nitrate, recycling, oxygen, food production, photosynthesis, life support system

1 Introduction

Human spaceflight missions to remote locations call for on-site food production and resource recirculation. In contrast to Low Earth Orbit, complete resupply of resources from Earth is challenged by increased mission duration and travel distances. Higher plants represent a key element for regeneration of air, water and food for astronauts (Wheeler et al., 2002; Pannico et al., 2022), either as part of stand-alone Bioregenerative Life Support Systems (BLSS), or in a combination with physicochemical methods. The MELiSSA project (Micro Ecological Life Support System Alternative) is an international collaboration led by the European Space Agency (ESA), emphasizing the development of a BLSS to support long-term space missions. In an integrated loop, waste streams from a crew compartment are to be processed by thermophilic, heterotrophic and nitrifying bacteria to provide input to photosynthetic compartments with higher plants and algae to regenerate mineralized nutrients and carbon dioxide (CO_2), and produce food, pure water, and oxygen (O_2) for the crew (Godia et al., 2002). An important objective of the MELiSSA project is to develop mathematical models that can predict critical processes such as plant growth, photosynthesis, and transpiration, based on parameters such as plant species, cultivation conditions, and the processed waste stream fed to the plants.

In a scenario of crop cultivation based on mineralized human waste, urine is a valuable resource due to its high nitrogen (N) content. N is an essential element and a critical input factor for crop cultivation, with profound effects on plant growth and development as a constituent of numerous vital compounds such as nucleic acids, chlorophyll, amino acids, proteins, ATP, phytohormones, auxin and cytokinins (Marschner and Marschner, 2012; Taiz, 2015; De Bang et al., 2021). The use of recycled organic waste for crop cultivation typically requires mineralization of organic compounds by physicochemical and/or microbial processes. N is primarily taken up by plant roots as inorganic ammonium (NH_4^+) and nitrate (NO_3^-) (Marschner and Marschner, 2012; Taiz, 2015), that may be derived from urine. While fresh urine is rich in urea-N (up to 12 g L^{-1}), this compound is rapidly hydrolyzed upon storage in a non-sterile environment to NH_4^+/NH_3 that may be further converted to NO_3^- by physicochemical and/or microbial processes (Udert et al., 2006; Larsen et al., 2021). As the result of this upstream treatment depends on the mineralization strategy and the process conditions, the resulting nutrient solution provided to the plants may vary in the absolute concentrations of NH_4^+ and NO_3^- and the ratio between them. This may in turn affect not only the plant uptake rates of these inorganic N species, but also other physiological and metabolic processes such as uptake of other nutrients, enzyme activity, photosynthesis and respiration, water balance, signaling pathways, leaf expansion, and root architecture - eventually influencing the overall plant growth and crop yield (Guo et al., 2007a; Guo et al., 2007c; Andrews et al., 2013; Liu and Von Wiren, 2017). A nutrient solution containing both NH_4^+ and NO_3^- is typically preferred to optimize plant growth and development rather than using either NO_3^- or NH_4^+ as the sole source of N, although the use of NH_4^+ as the dominant N source should be avoided to reduce risk of ammonium toxicity and reduced plant growth (Roosta and Schjoerring, 2008; Taiz, 2015; Song et al., 2021; Weil et al., 2021; Hameed et al., 2022). Beyond N, urine contains other plant macronutrients such as potassium, phosphorus, sulfur, and lower levels of calcium and magnesium (Udert et al., 2006; Larsen et al., 2021). On the other hand, feeding crops with processed urine introduces non-essential elements such as sodium (Na^+) and chloride (Cl^-). Plants naturally accumulate salts, and the presence of Na^+ and Cl^- in the nutrient solution may affect plant physiology and growth. At some concentrations, NaCl has been demonstrated to act as a eustressor with beneficial effects on crop quality (Kronzucker et al., 2013; Rouphael et al., 2018). However, high concentrations of salt is among the most limiting factors for plant growth and may cause injurious abiotic stress, altering morphological and physiological plant traits and ultimately reducing crop yield (Chinnusamy and Zhu, 2006; Acosta-Motos et al., 2017).

To make possible a new generation of scientific studies related to the higher plant compartment, one of the most complex compartments in the MELiSSA loop, a Plant Characterization Unit (PCU) was recently designed and assembled on the premises of Department of Agricultural Sciences of University of Naples Federico II in Italy as part of the ESA MELiSSA PaCMan (PlAnt Characterization unit for closed life support system – engineering, MANufacturing & testing) activity (Pannico et al., 2022). The PCU is a gas-tight cultivation chamber for characterization of higher plants, offering extensive monitoring and control of the cultivation environment, including its separated hydroponic and atmospheric loops.

Lettuce is a highly relevant species for bioregenerative life support systems with high harvest index, efficiency (per area, time, and volume), and potential yield (edible biomass, O_2 and water), combined with relatively modest horticultural requirements (Berkovich et al., 2004). Lettuce has been successfully cultivated onboard the International Space Station (Khodadad et al., 2020) and represents a healthy and nutritious addition to the human diet, rich in vitamin C, antioxidants, polyphenols and dietary fiber (Khodadad et al., 2020). Furthermore, it is one of the most used vegetables in terrestrial hydroponic cultivation systems (Zhu et al., 2020), illustrating the benefits of a deeper understanding of plant responses to nutrient solutions derived from organic waste in commercial crop production also on Earth, with the potential to improve resource utilization and reduce environmental impact of industrial food production systems.

The underlying hypotheses and scenario of this study was that strategies and operating conditions of upstream waste processing will affect the composition of the mineralized nutrients fed to the plants in a life support system. As these strategies and conditions may be designed and controlled, but also give rise to fluctuations and dynamics, it is critical to understand and predict consequences of nutrient solution composition on crop cultivation. More specifically, urine ammonification and nitrification may result in nutrient solutions with varying concentrations of NH_4^+ and NO_3^-, including their relative ratio, which will impact downstream crop

cultivation. Furthermore, beyond the incoming nutrient streams, nutrient utilization rates inside the plant compartment will dictate the evolution of the nutrient solution in a closed-loop scenario with complete recycling of water, nutrients and non-nutrients. This study aimed at investigating biological and system effects of high and low NH_4^+:N ratios on lettuce cultivated in a urine recycling scenario, exploiting the recently established PCU facility offering controlled hydroponic cultivation conditions and state of the art monitoring of critical parameters such as O_2 production.

2 Materials and methods

2.1 Lettuce seedling production

About 100 lettuce seeds (*Lactuca sativa* L. cultivar 'Grand Rapids') were disinfected in 5% sodium hypochlorite solution for 15 minutes followed by three rinsing cycles in ultrapure water. The disinfected seeds were dispersed onto absorbent paper, moist with ultrapure water and incubated at room temperature under indirect lighting. After 48 hours, germinated seeds with about 1 cm radicle were transferred to Styrofoam trays with vermiculite soaked in nutrient solution prepared according to Peiro et al. (2020) at 0.5X strength, and incubated at 24°C in a dedicated nursery with 65% relative humidity (RH), a light/dark regime of 16/8 hours and a light intensity of 400 ± 50 $\mu mol \cdot m^{-2} \cdot s^{-1}$ (PPFD). Ten days after sowing, 18 equally developed seedlings (evaluated by visual inspection) were selected from the pool of 100 germinated seeds. Each seedling was installed into a bottomless 50 mL test tube (CLS430829, Corning, NY, USA) filled with rockwool (Delta 4G 42/40, Grodan, Roermond, The Netherlands) cut into a cylindrical shape and vertically split in two. The seedling's root system was sandwiched between the two halves of the rockwool column and inserted into the 50 mL tube. The top surface of the rockwool was then covered with grafting mastic (Cortimax, Cisa Adriatica S.r.l., Pescara, Italy) to minimize gas exchange between the root and shoot zones of the cultivation chamber.

2.2 Cultivation chamber and cultivation conditions

For each of the two crop tests (designated $HiNH_4^+$ and $LoNH_4^+$), 18 lettuce plants were cultivated inside the PCU. Within one crop test, all plants shared the same nutrient solution (recirculated within the PCU's hydroponic loop) and the same atmosphere (recirculated within the PCU's atmospheric loop). The plants were cultivated for 28 days inside the PCU chamber to a total plant age of 38 days. The day/night cycle was 16/8 hours, with an average light intensity across the plant positions of 430 $\mu mol \cdot m^{-2} \cdot s^{-1}$ (PPFD represented by 23% blue, 20% green and 57% red light). PPFD and spectral composition were recorded by eighteen spectral scans (one per plant position, measured at a height of 3 cm above the medium surface) using a spectral radiometer (MSC15, Gigahertz-Optik, Türkenfeld, Germany). The largest deviation between this average light intensity and the intensity at any of the plant positions was 68 $\mu mol \cdot m^{-2} \cdot s^{-1}$ (PPFD), corresponding to 16% of the average intensity. The air temperature and RH were automatically controlled as described by Pannico et al. (2022), at 26°C and 50% during the day and 20°C and 70% during the night, respectively. The atmospheric CO_2 concentration was controlled at 1000 ppmv (parts per million by volume) by automatic injection of pure CO_2 during the day phase, while it was allowed to increase during the night phase due to respiration. Atmospheric O_2 concentration started at ambient levels and increased based on plant photosynthesis. The atmospheric O_2 concentration was not controlled beyond one chamber venting per crop test (Day 19) to avoid O_2 levels rising above 25%.

2.3 Nutrient solution preparation, monitoring, and maintenance

The nutrient solutions were based on the recipe described by Peiro et al. (2020) with the exception of i) the NH_4^+:N ratio was either reduced ($LoNH_4^+$ crop test) or increased ($HiNH_4^+$ crop test) using SO_4^{2-} as counter-ion for required charge balancing, and ii) Na^+ and Cl^- levels were increased (both crop tests). Identification of prioritized nutrient solutions for the two PCU crop tests was based on preliminary deep water crop cultivation experiments with various NH_4^+:N ratios (0.00, 0.11, 0.22, 0.44, 0.50 $mol \cdot mol^{-1}$), nutrient solution strengths (0.75, 1.00, 1.25 X) and NaCl concentrations (0, 5 mM). PCU crop cultivation conditions were selected aiming at the presence of NaCl (5 mM) to mimic a urine recycling scenario (see Results section), reduced nutrient solution strength (0.75 X) to minimize negative effects of elevated total ionic strength (maintaining same electrical conductivity for the $LoNH_4^+$ crop test as for the nutrient solution of Peiro et al. (2020), 1.9 mS/cm), and two NH_4^+:N ratios representing considerable differences (high and low) while still providing acceptable plant growth conditions and representing relevant degrees of nitrification in a BLSS perspective (see Results section). The nutrient solutions of the $LoNH_4^+$ and $HiNH_4^+$ crop tests were obtained by mixing the following A and B stock solutions made from reverse osmosis water: $LoNH_4^+$ Stock A consisted of 434 mM $Ca(NO_3)_2$, 90 mM $CaCl_2$, 9.6 mM $FeCl_3$ and 12 mM Na-EDTA. $HiNH_4^+$ Stock A consisted of 213 mM $Ca(NO_3)_2$, 311 mM $CaCl_2$, 9.6 mM $FeCl_3$ and 12 mM Na-EDTA. $LoNH_4^+$ Stock B consisted of 120 mM $MgSO_4$, 420 mM KNO_3, 180 mM KH_2PO_4, 207 mM NH_4NO_3, 187 mM $NaNO_3$, 590 mM NaCl, and micronutrients. $HiNH_4^+$ Stock B consisted of 120 mM $MgSO_4$, 420 mM KNO_3, 415 mM $(NH_4)_2SO_4$, 180 mM KH_2PO_4, 107 mM NH_4NO_3, 315 mM Na_2SO_4, 145 mM NaCl, and micronutrients. Micronutrients (part of Stock B) were 2.4 mM H_3BO_3, 0.42 mM $ZnSO_4$, 96 µM $CuSO_3$, 0.6 mM $MnSO_4$, and 60 µM H_2MoO_4. For the $LoNH_4^+$ crop test, $LoNH_4^+$ A and B stock solutions were added at a 1:1 ratio to achieve an electrical conductivity of 1.9 $mS \cdot cm^{-1}$ at startup, similar to that of Peiro et al. (2020). This resulted in a total N concentration of 11 mM. For the $HiNH_4^+$ crop test, $HiNH_4^+$ A and B stock solutions were added at a 1:1 ratio to achieve the same total N concentration (11 mM). This resulted in an electrical conductivity of 2.2 $mS \cdot cm^{-1}$ at startup, due to higher concentrations of SO_4^{2-} used for charge balancing. The measured ion concentrations, pH and EC of

both nutrient solutions are summarized in Table 1. The total liquid volume in the hydroponic loop was 265 - 275 L throughout both crop tests.

Water quality of the recirculating nutrient solution was continuously monitored, including pH (2 x Endress+Hauser Orbisint CPS11D Memosens, Germany), electrical conductivity (EC; 2 x Endress+Hauser Indumax CLS50D, Germany), dissolved O_2 (Mettler Toledo InPro 6860i, Switzerland), dissolved CO_2 (Labolytic optical CO_2 sensor 0-15 mg/L, Trondheim, Norway), and nitrate (Endress+Hauser Viomax CAS51D, Germany, installed in an at-line configuration with auto-sampling and auto-dilution of the nutrient solution). Nutrient solution temperature was continuously monitored and automatically controlled at 18 ± 0.5°C. For both crop tests, pH was adjusted to 5.9 at startup using 0.5 M H_2SO_4 and then maintained at 5.9 by automatic addition of 0.5 M KOH throughout both crop tests (no addition of acid necessary during the cultivation period). Throughout both crop tests, the actual pH of the nutrient solution typically deviated less than 0.05 pH units from the set-point, and never more than 0.2 pH units. During both crop tests, nutrient stock solutions A and B were automatically fed at a 1:1 ratio to maintain a constant NO_3^- concentration. The recirculating nutrient solution was mechanically filtered in three steps with reducing pore size from 1.6 to 0.45 µm, using filter cartridges (PP3 Sartopure - Sartobran, Sartorius, Goettingen, Germany). The filtration unit was implemented between the plant cultivation chamber and the stirred tank holding the nutrient solution that was continuously fed to the plants.

2.4 Data collection, sampling, and analysis

Atmospheric concentrations of O_2 and CO_2 inside the cultivation chamber were continuously measured by an O_2/CO_2 gas analyzer (California Analytical Instruments, 700 LX NDIR/O_2, Orange, CA, USA). Additionally, the O_2 and CO_2 concentrations of the pressure compensation system's gas tank were measured at crop test start and end, and before and after chamber venting. The amount of atmospheric gas inside the PCU was determined continuously based on ideal gas law, a total atmospheric volume of 4.9 m^3, and continuously measured gas pressure and temperature. This allowed computation of daily atmospheric leak rates and plant O_2 production (Pannico et al., 2022). To keep the air humidity constant, the water produced by the plant transpiration was condensed and collected (Pannico et al., 2022). During the crop tests presented in this study, the injection rates of CO_2 and water into the atmospheric loop were inaccurate, unfortunately preventing accurate mass balances for CO_2 and water and thereby also preventing calculation of consumed amounts of CO_2 and produced amounts of water.

TABLE 1 Characterization of the $LoNH_4^+$ and $HiNH_4^+$ nutrient solutions at start (0 days after transplant (DAT)) and end (28 DAT) of each crop test.

	$LoNH_4^+$		$HiNH_4^+$	
	0 DAT	28 DAT	0 DAT	28 DAT
NO_3^- [mM]	9.7	9.7	5.6	5.6
NH_4^+ [mM]	1.3	0.2	5.3	1.6
NO_2^- [mM]	0.0	0.0	0.0	0.5
Total N [mM]	11.0	10.0	10.9	7.8
HPO_4^{2-} [mM]	0.8	0.7	0.9	0.7
K^+ [mM]	3.7	3.1	3.5	7.4
Ca^{2+} [mM]	4.6	6.5	4.8	4.6
Mg^{2+} [mM]	0.7	0.8	0.7	0.6
SO_4^{2-} [mM]	0.8	0.9	4.9	4.7
Cl^- [mM]	4.5	5.2	4.7	4.2
Na^+ [mM]	5.1	6.4	4.9	4.8
NH_4^+:NO_3^- [mol·mol^{-1}]	0.14	0.03	0.95	0.28
NH_4^+:N [mol·mol^{-1}]	0.12	0.02	0.49	0.20
Na:N [mol·mol^{-1}]	0.46	0.64	0.46	0.62
Cl:N [mol·mol^{-1}]	0.41	0.52	0.43	0.54
K:N [mol·mol^{-1}]	0.33	0.31	0.32	0.96
pH	5.9	5.9	5.9	5.9
EC [mS·cm^{-1}]	1.9	1.9	2.2	2.3

Top-view images of the 1.2 m × 1.5 m cultivation chamber floor were acquired every hour (FLIR Blackfly S BFS-U3-200S6C-C @ 70 dpi), and projected leaf area as observed from above was calculated for images acquired every second day based on image segmentation by color. Projected Leaf Area Index (PLAI) was calculated as the measured projected leaf area of all 18 plants (m^2) per total cultivation area (m^2) (Zheng and Moskal, 2009). SPAD index for indication of chlorophyll content (average of ten measurements per plant; SPAD-502, Minolta Corp. Ltd, Osaka, Japan), dark-adapted chlorophyll fluorescence for the maximum quantum yield of photosystem II (F_v/F_m) (average of two measurements per plant; Plant Stress Kit, Opti-Sciences), and leaf color index (average of three measurements per plant; Chroma Meter CR-400, Konika Minolta) were measured immediately after opening the cultivation chamber at day of harvest. Fresh weight of shoot and stem, and leaf number were determined for each plant by destructive sampling. Additionally, total leaf area of each plant was determined from top-view images of the plant's individual leaves (Canon EOS 90D + Tamron SP 35 mm @ 59 dpi) based on image segmentation by color.

The lead taproot of each plant was isolated and imaged (Canon EOS 90D + Tamron SP 35 mm @ 294 dpi for $LoNH_4^+$ and 334 dpi for $HiNH_4^+$) in a tray with water. The lead taproot was defined as the medial root with the largest diameter in the basal zone, not considering the diameter of the laterals. Root length, diameter and number of links and forks were analyzed with WinRhizo (Pro 2021a, Regent Instruments Inc.). Following counting of leaf number and determination of shoot fresh weight (FW) of each plant, shoots and roots were oven-dried at 60°C until constant weight was reached for determination of dry weight (DW) per plant. Total plant DW was calculated as shoot DW + root DW, while harvest index was calculated as shoot DW per total plant DW. Dried samples of shoots and roots were analyzed for total carbon (C) and N content via combustion analysis by a Micro Elemental Analyser UNICUBE® (Elementar, Langenselbold Hesse, Germany) equipped with a thermal conductivity detector. Leaf soluble cations and anions were determined by liquid ion exchange chromatography (ICS-3000, Dionex, Sunnyvale, CA, USA) as described by Pannico et al. (2019).

Every two days, nutrient solution samples (25 mL) were extracted from the hydroponic loop for offline analysis. Nutrient ion concentrations were determined by ion exchange chromatography (ICS 3000 Dionex) and the results were smoothed by moving average to filter out noise from analysis uncertainty. N mass balance was calculated based on measured parameters at the start and end of each crop test, including concentrations of inorganic N in the nutrient solution (measured via optical sensor and ion chromatography methods described above), total liquid volume, total shoot and root biomass and their N content, in addition to the amount of nutrient stock solutions introduced and samples removed throughout the crop test.

Statistical analyses were performed with SPSS (IBM SPSS version 28.0.0.0), Anova with Tukey HSD post-test, tests of normality, Independent Samples t-test and Mann Whitney U test.

3 Results

Building on the background presented in the introduction, the results section first presents the experiment rationale with respect to nutrient solution composition and cultivation conditions. Representing the first scientific paper detailing crop cultivation results from the recently established PCU facility, plant growth and selected scientific datasets offered by this facility are then illustrated on a high level, before being explored in more detail to present effects of crop cultivation in low vs. high NH_4^+:N ratio.

3.1 Urine recycling scenario: Experiment rationale and nutrient solution design

The experiment rationale was built on the hypothesis presented in the introduction that both design and natural dynamics of upstream waste processing may result in mineralized waste streams with different NH_4^+:NO_3^- ratios, which in turn may affect the biology of a downstream plant compartment and thus the overall BLSS performance. Effects of different NH_4^+:NO_3^- ratios in the nutrient solution were explored in a mineralized urine scenario, using NH_4^+ and NO_3^- as the sole N sources. Two crop tests (two treatments), designated $LoNH_4^+$ and $HiNH_4^+$, were performed with NH_4^+ to total N ratios (NH_4^+:N) of 0.1 and 0.5 mol·mol^{-1}, respectively. Relating to a foreseen upstream nitrification process, the $LoNH_4^+$ scenario (0.1 mol·mol^{-1} NH_4^+:N) represents nearly complete nitrification, while the $HiNH_4^+$ scenario (0.5 mol·mol^{-1} NH_4^+:N) represents nitrification without increased alkalinity and thus limited by redox, as reviewed by Larsen et al. (2021). At the same time, these scenarios represent considerable different, low and high NH_4^+:N ratios for lettuce cultivation (Zhu et al., 2020; Du et al., 2022; Hameed et al., 2022) while still avoiding the use of NH_4^+ as the dominant N source to limit the potential of ammonium toxicity and thereby allow acceptable growth (see Materials and methods). To allow direct comparison of results, total N concentration was identical at startup of both crop tests (11 mM). Capitalizing on a state-of-the-art nutrient monitoring and control system, the NO_3^- concentration was kept constant (9.7 mM in $LoNH_4^+$; 5.6 mM in $HiNH_4^+$) throughout each of the two crop tests to minimize effects of the absolute NO_3^- concentration itself. This allowed the NH_4^+:N ratio to change throughout the cultivation period depending on the total consumption of NH_4^+ and NO_3^- in the system, demonstrating the development of the NH_4^+:N ratio over time.

In line with a urine recycling scenario, the crop tests were performed with an elevated NaCl concentration of 5 mM, representing a Na:N concentration ratio of 0.46 mol·mol^{-1}. This ratio was designed based on typical Na:N ratios of mineralized urine. While fresh urine is typically characterized by 0.17 mol·mol^{-1} Na:N and Cl:N (adapted from Udert et al., 2006), several reports illustrate ratios of approximately 0.25 mol·mol^{-1} in urine-based fertilizer solutions (adapted from Bonvin et al., 2015; Mauerer et al., 2018; Halbert-Howard et al., 2021). However, the final composition of the mineralized nutrient solutions depends on urine storage and ammonification and nitrification processes. As urine is prone to

ammonia volatilization, resulting Na:N and Cl:N ratios may be considerably elevated - exemplified by the real stored urine fraction by Udert and Wachter (2012) with Na:N and Cl:N ratios of 0.5 mol·mol^{-1}. Thus, the Na:N and Cl:N concentration ratios used in this study represent a urine-based nutrient solution, accounting for effects by urine storage and processing. However, effects of potential Na^+ accumulation over time in a closed loop system are not accounted for in this study, as such predictions would benefit from more insight in Na uptake ratios as function of nutrient solution composition and cultivation conditions.

Beyond NH_4^+/NO_3^- and Na^+/Cl^-, the two crop tests were run with similar concentrations of macro- and micronutrients, except for SO_4^{2-} used for charge balancing of NH_4^+/NO_3^-. The total strength of the nutrient solutions was designed so that the total electrical conductivity of the $LoNH_4^+$ nutrient solution at start was identical to that of Peiro et al. (2020) (1.9 mS·cm^{-1}) used for similar MELiSSA studies of hydroponic lettuce cultivation (resulting in an electrical conductivity of 2.2 mS·cm^{-1} for the $HiNH_4^+$ nutrient solution due to the elevated requirement of SO_4^{2-} for charge balancing). The resulting nutrient solutions based on the above design criteria are illustrated in Table 1.

3.2 Crop cultivation in the ESA MELiSSA Plant Characterization Unit

The results reported in this paper were obtained in the recently established ESA MELiSSA Plant Characterization Unit (PCU), in which 18 lettuce plants were hydroponically cultivated as deep-water culture for 28 days after transplant (DAT), to a total age of 38 days, across a 1.8 m^2 plant cultivation area (Figure 1). Extensive monitoring and control systems provided stable cultivation conditions, including atmospheric temperature and RH, and nutrient solution temperature, pH and NO_3^- concentration (see Materials and methods, Table 1; Figure 3). The closed nature of the atmospheric loop combined with continuous monitoring of atmospheric O_2 and CO_2 concentrations represent the basis for determination of O_2 production and CO_2 consumption by the plants. Atmospheric leak rates in percent gas volume per hour were calculated daily and demonstrated a stable and high system tightness with an average leak rate of 0.082 ± 0.017%·h^{-1} and 0.095 ± 0.022%·h^{-1} for the $LoNH_4^+$ and $HiNH_4^+$ crop tests, respectively. The atmospheric O_2 concentration increased during the day phase resulting from photosynthesis, while it decreased during the night phase due to respiration (Figure 2). As the O_2 production during the day phase exceeds the O_2 consumption during the night phase, atmospheric O_2 gradually increased throughout the crop tests creating a need to vent the cultivation chamber to stay below 25% O_2 for safety reasons (performed at Day 19 for both crop tests). Atmospheric CO_2 was controlled at a minimum of 1000 ppm during the day phase, while it increased due to respiration during the night phase (up to 2140 ppm during the $LoNH_4^+$ crop test). As the PCU chamber is sealed and only opened for venting and reduction of atmospheric O_2 concentration, sampling or physical inspection of the plants is not possible during a crop test. To demonstrate biomass development, Projected Leaf Area Index (PLAI) was calculated based on top-view images acquired by the PCU's internal color camera (Figure 4). To further indicate differences in biomass development over time (Figure 4) despite the lack of true biomass measurements, PLAI was used as a basis for calculating a specific growth rate, here introduced as μ_{PLAI}, according to Equation 1 where t symbolizes time (in DAT).

$$\mu_{PLAI} = \frac{\frac{d(PLAI)}{d(t)}}{PLAI} \qquad \text{Equation 1}$$

3.3 Plant development and physiology at high and low NH_4^+:NO_3^- ratios

3.3.1 Shoot development over time as observed by non-destructive methods

A relatively stable μ_{PLAI} during the first 16 - 18 days indicates close to exponential growth for plants in both the $HiNH_4^+$ crop test and the $LoNH_4^+$ crop test in this period. From approximately 20 DAT, as the plants mature and start to overlap, the PLAI-based specific growth rates of both treatments coincide and decrease (Figure 4). Regression analysis of PLAI from 0 to 16 DAT was performed using exponential trendlines (Figure 4; R^2 factors > 0.999), demonstrating a reduced μ_{PLAI} for plants growing in the $HiNH_4^+$ nutrient solution (0.18 per day) compared to that of $LoNH_4^+$ (0.22 per day). The initial PLAI of $HiNH_4^+$ and $LoNH_4^+$ plants were similar due to identical germination and seedling phases (both 0.010 m^2·m^{-2} at 2 DAT). The final PLAI of the $LoNH_4^+$ crop test at 28 DAT reached 0.70 m^2·m^{-2} corresponding to a projected leaf area of 1.3 m^2, while corresponding values of $HiNH_4^+$ were 44% lower with 0.39 m^2·m^{-2} PLAI and 0.71 m^2 projected leaf area. Closer inspection of the PLAI of the two crops illustrate that their differences stayed below approximately 20% during the first 10 days in the PCU, before it increased gradually up to approximately 45% at 18 DAT and remained at this level throughout the rest of the cultivation period.

3.3.2 Root and shoot biomass and morphology at harvest

In line with the differences demonstrated by non-destructive PLAI analysis, detailed inspection of the plants after destructive sampling at 28 DAT illustrated a total leaf area of the $HiNH_4^+$ crop which was 50% lower than that of the $LoNH_4^+$ crop (3.5 m^2 vs. 7.0 m^2, respectively, for the 18 plants; Table 2). The results demonstrate that the shoot biomass was affected in a similar way, with the $HiNH_4^+$ plants having 58% lower shoot fresh weight and 40% lower shoot dry weight compared to the $LoNH_4^+$ plants. The difference in these numbers illustrate a higher shoot dry weight content of the $HiNH_4^+$ plants compared to the $LoNH_4^+$ plants (10% vs. 7%, respectively). Furthermore, the $HiNH_4^+$ plants developed a significantly lower number of leaves (35%) compared to the $LoNH_4^+$ group.

The dry root biomass difference between the two crops (19% lower for $HiNH_4^+$ plants) was smaller than the shoot dry biomass difference (40% lower for $HiNH_4^+$), illustrating a higher root:shoot ratio and a lower harvest index of the $HiNH_4^+$ plants compared to those of $LoNH_4^+$ (Table 2). Following harvest and destructive sampling, the lead taproot of each plant (see Materials and methods) was isolated, imaged, and analyzed. The taproots of the $HiNH_4^+$ and $LoNH_4^+$ plants demonstrated considerable differences,

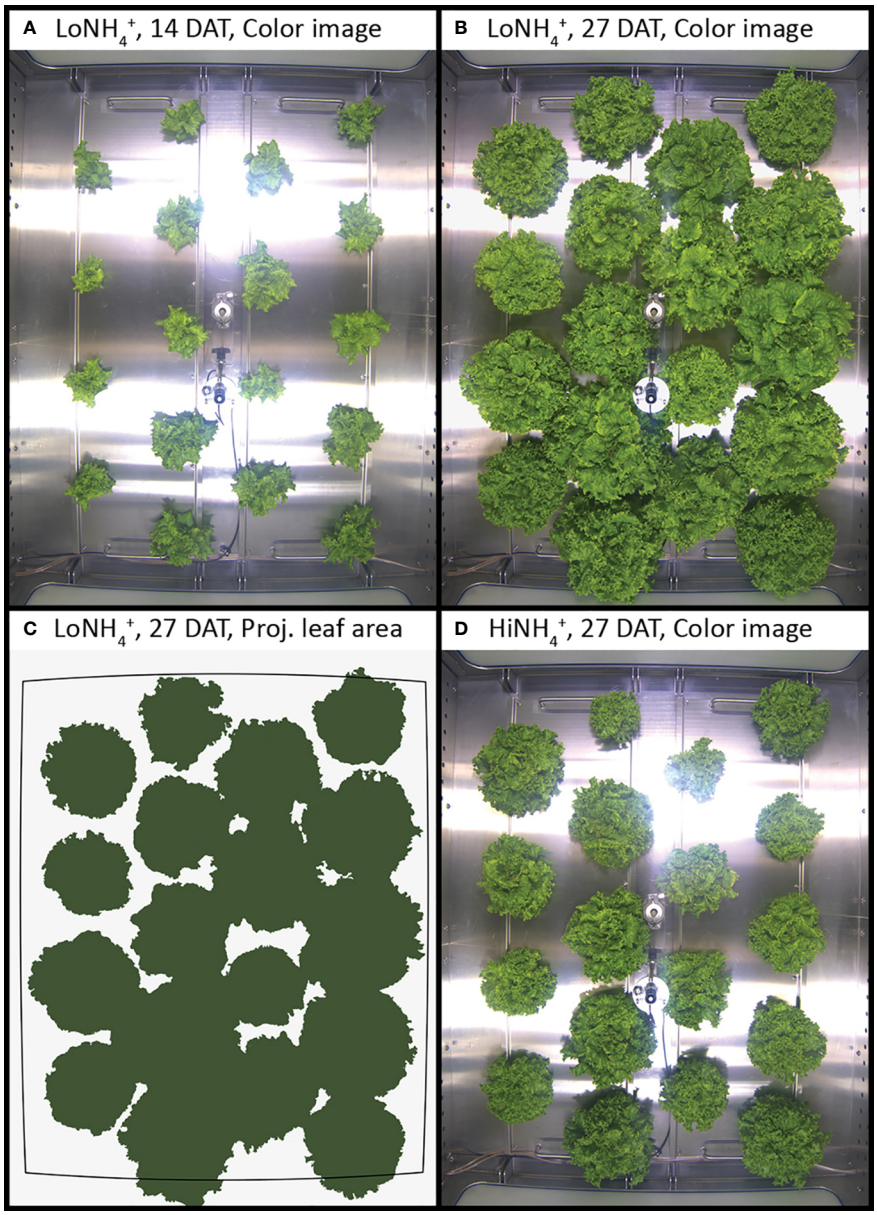

FIGURE 1
Top-view color images of lettuce inside the PCU cultivation chamber at 14 and 27 days after transplant (DAT), cultivated in $LoNH_4^+$ **(A, B)** and $HiNH_4^+$ nutrient solution **(D)**. Example illustrating image segmentation for determination of projected leaf area **(C)**.

as qualitatively indicated in Figure 5. In average, the lead taproots of $HiNH_4^+$ were shorter (55% reduction in total length, including both mother root and lateral roots), thinner (15% reduction in average diameter) and less branched (57% less forks) than those of the $LoNH_4^+$ plants.

3.3.3 Leaf chlorophyll content, color index and F_v/F_m at harvest

Dark-adapted chlorophyll fluorescence measurements of the maximum quantum yield of photosystem II (F_v/F_m) were identical for both treatments (Table 3), while an elevated SPAD index indicated a higher chlorophyll content of the leaves of the $HiNH_4^+$ plants. Color measurements illustrated significant differences as evaluated by the L*a*b color space, with the $HiNH_4^+$ leaf color shifted more towards green compared to the color of the $LoNH_4^+$ leaves.

3.3.4 Nutrient ion and element composition of shoots and roots at harvest

Nutrient ion and element analyses of lettuce shoot and root biomass harvested at 28 DAT demonstrated considerable differences between plants cultivated in the two different nutrient solutions (Table 4). The biomass content of NO_3^- and NH_4^+ varied in line with their concentrations and ratios in the nutrient solutions. The $HiNH_4^+$ plants exhibited an NH_4^+ root content nearly three

10.3389/fpls.2023.1229476

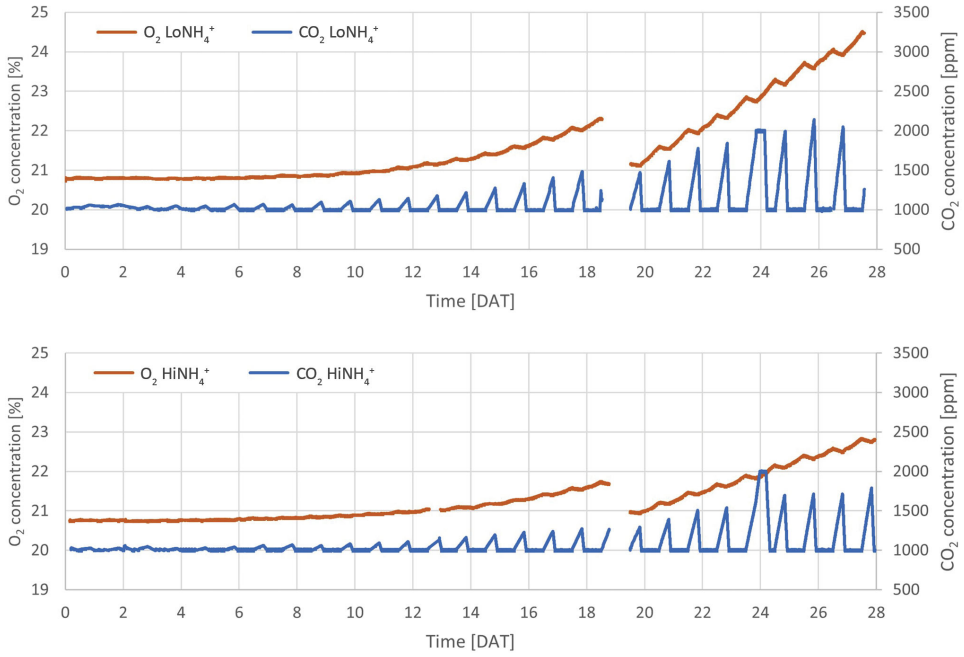

FIGURE 2
Absolute concentrations of atmospheric O_2 and CO_2 throughout the $LoNH_4^+$ (upper graph) and $HiNH_4^+$ (lower graph) crop tests. Missing data from 19 DAT represents a venting event in which the cultivation chamber was opened to reduce the O_2 concentration.

times higher and a NO_3^- shoot and root content 7 – 8 times lower than that of the $LoNH_4^+$ plants. Considering total N, the most significant differences were observed for the roots, for which the total N content was 28% higher in the $HiNH_4^+$ plants. Additionally, the C content of $HiNH_4^+$ plants was higher than that of the $LoNH_4^+$ plants (9% higher in shoot content and 15% higher in root content). The content of other nutrient ions was generally lower in plants cultivated in $HiNH_4^+$ nutrient solution compared to those cultivated in $LoNH_4^+$. This includes the cations K^+ (52% lower shoot content and 36% lower root content), Na^+ (32% lower shoot

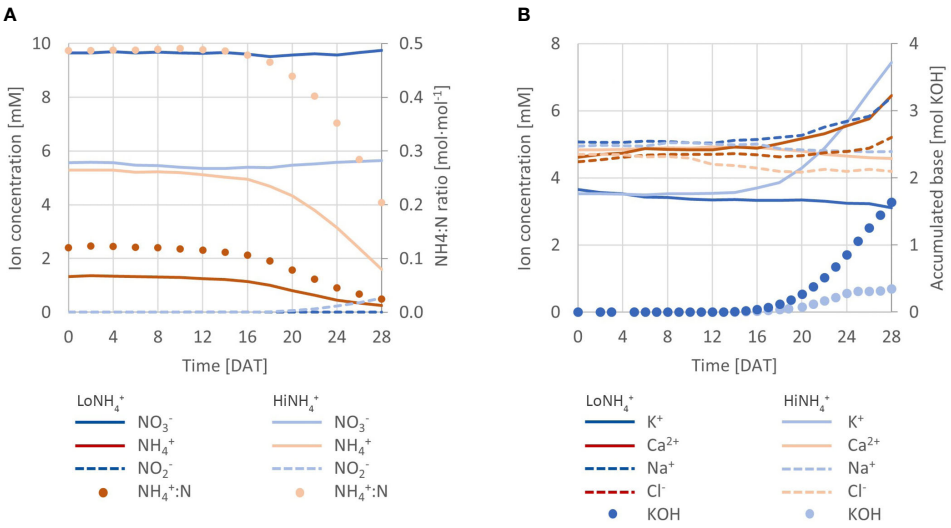

FIGURE 3
(A) Measured concentration of NO_3^-, NH_4^+, and NO_2^- throughout the $LoNH_4^+$ and $HiNH_4^+$ crop tests (lines; left Y-axis), in addition to the ratio of NH_4^+ to total N (NH_4^+:N; dots; right Y-axis). **(B)** Development of K^+, Ca^{2+}, Na^+ and Cl^- concentrations in the nutrient solutions of both crop test (lines; left Y-axis), in addition to accumulated addition of base (KOH; dots; right Y-axis).

10.3389/fpls.2023.1229476

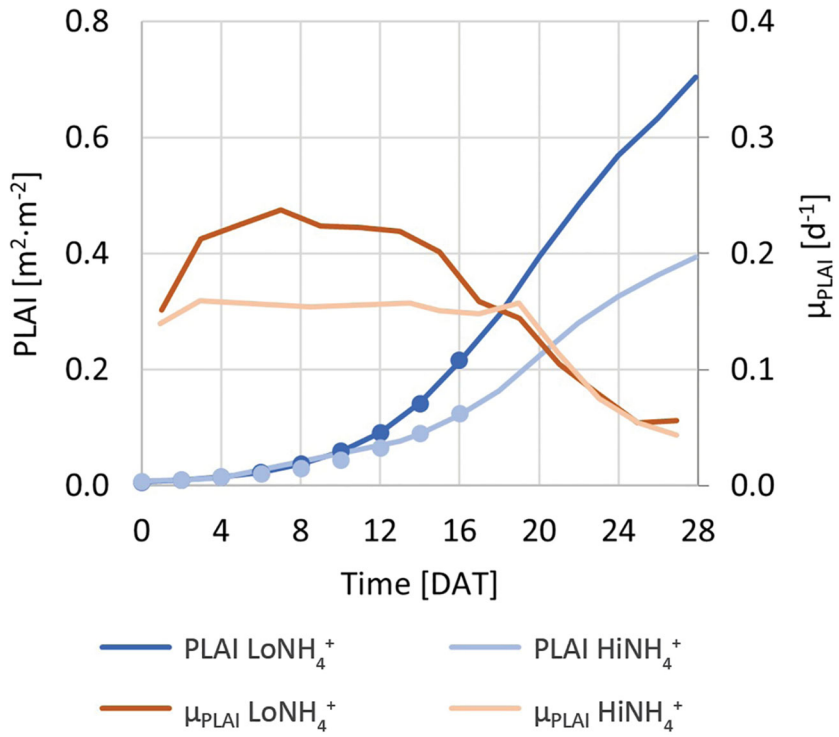

FIGURE 4
Blue solid lines (left Y-axis): PLAI (Projected Leaf Area Index) of the $LoNH_4^+$ and $HiNH_4^+$ crop tests. Blue circles (left Y-axis): Trendlines based on exponential regression of a subset of the PLAI dataset from 0 to 16 DAT (coinciding with the PLAI dataset in blue solid lines). Red lines (right Y-axis): PLAI-based specific growth rate, μ_{PLAI}, of the $LoNH_4^+$ and $HiNH_4^+$ plants.

content and 22% lower root content), and Mg^{2+} (47% lower shoot content). Ca^{2+} illustrated the same trend (55% lower shoot content and 17% lower root content in $HiNH_4^+$) although the differences were not statistically significant due to high variability in the results. Reduced nutrient ion content of $HiNH_4^+$ plants could also be observed for the anions HPO_4^{2-} (44% lower shoot content) and Cl^- (72% lower root content), while no statistically significant differences could be observed for SO_4^{2-}.

3.4 Crop performance and system dynamics at high and low NH_4^+:NO_3^- ratios

3.4.1 O_2 production

Continuous monitoring of the atmospheric O_2 and CO_2 concentrations inside the cultivation chamber illustrated O_2 production during the day (when CO_2 was controlled at 1000 ppm by automatic CO_2 injection), and O_2 consumption and CO_2

TABLE 2 Biomass characteristics of plants from the $LoNH_4^+$ and $HiNH_4^+$ crop tests, measured at harvest (28 DAT).

	$LoNH_4^+$	$HiNH_4^+$	Statistical significance
Shoot fresh weight per plant [g]	289 ± 122	121 ± 51	$p < 0.01$
Shoot dry weight per plant [g]	19 ± 5	11 ± 4	$p < 0.01$
Shoot dry weight content [%]	6.9 ± 1.3	9.8 ± 1.6	$p < 0.01$
Root dry weight per plant [g]	2.4 ± 0.7	1.9 ± 0.6	$p < 0.05$
Total dry weight per plant [g]	21 ± 6	13 ± 4	$p < 0.01$
Harvest index	0.88 ± 0.02	0.85 ± 0.02	$p < 0.01$
Root:shoot ratio	0.14 ± 0.02	0.19 ± 0.03	$p < 0.01$
Stem diameter per plant [mm]	18 ± 3	15 ± 3	$p < 0.01$
Leaf number per plant	40 ± 19	26 ± 8	$p < 0.05$
Total leaf area per plant [cm^2]	3907 ± 724	1961 ± 712	$p < 0.01$

All values are tabulated as mean value ± standard deviation based on separate analyses of 18 individual plants from each crop test. Statistical significance between the two crop tests is indicated as p-values. The shoot dry weight content was calculated as shoot dry weight divided by shoot fresh weight, the harvest index was calculated as shoot dry weight divided by total dry weight, while the root:shoot ratio was calculated based on dry weight.

10.3389/fpls.2023.1229476

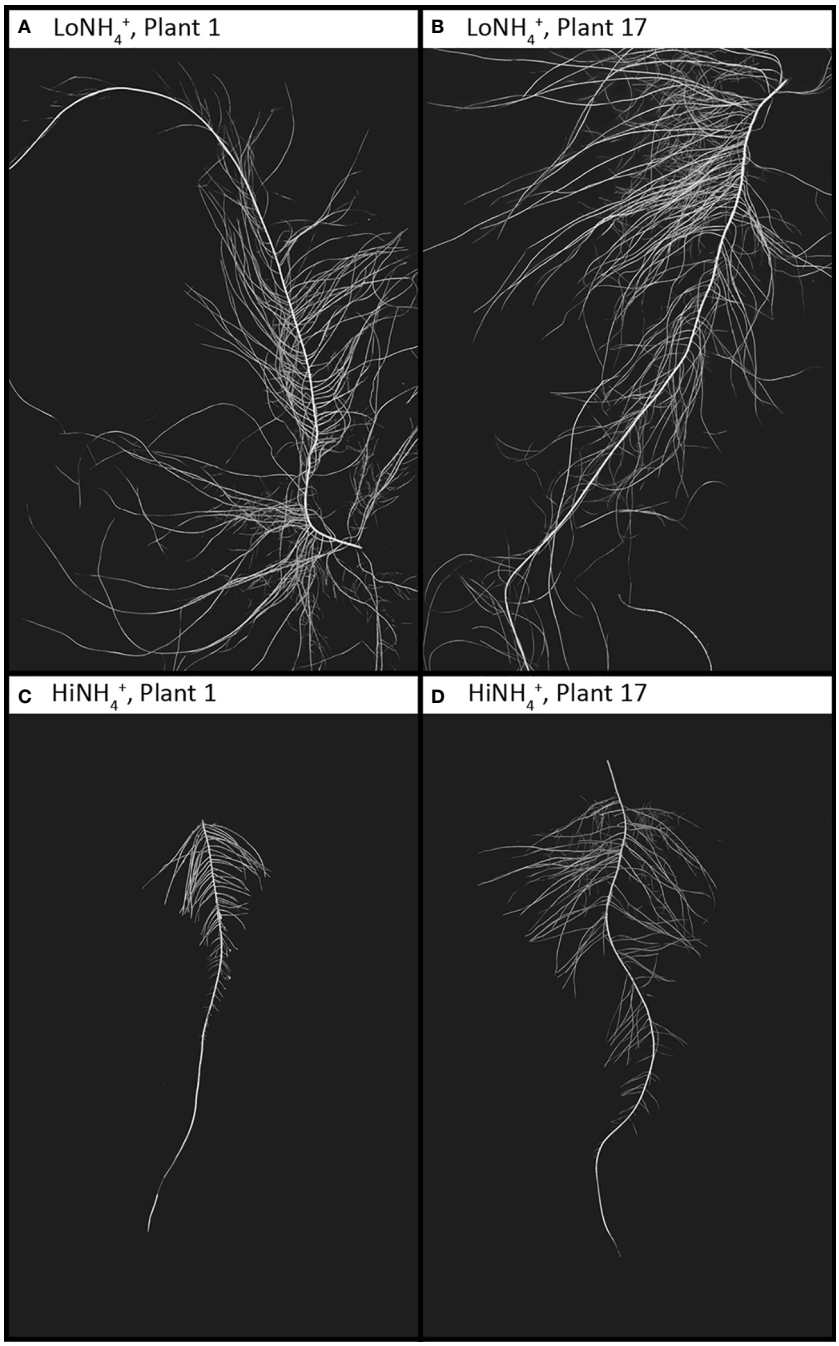

FIGURE 5
Lead taproots of two example $LoNH_4^+$ plants **(A, B)** and two $HiNH_4^+$ plants **(C, D)** from harvest at 28 DAT. All images are represented at the same resolution, covering a 20 x 30 cm area. Root and background contrast and color levels have been modified from the raw images to enhance root morphology.

production during the night (Figure 2). Detailed inspection of the datasets illustrates an immediate increase in atmospheric CO_2 concentration and a corresponding decrease in O_2 starting from the time at which the cultivation chamber LEDs were turned off, as illustrated in Figure 6A, detailing the first two days after the chamber venting. Reversely, an immediate decrease of CO_2 concentration and increase of O_2 was initiated when the LEDs were reactivated at the end of the night phase. During the 16-hour day phase of the 21st day (20 DAT), the O_2 concentration of the cultivation chamber increased 0.48 vol-% in the $LoNH_4^+$ crop test, and 0.26 vol-% in the $HiNH_4^+$ crop test. During this day, the $LoNH_4^+$ plants covered a 0.71 m^2 cultivation area, while the $HiNH_4$ plants covered 0.40 m^2 (as evaluated by projected leaf area). During the following 8-hour night phase, the CO_2 concentration increased linearly to 1614 ppm ($LoNH_4^+$) and 1391 ppm ($HiNH_4^+$) (with no injection of CO_2). After reactivating the LEDs, the atmospheric CO_2 concentration returned to 1000 ppm after 1.5 hours ($LoNH_4^+$) and 1.6 hours ($HiNH_4^+$) of daylight. Corresponding analyses at the end

TABLE 3 F_v/F_m (average of two measurements per plant), SPAD (average of ten measurements per plant) and Color index (average of three measurements per plant) values of the 18 $LoNH_4^+$ and 18 $HiNH_4^+$ plants as measured at harvest (28 DAT).

Parameter	$LoNH_4^+$	$HiNH_4^+$	Statistical significance
F_v/F_m	0.83 ± 0.01	0.83 ± 0.01	*Not sign.*
SPAD index	20 ± 3	23 ± 2	$p < 0.01$
Color index L	53 ± 3	51 ± 3	*Not sign.*
Color index a	-18.8 ± 0.5	-18.3 ± 0.5	$p < 0.01$
Color index b	34.3 ± 1.3	32.6 ± 1.8	$p < 0.01$

All values are tabulated as mean value ± standard deviation. Statistical significance between the two treatments is indicated as p-values.

of the crop tests demonstrated an increase in O_2 concentration of 0.59 vol-% by the $LoNH_4^+$ plants (1.21 m^2 projected leaf area), and 0.33 vol-% by the $HiNH_4^+$ plants (0.71 m^2 projected leaf area) during the day phase of the 28th day. The total O_2 amount inside the PCU atmospheric loop and its pressure compensation system was precisely determined at the time of cultivation chamber closing and opening (see Materials and methods). Compensating for the accurately determined chamber gas leaks, this allows detailed calculations of the O_2 amount produced by the plants during the two phases of each crop test before (0 - 18 DAT) and after (20 - 28 DAT) chamber venting (totaling 26.6 days; Table 5). Considering the absolute O_2 production, the $HiNH_4^+$ plants produced 34% less O_2 during the first phase (0 - 18 DAT) and 43% less O_2 during the second phase (20 - 28 DAT) compared to the $LoNH_4^+$ plants.

TABLE 4 Average shoot and root nutrient ion and element content of the 18 $LoNH_4^+$ and 18 $HiNH_4^+$ lettuce plants as measured at harvest (28 DAT).

		$LoNH_4^+$	$HiNH_4^+$	Statistical significance
Shoots	Total C	382 ± 11	416 ± 9	$p < 0.01$
	Total N	39 ± 7	34 ± 5	$p < 0.05$
	NO_3-N	6.0 ± 2.6	0.8 ± 0.3	$p < 0.01$
	NH_4-N	1.0 ± 0.3	1.1 ± 0.2	*Not sign.*
	PO_4-P	4.8 ± 1.1	2.7 ± 0.5	$p < 0.01$
	K^+	71 ± 15	34 ± 6	$p < 0.01$
	Ca^{2+}	3.8 ± 0.7	1.7 ± 0.3	*Not sign.*
	Mg^{2+}	1.9 ± 0.3	1.00 ± 0.14	$p < 0.01$
	SO_4-S	1.1 ± 0.3	1.3 ± 0.3	*Not sign.*
	Na^+	4.6 ± 0.6	3.1 ± 1.4	$p < 0.01$
	Cl^-	20 ± 5	17 ± 3	*Not sign.*
Roots	Total C	335 ± 19	384 ± 6	$p < 0.01$
	Total N	56 ± 2	72 ± 5	$p < 0.01$
	NO_3-N	18 ± 3	2.7 ± 0.6	$p < 0.01$
	NH_4-N	1.3 ± 0.2	3.5 ± 0.3	$p < 0.01$
	PO_4-P	13.9 ± 1.0	15.2 ± 1.4	*Not sign.*
	K^+	97 ± 11	62 ± 4	$p < 0.01$
	Ca^{2+}	1.03 ± 0.17	0.9 ± 0.2	*Not sign.*
	Mg^{2+}	1.07 ± 0.13	1.20 ± 0.12	*Not sign.*
	SO_4-S	8.8 ± 1.7	9.4 ± 0.7	*Not sign.*
	Na^+	4.7 ± 0.8	3.7 ± 1.0	$p < 0.01$
	Cl^-	6.7 ± 1.4	1.9 ± 0.6	$p < 0.01$

All values are tabulated as mean value ± standard deviation in unit g/kg dry weight based on separate analyses of individual plants. Statistical significance between the two treatments is indicated as p-values.

10.3389/fpls.2023.1229476

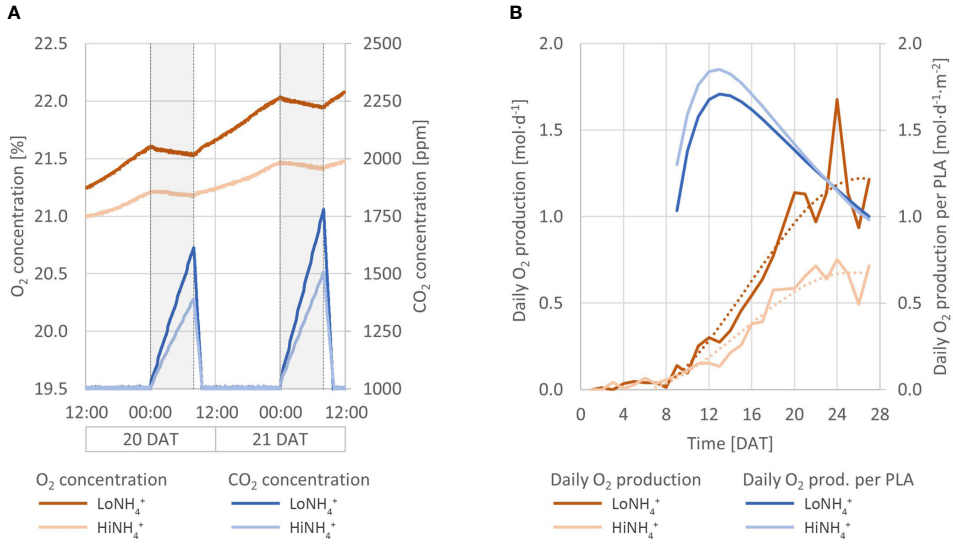

FIGURE 6
(A) Atmospheric O_2 (red lines) and CO_2 (blue lines) concentration inside the PCU cultivation chamber over 48 hours (20 - 21 DAT) for the $LoNH_4^+$ and $HiNH_4^+$ crop tests. Night phases are indicated with gray background. **(B)** Daily O_2 production (by 18 plants; solid red lines) of the $LoNH_4^+$ and $HiNH_4^+$ crop tests, plotted together with smoothed datasets based on 3rd degree polynomial regression (dotted red lines). Additionally, daily O_2 production per projected leaf area (PLA; blue lines).

However, accounting for the smaller projected leaf area (PLA) of the $HiNH_4^+$ plants, average O_2 production per day and projected leaf area was similar for the $LoNH_4^+$ and $HiNH_4^+$ plants both during the first phase of the crop tests (1.2 vs 1.3 mol·d^{-1}·m^{-2}, respectively) and during the second phase (both 1.1 mol·d^{-1}·m^{-2}). Furthermore, relating the total O_2 production to the total shoot DW at harvest also demonstrates similar values for the two crops, with 37 mol O_2 produced (over 26.6 days) per kg shoot DW for both crops. Estimated daily O_2 production throughout the crop tests was calculated based on the O_2 concentration in the cultivation chamber, the leak rate, and estimated daily gas composition of the atmospheric pressure compensation system (see Materials and methods). As the latter introduces a modest uncertainty in the calculations of daily O_2 production, the resulting datasets were smoothed by polynomial regression (Figure 6B). Evaluating the differences in daily O_2 production at 10, 14, 18, 22 and 26 DAT based on these datasets, the $HiNH_4^+$ plants produced 26, 37, 40, 42 and 45% less compared to the $LoNH_4^+$ plants, respectively.

To account for the considerable difference in biomass between the two treatments, the daily O_2 production (smoothed dataset) was evaluated per projected leaf area (PLA), measured non-destructively throughout the crop tests. These results (Figure 6B), illustrate similar daily O_2 productions per PLA for both treatments, with an indication of an increased O_2 production per PLA for the $HiNH_4^+$ plants during the early phase of the crop tests (15, 7, and 4% increase at 10, 14 and 18 DAT, respectively, and no difference

TABLE 5 Total O_2 production of 18 plants during the $LoNH_4^+$ and $HiNH_4^+$ crop tests, tabulated for the cultivation periods before (18.1 days) and after (8.5 days) the chamber venting, in addition to the full crop test period (26.6 days, not accounting for the day of venting at 19 DAT).

	Phase (duration)	$LoNH_4^+$	$HiNH_4^+$
Total O_2 production [mol]	0 - 18 DAT (18.1 days)	3.61	2.40
Average daily O_2 production [mol·d^{-1}]		0.20	0.13
Average PLA [m^2]		0.16	0.10
PLA-specific daily O_2 production [mol·d^{-1}·m^{-2}]		1.22	1.32
Total O_2 production [mol]	20 - 28 DAT (8.5 days)	8.74	4.97
Average daily O_2 production [mol·d^{-1}]		1.03	0.59
Average PLA [m^2]		0.97	0.55
PLA-specific daily O_2 production [mol·d^{-1}·m^{-2}]		1.06	1.06
Total O_2 production (26.6 days) [mol]	(26.6 days)	12.4	7.37

Average daily O_2 production and average projected leaf area (PLA) are calculated based on the tabulated period durations, as a basis for calculation of PLA-specific daily O_2 production.

TABLE 6 Nitrogen (N) mass balance of the $LoNH_4^+$ and $HiNH_4^+$ crop tests.

	Parameter and unit	$LoNH_4^+$	$HiNH_4^+$
Nutrient solution	NO_3^- at start [mol]	2.66	1.47
	NH_4^+ at start [mol]	0.36	1.39
	Total inorganic N at start [mol]	3.02	2.87
	NO_3^- addition [mol]	0.82	0.03
	NH_4^+ addition [mol]	0.10	0.03
	Total inorganic N net addition [mol]	0.90	0.05
	NO_3^- at end [mol]	2.58	1.54
	NH_4^+ at end [mol]	0.07	0.43
	NO_2^- at end [mol]	0.00	0.14
	Total inorganic N at end [mol]	2.65	2.12
	Total inorganic N consumption [mol]	1.28	0.80
Plants	N in shoots [mol]	1.02	0.53
	N in roots [mol]	0.17	0.18
	N in biomass [mol]	1.19	0.70
Mass balance	Mass balance closure [%]	94	89

Total inorganic N net addition accounts for addition of inorganic N (as NO_3^- and NH_4^+) and samples removed throughout the crop tests. Mass balance closure is calculated as the amount of N in the total biomass divided by the total consumption of inorganic N.

from 20 to 28 DAT). The highest specific O_2 productivity (per time and PLA) estimated was 1.85 mol·d^{-1}·m^{-2} for the $HiNH_4^+$ crop (13 DAT) and 1.71 mol·d^{-1}·m^{-2} for the $LoNH_4^+$ crop (13 DAT).

3.4.2 Nutrient solution development

From start, the total N concentration was the same in both crop tests (11 mM; Table 1), while the NH_4^+:N ratios were different (0.1 mol·mol^{-1} for $LoNH_4^+$, 0.5 mol·mol^{-1} for $HiNH_4^+$). Based on an advanced PCU nutrient management system, automatic feeding of nutrient stock solutions (with the same NH_4^+:N ratios as from start, thus 0.1 or 0.5 mol·mol^{-1}, see Materials and methods) successfully maintained a constant NO_3^- concentration throughout both crop tests (Figure 3A), at 9.7 mM for $LoNH_4^+$ and 5.6 mM for $HiNH_4^+$ (Table 1). While this control strategy required considerable feeding of nutrient stock solutions during the $LoNH_4^+$ crop test (0.5 L of each stock solution), practically no nutrient stock solution feeding was required during the $HiNH_4^+$ crop test (0.03 L of each), indicating a considerable NO_3^- consumption during the $LoNH_4^+$ crop test, and practically no NO_3^- consumption during the $HiNH_4^+$ crop test.

Without control of nutrient solution NH_4^+ concentration, NH_4^+ levels were allowed to vary based on N consumption. Throughout both crop tests, the NH_4^+ concentration was considerably reduced (Table 1), demonstrating a higher consumption of NH_4^+ relative to total N than the NH_4^+:N ratio of the nutrient solution. In consequence, the nutrient solution NH_4^+:N ratio during the $LoNH_4^+$ crop test was reduced from 0.12 to 0.02 mol·mol^{-1}, while it was reduced from 0.49 to 0.20 mol·mol^{-1} during the $HiNH_4^+$ crop test.

Nitrite (NO_2^-) could not be detected (< 1 mg N L^{-1}) throughout the full $LoNH_4^+$ crop test and throughout the close-to-exponential phase of the $HiNH_4^+$ crop test (up to 20 DAT). During the latter test, NO_2^- was detected during the last 6 days of cultivation (0.1 mM at 22 DAT, increasing to 0.5 mM at 28 DAT). To rule out major effects of nitrification on observed NH_4^+ consumption, operation of the cultivation facility was prolonged after removal of all plants from the system. Over the next 6 days, the NH_4^+ concentration decreased 0.5 mM in parallel with a further 0.4 mM increase of NO_2^-. Nutrient solution pH was kept constant by automatic pH control with KOH and H_2SO_4. No acid addition was required in any of the crop tests, while base addition was characterized by a considerably higher KOH consumption during the $HiNH_4^+$ crop test (1.6 mol OH^-) than during the $LoNH_4^+$ crop test (0.3 mol OH^-) (Figure 3B).

Despite no control of electrical conductivity (EC), the NO_3^- based feeding of nutrient stock solutions and the pH-based feeding of base resulted in a relatively constant EC of 1.9 mS/cm during the $LoNH_4^+$ crop test and 2.2 - 2.3 mS/cm during the $HiNH_4^+$ crop test (Table 1).

Development of macronutrient concentrations (Figure 2B) in the nutrient solution was most profound for K^+, with a considerable increase from 3.5 to 7.4 mM during the $HiNH_4^+$ crop test (KOH was automatically added to maintain pH at setpoint). In contrast, K^+ concentration decreased by 0.6 mM over the $LoNH_4^+$ crop test. Other ions demonstrating a concentration change of more than 0.2 mM over the course of a crop test (beyond K^+ and N ion species) included Ca^{2+}, Na^+ and Cl^-, demonstrating an increase during the $LoNH_4^+$ crop test (requiring considerable feeding of nutrient stock

solutions) and a decrease during the $HiNH_4^+$ (conducted practically without feeding of nutrient stock solutions). For other macronutrients, including HPO_4^{2-}, Mg^{2+}, and SO_4^{2-}, analyses throughout the crop tests demonstrated stable levels (Table 1).

3.4.3 N mass balance

With a considerable nutrient solution volume (270 L), a limited cultivation area (1.8 m^2), and a crop with modest nutrient requirements (lettuce), mass balances are vulnerable to measurement inaccuracies especially with respect to ion concentrations in the nutrient solution. Nevertheless, a N mass balance was calculated (Table 6) based on the available datasets, demonstrating a mass balance closure of 94% ($LoNH_4^+$) and 89% ($HiNH_4^+$).

The total consumption of NO_3^- and NH_4^+ during the $LoNH_4^+$ crop test was 0.9 and 0.4 mol, respectively, illustrating an apparent NH_4^+:N consumption ratio of 0.31 mol·mol^{-1} during the $LoNH_4^+$ crop test. In contrast, with no observed consumption of NO_3^- during the $HiNH_4^+$ crop test, N consumption was apparently based on NH_4^+ only. Relative to the produced biomass (Table 2), the consumption of inorganic N (Table 6) was 3.1 mol·$kgDW^{-1}$ for both crop tests.

3.4.4 Incorporation of C and N into edible biomass

To illustrate C and N recycling in a BLSS perspective, the amounts of C and N incorporated into edible biomass (18 plants per crop) was calculated for both crop tests (Figure 7) based on measured shoot DW at harvest (Table 2), and their composition (Table 4). The edible biomass of the $HiNH_4^+$ crop (202 g DW) was 40% lower than that of the $LoNH_4^+$ crop (337 g DW), while the relative shoot C content of the $HiNH_4^+$ crop (42%) was higher than that of the $LoNH_4^+$ crop (38%). In sum, the $HiNH_4^+$ crop incorporated 35% less C (84 g) into total edible biomass compared to the $LoNH_4^+$ crop (128 g). For N, the relative shoot content of the $HiNH_4^+$ crop (3.4%) was lower than that of the $LoNH_4^+$ crop (3.9%). In sum, the $HiNH_4^+$ crop incorporated 48% less N (7 g) into total edible biomass compared to the $LoNH_4^+$ crop (13 g).

4 Discussion

During long duration human space missions, bioregenerative life support systems may provide food, regenerated water, and O_2 for the astronauts. Given the limited availability of nutrient resources for plant production in this scenario, recycling and reuse of nutrients such as N from human urine is important. Depending on the upstream mineralization process of urine, the nutrient solution may have various NH_4^+:NO_3^- ratios and elevated NaCl concentrations. To maximize production of food, O_2 and clean water, crop cultivation conditions should be optimized. However, as a BLSS consists of multiple processes, the performance of the regenerative loop including ammonification and nitrification needs to be evaluated and optimized as a whole. This illustrates a possible trade-off between the overall BLSS efficiency and crop cultivation and yield, which should be considered in a long-term perspective with continuous operation. Increased knowledge on plant responses to various optimal and sub-optimal cultivation conditions and nutrient solutions will contribute to improved computer models, BLSS efficiency and improvement in design and control of integrated processes linking waste management and crop cultivation.

4.1 Biomass production and morphology

In this research campaign, considerable differences were identified between lettuce plants cultivated in nutrient solutions containing high and low NH_4^+:N ratios. In a BLSS perspective, the results demonstrate that both NH_4^+:N ratios, representing considerably different scenarios of upstream waste treatment, allow plant growth and development, and thus fixation of C and N into edible biomass. There is, however, a clear impact on biomass productivity (produced amount per time) and therefore on the total production over a given time. Under the conditions tested during the 28-day crop tests performed in this campaign, the $HiNH_4^+$ crop provided 40% lower edible biomass (shoot dry weight), resulting in the incorporation of 35% less C and 48% less N into edible biomass compared to the crop cultivated at low NH_4^+:N. These results are in line with previous research on lettuce, illustrating that increased ammonium concentrations strongly affect growth, resulting in decreased root and shoot biomass accumulation (Qiu et al., 2014; Wenceslau et al., 2021; Du et al., 2022; Hameed et al., 2022). Furthermore, the results are in line with general effects of ammonium toxicity on plant growth, demonstrating a biomass-reducing effect of high ammonium concentrations attributed to for example oxidative stress, nutrient imbalances and reduced photosynthesis (Barickman and Kopsell, 2016; Song et al., 2021; Weil et al., 2021). In line with the biomass results, the total leaf area per plant at time of harvest was reduced by a 2-factor for the $HiNH_4^+$ plants compared to the $LoNH_4^+$ plants. This effect is supported by other reports on hydroponically grown lettuce and other plants, demonstrating lower leaf areas with increasing ammonium concentrations (Guo et al., 2007a; Guo et al., 2007b; Urlic et al., 2017; Wenceslau et al., 2021). Beyond the NH_4^+:N ratio, other potential stress factors include the nutrient solution's total ionic strength and the presence of Na^+ and Cl^- added to mimic a urine recycling scenario. While several studies indicate no or minor growth retardation of lettuce cultivated in the presence of seawater, elevated electrical conductivity and/or Na^+ and Cl^- concentrations similar to the cultivation conditions used in the presented work (Atzori et al., 2019 and references within), one should not rule out combined effects of salinity and NH_4^+:N ratio especially in a foreseen future closed-loop scenario with accumulating Na^+ and Cl^- concentrations and increasing total electrical conductivity.

Calculation of PLAI throughout the crop tests offered a method to evaluate plant growth and PLAI-based growth rate without opening the closed cultivation chamber. While noticeable differences in PLAI (and thus biomass) between the $HiNH_4^+$ and $LoNH_4^+$ crops could not easily be observed until after approximately 10 days of cultivation, calculation of μ_{PLAI} indicated a difference in specific growth rate between the two

10.3389/fpls.2023.1229476

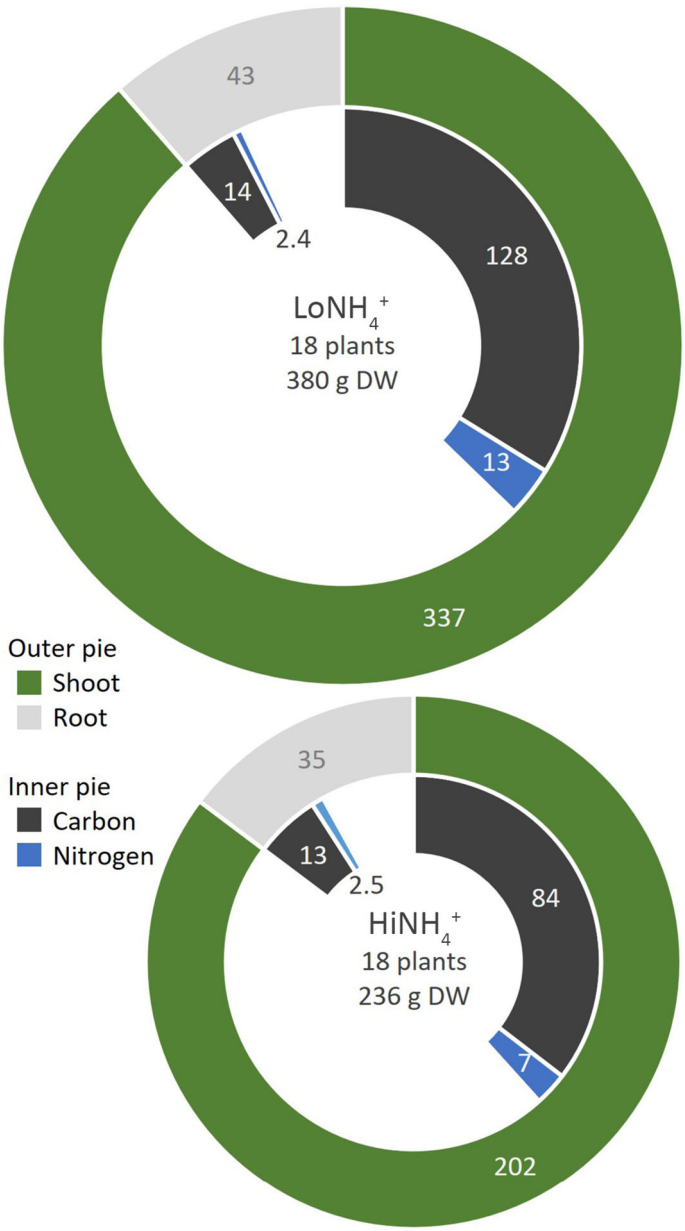

FIGURE 7
Incorporation of C (black) and N (blue) into shoots (green) and roots (gray) of the $LoNH_4^+$ (upper) and $HiNH_4^+$ (lower) crops. All numbers represent element or biomass dry weight in gram and relate to the full crop consisting of 18 plants. The relative difference in total pie area corresponds to the relative difference in total dry weight of the two crops.

crops starting already in the early cultivation phase. This indicates that under the conditions tested, the elevated NH_4^+:N ratio introduced negative effects on plant growth also during the close-to-exponential cultivation period. At the same time, this indicates that the observed NO_2^- in the nutrient solution was not the main cause of the observed differences in biomass production (and thus O_2 production, see below). While elevated NO_2^- concentrations in the nutrient solution may cause reduced growth (Hoque et al., 2008), NO_2^- was not observed until the late cultivation phase of the $HiNH_4^+$ crop, at a time which μ_{PLAI} of both crops had started to decrease and coincided. Coinciding μ_{PLAI} towards the end of the cultivation period may be explained by reduced specific growth rates as plants mature, and the fact that the presented growth rates are based on PLAI which, by definition, cannot exceed a factor of 1 due to a limited cultivation area and overlapping leaves.

Beyond the overall reduction in biomass production of the $HiNH_4^+$ crop, these plants displayed a significantly higher root:shoot ratio than the $LoNH_4^+$ plants, indicating a higher relative use of energy towards root growth. This is in line with previous research showing increasing root:shoot ratio with increasing NH_4^+:NO_3^- ratio in several species, including lettuce (Zhu et al., 2020), tobacco (Walch-Liu et al., 2000) and cucumber (Zhou et al., 2017). More specifically, alteration of biomass partitioning between root and shoot is a known plant response to nutritional stress (Maskova and Herben, 2018) and NH_4^+:K^+

imbalance has been demonstrated to negatively influence carbohydrate accumulation, disturbing the root-to-shoot biomass partitioning (Zhao et al., 2020). In our study, NH_4^+ and K^+ were among the nutrient ions that demonstrated the greatest differences between the biomass content of the $HiNH_4^+$ and $LoNH_4^+$ crops. Additionally, the two crops demonstrated differences in root size and morphology. The $HiNH_4^+$ plants exhibited shorter primary and secondary roots, along with a significantly lower number of forks and links illustrating less branching. This is likely to be caused by the nutrient availability (especially of NH_4^+ and NO_3^-) and plant nutritional status, which are known to strongly influence the development of the root system (Lima et al., 2010). NH_4^+ is known to affect root architecture by inhibition of primary root growth and elongation, while promoting lateral branching (Liu and Von Wiren, 2017; Liu et al., 2013). Conversely, NO_3^- has been shown to stimulate lateral root elongation (Lima et al., 2010; Marschner and Marschner, 2012). These observations represent valuable details for mathematical modelling of plant growth and development, as the root's surface area is critical for mass and energy transfer.

4.2 O_2 production

In total, the $HiNH_4^+$ crop produced 41% less O_2 than the $LoNH_4^+$. However, as the growth of the $HiNH_4^+$ plants was impaired, the O_2 production should be evaluated also in terms of specific production. When O_2 production was normalized by shoot dry weight at harvest, the amount of O_2 produced was 37 mol·kg^{-1} for both the $LoNH_4^+$ and the $HiNH_4^+$ crops. On a high level, O_2 production following biomass production is in line with the general mechanism of photosynthesis, converting light energy to chemical energy utilized for the synthesis and accumulation of organic matter (Evert and Eichhorn, 2013; Taiz, 2015), and hence, the photosynthetic rate is determining for biomass productivity. Furthermore, measurements of chlorophyll fluorescence on dark-adapted leaves demonstrated that the F_v/F_m of both crops (0.83) was within a range indicating a healthy and well-functioning photosystem II (0.79 – 0.84) (Bjorkman and Demmig, 1987).

The total O_2 production, when normalized per unit leaf area at harvest, was 1.8 and 2.1 mol·m^{-2} for the $LoNH_4^+$ and $HiNH_4^+$ crops, respectively. Similarly, O_2 production per PLA demonstrates no reduction in specific O_2 production of the $HiNH_4^+$ plants compared to the $LoNH_4^+$ plants. On the contrary, detailed examination of the data indicates a marginal increase of the specific O_2 production per PLA by the $HiNH_4^+$ plants during the second and third week of the cultivation period. This indication is in line with a higher SPAD index of the leaves of the $HiNH_4^+$ plants, and a color index more towards green compared to the $LoNH_4^+$ plants. These findings are again in line with other investigations on both lettuce and species such as Arabidopsis and kohlrabi, demonstrating a higher chlorophyll concentration in leaves of plants cultivated with a higher proportion of NH_4^+ in the fertilizer (Blanke et al., 1996; Qiu et al., 2014; Hu et al., 2015). However, the scientific literature on chlorophyll content as a response to NH_4^+ concentration and NH_4^+:NO_3^- ratio demonstrate complex relationships and varying results. Song et al. (2021) demonstrated that lettuce and cabbage chlorophyll content was higher in plants exposed to an NH_4^+:NO_3^- ratio of 50:50, than both 0:100 and 100:0, while Zhu et al. (2020) reported a higher chlorophyll concentration in lettuce seedlings exposed to an NH_4^+:NO_3^- ratio 25:75 than both 100:0, 50:50 and 0:100. Studies of other species also show varying results, for example, an increase in chlorophyll content with increasing NH_4^+:NO_3^- ratios was not discovered in kale (Assimakopoulou et al., 2019). Different theories are proposed to explain an increased chlorophyll content as a response to high ammonium. The higher chlorophyll concentration may be caused by ammonium-stress inhibiting leaf expansion, resulting in a denser chlorophyll content rather than an actual total increase (Sanchez-Zabala et al., 2015). Furthermore, carbon skeletons in the leaves favor NH_4^+ assimilation. Based on this, it has been proposed that a higher chlorophyll content might be a strategy to increase photosynthetic CO_2 assimilation to produce more carbon skeletons and thereby mitigate NH_4^+ accumulation (Sanchez-Zabala et al., 2015).

4.3 Biomass composition

The 3-fold increase of root NH_4^+ content of the $HiNH_4^+$ plants compared to the $LoNH_4^+$ plants is comparable to the difference between the two nutrient solutions, with 3 to 5-fold elevated NH_4^+ concentration (at start and end, respectively) and 3 to 7-fold elevated NH_4^+:N ratio in the $HiNH_4^+$ nutrient solution compared to the $LoNH_4^+$ nutrient solution. Such elevated root NH_4^+ content is consistent with the roots being the primary site for initial NH_4^+ accumulation, where it is incorporated into organic complexes, while N is typically transported to the shoots in other forms such as amino acids (Mengel and Kirkby, 2001; Marschner and Marschner, 2012). Additionally, the biomass NO_3^- content varied considerably between the crops, and in line with the nutrient solution composition. The shoots and roots of the $HiNH_4^+$ plants demonstrated an 87% and 85% reduction compared to those of the $LoNH_4^+$ plants, respectively, in line with the 42% lower NO_3^- concentration in the nutrient solution. A similar reduction of leaf NO_3^- content with increasing NH_4^+:N ratio in the nutrient solution was reported for example for rocket salad (Kim et al., 2006). The average nitrate content of the $LoNH_4^+$ and $HiNH_4^+$ edible biomass (shoots) was 6.0 and 0.8 g NO_3-N per kg dry weight, respectively (Table 4). Considering the shoot dry weight content (Table 2), this corresponds to 1.8 g and 0.3 g NO_3^- per kg fresh weight, respectively, both below the maximum nitrate levels set by the European Union (Commission Regulation No 1258/2011).

Analyses of the shoot and root content of nutrient ions beyond N species demonstrated an overall trend of similar or lower content of both anions and cations in the $HiNH_4^+$ plants compared to the $LoNH_4^+$ plants. As demonstrated by the ionic concentration trend of the nutrient solution, all macronutrients beyond NH_4^+ were available at relatively stable concentrations throughout the crop tests, indicating that the differences between the two crops were not governed by nutrient availability, but rather by direct or indirect consequences of the difference in NH_4^+ concentration and/or NH_4^+:N ratio. This is in line with reports on reduced uptake of ions such as K^+, Ca^{2+} and Mg^{2+} with increasing NH_4^+ concentration and NH_4^+:NO_3^- ratio in the nutrient solution (Britto and Kronzucker,

2002; Savvas et al., 2006; Roosta and Schjoerring, 2008; Fallovo et al., 2009). For example, Weil et al. (2021) reported that the concentration of both K^+ and Ca^{2+} in lettuce shoots declined significantly with increasing nutrient solution NH_4^+:N ratio, concluding that the uptake of cationic nutrients and the plant growth were reduced when the NH_4^+:N ratio exceeded 0.50 mol·mol^{-1}. The observed effects on nutrient ion content have been explained by antagonism (Lasa et al., 2001; Marschner and Marschner, 2012); that the NH_4^+ ion resembles the K^+ ion in radius and hydration shell size and may therefore move through K^+ channels (Marschner and Marschner, 2012), and that uptake of NO_3^- occurs simultaneously with the uptake of Ca^{2+} or K^+ so that an increasing proportion of NO_3^- will increase the content of Ca^{2+} and K^+ in leaves (Du et al., 2022).

The content of NaCl in the nutrient solutions, which was designed to mimic a urine recycling scenario, may have impacted plant nutrient uptake in both the high and low NH_4^+- scenarios. In general, excess Na^+ uptake lowers the uptake of essential ions and disturbs the root-shoot transport. It has been widely observed that Na^+, even at low levels, inhibits the transport systems for K^+ uptake due to the chemical similarities between the two ions (Amini and Ehsanpour, 2005; Kronzucker et al., 2013). For some functions, Na^+ may also replace potassium, such as for example for maintenance of vacuole osmotic potential (Wakeel et al., 2011). Na^+ may cause osmotic stress, which decreases the passive uptake of calcium, resulting in a lower concentration of calcium in the plant. Another possible effect of NaCl in plant nutrition, is that Cl^- may antagonize the uptake of nitrate, while it assists uptake of ammonium (Song et al., 2021).

The $HiNH_4^+$ lettuce crop demonstrated a higher carbon content in both leaves and roots compared to the $LoNH_4^+$ plants. During stress conditions that affect plant growth but still allow for photosynthesis, accumulation of sugars is commonly observed Peshev and Van Den Ende, 2013). Exposed to high NH_4^+ concentrations, plants have been shown to synthesize sugars to provide carbon skeletons to increase NH_4^+ assimilation (Raab and Terry, 1994). Additionally, plants exposed to abiotic stress often accumulate reactive oxygen species (ROS). Accumulation of soluble sugars can mitigate this toxic effect caused by plant stress by contributing to ROS scavenging (Keunen et al., 2013; Peshev and Van Den Ende, 2013). Sugars can also protect chloroplasts and thereby stabilize photosynthesis under stress conditions, and they may serve as osmoprotectants (Peshev and Van Den Ende, 2013). Additionally, the uptake of NO_3^- against the electrochemical gradient requires more use of fixed carbon compared to acquisition of NH_4^+ (Britto and Kronzucker, 2013).

4.4 Nutrient consumption and nutrient solution evolution in a long-term perspective

Maximizing resource utilization limits the possibilities of flushing the hydroponic loop and restarting the system with a fresh and balanced nutrient solution. Thus, long term development of the nutrient solution needs to be understood, modelled, and ultimately designed and controlled in a trade off with the productivity of the plants and the design and performance of upstream processes. In light of the observed effects of the NH_4^+:N ratio, the development of this ratio over time should be considered. The results obtained under the conditions tested indicate a preference for NH_4^+ during the $HiNH_4^+$ crop test, in which N consumption apparently almost exclusively could be attributed to NH_4^+ consumption, although one cannot rule out that a modest nitrification activity could convert some NH_4^+ to NO_3^- and thus mask some NO_3^- consumption by the plants. Also, during the $LoNH_4^+$ crop test, the consumption of NH_4^+ relative to total N in the system was higher than the concentration of NH_4^+ relative to total N in the nutrient solution. In consequence, the nutrient solution NH_4^+:N ratio decreased over time during both crop tests (from 0.12 to 0.02 mol·mol^{-1} in the $LoNH_4^+$ crop test; from 0.49 to 0.20 in the $HiNH^+_4$ crop test). Even after a hypothetical addition of nutrient stock solutions to restore the total N concentration before an additional plant cultivation period, the initial NH_4^+:N ratio of the second period will be lower than that of the first (0.03 mol·mol^{-1} after topping up the remaining $LoNH_4^+$ nutrient solution to the initial 11 mM total N; 0.29 mol·mol^{-1} after topping up the remaining $HiNH_4^+$ nutrient solution to the initial 11 mM total N). These considerations illustrate a potential to combine high-NH_4^+:N stock solutions generated by upstream waste treatment processes with efficient long-term plant biomass and O_2 productivity despite initially reduced productivity. In a modelling perspective, it illustrates the importance of understanding the relative NH_4^+:NO_3^- consumption in the higher plant compartment combined with the effects of the NH_4^+:NO_3^- ratio of the mineralized waste from upstream compartments. High NH_4^+ to NO_3^- preference has been observed in several other studies, including a study of N absorption by tomato, in which 50% of plant N was absorbed as NH_4^+ even though this ion represented only 10% of available N (the remaining 90% being NO_3^-) (Glass et al., 2002). N preference may be linked to energy considerations as uptake of NO_3^- requires energy while NH_4^+ can be directly absorbed, hence many plants prefer to take up NH_4^+ if both are available (Mengel and Kirkby, 2001; Marschner and Marschner, 2012; Du et al., 2022). Additionally, NO_3^- uptake is inhibited by ammonium, and lettuce appears to absorb ammonium faster than NO_3^- when the source contains both N-forms (Savvas et al., 2006; Britto and Kronzucker, 2013). However, plant preference for NH_4^+ or NO_3^- is known to vary across plant species, physiological phase and environmental conditions (Britto and Kronzucker, 2013), and thus observed N preference may only be valid for a given species, developmental stage, and cultivation conditions. An improved understanding of the NH_4^+ to NO_3^- preference, for example as function of cultivation conditions, should be further pursued, as this may hold potential to reduce ammonium toxicity even at conditions of high NH_4^+:N ratios.

During the $LoNH_4^+$ crop test which required a considerable amount of nutrient stock solution feeding, accumulation of Na^+, Ca^{2+} and to a certain extent Cl^- was observed together with a marginal reduction of K^+. This illustrates imbalance between the system's feed rates and consumption rates. Nutrient ion levels in the nutrient stock solutions may be tuned relative to for example total N as far as charge balancing allows in order to achieve a balanced nutrient solution. Accumulation of Na^+ and Cl^-, however, represents a potential general challenge for the utilization of

mineralized human waste. Accumulation of Na^+ in the nutrient solution may to a certain extent be mitigated by increased plant Na^+ uptake rates with increasing Na^+ concentrations in the nutrient solution (Neocleous and Savvas, 2017; Breś et al., 2022). Nevertheless, the extent and the implications of long-term accumulation of non-nutrients in crop cultivation based on human waste are important aspects that would benefit from further attention in a BLSS perspective.

The ratio between consumed NH_4^+ and consumed NO_3^- affects nutrient solution pH. NH_4^+ uptake causes release of protons and thereby reduced pH in the root zone, which again may impact nutrient uptake (Lasa et al., 2001; Marschner and Marschner, 2012; Weil et al., 2021). This effect was clearly demonstrated during the $HiNH_4^+$ crop test with a substantial amount of base added to maintain a constant pH. The $HiNH_4^+$ scenario, with an NH_4^+:N ratio of 0.5 mol·mol^{-1} is based on urine ammonification and partly nitrification without addition of alkalinity (Larsen et al., 2021). In a BLSS scenario, the results presented illustrate that no or low alkalinity addition during the nitrification step results in increased alkalinity requirement during the crop cultivation step instead. In this case, addition of OH^- during crop cultivation should be carefully balanced with appropriate anions to avoid nutrient imbalance over time. In this context, it is interesting to notice that addition of macronutrient ions prone to be present at low concentrations in mineralized urine due to precipitation (such as Ca^{2+}) could possibly serve a dual purpose of being a counter ion for OH^- charge balancing and being a required nutrient solution supplement. Such feeding strategies must, however, be carefully tuned and consider factors such as salt availability and solubility.

4.5 Strategies to maximize food and O_2 production in a BLSS perspective

In a Lunar greenhouse perspective, cultivation area will be limited and should be utilized in an efficient way. In a scenario of constant plant density throughout the cultivation period, plants should be cultivated to an adult stage, as the plant growth rate (g per day) and the O_2 production rate (mol per day) are highest during the end of the cultivation period, thus increasing also the average growth rate and the average O_2 production rate as evaluated over the full cultivation period. However, such a strategy comes at the cost of a low utilization rate of the available cultivation area (low PLAI), especially during the first part of the cultivation period. In a more optimized scenario, initial plant density can be high to achieve a high PLAI even with small plants. As the plants grow, the plant density can be reduced to give room for the expanding plants. In such an optimized scenario, specific production per time and PLA should be considered when aiming at optimizing food (biomass) and O_2 production. Under the conditions tested, the specific O_2 production per time and PLA reached a maximum around 13 DAT (Figure 6B), indicating that adolescent lettuce plants were more effective in O_2 production per time and PLA than seedlings and adult plants. With O_2 production linked to biomass production, this period with the highest specific O_2 production per time and PLA coincides with the period of highest specific growth rate (here estimated as μ_{PLAI}; Figure 4). Thus, in an optimized scenario with dynamic plant density to continuously operate at a high PLAI, the results obtained under the conditions tested suggest that plants should be cultivated up to approximately 16 - 20 days after transplant (26 - 30 days after germination) to maintain a maximized specific biomass (food) production per time and PLA and a maximized specific O_2 production per time and PLA. Furthermore, it is interesting to notice the indication of a higher O_2 production per time and PLA of the $HiNH_4^+$ crop compared to that of the $LoNH_4^+$ crop (Figure 6B), illustrating that as long as PLAI is kept high, O_2 productivity may be high even under cultivation conditions suboptimal for growth. Such an effect, that may be attributed to the plant's complex physiological response to mitigate suboptimal cultivation conditions, is especially interesting considering the possible need to accept suboptimal conditions for a given BLSS step in order to maximize the total efficiency of the whole loop.

5 Conclusion

The results of this study demonstrate the importance of understanding and considering direct and indirect effects of upstream waste processing on crop cultivation in BLSS. The urine utilization scenarios of 0.1 and 0.5 mol·mol^{-1} NH_4^+:N demonstrated significant effects on plant development, plant nutrient composition and O_2 production. Under the conditions tested, plants cultivated at the high NH_4^+:N ratio demonstrated a high preference for ammonium combined with a reduced specific growth rate and thus a reduced total biomass production. O_2 production per time and projected leaf area reached a maximum during the adolescent plant phase, coinciding with exponential growth and indicating a strong relationship between biomass and O_2 production. Interestingly, the specific O_2 production per time and projected leaf area was marginally higher for the plants cultivated at high NH_4^+:N ratio, in line with a higher chlorophyll content. In a life support perspective, the results illustrate design concepts for crop cultivation strategies depending on the performance of upstream processes (e.g. urine mineralization and high/low NH_4^+:N) and downstream needs (food or O_2). In addition, parameters such as plant density and cultivation duration may be adjusted or balanced against each other to optimize performance. Ultimately, the results may guide the design and control of both crop cultivation and other processes in a regenerative BLSS loop towards a common trade-off and to achieve a greater good rather than optimizing individual processes.

The unique features of the ESA MELiSSA Plant Cultivation Unit (PCU) with its gas-tight atmospheric and hydroponic loops with extensive monitoring and control enabled collection of comprehensive and detailed data on crop O_2 production, plant growth via image-based analyses, and nutrient solution dynamics throughout the entire cultivation period. Together with future expanded capabilities of the PCU, such as analyses of CO_2 consumption and water production, this will contribute to improved understanding of plant responses and further advancement of computer models for predictions of plant growth and production in various BLSS and cultivation scenarios.

This study represents a further advancement towards increased waste- and resource recycling in plant-based food production systems. A deeper understanding of these processes and their impacts is crucial for the production of food and for the regeneration of water and O_2 in future human space exploration. Additionally, considering relevant terrestrial challenges such as depletion of mineral resources and pollution of ground waters due to nutrient runoff, nutrient recycling fuels sustainable agriculture also on Earth. Exploitation of waste streams for plant production illustrates synergies between space exploration and terrestrial food production, and knowledge on plant responses to different resource utilization scenarios improves the development and design of systems and processes for both Earth and space.

Data availability statement

The raw data supporting the conclusions of this article will be made available by the authors, without undue reservation.

Author contributions

ØJ, MS and A-IJ designed the experiment. MS, ØJ, AP and CQ executed the crop tests and performed analyses and calculations. All authors contributed to interpretation of results. MS and ØJ prepared the draft manuscript. All authors contributed to the article and submitted and approved the submitted section.

Funding

This research was funded by the European Space Agency (ESA) through the MELiSSA PaCMan 2 project (Plant characterization unit for closed life support system - engineering, manufacturing and testing), contract number 4000115852/15/NL/AT.

Acknowledgments

The authors would like to thank Luigi Duri (University of Naples Federico II) for his invaluable assistance during the laboratory work. Furthermore, the full PaCMan project team is acknowledged for the PCU development efforts, with special thanks for valuable technical and scientific discussions to Lorenzo Bucchieri (EnginSoft S.p.A.), Emmanuel Frossard, Geremia Pellegri and Icíar Giménez de Azcárate Bordóns (ETH Zürich), Youssef Rouphael and Stefania de Pascale (University of Naples Federico II), Adam Harper and Matt Whiteley (Hosokawa Micron Ltd.), Gionata Cimini (Odys S.r.l.) and Christel Paille (ESA/ESTEC).

Conflict of interest

CQ is employed by EnginSoft S.p.a.

The remaining authors declare that the research was conducted in the absence of any commercial or financial relationships that could be construed as a potential conflict of interest.

Publisher's note

All claims expressed in this article are solely those of the authors and do not necessarily represent those of their affiliated organizations, or those of the publisher, the editors and the reviewers. Any product that may be evaluated in this article, or claim that may be made by its manufacturer, is not guaranteed or endorsed by the publisher.

References

Acosta-Motos, J. R., Ortuno, M. F., Bernal-Vicente, A., Diaz-Vivancos, P., Sanchez-Blanco, M. J., and Hernandez, J. A. (2017). Plant responses to salt stress: adaptive mechanisms. *Agronomy-Basel* 7. doi: 10.3390/agronomy7010018

Amini, F., and Ehsanpour, A. A. (2005). Soluble Proteins, Proline, Carbohydrates and Na +/K+ Changes in Two Tomato (Lycopersicon esculentum Mill.) Cultivars under in *vitro* Salt Stress. *Am. J. Biochem. Biotechnol.* 1, 212–216. doi: 10.3844/ajbbsp.2005.212.216

Andrews, M., Raven, J. A., and Lea, P. J. (2013). Do plants need nitrate? The mechanisms by which nitrogen form affects plants. *Ann. Appl. Biol.* 163, 174–199. doi: 10.1111/aab.12045

Assimakopoulou, A., Salmas, I., Kounavis, N., Bastas, A. I., Michopoulou, V., and Michail, E. (2019). The impact of ammonium to nitrate ratio on the growth and nutritional status of kale. *Notulae Botanicae Horti Agrobotanici Cluj-Napoca* 47, 848–859. doi: 10.15835/nbha47311466

Atzori, G., Mancuso, S., and Masi, E. (2019). Seawater potential use in soilless culture: A review. *Scientia Hortic.* 249, 199–207. doi: 10.1016/j.scienta.2019.01.035

Barickman, T. C., and Kopsell, D. A. (2016). Nitrogen form and ratio impact Swiss chard (Beta vulgaris subsp cicla) shoot tissue carotenoid and chlorophyll concentrations. *Scientia Hortic.* 204, 99–105. doi: 10.1016/j.scienta.2016.04.007

Berkovich, Y. A., Chetirkin, P. V., Wheeler, R. M., and Sager, J. C. (2004). Evaluating and optimizing horticultural regimes in space plant growth facilities. *Adv. Space Res.* 34, 1612–1618. doi: 10.1016/j.asr.2003.08.080

Bjorkman, O., and Demmig, B. (1987). Photon Yield of O-2 Evolution and Chlorophyll Fluorescence Characteristics at 77-K among Vascular Plants of Diverse Origins. *Planta* 170, 489–504. doi: 10.1007/BF00402983

Blanke, M. M., Bacher, W., Pring, R. J., and Baker, E. A. (1996). Ammonium nutrition enhances chlorophyll and glaucousness in Kohlrabi. *Annals of Botany* 78, 599–604.

Bonvin, C., Etter, B., Udert, K. M., Frossard, E., Nanzer, S., Tamburini, F., et al. (2015). Plant uptake of phosphorus and nitrogen recycled from synthetic source-separated urine. *Ambio* 44 Suppl 2, S217–S227. doi: 10.1007/s13280-014-0616-6

Breś, W., Kleiber, T., Markiewicz, B., Mieloszyk, E., and Mieloch, M. (2022). The effect of naCl stress on the response of lettuce (Lactuca sativa L.). *Agronomy* 12, 244. doi: 10.3390/agronomy12020244

Britto, D. T., and Kronzucker, H. J. (2002). NH4+ toxicity in higher plants: a critical review. *J. Plant Physiol.* 159, 567–584. doi: 10.1078/0176-1617-0774

Britto, D. T., and Kronzucker, H. J. (2013). Ecological significance and complexity of N-source preference in plants. *Ann. Bot.* 112, 957–963. doi: 10.1093/aob/mct157

Chinnusamy, V., Zhu, J., and Zhu, J. K. (2006). Salt Stress Signaling and Mechanisms of Plant Salt Tolerance. In: Setlow, J.K. (eds) *Genetic Engineering.* Genetic Engineering: Principles and Methods (Boston, MA: Springer). 27, 141–177. doi: 10.1007/0-387-25856-6_9

De Bang, T. C., Husted, S., Laursen, K. H., Persson, D. P., and Schjoerring, J. K. (2021). The molecular-physiological functions of mineral macronutrients and their

consequences for deficiency symptoms in plants. *New Phytol.* 229, 2446–2469. doi: 10.1111/nph.17074

Du, K. K., Zhang, J. L., Han, Y. Y., Hao, J. H., Qin, X. X., Liu, C. J., et al. (2022). Effects of varying NO3-:NH4+ Ratios on lettuce (Lactuca sativa L.) nitrogen metabolism. *Pakistan J. Bot.* 54, 2081–2088. doi: 10.30848/PJB2022-6(37)

Evert, R. F., and Eichhorn, S. E. (2013). *Raven biology of plants* (Peter Marshall, Macmillan Education).

Fallovo, C., Colla, G., Schreiner, M., Krumbein, A., and Schwarz, D. (2009). Effect of nitrogen form and radiation on growth and mineral concentration of two Brassica species. *Scientia Hortic.* 123, 170–177. doi: 10.1016/j.scienta.2009.09.003

Glass, A. D. M., Britto, D. T., Kaiser, B. N., Kinghorn, J. R., Kronzucker, H. J., Kumar, A., et al. (2002). The regulation of nitrate and ammonium transport systems in plants. *J. Exp. Bot.* 53, 855–864. doi: 10.1093/jexbot/53.370.855

Godia, F., Albiol, J., Montesinos, J. L., Perez, J., Creus, N., Cabello, F., et al. (2002). MELISSA: a loop of interconnected bioreactors to develop life support in space. *J. Biotechnol.* 99, 319–330. doi: 10.1016/S0168-1656(02)00222-5

Guo, S. W., Chen, G., Zhou, Y., and Shen, Q. R. (2007b). Ammonium nutrition increases photosynthesis rate under water stress at early development stage of rice (Oryza sativa L.). *Plant Soil* 296, 115–124. doi: 10.1007/s11104-007-9302-9

Guo, S. W., ZHOU, Y., GAO, Y. X., LI, Y., and SHEN, Q. R. (2007c). New insights into the nitrogen form effect on photosynthesis and photorespiration. *Pedosphere* 17, 601–610. doi: 10.1016/S1002-0160(07)60071-X

Guo, S., Zhou, Y., Shen, Q., and Zhang, F. (2007a). Effect of ammonium and nitrate nutrition on some physiological processes in higher plants - Growth, photosynthesis, photorespiration, and water relations. *Plant Biol.* 9, 21–29. doi: 10.1055/s-2006-924541

Halbert-Howard, A., Häfner, F., Karlowsky, S., Schwarz, D., and Krause, A. (2021). Evaluating recycling fertilizers for tomato cultivation in hydroponics, and their impact on greenhouse gas emissions. *Environ. Sci. pollut. Res.* 28, 59284–59303. doi: 10.1007/s11356-020-10461-4

Hameed, M. K., Umar, W., Razzaq, A., Aziz, T., Maqsood, M. A., Wei, S. W., et al. (2022). Differential metabolic responses of lettuce grown in soil, substrate and hydroponic cultivation systems under NH4+/NO3- application. *Metabolites* 12. doi: 10.3390/metabo12050444

Hoque, M. M., Ajwa, H. A., and Smith, R. (2008). Nitrite and ammonium toxicity on lettuce grown under hydroponics. *Commun. Soil Sci. Plant Anal.* 39, 207–216. doi: 10.1080/00103620701759194

Hu, L. L., Yu, J. H., Liao, W. B., Zhang, G. B., Xie, J. M., Lv, J., et al. (2015). Moderate ammonium:nitrate alleviates low light intensity stress in mini Chinese cabbage seedling by regulating root architecture and photosynthesis. *Scientia Horticulturae* 186, 143–153.

Keunen, E., Peshev, D., Vangronsveld, J., Van Den Ende, W., and Cuypers, A. (2013). Plant sugars are crucial players in the oxidative challenge during abiotic stress: extending the traditional concept. *Plant Cell Environ.* 36, 1242–1255. doi: 10.1111/pce.12061

Khodadad, C. L. M., Hummerick, M. E., Spencer, L. E., Dixit, A. R., Richards, J. T., Romeyn, M. W., et al. (2020). Microbiological and nutritional analysis of lettuce crops grown on the international space station. *Front. Plant Sci.* 11. doi: 10.3389/fpls.2020.00199

Kim, S. J., Kawaharada, C., and Ishii, G. (2006). Effect of ammonium: nitrate nutrient ratio on nitrate and glucosinolate contents of hydroponically-grown rocket salad (Eruca sativa Mill.). *Soil Sci. Plant Nutr.* 52, 387–393. doi: 10.1111/j.1747-0765.2006.00048.x

Kronzucker, H. J., Coskun, D., Schulze, L. M., Wong, J. R., and Britto, D. T. (2013). Sodium as nutrient and toxicant. *Plant Soil* 369, 1–23. doi: 10.1007/s11104-013-1801-2

Larsen, T. A., Riechmann, M. E., and Udert, K. M. (2021). State of the art of urine treatment technologies: A critical review. *Water Research X*, 13. doi: 10.1016/j.wroa.2021.100114

Lasa, B., Frechilla, S., Lamsfus, C., and Aparicio-Tejo, P. M. (2001). The sensitivity to ammonium nutrition is related to nitrogen accumulation. *Scientia Hortic.* 91, 143–152. doi: 10.1016/S0304-4238(01)00239-4

Lima, J. E., Kojima, S., Takahashi, H., and Von Wiren, N. (2010). Ammonium triggers lateral root branching in Arabidopsis in an AMMONIUM TRANSPORTER1;3-dependent manner. *Plant Cell* 22, 3621–3633. doi: 10.1105/tpc.110.076216

Liu, Y., Lai, N. W., Gao, K., Chen, F. J., Yuan, L. X., and Mi, G. H. (2013). Ammonium inhibits primary root growth by reducing the length of meristem and elongation zone and decreasing elemental expansion rate in the root apex in arabidopsis thaliana. *PloS One* 8. doi: 10.1371/journal.pone.0061031

Liu, Y., and Von Wiren, N. (2017). Ammonium as a signal for physiological and morphological responses in plants. *J. Exp. Bot.* 68, 2581–2592. doi: 10.1093/jxb/erx086

Marschner, H., and Marschner, P. (2012). *Marschner's mineral nutrition of higher plants* (London, UK: Elsevier).

Maskova, T., and Herben, T. (2018). Root:shoot ratio in developing seedlings: How seedlings change their allocation in response to seed mass and ambient nutrient supply. *Ecol. Evol.* 8, 7143–7150. doi: 10.1002/ece3.4238

Mauerer, M., Rocksch, T., Dannehl, D., Schuch, I., Mewis, I., Förster, N., et al. (2018). Impact of different concentrations of nitrified urine in a recirculating nutrient solution on growth, yield and quality of lettuce. *DGG Proc.* 8, 1–5. doi: 10.5288/dgg-pr-mm-2018

Mengel, K., and Kirkby, E. A. (2001). *Principles of plant nutrition 5th edition* (Dordrecht, Netherlands: Kluwer Academic Publishers).

Neocleous, D., and Savvas, D. (2017). Simulating NaCl accumulation in a closed hydroponic crop of zucchini: Impact on macronutrient uptake, growth, yield, and photosynthesis. *J. Plant Nutr. Soil Sci.* 180, 283–293. doi: 10.1002/jpln.201600338

Pannico, A., Cimini, G., Quadri, C., Paradiso, R., Bucchieri, L., Rouphael, Y., et al. (2022). A plant characterization unit for closed life support. *Front. Astronomy Space Sci.* 9. doi: 10.3389/fspas.2022.820752

Pannico, A., El-Nakhel, C., Kyriacou, M. C., Giordano, M., Stazi, S. R., De Pascale, S., et al. (2019). Combating micronutrient deficiency and enhancing food functional quality through selenium fortification of select lettuce genotypes grown in a closed soilless system. *Front. Plant Sci.* 10. doi: 10.3389/fpls.2019.01495

Peiro, E., Pannico, A., Colleoni, S. G., Bucchieri, L., Rouphael, Y., De Pascale, S., et al. (2020). Air distribution in a fully-closed higher plant growth chamber impacts crop performance of hydroponically-grown lettuce. *Front. Plant Sci.* 11. doi: 10.3389/fpls.2020.00537

Peshev, D., and Van Den Ende, W. (2013). "Sugars as antioxidants in plants," in *Crop improvement under adverse conditions*. Eds. N. Tuteja and S. S. Gill (London: Springer).

Qiu, Z. P., Yang, Q. C., and Liu, W. K. (2014). Effects of nitrogen fertilizer on nutritional quality and root secretion accumulation of hydroponic lettuce. *Int. Symposium New Technol. Environ. Control Energy-Saving Crop Production Greenhouse Plant Factory - Greensys 2013* 1037, 679–685. doi: 10.17660/ActaHortic.2014.1037.87

Raab, T. K., and Terry, N. (1994). Nitrogen-source regulation of growth and photosynthesis in beta-vulgaris L. *Plant Physiol.* 105, 1159–1166. doi: 10.1104/pp.105.4.1159

Roosta, H. R., and Schjoerring, J. K. (2008). Effects of nitrate and potassium on ammonium toxicity in cucumber plants. *J. Plant Nutr.* 31, 1270–1283. doi: 10.1080/01904160802135050

Rouphael, Y., Petropoulos, S. A., Cardarelli, M., and Colla, G. (2018). Salinity as eustressor for enhancing quality of vegetables. *Scientia Hortic.* 234, 361–369. doi: 10.1016/j.scienta.2018.02.048

Sanchez-Zabala, J., Gonzalez-Murua, C., and Marino, D. (2015). Mild ammonium stress increases chlorophyll content in Arabidopsis thaliana. *Plant Signaling Behav.* 10. doi: 10.4161/15592324.2014.991596

Savvas, D., Passam, H. C., Olympios, C., Nasi, E., Moustaka, E., Mantzos, N., et al. (2006). Effects of ammonium nitrogen on lettuce grown on pumice in a closed hydroponic system. *Hortscience* 41, 1667–1673. doi: 10.21273/HORTSCI.41.7.1667

Song, J., Yang, J., and Jeong, B. R. (2021). Growth, Quality, and Nitrogen Assimilation in Response to High Ammonium or Nitrate Supply in Cabbage (Brassica campestris L.) and Lettuce (Lactuca sativa L.). *Agronomy-Basel* 11. doi: 10.3390/agronomy11122556

Taiz, L. (2015). *Plant Physiology and Development, sixth edition* (Sunderland CT, USA: Sinauer Associates Inc).

Udert, K. M., Larsen, T. A., and Gujer, W. (2006). Fate of major compounds in source-separated urine. *Water Sci. Technol.* 54, 413–420. doi: 10.2166/wst.2006.921

Udert, K. M., and Wachter, M. (2012). Complete nutrient recovery from source-separated urine by nitrification and distillation. *Water Res.* 46, 453–464. doi: 10.1016/j.watres.2011.11.020

Urlic, B., Spika, M. J., Becker, C., Klaring, H. P., Krumbein, A., Ban, S. G., et al. (2017). Effect of NO3 and NH4 concentrations in nutrient solution on yield and nitrate concentration in seasonally grown leaf lettuce. *Acta Agriculturae Scandinavica Section B-Soil Plant Sci.* 67, 748–757. doi: 10.1080/09064710.2017.1347704

Wakeel, A., Farooq, M., Qadir, M., and Schubert, S. (2011). Potassium substitution by sodium in plants. *Crit. Rev. Plant Sci.* 30, 401–413. doi: 10.1080/07352689.2011.587728

Walch-Liu, P., Neumann, G., Bangerth, F., and Engels, C. (2000). Rapid effects of nitrogen form on leaf morphogenesis in tobacco. *J. Exp. Bot.* 51, 227–237. doi: 10.1093/jexbot/51.343.227

Weil, S., Barker, A. V., Zandvakili, O. R., and Etemadi, F. (2021). Plant growth and calcium and potassium accumulation in lettuce under different nitrogen regimes of ammonium and nitrate nutrition. *J. Plant Nutr.* 44, 270–281. doi: 10.1080/01904167.2020.1806313

Wenceslau, D., Oliveira, D. F., Rabelo, H., Ferbonink, G. F., Gomes, L. A. A., Leonel, E. C. A., et al. (2021). Nitrate concentration and nitrate/ammonium ratio on lettuce grown in hydroponics in Southern Amazon. *Afr. J. Agric. Res.* 17, 862–868.

Wheeler, R. M., Stutte, G. W., Subbarao, G. V., and Yorio, N. C. (2002). "Plant growth and human life support for space travel," in *Handbook of plant and crop physiology, 2 ed*. Ed. M. Pessarakli (New York: Marcel Dekker Inc).

Zhao, H. Y., Sun, S. M., Zhang, L. H., Yang, J. J., Wang, Z. Y., Ma, F. W., et al. (2020). Carbohydrate metabolism and transport in apple roots under nitrogen deficiency. *Plant Physiol. Biochem.* 155, 455–463. doi: 10.1016/j.plaphy.2020.07.037

Zheng, G., and Moskal, L. M. (2009). Retrieving leaf area index (LAI) using remote sensing: theories, methods and sensors. *Sensors* 9, 2719–2745. doi: 10.3390/s90402719

Zhou, J. Y., Wang, M., Sun, Y. M., Gu, Z. C., Wang, R. R., Saydin, A., et al. (2017). Nitrate increased cucumber tolerance to fusarium wilt by regulating fungal toxin production and distribution. *Toxins* 9. doi: 10.3390/toxins9030100

Zhu, X., Yang, R., Han, Y. Y., Hao, J. H., Liu, C. J., and Fan, S. X. (2020). Effects of different NO3-:NH4+ ratios on the photosynthesis and ultrastructure of lettuce seedlings. *Horticulture Environ. Biotechnol.* 61, 459–472. doi: 10.1007/s13580-020-00242-w

frontiers | Frontiers in Astronomy and Space Sciences

TYPE Original Research
PUBLISHED 16 August 2023
DOI 10.3389/fspas.2023.1198689

Check for updates

OPEN ACCESS

EDITED BY
Cyprien Verseux,
University of Bremen, Germany

REVIEWED BY
Lucie Poulet,
UMR6602 Institut Pascal (IP), France
Gabriela Soreanu,
Gheorghe Asachi Technical University of Iași, Romania

*CORRESPONDENCE
Angelo C. J. Vermeulen,
a.c.j.vermeulen@tudelft.nl

RECEIVED 01 April 2023
ACCEPTED 07 July 2023
PUBLISHED 16 August 2023

CITATION
Vermeulen ACJ, Papic A, Nikolic I and Brazier F (2023), Stoichiometric model of a fully closed bioregenerative life support system for autonomous long-duration space missions.
Front. Astron. Space Sci. 10:1198689.
doi: 10.3389/fspas.2023.1198689

COPYRIGHT
© 2023 Vermeulen, Papic, Nikolic and Brazier. This is an open-access article distributed under the terms of the Creative Commons Attribution License (CC BY). The use, distribution or reproduction in other forums is permitted, provided the original author(s) and the copyright owner(s) are credited and that the original publication in this journal is cited, in accordance with accepted academic practice. No use, distribution or reproduction is permitted which does not comply with these terms.

Stoichiometric model of a fully closed bioregenerative life support system for autonomous long-duration space missions

Angelo C. J. Vermeulen[1,2]*, Alvaro Papic[2], Igor Nikolic[1] and Frances Brazier[1]

[1]Systems Engineering and Simulation, Faculty of Technology, Policy and Management, Delft University of Technology, Delft, Netherlands, [2]SEADS (Space Ecologies Art and Design), Temse, Belgium

Bioregenerative life support systems (BLSS) are vital for long-duration and remote space missions to increase mission sustainability. These systems break down human waste materials into nutrients and CO_2 for plants and other edible organisms, which in turn provide food, fresh water, and oxygen for astronauts. The central idea is to create a materially closed loop, which can significantly reduce mission mass and volume by cutting down or even eliminating disposable waste. In most BLSS studies only a fraction of the resources, such as food, are provided by the system itself, with the rest taken on board at departure or provided through resupply missions. However, for autonomous long-duration space missions without any possibility of resupply, a BLSS that generates all resources with minimal or no material loss, is essential. The goal of this study is to develop a stoichiometric model of a conceptually fully closed BLSS that provides all the metabolic needs of the crew and organisms. The MELiSSA concept of the European Space Agency is used as reference system, consisting of five interconnected compartments, each inhabited by different types of organisms. A detailed review of publicly available MELiSSA literature from 1989 to 2022 revealed that no existing stoichiometric model met the study's requirements. Therefore, a new stoichiometric model was developed to describe the cycling of the elements C, H, O, and N through all five MELiSSA compartments and one auxiliary compartment. A compact set of chemical equations with fixed coefficients was established for this purpose. A spreadsheet model simulates the flow of all relevant compounds for a crew of six. By balancing the dimensions of the different compartments, a high degree of closure is attained at steady state, with 12 out of 14 compounds exhibiting zero loss, and oxygen and CO_2 displaying only minor losses between iterations. This is the first stoichiometric model of a MELiSSA-inspired BLSS that describes a continuous provision of 100% of the food and oxygen needs of the crew. The stoichiometry serves as the foundation of an agent-based model of the MELiSSA loop, as part of the Evolving Asteroid Starships (E|A|S) research project.

KEYWORDS

space exploration, human spaceflight, bioregenerative life support, waste processing, food production, ecosystem modeling, simulation, MELiSSA

1 Introduction

Bioregenerative life support systems (BLSS) will be a key component of future long-duration space exploration, as they can reduce mission mass and volume (Imhof et al, 2017; Audas et al, 2022). A BLSS recycles human waste by feeding it to an artificial ecosystem consisting of a range of different organisms, such as higher plants, microalgae, and bacteria. These organisms gradually break down the waste and in the process provide fresh food, generate oxygen, and clean water for the crew (Nelson et al, 2010; Escobar and Nabity, 2017; Pannico et al, 2022). As a result, there is less reliance on constant resupply from Earth, which greatly reduces the material footprint needed for extended missions in space (Macelroy and Averner, 1978; Häder, 2020; Audas et al, 2022). Because of its constant fresh food provision, a BLSS also solves the problem that essential nutrients in processed and prepackaged food are deficient and degrade over time (Cooper et al, 2017; Carillo et al, 2020). Biological systems are also capable of self-repair, unlike mechanical systems that need separate systems to be repaired. Surviving organisms and tissues in a damaged BLSS can potentially recover to their original size on their own, even after significant damage (Bartsev et al, 1996).

MELiSSA is a BLSS concept developed by ESA with a consortium of 15 international partners and the involvement of approximately 50 organizations (MELiSSA Foundation, 2023). It is an artificial ecosystem consisting of five interconnected compartments inhabited by higher plants, microalgae, microorganisms, and humans (abbreviated as C1 to C5, Figure 1; Table 1). Each of the compartments has its own specific metabolic function within the entire MELiSSA loop. First, all human waste is broken down through a sequence of three bioreactor types: a thermophilic anaerobic compartment (C1), photoheterotrophic compartment (C2) and nitrifying compartment (C3). This results in nutrients and CO_2 for microalgae and plants (C4a and C4b) that, in turn, provide food, oxygen, and fresh water for the crew (C5), thus closing the loop (Hendrickx and Mergeay, 2007; Clauwaert et al, 2017; Vermeulen et al, 2020a). The operational pilot plant at Universitat Autònoma de Barcelona consists of a number of connected MELiSSA compartments and demonstrates a part of the system's entire metabolic loop (Gòdia et al, 2004; Garcia-Gragera et al, 2021). Mathematical models of the MELiSSA loop have been developed and improved since the beginning of the MELiSSA project in 1989 (MELiSSA, 1989; Dussap and Gros, 1991). Some of these models are used for predictive control, to be run alongside the actual physical system. The MELiSSA models help in understanding the dynamics of mass flow fluctuations and achieving long-term reliability of the system (Cornet et al, 2001; Ciurans Molist et al, 2020; Poulet et al, 2020). Such ecosystem models can also be used to simulate the impact of unforeseen perturbations, deliberate interventions, or design changes in the system (Volk and Rummel, 1987; Pilo Teniente, 2015; Vermeulen et al, 2019).

To describe the material flows in an ecosystem model, the stoichiometric relations governing these flows need to be developed (Volk and Rummel, 1987; Begon and Townsend, 2021). Several authors have described mass flow models of biological life support systems (Volk and Rummel, 1987; Garland, 1989; Loader et al, 1997; Finn, 1998), but not all studies contain the underlying chemical stoichiometric equations. The stoichiometric equations describing mass flows in the MELiSSA BLSS have been published in publicly-available MELiSSA literature, both in peer-reviewed papers and research reports disseminated by the MELiSSA Foundation (Table 1). In less than half of the listed studies, all five MELiSSA compartments were modeled. The other studies describe either a smaller number of compartments, or just one. The loop is never fully closed in any of the listed studies. There are a number of reasons for this. First of all, it may indicate that certain compounds are not part of the regenerative logic of the system and are not generated within the loop, and therefore need to be fully supplied from the outside (Dussap et al, 1993; Poughon et al, 2009). Secondly, it may indicate an output that does not get regenerated, such as a residual indigestible material (Fulget et al, 1999; Poughon et al, 2000). Because of the resulting accumulation of that material, external supply is required to keep the system running. And thirdly, it may be a deliberate system design choice that only a fraction of a particular compound or resource is generated by the BLSS. Several MELiSSA studies, for example, explicitly specify that only a part of the needed food is generated by the loop (Poughon et al, 2000; Guirado and Podhajsky, 2008; Thiron, 2020). The rest is supplied externally. One of the main motivations for such a choice is the limited space that is available in common spacecraft and habitat designs to integrate bioreactors and plant growth chambers (Johnson et al, 2021; Gorce et al, 2022).

Almost three-quarters of the researched MELiSSA studies list all the stoichiometric equations of their models. The other studies limit themselves to a few selected equations as examples. The stoichiometric coefficients in the chemical equations can either be fixed beforehand, or dynamically calculated on the fly, during the simulation run. For example, in simulating the production of *Limnospira indica* in C4a, the elementary composition of its biomass is determined by the variable light irradiation inside the photobioreactor (Guirado and Podhajsky, 2008; Poughon et al, 2009). This then necessitates the recalculation of all subsequent stoichiometric equations that contain this dynamic empirical biomass formula.

Whenever creating a stoichiometry to describe mass flows in an ecosystem, choices need to be made about which compounds will be considered, and which level of detail will be used to describe the ecosystem's biochemical processes (Dubitzky et al, 2011; Begon and Townsend, 2021). This choice is influenced by the level of knowledge about the individual metabolism of the different species in the ecosystem, but ultimately depends on the objective and scope of the study. In light of this, the reviewed MELiSSA studies contain varying assumptions concerning the role of different compounds such as lipids, VFAs, and CO_2. This is partially due to the fact that over time the MELiSSA models became more detailed, incorporating more processes. Early MELiSSA papers assume that all lipids consumed by the astronauts are oxidized and no traces of lipids are found in the feces (Dussap and Gros, 1991; Dussap et al, 1993). This is later adjusted, and lipids become an explicit part of the feces input in C1 (Poughon et al, 2000). The mix of VFAs that is generated as output of C1 varies quite significantly between the different studies. In the earliest studies only acetic acid and butyric acid are considered (Dussap and Gros, 1991; Dussap et al, 1993), but in later studies, a broader range of VFAs is included in the stoichiometry (Poughon, 2007b).

10.3389/fspas.2023.1198689

TABLE 1 Systematic review of the stoichiometric descriptions of mass flows in the various compartments of the MELiSSA loop, as documented in publicly available literature. Only modeling studies containing at least one chemical equation are listed. "Full closure" indicates that all material outputs are utilized as inputs without the need for any external supplies. "Chemical equations" indicates the number of involved chemical equations that are factually listed in the publication. "Stoichiometrically balanced" indicates that the publication includes the stoichiometric coefficients for all fixed equations. Stoichiometric coefficients are described as dynamic when coefficients within at least one chemical equation fluctuate throughout a simulation run. The macromolecule composition is described as dynamic when the proportion of CHON elements in at least one chemical formula varies over time. C, compartment; N/A, not applicable.

MELiSSA compartments	Full closure	Chemical equations	Stoichiometrically balanced	Stoichiometric coefficients	Macromolecule composition	References
C1-C5[a]	No	Partly	Yes	Fixed	Fixed	MELiSSA (1989)
C1-C5[a]	No	Complete	Yes	Fixed	Fixed	Dussap and Gros (1991)
C1-C5[a]	No	Complete	Yes	Fixed	Fixed	Dussap et al (1993)
C1-C5[a]	No	Complete	Yes	Fixed + dynamic	Fixed + dynamic	Poughon et al (1994)
C1-C5[a]	No	Complete	Yes	Fixed	Fixed	Fulget (1996)
C1-C5[a]	No	Examples	Yes	Fixed + dynamic	Fixed + dynamic	Fulget et al (1999)
C1-C5	No	Complete	Incomplete	Fixed + dynamic	Fixed + dynamic	Poughon et al (2000)
C1-C5	No	Complete	Yes	Fixed + dynamic	Fixed + dynamic	Poughon (2007b)
C1-C5	No	Complete	Yes	Fixed + dynamic	Fixed + dynamic	Guirado and Podhajsky (2008)
C1-C5	No	Examples	Yes	Fixed + dynamic	Fixed + dynamic	Poughon et al (2009)
C1-C5	No	Complete	Yes	Fixed + dynamic	Fixed + dynamic	Thiron (2020)
C1-C4a	No info	Complete	No	None	Fixed	Hendrickx et al (2006)
C2+C5	No	Complete	Yes	Fixed	Fixed	Poughon (1994b)
C4a-C5	No	Partly	Yes	Fixed + dynamic	Fixed + dynamic	Poughon (2007a)
C4a-C5	No	Partly	Yes	Fixed	Fixed	Pilo Teniente (2015)
C4a-C5	No	Partly	Yes	Fixed	Fixed	Alemany et al (2019)
C2	N/A	Complete	Yes	Fixed	Fixed	Cornet and Dussap (2000)
C3	N/A	Complete	Yes	Fixed	Fixed	Cruvellier et al (2016)
C4a	N/A	Complete	Yes	Fixed	Fixed	Poughon (1994a)
C4a	N/A	Complete	Yes	Fixed	Fixed	Cornet et al (1998)
C4a	N/A	Complete	Yes	Fixed	Fixed	Cornet et al (2003)
C4a	N/A	Complete	Yes	Dynamic	Dynamic	Poughon et al (2020)
C4b	N/A	Complete	No	None	No info	Maclean et al (2010)
C4b	N/A	Complete	Yes	Fixed	Fixed	Poulet et al (2020)

[a]Only C4a (*Limnospira* compartment), no C4b (higher plant compartment).

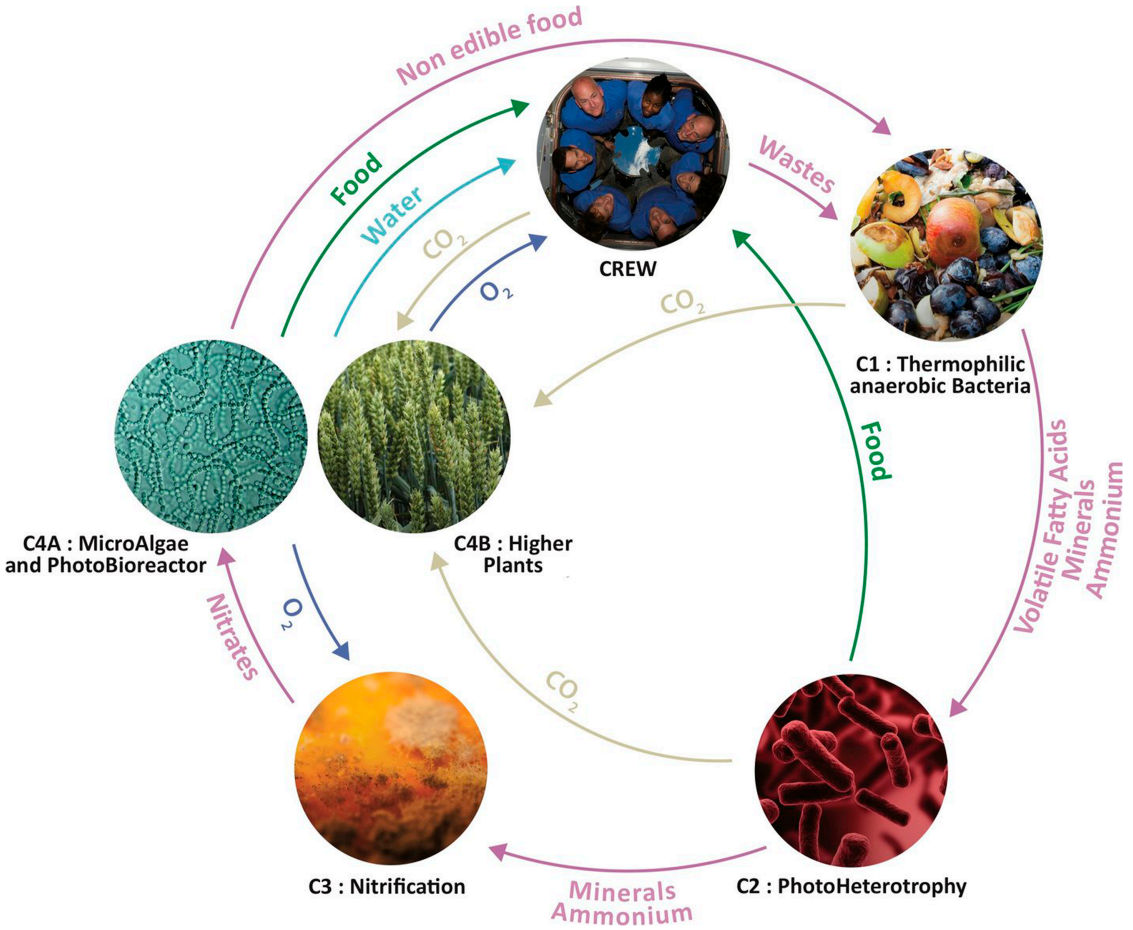

FIGURE 1
Overview of the MELiSSA loop with its five main compartments and a schematic overview of the different material flows. Some of these material flows have been adjusted in the stoichiometric model. See Section 3 Stoichiometric model assumptions for more details. Image by the MELiSSA Foundation.

The stoichiometric model presented in this paper provides the basis for an agent-based model (ABM) of the MELiSSA loop to study the interactions and emergent behavior of the MELiSSA system from a theoretical perspective. MELiSSA is fundamentally a complex system, and properties such as nonlinearity, stochasticity and chaos may play an important role in the overall behavior of the system, just like in any ecosystem (Bjørnstad, 2015). Because all functions in the MELiSSA loop are tightly coupled and since there are no large buffers in space (e.g., no large atmosphere or water bodies), slight variations in any of the loop's pathways can have dramatic consequences for the entire loop (Macelroy and Averner, 1978; Poulet et al, 2018). It is precisely such tightly coupled systems that are potentially susceptible to irregular fluctuations (Bjørnstad, 2015). ABMs offer a modeling approach that helps to gain insight in such dynamics and helps to explore different design strategies for improved system robustness. ABMs are used to understand those aspects of the behavior of a system, that are not easily represented in population-level differential equations, such as variation among individuals or variation of individuals during their life cycle (Deangelis and Grimm, 2014). Such exploratory models of complex systems lead to insights about essential mechanisms and principles, a use of modeling that is different from modeling aimed at making accurate predictions (Forrest and Mitchell, 2016). MELiSSA modeling studies to date focus on predictive modeling because this is a critical step to develop a durable and reliable BLSS. The MELiSSA modelling approach is mechanistic, allowing for better understanding and improved predictions. With its exploratory approach, this study can be considered as being complementary to the existing MELiSSA modeling efforts. In order to build an ABM of MELiSSA, a stoichiometric model is needed that describes essential mass flows between all involved agents (bacteria, microalgae, higher plants and humans). The key metabolic processes in all MELiSSA compartments need to be described with enough detail to enable studying the interactions. At the same time, they need to remain abstracted enough to tlead to an efficient model and retain relevance for the objectives of the ABM which are centered around investigating the impact of heterogeneity in the system and capturing nonlinear dynamics.

The research objective of this paper is to develop a stoichiometric model of a hypothetical BLSS that provides a crew with fresh food and oxygen during long-duration space missions, without the need for any resupply. The

envisioned stoichiometric model should conform to the following requirements:

- The system provides 100% of all the food and oxygen needed by the crew, and 100% of the resources needed by every other organism in the loop.
- The stoichiometric model is fully closed. Every single output is used as input, and no additional external supplies are needed during steady state.
- No kinetic limitations of the stoichiometric reactions are used. Macromolecules do not have a dynamic composition (e.g., biomass composition does not depend on light), and all stoichiometric coefficients are fixed. Such a static approach is sufficient for the current goals of the ABM of MELiSSA that is developed on top of this stoichiometry.

The current literature (listed in Table 1) has, to the authors' knowledge, not included such a stoichiometric model of the MELiSSA loop. As described above, the loop is always considered to be partially open, primarily for practical reasons. The research reported in this paper is more theoretical in nature, focusing on the internal dynamics of hypothetically fully closed systems.

2 Materials and methods

This section describes the empirical formulas, stoichiometric equations, and the setup of a static spreadsheet model.

2.1 Empirical formulas

Table 2 provides an overview of the empirical formulas of the large biomolecules. More detailed descriptions of the origin of each formula are then discussed. The empirical formulas of biomass and feces are provided for comparative purposes only, since both biomass and feces are represented as proportions of carbohydrates, proteins and lipids.

2.1.1 Carbohydrates, proteins, and lipids

The formula for carbohydrates is the general formula for polysaccharides, used in many of the MELiSSA modeling studies (e.g., in (Dussap et al, 1993) and (Thiron, 2020)). There are, however, a range of different general formulas used for proteins in the MELiSSA literature (Fulget, 1996; Duatis et al, 2008; Thiron, 2020). Our approach was to first calculate the average protein composition of the different organisms generating biomass in our model, and then compare this result to general protein formulas published in multiple BLSS studies. In our stoichiometric model, the higher plants are represented by a generalized "ideal plant", in line with previous MELiSSA studies (Poughon, 2007b; Guirado and Podhajsky, 2008). It is conceived as an average of the nutritional properties of bread wheat, durum wheat, potato and soybean. The CHON composition of the protein of this ideal plant is then averaged with that of *Limnospira* and *Rhodobacter*, all using values listed in MELiSSA literature (Dussap et al, 1993; Duatis et al, 2008). This results in $CH_{1.5799}O_{0.3134}N_{0.2558}$. This composition comes very close to $CH_{1.5900}O_{0.3100}N_{0.2500}$ used as general protein formula in studies of the Lunar Palace BLSS (Hu et al, 2010; Fu et al, 2016), and hence this latter formula was selected. Palmitic acid is often used as lipid in stoichiometries of ecosystems (Volk and Rummel, 1987; Guirado and Podhajsky, 2008). However, vegetable oils mainly consist of more complex triacylglycerols (Zambelli et al, 2015). Therefore in this stoichiometric model, lipids are represented by tripalmitin, consisting of one glycerol molecule bonded to three palmitic acid molecules. Just like with palmitic acid, the fermentation of glycerol also leads to VFAs, further contributing to the overall VFA output of C1.

2.1.2 Biomass

Throughout the MELiSSA literature the empirical formulas of the biomass of specific organisms differ to varying degrees. The empirical formula that describes the biomass of the purple sulphur bacteria *Rhodobacter* varies, for example, between (Dussap et al, 1993), (Hendrickx et al, 2006), and (Thiron, 2020). This is to be expected since empirical formulas are always approximations. Moreover, in several MELiSSA modeling studies, biomass composition is dependent on environmental parameters such as light input, and consequently the biomass composition varies throughout the course of a simulation (Table 1). In the current stoichiometric model, biomass is consistently represented as a combination of carbohydrates, proteins, and lipids, and not as one single molecule. This makes it possible to trace the levels of each individual compound throughout the loop. To establish the

TABLE 2 Empirical formulas of all large biomolecules used in the stoichiometric model.

Compound	Empirical formula	References and notes
Carbohydrates	$CH_{1.6667}O_{0.8333}$	General polysaccharides
Proteins	$CH_{1.5900}O_{0.3100}N_{0.2500}$	Hu et al, 2010, Fu et al, 2016
Lipids	$CH_{1,9216}O_{0,1177}$	Tripalmitin
Biomass Rhodospirillum rubrum	$CH_{1.6472}O_{0.3598}N_{0.1788}$	18% carbohydrates, 72% proteins, 10% lipids, literature
Biomass Limnospira sp.	$CH_{1.6472}O_{0.3598}N_{0.1788}$	18% carbohydrates, 72% proteins, 10% lipids, literature
Biomass higher plants (edible)	$CH_{1.6889}O_{0.6090}N_{0.05487}$	70% carbohydrates, 20% proteins, 10% lipids, literature
Biomass higher plants (non-edible)	$CH_{1.6667}O_{0.8333}$	100% carbohydrates, 0% proteins, 0% lipids, literature
Feces	$CH_{1.6676}O_{0.6028}N_{0.07715}$	66% carbohydrates, 28% proteins, 6% lipids, calculated

composition of the different types of biomass, in this study an estimate was made based on averaged values from literature. As validation, the corresponding empirical formula was then compared with formulas published in MELiSSA literature.

In correspondence with the MELiSSA study of (Hendrickx et al, 2006), the same biomass composition was chosen for both *Rhodospirillum rubrum* and *Limnospira sp*. Based on literature (e.g., Dussap et al, 1993; Kobayashi and Kobayashi, 1995; Teuling et al, 2017), the following biomass composition was established (dry weight, or DW): 18% carbohydrates, 72% proteins, and 10% lipids. Both organisms contain high amounts of protein, hence their interesting potential as food sources (Vrati, 1984; Clauwaert et al, 2017; Muys et al, 2019). Using the previously established CHON compositions of carbohydrates, proteins and lipids, the overall biomass composition corresponds to the empirical formula $CH_{1.6472}O_{0.3598}N_{0.1788}$. This is in the same range as the biomass formulas used in the MELiSSA modeling studies of (Hendrickx et al, 2006) and (Thiron, 2020).

Carbohydrates are typically the most abundant compound in plants, encompassing both structural (e.g., cellulose) and non-structural (e.g., starch and glucose) carbohydrates (Moore and Hatfield, 1994). As explained before, an 'ideal plant' is used in the current model. Four energy- and/or protein-rich crops were selected and combined based on (Paradiso et al, 2013): bread and durum wheat, potato and soybean. Averaging the carbohydrate, protein and lipid fractions of these four crops (Molders et al, 2012; Stasiak et al, 2012; Page and Feller, 2013; Paradiso et al, 2013), leads to the following edible plant biomass composition (DW): 70% carbohydrates, 20% proteins, and 10% lipids. Taking into account the above CHON compositions of carbohydrates, proteins and lipids, this corresponds to the empirical macroformula $CH_{1.6889}O_{0.6090}N_{0.05487}$. This is in line with the "food" descriptions in other MELiSSA studies (Fulget, 1996; Thiron, 2020). The inedible part of the plant is considered to be 100% carbohydrates, assuming that it is only composed of cellulose.

2.1.3 Feces

Just like with biomass, feces are expressed in the model as a combination of carbohydrates, proteins and lipids. The composition of feces was calculated by stoichiometrically balancing the equation for human metabolism (see 5.5). The proportions of carbohydrates, proteins and lipids as reported in literature [review in (Rose et al, 2015)] were used as a guideline to solve the stoichiometry. The resulting empirical formula is $CH_{1.6676}O_{0.6028}N_{0.07715}$.

2.2 Establishing the stoichiometric equations

As a general method to balance the equations that represent the reactions occurring in each compartment, each one is stated as a linear programming problem–or non-linear when the constraints of the particular reaction so require–where the goal is to minimize the total amount of matter used. The variables are defined as the number of moles of each compound on either side of the equation. The objective function is subject to the linear constraint of keeping the number of atoms of a given element equal on both sides of the equation. Additionally for each problem *ad hoc* constraints are described e.g., to keep proportions of VFA's produced similar to experimental data on C2. The solving engine for these problems is MS Excel's built-in optimization tool. For linear problems Simplex is used and for non-linear problems GRN non-linear, both on their default configurations settings. In reporting throughout this paper 4 significant decimals are used, but during calculations in Excel 14 decimals were used.

This stoichiometry is a full revision of a version of that was concisely published in two IAC conference papers (Vermeulen et al, 2018b; 2019) and presented at two MELiSSA conferences (Vermeulen et al, 2018a; 2020b). The revisions were based on a detailed validation session and on further literature study. The main changes were the following:

- All biomass compositions were re-evaluated (*Limnospira*, *Rhodospirillum* and higher plants) to more accurately represent their carbohydrate, protein and lipid content.
- No more distinction between fecal and bacterial protein, in line with the singular use of carbohydrates and lipids in the stoichiometry.
- The VFA spectrum was extended beyond acetic acid and butyric acid.
- Instead of representing urine as NH_3, it is now represented as urea, in order to bring carbon into the urine cycling. Hence, a new subsystem with its own stoichiometry representing the breakdown of urea was added.

2.3 Static spreadsheet model to test the closure level

To calculate the steady state flow values for each stream, each compartment's equation is linked, thus building an equation based model that represents the whole cycle. To solve it, the one *a priori* known value is used: the consumption rate of the crew compartment, which has been set at 3,000 kcal/day/person. Knowing these requirements for C5, the required food outputs of C4a and C4b are calculated. By continuing to work backwards through the entire stoichiometry, the flow rates through the entire loop could be established over a period of 1 day for a crew of six.

Since there is a subcycle between C1 and C2 the exchange flows between them need to be calculated (Figure 2). Having the required steady state flows into C1, and out of C2 (except the subcycle flows into each other), the process of exchange between C1 and C2 can be examined. This requires an iterative approach in which, given an initial output of VFAs from C1 to C2, a subsequent C2 to C1 flow of biomass is calculated. This, in turn, updates the flow from C1 to C2 again. This eventually converges into a stable exchange between C1 and C2, with complete processing of all VFAs. This then results in cycle-wide steady state flow rates.

3 Stoichiometric model assumptions

This section describes the general assumptions behind the model and those per compartment.

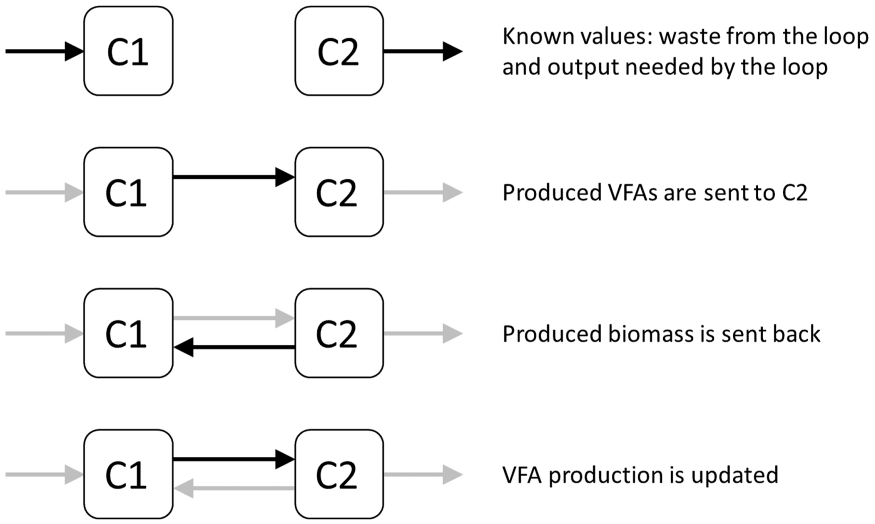

FIGURE 2
Diagram representing the subcycle between C1 and C2, and the process of converging to a stable exchange of VFAs and biomass between the two compartments.

3.1 General assumptions

This stoichiometry is based on the four CHON elements; sulfur and phosphor are not yet included. Throughout the entire loop, food and feces are described as a proportion of carbohydrates, proteins and lipids. The water in this stoichiometric model is what is used in the chemical reactions. The actual water needs of a human crew (drinking and hygiene water) have not been included. Net biomass production only occurs in C2, C4a, and C4b because this biomass is a material input for other compartments. For the other compartments it is assumed there is no growth, and hence no net biomass production occurs. This has an impact on the stoichiometric approach for each compartment, which differs when describing a growth metabolism vs. a maintenance metabolism without growth (Cruvellier et al, 2016). It is further assumed that all waste materials are fully digested in C1, and no undigestible residues are left. And there is no limitation in terms of available space and hence the number of bioreactors and growth chambers that can be included.

3.2 MELiSSA loop adjustments

Several adjustments have been made to the official concept of the MELiSSA loop, as illustrated in Figure 1. They can be summarized as follows (more details further down in this section):

- The *Rhodospirillum* biomass that is produced in C2 is not used for human consumption, but is sent to C1 where it is anaerobically digested, together with the other organic waste.
- C2 does not produce any net CO_2.
- Urea is included as an individual waste product and is processed by C3.
- C3 consists of two subcompartments, C3a and C3b, to respectively process ammonia and urea.
- An auxiliary compartment has been added to burn surplus hydrogen and generate water.

3.3 Assumptions for Compartment 1: anaerobic fermentation

In C1, the thermophilic anaerobic bacteria can convert up to 70% of the waste under experimental conditions (Lasseur et al, 2010). This is because cellulose and hemicellulose can only be hydrolyzed slowly, further hampered by the fact that both are often intermeshed with lignin in lignocellulose, which is even more difficult to break down (Liebetrau et al, 2017). In this model it is assumed that all organic waste is fully converted in C1. In the MELiSSA system up to 71% of the organic nitrogen in the waste is converted into ammonium (Clauwaert et al, 2017). In our stoichiometric model it is assumed that this is 100%. The VFA spectrum produced by C1 consists of four VFAs: acetic acid, propionic acid, butyric acid and valeric acid. These VFAs are characteristically produced during acidogenesis (Jiang et al, 2013; Khan et al, 2016).

3.4 Assumptions for Compartment 2: *Rhodospirillum* culture

In the original conceptualization of MELiSSA, it was assumed that in addition to the microalgae and crops from C4, the edible purple sulfur bacteria from C2 would also serve as a food supply for the crew (Lasseur et al, 1996; Albiol et al, 2000; Figure 1). However, because of close proximity, there is always a chance that pathogens associated with fecal matter in C1 pass through membrane filtration and end up with the edible bacteria in C2 (Clauwaert et al, 2017). Therefore, the produced biomass from this compartment is sent back

TABLE 3 Assumptions about the human metabolism. Listed values are for one crew member.

Parameter	Value	References and notes
Daily caloric intake	3,000 kcal	Poughon et al, 1994; Ewert et al, 2022
Daily caloric intake from higher plants	2,700 kcal	90%
Daily caloric intake from Limnospira	300 kcal	10%
Oxygen consumption	0.84 kg/day or 52.50 mol/day	Jones, 2003
CO_2 production	1 kg/day or 22.72 mol/day	Jones, 2003
Urea production	0.1239–0.7758 mol/day	Based on Putnam, 1971; MedlinePlus, 2023.
Feces production	Stoichiometrically determined	—

to C1 for anaerobic degradation. This is in correspondence with other MELiSSA modeling studies (Poughon et al, 2000; Waters et al, 2004; Thiron, 2020). The overall diet of the crew should only contain a limited amount of microbial single-cell protein, because of increased nucleic acid contents and lower palatability (Tusé and Miller, 1984; Tranquille and Emeis, 1996). The crew is already using another microbial food source (*Limnospira* from C4a, Figure 1), and this might be an additional argument to avoid consuming the bacteria from C2. Theoretically, the assimilation of the VFAs by purple sulfur bacteria in C2 could generate a net CO_2 output (Hendrickx and Mergeay, 2007). However, in practice, this has not been observed yet in MELiSSA bioreactor experiments with C1 effluent as VFA source (Mastroleo et al, 2020).

3.5 Assumptions for Compartment 3: processing ammonia and urea

Analogous to C4, this compartment also consists of two subcompartments, C3a and C3b. C3a processes ammonia and produces nitrate. C3b is a urine treatment unit based on C3a, and also produces nitrate. It is assumed that all incoming ammonia and urea are converted to nitrate.

3.6 Assumptions for Compartment 5: human metabolism

The assumptions about the human metabolism are summarized in Table 3. The reference caloric value of the higher plants is estimated to be 4,000 kcal/kg dry weight (DW). This is based on the reported caloric values of the four crops that constitute the ideal plant (adjusted for their moisture content): bread wheat and durum wheat (Kaleta and Górnicki, 2013; Knowledge4 Policy, 2021; WebMD, 2021), potato (Decker and Ferruzzi, 2013; U.S. Food & Drug Administration, 2017), and soybean (Food Data Central, 2019b). The reference caloric value of *Limnospira* (commercially available as Spirulina) is estimated to be 3,000 kcal/kg DW (Food Data Central, 2019a). Solid output of the human metabolism is described as feces and urea. All other body wastes such as dead skin cells, sweat solids, hair, nails, etc. (Hu et al, 2010) are assumed to be part of the feces. H_2O is only integrated in the stoichiometry as a metabolite, and as such the amounts do not represent actual water consumption. It is assumed that the anabolism and catabolism of the crew are in dynamic equilibrium, and that the crew neither gains or loses weight.

4 Results

This section describes the results of the stoichiometry development, and the simulation results.

4.1 Stoichiometric equations

For each compartment a set of chemical equations with fixed stoichiometric coefficients has been developed, making sure that all types of output are also used as input in the loop, thus enabling full closure. The equations are partially based on existing equations from the MELiSSA literature, but were tailored to serve the needs of this study based on additional literature.

4.1.1 Compartment 1: fermentation with thermophilic anaerobic bacteria

The first compartment of the MELiSSA loop is an anaerobic digester with a consortium of thermophilic bacteria that receives fecal material and other wastes, such as inedible plant material (Michel et al, 2005; Mastroleo, 2009; Poughon et al, 2013). Anaerobic digestion is a natural process that typically consists of four subsequent stages: hydrolysis, acidogenesis, acetogenesis and methanogenesis. Volatile fatty acids are intermediate products in this process, while methane is the main end product (Hendrickx and Mergeay, 2007; Khan et al, 2016). In the MELiSSA system a partial anaerobic transformation is used with a maximal yield of volatile fatty acids (VFAs), all while avoiding the production of methane. The VFAs are useful biomolecules that can be utilized as nutrients for other microorganisms downstream in the MELiSSA loop. Such partial anaerobic digestion is achieved by operating the bioreactor under slightly acidified conditions (pH 5.3) which inhibits methanogenic activity (Mastroleo, 2009; Clauwaert et al, 2017).

Organic waste typically consists of polymers (carbohydrates and proteins), as well as fats (Liebetrau et al, 2017). These cannot be taken up by the microbial cells and have to be broken

down into smaller compounds first. During hydrolysis, bacteria excrete hydrolytic enzymes which split these substances into sugars, amino acids, fatty acids, and glycerol. These water-soluble hydrolysis products are then converted into volatile fatty acids, CO_2 and hydrogen during anaerobic fermentation (or acidogenesis) (Lauwers et al, 2013; Liebetrau et al, 2017). C1 receives input from three different sources: feces from the crew, inedible plant material, and biomass from C2. The next paragraphs describe the stoichiometries of the fermentation of, respectively, carbohydrates, proteins, and lipids.

4.1.1.1 Carbohydrate fermentation

Carbohydrate fermentation in the MELiSSA loop has been described in multiple studies, and results in the production of VFAs, CO_2 and hydrogen. In Hendrickx et al (2006) only one generic formula representing all VFAs is used, while in all the other consulted MELiSSA studies just two VFAs are produced (e.g., Dussap et al, 1993; Poughon et al, 2009). In some studies this is complemented with the production of bacterial biomass (Guirado & Podhajsky, 2008; Thiron, 2020). As stated above, in the current stoichiometry, four VFAs are used and no biomass production is needed in the equation of this compartment. As a consequence, a new stoichiometry had to be calculated. Proportions of acetic acid, propionic acid, butyric acid and valeric acid were used from (Yin et al, 2016), describing the anaerobic fermentation of glucose as model carbohydrate at pH 6. In below equation, the proportions of these four VFAs were used since the MELiSSA C1 bioreactor also operates at a low pH of 5.3 (Clauwaert et al, 2017). CO_2 and hydrogen are produced in equal proportions, in line with other published balanced carbohydrate fermentation reactions (Dussap et al, 1993; Yin et al, 2016).

$$\begin{aligned} CH_{1.6667}O_{0.8333} + 0.1666\,H_2O \rightarrow\ & 0.04651\ \underset{\text{acetic acid}}{C_2H_4O_2} + 0.0711\ \underset{\text{propionic acid}}{C_3H_6O_2} \\ & + 0.09535\ \underset{\text{butyric acid}}{C_4H_8O_2} + 0.006313\ \underset{\text{valeric acid}}{C_5H_{10}O_2} \\ & + 0.2807\,CO_2 + 0.2807\,H_2 \end{aligned} \quad (1)$$

4.1.1.2 Protein fermentation

Just like with carbohydrates, there are several stoichiometric descriptions of the fermentation of proteins in the MELiSSA literature. Older studies use acetic acid and butyric acid as VFA output (e.g., Dussap & Gros, 1991), subsequent studies use up to 5 VFAs (e.g., Guirado & Podhajsky, 2008; Thiron, 2020). In these latter studies, microbial biomass is also included as an output. As biomass output is not necessary in this part of our stoichiometric model, and as a slightly differing empirical formula for protein is used, a new stoichiometric balance needs to be calculated. Proteins are polymers consisting of amino acids. During anaerobic fermentation, proteins are first broken down into their individual amino acids. The subsequent fermentation of these amino acids can be described using a single reaction step, and results in the production of VFAs, CO_2, hydrogen and ammonia (Ramsay and Pullammanappallil, 2001; Poughon et al, 2009). In stoichiometric equations, CO_2, hydrogen and ammonia are generally being produced in a similar order of magnitude (Poughon, 2007b; Thiron, 2020). Tepari (2019) investigated protein fermentation during anaerobic wastewater treatment, and used bovine serum albumin (BSA) as model protein. At pH 5, only acetic acid (37.4%), propionic acid (13.7%) and butyric acid (48.9%) were produced, and no valeric acid. These proportions were used to calculate the following stoichiometric equation:

$$\begin{aligned} CH_{1.59}O_{0.31}N_{0.25} + 0.4962\,H_2O \rightarrow\ & 0.1056\ \underset{\text{acetic acid}}{C_2H_4O_2} + 0.03867\ \underset{\text{propionic acid}}{C_3H_6O_2} \\ & + 0.138\ \underset{\text{butyric acid}}{C_4H_8O_2} + 0.1209\,CO_2 \\ & + 0.037\,H_2 + 0.25\,NH_3 \end{aligned} \quad (2)$$

4.1.1.3 Lipid fermentation

As described above, tripalmitin is used as model lipid in this model. Since in previous MELiSSA modeling studies, palmitic acid is used, a new stoichiometric equation has to be calculated. When lipids such as triacylglycerols are anaerobically digested, they are first hydrolyzed to glycerol and long-chain fatty acids (LCFAs) (Mackie et al, 1991; Li et al, 2002; Cirne et al, 2007). Subsequently, the glycerol is degraded into VFAs, while the LCFAs are broken down into acetic acid and hydrogen through beta-oxidation (Weng and Jeris, 1976; Ceron-Chafla et al, 2021; Holohan et al, 2022). Firstly, the glycerol and LCFA fermentations will be individually described, after which they will be integrated into one equation.

The hydrolysis of tripalmitin can be written as follows:

$$\underset{\text{tripalmitin}}{C_{51}H_{98}O_6} + 3\,H_2O \rightarrow \underset{\text{glycerol}}{C_3H_8O_3} + 3\,\underset{\text{palmitic acid}}{C_{16}H_{32}O_2} \quad (3)$$

In experiments by Yin et al, 2016, glycerol was subjected to (non-strict) anaerobic fermentation at pH 6. The study presents three individual stoichiometric reactions, each describing the degradation of glycerol into acetic acid, propionic acid, and butyric acid. The experiment resulted in a production of 32% acetic acid, 52% propionic acid, and 16% butyric acid. Integrating the three individual stoichiometric reactions, taking into account the above mentioned proportion, leads to the following single equation:

$$\begin{aligned} \underset{\text{glycerol}}{C_3H_8O_3} + 0.2727\,H_2O \rightarrow\ & 0.2727\ \underset{\text{acetic acid}}{C_2H_4O_2} + 0.4481\ \underset{\text{propionic acid}}{C_3H_6O_2} \\ & + 0.1396\ \underset{\text{butyric acid}}{C_4H_8O_2} + 0.5519\,CO_2 \\ & + 1.3766\,H_2 + 0.4481\,H_2O \end{aligned} \quad (4)$$

The stoichiometric equation for palmitic beta-oxidation is described by Li et al (2018):

$$\underset{\text{palmitic acid}}{C_{16}H_{32}O_2} + 14\,H_2O \rightarrow 8\ \underset{\text{acetic acid}}{C_2H_4O_2} + 14\,H_2 \quad (5)$$

Integrating Eqs 3–5 leads to:

$$\begin{aligned} CH_{1.9216}O_{0.1177} + 0.8789\,H_2O \rightarrow\ & 0.4759\ \underset{\text{acetic acid}}{C_2H_4O_2} + 0.008786\ \underset{\text{propionic acid}}{C_3H_6O_2} \\ & + 0.002737\ \underset{\text{butyric acid}}{C_4H_8O_2} \\ & + 0.01082\,CO_2 + 0.8505\,H_2 \end{aligned} \quad (6)$$

4.1.2 Compartment 2: VFA processing by photoheterotrophic bacteria

The purpose of MELiSSA C2 is to recycle the VFAs produced in C1. The purple non-sulphur phototrophic bacteria *Rhodospirillum*

rubrum is utilized for this. Under anaerobic conditions, it uses light as an energy source to convert VFAs into biomass (Mastroleo, 2009; De Meur et al, 2020). Because we use a custom composition of *Rhodospirillum* biomass in this model, a new stoichiometry had to be calculated. Anaerobic digestion of organic matter may lead to fluctuating proportions of different VFAs (Alloul et al, 2018). Because of the variable VFA spectrum coming out of C1, it was decided to develop a individual equation for each VFA. The assimilation process consumes CO_2 and NH_3, and for acetic acid also hydrogen (Dussap et al, 1993; Fulget, 1996; Thiron, 2020). As explained above, no net CO_2 production occurs in the following equations.

$$\underset{\text{acetic acid}}{C_2H_4O_2} + H_2 + 0.2774\,CO_2 + 0.4073\,NH_3 \rightarrow \Big[0.3327\,\underset{\text{carbohydrates}}{CH_{1.6667}O_{0.8333}} + 1.6291\,\underset{\text{proteins}}{CH_{1.5900}O_{0.3100}N_{0.2500}} + 0.3155\,\underset{\text{lipids}}{CH_{1,9216}O_{0,1177}}\Big]_{\text{Rhodospirillum}} + 1.7353\,H_2O \quad (7)$$

$$0.8556\ \underset{\text{propionic acid}}{C_3H_6O_2} + 0.1611\,CO_2 + 0.4879\,NH_3 \rightarrow \Big[0.3986\,\underset{\text{carbohydrates}}{CH_{1.6667}O_{0.8333}} + 1.9515\,\underset{\text{proteins}}{CH_{1.5900}O_{0.3100}N_{0.2500}} + 0.3780\,\underset{\text{lipids}}{CH_{1,9216}O_{0,1177}}\Big]_{\text{Rhodospirillum}} + 1.052\,H_2O \quad (8)$$

$$0.5563\ \underset{\text{butyric acid}}{C_4H_8O_2} + 0.3086\,CO_2 + 0.4532\,NH_3 \rightarrow \Big[0.3702\,\underset{\text{carbohydrates}}{CH_{1.6667}O_{0.8333}}\ 1.8127\,\underset{\text{proteins}}{CH_{1.5900}O_{0.3100}N_{0.2500}} + 0.3511\,\underset{\text{lipids}}{CH_{1,9216}O_{0,1177}}\Big]_{\text{Rhodospirillum}} + 0.8182\,H_2O \quad (9)$$

$$0.4084\,\underset{\text{valeric acid}}{C_5H_{10}O_2} + 0.3762\,CO_2 + 0.4325\,NH_3 \rightarrow \Big[0.3533\,\underset{\text{carbohydrates}}{CH_{1.6667}O_{0.8333}} + 1.7299\,\underset{\text{proteins}}{CH_{1.5900}O_{0.3100}N_{0.2500}} + 0.335\,\underset{\text{lipids}}{CH_{1,9216}O_{0,1177}}\Big]_{\text{Rhodospirillum}} + 0.6991\,H_2O \quad (10)$$

4.1.3 Compartment 3: nitrification of ammonia and ureolysis

In some cases, ammonia and urea can be taken up directly by plants or microorganisms grown for food production. However, in a BLSS it is desirable to convert ammonia and urea to nitrate because it is a less volatile and less reactive molecule (Clauwaert et al, 2017; De Paepe et al, 2018; Sachdeva et al, 2021). MELiSSA C3 receives ammonia from C2 and urine from C5, and transforms both into nitrate for the plants and microalgae in C4 (Duatis and Moreno, 2009; 2010). Ammonia is processed in a nitrifying bioreactor, while urine is processed separately in a modified version of the nitrifying bioreactor, the so-called Urine Treatment Unit (UTU) (Guirado and Podhajsky, 2008). As both bioreactors process different compounds, two separate compartments are defined in the stoichiometric model: 3a and 3b.

4.1.3.1 Compartment 3a: nitrification of ammonia by nitrifying bacteria

The nitrifying bioreactor as defined in the MELiSSA project is a cylindrical packed-bed bioreactor with polystyrene beads that are colonized by a biofilm of *Nitrosomonas europaea* and *Nitrobacter winogradsky* (Cruvellier et al, 2016; Garcia-Gragera et al, 2021). The nitrification of ammonia happens in two steps, each step carried out by one of the bacterial species (Cruvellier et al, 2016):

$$2\,NH_3 + 3\,O_2 \underset{\text{Nitrosomonas}}{\rightarrow} 2\,HNO_2 + 2\,H_2O \quad (11)$$

$$2\,HNO_2 + O_2 \underset{\text{Nitrobacter}}{\rightarrow} 2\,HNO_3 \quad (12)$$

Taken together this results in:

$$NH_3 + 2\,O_2 \rightarrow HNO_3 + H_2O \quad (13)$$

4.1.3.2 Compartment 3b: breakdown of urea by ureolytic heterotrophic bacteria

In a recent MELiSSA study of a UTU concept (Christiaens et al, 2019), showed how human urine can be nitrified with the use of a synthetic microbial community of ureolytic heterotrophic bacteria and nitrifying bacteria cultivated in a continuous stirred tank reactor. First, during ammonification, the ureolytic heterotrophic bacteria break down urea into ammonia and CO_2, a process catalyzed by the enzyme urease (Nicolau et al, 2010; De Paepe et al, 2018). Subsequently, the ammonia is further converted into nitrate by the nitrifying bacteria as described above. The stoichiometric equation describing the ammonification of urea can be found in (Guirado and Podhajsky, 2008):

$$\underset{\text{urea}}{CO(NH_2)_2} + H_2O \rightarrow 2\,NH_3 + CO_2 \quad (14)$$

Taken together with (13), this results in:

$$\underset{\text{urea}}{CO(NH_2)_2} + 4\,O_2 \rightarrow 2\,HNO_3 + H_2O + CO_2 \quad (15)$$

4.1.4 Compartment 4: food production

4.1.4.1 Compartment 4a: photoautotrophic cyanobacteria growth

The edible microalgae *Limnospira platensis* and *indica* (previously *Arthrospira platensis* and *indica*) are cyanobacteria that consume nitrate and CO_2 that are produced in other compartments of the loop, and generate oxygen and food for the crew (Clauwaert et al, 2017; Alemany et al, 2019; Sachdeva et al, 2021). *Limnospira* is grown inside a gas lift photobioreactor with illumination and a gas injection system (Garcia-Gragera et al, 2021; Poughon et al, 2021). Since a custom biomass composition is used in our model, a new stoichiometric balance had to be calculated (generated biomass is dry mass):

$$CO_2 + 0.1788\,HNO_3 + 0.7342\,H_2O \rightarrow \Big[0.1461\,\underset{\text{carbohydrates}}{CH_{1.6667}O_{0.8333}} + 0.7154\,\underset{\text{proteins}}{CH_{1.5900}O_{0.3100}N_{0.2500}} + 0.1385\,\underset{\text{lipids}}{CH_{1,9216}O_{0,1177}}\Big]_{\text{Limnospira}} + 1.4554\,O_2 \quad (16)$$

4.1.4.2 Compartment 4b: higher plant growth

Edible crops are grown in C4b of the MELiSSA loop (Pannico et al, 2022). The goal of this compartment is in line with that of C4a: recycling nitrate and CO_2, and producing oxygen and food (Lasseur et al, 2010; Peiro et al, 2020). In the current model, a harvest index of 50% is used, which means that half of the plant biomass is edible, while the other half is not. The non-edible part is considered as waste and is used as feed for the thermophilic anaerobic bacteria in C1. This can be summarized in the general equation:

$$CO_2 + H_2O + HNO_3 \rightarrow [\text{biomass}]_{\text{higher plants edible}} + 0.8965\,[\text{biomass}]_{\text{higher plants non-edible}} + O_2 \quad (17)$$

This corresponds to the following stoichiometric equation (generated biomass is dry mass):

$$\begin{aligned} &2.9101\,CO_2 + 0.0842\,HNO_3 + 2.4\,H_2O \\ &\rightarrow \Big[0.9629\,\underset{\text{carbohydrates}}{CH_{1.6667}O_{0.8333}} + 0.3368\,\underset{\text{proteins}}{CH_{1.5900}O_{0.3100}N_{0.2500}} + 0.2348\,\underset{\text{lipids}}{CH_{1,9216}O_{0,1177}}\Big]_{\text{higher plants edible}} \\ &+ \Big[1.3756\,\underset{\text{carbohydrates}}{CH_{1.6667}O_{0.8333}}\Big]_{\text{higher plants non-edible}} + 3.1961\,O_2 \end{aligned} \quad (18)$$

4.1.5 Compartment 5: human metabolism

The general equation for the human metabolism can be summarized as follows (Guirado and Podhajsky, 2008):

$$[\text{biomass}]_{\text{higher plants edible}} + [\text{biomass}]_{\text{Limnospira}} + O_2 \rightarrow [\text{feces}] + CO(NH_2)_2 + H_2O + CO_2 \quad (19)$$

To determine the final stoichiometric equation, a few preparatory calculations are needed. Firstly, the right proportion between edible higher plant biomass and *Limnospira* biomass needs to be established. In the model, 90% of the caloric content of the food comes from the higher plants, and 10% comes from *Limnospira*. Higher plants and *Limnospira* are considered to have a caloric content of respectively 4,000 and 3000 kcal/kg. This amounts to a target daily food intake of 675 g DW (27.86 mol) of higher plant biomass and 100 g DW (4.56 mol) of *Limnospira* biomass per crew member. Using the biomass compositions, this can then be translated into corresponding values for carbohydrates, proteins, and lipids. For oxygen, CO_2, and urea, reported daily values were transformed into moles (Table 2), and this was then used for calculating a stoichiometry with realistic proportions between these compounds and biomass uptake. The amount of feces is calculated by solving the stoichiometric equation. Below equation describes the metabolism of one crew member:

$$\begin{aligned} &\Big[17.6580\,\underset{\text{carbohydrates}}{CH_{1.6667}O_{0.8333}} + 6.1760\,\underset{\text{proteins}}{CH_{1.5900}O_{0.3100}N_{0.2500}} + 4.3059\,\underset{\text{lipids}}{CH_{1,9216}O_{0,1177}}\Big]_{\text{higher plants edible}} + \Big[0.6594\,\underset{\text{carbohydrates}}{CH_{1.6667}O_{0.8333}} \\ &+ 3.2286\,\underset{\text{proteins}}{CH_{1.5900}O_{0.3100}N_{0.2500}} + 0.6253\,\underset{\text{lipids}}{CH_{1,9216}O_{0,1177}}\Big]_{\text{Limnospira}} + 24.2893\,O_2 \rightarrow \Big[6.1661\,\underset{\text{carbohydrates}}{CH_{1.6667}O_{0.8333}} \\ &+ 3.1982\,\underset{\text{proteins}}{CH_{1.5900}O_{0.3100}N_{0.2500}} + 0.9989\,\underset{\text{lipids}}{CH_{1,9216}O_{0,1177}}\Big]_{\text{feces}} + 0.7758\,\underset{\text{urea}}{CO(NH_2)_2} + 17.2869\,H_2O + 21.5142\,CO_2 \end{aligned} \quad (20)$$

4.1.6 Auxiliary processes

4.1.6.1 Excess hydrogen burn-off

One auxiliary process has been added to the loop with the function to burn any excess hydrogen. This is in correspondence with other MELiSSA modeling studies such as (Poughon et al, 2000).

$$2\,H_2 + O_2 \rightarrow 2\,H_2O$$

4.2 Simulation results

The results of the stoichiometric spreadsheet model running in steady state conditions can be found in Table 4. The overall input and output values of all compounds in the loop are listed, for a crew of six over a period of 1 day (the time unit used in the ABM for which this stoichiometry was developed). All different stoichiometric equations were successfully balanced with each other, which resulted in a very high closure level with 12 out of 14 values reaching full closure, with no material loss. Oxygen displays an almost neglectable loss of 0.00021%, and CO_2 0.00001%. This is assumed to be caused by the numerical limitations of the software tools (e.g., number of decimals and rounding). The values correspond to respectively 2.13 mg O_2 and 1.47 mg CO_2 material loss per person per day. Over the course of a year, this would amount to 4.67 g O_2 and 3.21 g CO_2 for the entire crew. The VFA spectrum (weight-based) at steady state consists of 57.20% acetic acid, 12.59% propionic acid, 29.98% butyric acid and 0.23% valeric acid.

5 Discussion

This study presents a stoichiometric model of the MELiSSA BLSS, which describes the main metabolic processes in all compartments using a series of static chemical equations. In steady state, 100% of the necessary food and oxygen for the crew, as well as 100% of the compounds required for all other organisms in the loop, are generated. Using the assumption that all waste compounds in the loop can be broken down again, full closure was achieved in the static model by balancing the size of each compartment relative to all the other compartments. This is the first time a fully closed static MELiSSA model is described that can provide all the food and oxygen for astronauts. The model is a useful tool for theoretical

TABLE 4 Input and output values of the different compounds, after reaching steady state. Values for a crew of six, over a period of 1 day.

Compound	Input (mol)	Output (mol)	Material loss(mol)	Material loss(%)
Carbohydrates	1832.2836	1832.2836	0.0000	0.00000%
Protein	7587.0675	7587.0675	0.0000	0.00000%
Lipids	1490.3754	1490.3754	0.0000	0.00000%
Acetic acid	1570.2506	1570.2506	0.0000	0.00000%
Propionic acid	426.4730	426.4730	0.0000	0.00000%
Butyric acid	1207.5497	1207.5497	0.0000	0.00000%
Valeric acid	10.8735	10.8735	0.0000	0.00000%
Urea	4.6548	4.6548	0.0000	0.00000%
NH_3	1882.6600	1882.6601	0.0001	0.00000%
HNO_3	14.1068	14.1068	0.0000	0.00000%
H_2O	5591.1996	5591.1994	-0.0001	0.00000%
H_2	2004.4967	2004.4967	0.0000	0.00000%
O_2	391.0724	391.0716	-0.0008	-0.00021%
CO_2	1543.0613	1543.0611	-0.0002	-0.00001%

research on autonomous BLSSs for long-duration space exploration, allowing tracing of the elements over the entire cycle.

However, in practice, no system can be 100% closed. There are always potential outfluxes from the system, for example, through a buildup of recalcitrant organic matter (Hendrickx and Mergeay, 2007; Lasseur et al, 2010; Zhang et al, 2018) or the accumulation of different precipitates such as carbonates and phosphates (De Paepe et al, 2018; Christiaens et al, 2019). Recalcitrant organic matter consists mainly of plant fibers that do not rapidly biodegrade. Plant cell walls are composed of cellulose, hemicellulose, pectin, and lignin and are among the least degradable polymers in a BLSS (Hendrickx and Mergeay, 2007; Zhang et al, 2018). As a result, up to about 70% of the organic waste could be digested in MELiSSA lab experiments (Farges et al, 2008; Lasseur et al, 2010). The MELiSSA community has investigated additional methods to break down the remaining recalcitrant matter using hydrothermal and chemical oxidation, and anaerobic and hyperthermophilic cellulose-degrading bacteria (Hendrickx & Mergeay, 2007; Lasseur et al, 2010). The most efficient results were obtained by using supercritical water oxidation (SCWO) in which up to 98% of all organic matter could be broken down (Hendrickx and Mergeay, 2007; Zhang et al, 2018). Hydrogen peroxide was used as an oxidizer in these tests, which is a compound that can be generated within a BLSS loop (Tikhomirov et al, 2011; Vijapur et al, 2017; Nelson et al, 2020). Nevertheless, it is safe to assume that, in reality, there will always be some level of material loss in any BLSS loop. It would therefore be interesting to investigate what accumulates over a long period of time and then calculate the dimensions of the reserve storage required to mitigate the resulting material shortages.

The interaction between compartments C1 and C2 represents a subcycle in this model. The *Rhodospirillum* biomass generated in C2 is fed back into C1 as organic waste. The goal of this subcycle is to produce a surplus of CO_2, H_2, and NH_3 that is needed in the other compartments of the MELiSSA loop. Steady state of this subcycle is reached gradually until enough biomass from C2 is sent back to C1 to ensure that the exact amount of VFAs is produced to sustain a stable *Rhodospirillum* culture. If too few VFAs are provided, C2 will underperform due to a lack of *Rhodospirillum* growth. If too many VFAs are provided, the *Rhodospirillum* culture will not be able to process all of them, leading to accumulation and negative impacts on the mass flows and efficiency of the entire loop. At steady state, this subcycle generates the following surplus (per day, for a crew of six): 213 mol CO_2, 434 mol H_2, and 126 mol NH_3. The subcycle also explains the dominant amount of protein present in the loop, despite the food provided to the crew containing much less protein (Table 4). Due to the need for a significant mass of *Rhodospirillum* to process the VFAs and their high protein content (72%), a lot of protein is present in the loop in general. Bio-electrochemical oxidation is a potentially more efficient approach to convert the VFAs into CO_2. In a study by Luther et al, 2018, using bio-electrochemical oxidation within a microbial electrolysis cell, 80%–100% of the VFAs in the effluent of MELiSSA's C1 were converted into CO_2 in 7 days. With further process development and optimization, bio-electrochemical oxidation can potentially entirely replace the use of *Rhodospirillum* in C2.

(Jiang et al, 2013) conducted a series of experiments on anaerobic digestion of food waste. At a pH of 5.0, the resulting VFA spectrum consisted of 60.40% acetic acid, 8.32% propionic acid, 31.13% butyric acid, and 0.15% valeric acid, which falls within the same range as the results achieved in our model at steady state. Another study by Lim et al, 2008 also involved anaerobic digestion of food waste. At a pH of 5.5, the resulting VFA spectrum had a more variable composition, but acetic acid was generally the dominant VFA. These reported results are consistent with the results of our static model, which suggests that the theoretical VFA outcome is a potentially realistic scenario. However, it must be noted that VFA spectra generated during anaerobic fermentation are highly variable and depend on various factors such as substrate composition and inoculum (Poughon et al,

2013; Khan et al, 2016), pH and temperature (Shin et al, 2004; Jiang et al, 2013; Khan et al, 2016), and bioreactor design and operation (Lim et al, 2008; Bharathiraja et al, 2016). For instance, in experiments using food waste by Shin et al (2004), and in MELiSSA experiments using a synthetically composed organic waste (Luther et al, 2018; Zhang et al, 2019), both acetic acid and butyric acid were the main VFAs, with butyric acid being dominant.

Growing enough plants to meet the food requirements of a human crew typically results in the production of more oxygen than the crew needs. This is because the harvest index of the crops is often less than 100%, meaning that only a portion of the grown biomass is used for food (Jones, 2003). However, the unused biomass still generates oxygen. In a closed loop system, this could lead to an accumulation of excess oxygen (as e.g., observed in Poughon et al, 2000; Gros et al, 2003) and, eventually, the collapse of the system. In our model, the excess oxygen is used to hydrolyze solid waste in C1, in the form of H_2O. The hydrogen-burning auxiliary helps to transform any remaining oxygen gas into H_2O. Since oxygen originates from splitting H_2O during photosynthesis, the amount of surplus oxygen matches the amount of surplus hydrogen in the system.

In our model, the human crew consumes 21.51 mol/person/day of CO_2, which is very close to the target value of 22.72 mol/person/day used for calculating the stoichiometry. However, the human crew only uses 24.29 mol/person/day of oxygen, much lower than the target value of 52.50 mol/person/day. The proportion between consumed oxygen and produced CO_2 should be 2.31, but in our model, this proportion is 1.13, precisely because of the lower oxygen consumption. Remarkably, other BLSS modeling studies show the same tendency. In MELiSSA studies, the proportion is 1.20 (Fulget, 1996; Thiron, 2020) and in Lunar Palace studies, it ranges from 1.13 to 1.38 (Hu et al, 2010; Fu et al, 2016). This suggests that the description of the O_2 consumption in all of these studies is not entirely complete. This could be due to the fact that in reality, more compounds are oxidized than represented in the simplified stoichiometric equation for human metabolism. The total mass of consumed food per person per day corresponds to 781 g DW/day. This is slightly higher than the range of baseline values used in MELiSSA studies and reference documents. Adjusted to a daily food intake of 3,000 kcal/person, the values in these studies and documents range from 509 to 748 g DW/day (e.g. (Dussap et al, 1993; Poughon et al, 2000; Thiron, 2020)).

The composition of feces was calculated by solving the stoichiometric equation for human metabolism, using the general characterization of feces reported in the literature as a starting point (Rose et al, 2015). After solving the equation for human metabolism, the resulting feces composition was found to be 66% carbohydrates, 28% proteins, and 6% lipids, corresponding to the empirical formula $CH_{1.6676}O_{0.6028}N_{0.07715}$. This formula is similar to the one used in BLSS studies by Hu et al, 2010 and Fu et al, 2016, which is $CH_{1.70}O_{0.60}N_{0.05}$. Because the MELiSSA diet is a vegan diet, it is expected that there is a high fiber intake and a resulting high amount of fiber in the feces (Brodribb et al, 1980; Kay, 1982; Forsum et al, 1990). As a result, the overall carbohydrate fraction could be quite significant. It should be noted that the fraction of protein in the feces could be an underestimation, as bacteria can compose up to half of the fecal solids and may have a significant protein content (Cummings, 2001; Rose et al, 2015). Intestinal bacterial growth is not included in the human stoichiometry, which is justifiable as it means more digestion is done by the same groups of microbes in C1. The amount of feces produced is 253 g DW/person/day. Jenkins et al, 2001 measured 160 ± 24 g DW/person/day for a vegetarian diet. It should be noted that no other solid body wastes have been included in the stoichiometry, and as such the 'feces' in the equation represent a more general representation of all wastes combined.

Further development of the stoichiometric model could focus on increasing its granularity. This could involve expanding the model to include more elements beyond CHON, incorporating a greater diversity of crops, and using a more detailed description of human metabolism. Nitrogen, phosphorus, and potassium are the three major macro-elements for plants (Usherwood and Segars, 2001; Kanazawa et al, 2008). Therefore, including the latter two elements in the next version of the model seems like a logical step. Fertilizers typically contain these three elements, but it is crucial that they are applied in the correct ratio (Usherwood and Segars, 2001; Chun et al, 2017), which must also be factored into the model. Diverse plant crops could be used instead of the concept of an 'ideal plant', allowing for a more detailed description of the crew's daily diet. Integrating water usage beyond it's role as a metabolite will result in a more accurate description of the entire water budget. For example, water transpiration, water excretion, and free water inside the plant could be factored in. By integrating solid body wastes other than feces, the stoichiometry of human metabolism could also be further refined.

Data availability statement

The raw data supporting the conclusion of this article will be made available by the authors, without undue reservation.

Author contributions

AV and AP conceived and designed the study and performed the MELiSSA literature review. AV did the background research for the stoichiometry, while AP developed the tool in Excel to balance the chemical equations. The stoichiometric spreadsheet model was created in Excel by AP. AV wrote the first draft of the manuscript, and AP contributed sections. All authors contributed to the article and approved the submitted version.

Acknowledgments

The first, and shorter, version of the stoichiometry was compiled in collaboration with Jason Kiem from SmartCrops BV. Prof. Siegfried Vlaeminck from the University of Antwerp provided validation of this initial version and offered suggestions for further development. The authors would like to express their gratitude to Christophe Lasseur and Christel Paille from MELiSSA at ESTEC, as well as Prof. Claude-Gilles Dussap from Polytech Clermont, for providing input and feedback throughout the research. Ralph

Lindeboom from Delft University of Technology also provided valuable feedback on a previous version of the manuscript.

Conflict of interest

The authors declare that the research was conducted in the absence of any commercial or financial relationships that could be construed as a potential conflict of interest.

Publisher's note

All claims expressed in this article are solely those of the authors and do not necessarily represent those of their affiliated organizations, or those of the publisher, the editors and the reviewers. Any product that may be evaluated in this article, or claim that may be made by its manufacturer, is not guaranteed or endorsed by the publisher.

References

Albiol, J., Gòdia, F., Montesinos, J., Perez, J., Vernerey, A., Cabello, F., et al. (2000). Biological life support system demostration facility: the melissa pilot plant. *SAE Tech. Pap*. doi:10.4271/2000-01-2379

Alemany, L., Peiro, E., Arnau, C., Garcia, D., Poughon, L., Cornet, J.-F., et al. (2019). Continuous controlled long-term operation and modeling of a closed loop connecting an air-lift photobioreactor and an animal compartment for the development of a life support system. *Biochem. Eng. J.* 151, 107323. doi:10.1016/j.bej.2019.107323

Alloul, A., Ganigué, R., Spiller, M., Meerburg, F., Cagnetta, C., Rabaey, K., et al. (2018). Capture–ferment–upgrade: a three-step approach for the valorization of sewage organics as commodities. *Environ. Sci. Technol.* 52, 6729–6742. doi:10.1021/acs.est.7b05712

Audas, C., Ortega Ugalde, S., Paille, C., Lamaze, B., and Lasseur, C. (2022). Life support systems beyond low Earth orbit advocates for an improved resources management approach. *Ecol. Eng. Environ. Prot.* 2022, 5–13. doi:10.32006/eeep.2022.1.0513

Bartsev, S. I., Gitelson, J. I., Lisovsky, G. M., Mezhevikin, V. V., and Okhonin, V. A. (1996). Perspectives of different type biological life support systems (BLSS) usage in space missions. *Acta Astronaut.* 39, 617–622. doi:10.1016/S0094-5765(97)00012-X

Begon, M., and Townsend, C. R. (2021). *Ecology: from individuals to ecosystems*. New Jersey, United States: John Wiley & Sons.

Bharathiraja, B., Sudharsanaa, T., Bharghavi, A., Jayamuthunagai, J., and Praveenkumar, R. (2016). Biohydrogen and Biogas – an overview on feedstocks and enhancement process. *Fuel* 185, 810–828. doi:10.1016/j.fuel.2016.08.030

Bjørnstad, O. N. (2015). Nonlinearity and chaos in ecological dynamics revisited. *Proc. Natl. Acad. Sci.* 112, 6252–6253. doi:10.1073/pnas.1507708112

Brodribb, J., Condon, R. E., Cowles, V., and DeCosse, J. J. (1980). Influence of dietary fiber on transit time, fecal composition, and myoelectrical activity of the primate right colon. *Dig. Dis. Sci.* 25, 260–266. doi:10.1007/BF01308515

Carillo, P., Morrone, B., Fusco, G. M., De Pascale, S., and Rouphael, Y. (2020). Challenges for a sustainable food production system on board of the international space station: a technical review. *Agronomy* 10, 687. doi:10.3390/agronomy10050687

Ceron-Chafla, P., Chang, Y., Rabaey, K., van Lier, J. B., and Lindeboom, R. E. F. (2021). Directional selection of microbial community reduces propionate accumulation in glycerol and glucose anaerobic bioconversion under elevated pCO_2. *Front. Microbiol.* 12, 675763. doi:10.3389/fmicb.2021.675763

Christiaens, M. E. R., De Paepe, J., Ilgrande, C., De Vrieze, J., Barys, J., Teirlinck, P., et al. (2019). Urine nitrification with a synthetic microbial community. *Syst. Appl. Microbiol.* 42, 126021. doi:10.1016/j.syapm.2019.126021

Chun, J.-H., Kim, S., Arasu, M. V., Al-Dhabi, N. A., Chung, D. Y., and Kim, S.-J. (2017). Combined effect of Nitrogen, Phosphorus and Potassium fertilizers on the contents of glucosinolates in rocket salad (Eruca sativa Mill). *Saudi J. Biol. Sci.* 24, 436–443. doi:10.1016/j.sjbs.2015.08.012

Cirne, D. G., Paloumet, X., Björnsson, L., Alves, M. M., and Mattiasson, B. (2007). Anaerobic digestion of lipid-rich waste—effects of lipid concentration. *Renew. Energy* 32, 965–975. doi:10.1016/j.renene.2006.04.003

Ciurans Molist, C., Bazmohammadi, N., Vasquez, J. C., Dussap, C.-G., Guerrero, J., and Gòdia, F. (2020). Hierarchical control of space closed ecosystems - expanding microgrid concepts to bioastronautics. *IEEE Ind. Electron. Mag.* 15, 16–27. doi:10.1109/MIE.2020.3026828

Clauwaert, P., Muys, M., Alloul, A., De Paepe, J., Luther, A., Sun, X., et al. (2017). Nitrogen cycling in Bioregenerative Life Support Systems: challenges for waste refinery and food production processes. *Prog. Aerosp. Sci.* 91, 87–98. doi:10.1016/j.paerosci.2017.04.002

Cooper, M., Perchonok, M., and Douglas, G. L. (2017). Initial assessment of the nutritional quality of the space food system over three years of ambient storage. *npj Microgravity* 3, 17. doi:10.1038/s41526-017-0022-z

Cornet, J.-F., Dussap, C. G., and Gros, J.-B. (1998). "Kinetics and energetics of photosynthetic micro-organisms in photobioreactors," in *Bioprocess and algae reactor Technology, apoptosis advances in biochemical engineering biotechnology* (Berlin, Heidelberg: Springer), 153–224. doi:10.1007/BFb0102299

Cornet, J.-F., Dussap, C. G., and Leclercq, J.-J. (2001). "Simulation, design and model based predictive control of photobioreactors," in *Engineering and Manufacturing for biotechnology focus on biotechnology*. Editors M. Hofman, and P. Thonart (Dordrecht: Springer Netherlands), 227–238. doi:10.1007/0-306-46889-1_15

Cornet, J.-F., Favier, L., and Dussap, C.-G. (2003). Modeling stability of photoheterotrophic continuous cultures in photobioreactors. *Biotechnol. Prog.* 19, 1216–1227. doi:10.1021/bp034041l

Cornet, J. F., and Dussap, C. G. (2000). Kinetic and stoichiometric analysis of Rhodospirillum rubrum growth under carbon substrate limitations in rectangular photobioreactors. MELiSSA Technical Note 45.5. Laboratoire de Génie Chimique et Biochimique Available at: https://www.melissafoundation.org/download/469 (Accessed March 23, 2023).

Cruvellier, N., Poughon, L., Creuly, C., Dussap, C.-G., and Lasseur, C. (2016). Growth modelling of Nitrosomonas europaea ATCC® 19718 and nitrobacter winogradskyi ATCC® 25391: a new online indicator of the partial nitrification. *Bioresour. Technol.* 220, 369–377. doi:10.1016/j.biortech.2016.08.090

Cummings, J. (2001). "The effect of dietary fiber on fecal weight and composition," in *CRC handbook of dietary fiber in human nutrition*. Editor G. Spiller (Florida, United States: CRC Press), 183–252. doi:10.1201/9781420038514.ch4.4

De Meur, Q., Deutschbauer, A., Koch, M., Bayon-Vicente, G., Cabecas, P., Ruddy, W., et al. (2020). New perspectives on butyrate assimilation in Rhodospirillum rubrum S1H under photoheterotrophic conditions. *BMC Microbiol.* 20, 126. doi:10.1186/s12866-020-01814-7

De Paepe, J., Lindeboom, R. E. F., Vanoppen, M., De Paepe, K., Demey, D., Coessens, W., et al. (2018). Refinery and concentration of nutrients from urine with electrodialysis enabled by upstream precipitation and nitrification. *Water Res.* 144, 76–86. doi:10.1016/j.watres.2018.07.016

Deangelis, D., and Grimm, V. (2014). Individual-based models in ecology after four decades. *F1000prime Rep.* 6, 39. doi:10.12703/P6-39

Decker, E. A., and Ferruzzi, M. G. (2013). Innovations in food chemistry and processing to enhance the nutrient profile of the white potato in all forms. *Adv. Nutr.* 4, 345S–350S. doi:10.3945/an.112.003574

Duatis, J., Guirado, V., and Podhajsky, S. (2008). MELiSSA adaptation for space. Phase II. Preliminary life support system design. MELiSSA Technical Note 88.3. NTE SA (Werfen Group) Available at: https://www.melissafoundation.org/download/174.

Duatis, J., and Moreno, D. (2009). *MELiSSA adaptation for space. Phase II. LIfe support system recommended design for a demonstration in a moon base*. Barcelona, Spain: NTE-SENER. MELiSSA Technical Note 88.5.

Duatis, J., and Moreno, D. (2010). MELiSSA adaptation for space. Phase II. Recommendations and future work. PreliminaryDevelopment plan. MELiSSA technical note 88.6. NTE-SENER Available at: https://www.melissafoundation.org/download/238 (Accessed March 23, 2023).

Dubitzky, W., Southgate, J., and Fuß, H. (Editors) (2011). "Adaptation and self-organizing systems," *Understanding the dynamics of biological systems* (New York, NY: Springer). doi:10.1007/978-1-4419-7964-3

Dussap, C.-G., Cornet, J.-F., and Gros, J.-B. (1993). Simulation of mass fluxes in the MELISSA microorganism based ecosystem. *Warrendale, PA SAE Int.*, 932125. doi:10.4271/932125

Dussap, C. G., and Gros, J. B. (1991). Simulation des flux de matières dans l'écosystème MELiSSA. MELiSSA Technical Note 14.1. Laboratoire de Génie Chimique et Biochimique Available at: https://www.melissafoundation.org/download/600 (Accessed March 23, 2023).

Escobar, C., and Nabity, J. (2017). "Past, present, and future of closed human life support ecosystems-a review," in Proceedings of the 47th International Conference on Environmental Systems, Charleston, South Carolina, July 2017, 16–20.

Ewert, M. K., Chen, T. T., and Powell, C. D. (2022). Life support baseline values and assumptions document. Available at: https://ntrs.nasa.gov/citations/20210024855 (Accessed April 1, 2023).

Farges, B., Poughon, L., Creuly, C., Cornet, J.-F., Dussap, C.-G., and Lasseur, C. (2008). Dynamic aspects and controllability of the MELiSSA project: a bioregenerative system to provide life support in space. *Appl. Biochem. Biotechnol.* 151, 686–699. doi:10.1007/s12010-008-8292-2

Finn, C. K. (1998). *Steady-state system mass balance for the BIO-plex*. Warrendale, PA: SAE International. doi:10.4271/981747

FoodData Central (2019a). Seaweed, spirulina, dried. Available at: https://fdc.nal.usda.gov/fdc-app.html#/food-details/170495/nutrients (Accessed March 23, 2023).

FoodData Central (2019b). Soybeans, mature cooked, boiled, without salt. Available at: https://fdc.nal.usda.gov/fdc-app.html#/food-details/174271/nutrients (Accessed March 23, 2023).

Forrest, S., and Mitchell, M. (2016). Adaptive computation: the multidisciplinary legacy of John H. Holland. *Commun. ACM* 59, 58–63. doi:10.1145/2964342

Forsum, E., Eriksson, C., Göranzon, H., and Sohlström, A. (1990). Composition of faeces from human subjects consuming diets based on conventional foods containing different kinds and amounts of dietary fibre. *Br. J. Nutr.* 64, 171–186. doi:10.1079/BJN19900019

Fu, Y., Li, L., Xie, B., Dong, C., Wang, M., Jia, B., et al. (2016). How to establish a bioregenerative life support system for long-term crewed missions to the moon or mars. *Astrobiology* 16, 925–936. doi:10.1089/ast.2016.1477

Fulget, N. (1996). Complete loop control: first study. MELiSSA technical note 28.3. ADERSA. Available at: https://www.melissafoundation.org/download/552 (Accessed March 23, 2023).

Fulget, N., Poughon, L., Richalet, J., and Lasseur, Ch. (1999). Melissa: global control strategy of the artificial ecosystem by using first principles models of the compartments. *Adv. Space Res.* 24, 397–405. doi:10.1016/S0273-1177(99)00490-1

Garcia-Gragera, D., Arnau, C., Peiro, E., Dussap, C.-G., Poughon, L., Gerbi, O., et al. (2021). Integration of nitrifying, photosynthetic and animal compartments at the MELiSSA pilot plant. *Front. Astron. Space Sci.* 8, 750616. doi:10.3389/fspas.2021.750616

Garland, J. L. (1989). A simple, mass balance model of carbon flow in a controlled ecological life support system. Available at: https://ntrs.nasa.gov/citations/19900001255 (Accessed March 23, 2023).

Gòdia, F., Albiol, J., Pérez, J., Creus, N., Cabello, F., Montràs, A., et al. (2004). The MELISSA pilot plant facility as an integration test-bed for advanced life support systems. *Adv. Space Res.* 34, 1483–1493. doi:10.1016/j.asr.2003.08.038

Gorce, B., Garnier, L., Ssi Yan Kai, H., Schini, P.-Y., Lefevre, A., Afuera, E., et al. (2022). "Conceptual design of an environment control and life support system for a mars transit mission," in MELiSSA Conference 2022, Toulouse, France, November 2022, 8–10. Available at: https://www.melissafoundation.org/download/932 (Accessed March 23, 2023).

Gros, J. B., Poughon, L., Lasseur, C., and Tikhomirov, A. A. (2003). Recycling efficiencies of C,H,O,N,S, and P elements in a biological life support system based on micro-organisms and higher plants. *Adv. Space Res.* 31 (1), 195–199. doi:10.1016/S0273-1177(02)00739-1

Guirado, V., and Podhajsky, S. (2008). MELiSSA adaptation for space. Phase II. Summary of the European life support systems technologies. MELiSSA Technical Note 88.2. NTE SA (Werfen Group) Available at: https://www.melissafoundation.org/download/173 (Accessed March 23, 2023).

Häder, D. (2020). On the way to mars—flagellated algae in bioregenerative life support systems under microgravity conditions. *Front. Plant Sci.* 10, 1621. doi:10.3389/fpls.2019.01621

Hendrickx, L., De Wever, H., Hermans, V., Mastroleo, F., Morin, N., Wilmotte, A., et al. (2006). Microbial ecology of the closed artificial ecosystem MELiSSA (Micro-Ecological Life Support System Alternative): reinventing and compartmentalizing the Earth's food and oxygen regeneration system for long-haul space exploration missions. *Res. Microbiol.* 157, 77–86. doi:10.1016/j.resmic.2005.06.014

Hendrickx, L., and Mergeay, M. (2007). From the deep sea to the stars: human life support through minimal communities. *Curr. Opin. Microbiol.* 10, 231–237. doi:10.1016/j.mib.2007.05.007

Holohan, B. C., Duarte, M. S., Szabo-Corbacho, M. A., Cavaleiro, A. J., Salvador, A. F., Pereira, M. A., et al. (2022). Principles, advances, and perspectives of anaerobic digestion of lipids. *Environ. Sci. Technol. Wash.* 56, 4749–4775. doi:10.1021/acs.est.1c08722

Hu, E., Bartsev, S., and Liu, H. (2010). Conceptual design of a bioregenerative life support system containing crops and silkworms. *Adv. Space Res.* 45, 929–939. doi:10.1016/j.asr.2009.11.022

Imhof, B., Weiss, P., Vermeulen, A., Flynn, E., Hyams, R., Kerrigan, C., et al. (2017). "Space architectures," in *Star Ark: a Living, Self-Sustaining Spaceship*. Editor R. Armstrong (Cham: Springer International Publishing), 287–340. doi:10.1007/978-3-319-31042-8_12

Jenkins, D., Kendall, C., Popovich, D., Vidgen, E., Mehling, C., Vuksan, V., et al. (2001). Effect of a very-high-fiber vegetable, fruit, and nut diet on serum lipids and colonic function. *Metabolism Clin. Exp.* 50, 494–503. doi:10.1053/meta.2001.21037

Jiang, J., Zhang, Y., Li, K., Wang, Q., Gong, C., and Li, M. (2013). Volatile fatty acids production from food waste: effects of pH, temperature, and organic loading rate. *Bioresour. Technol.* 143, 525–530. doi:10.1016/j.biortech.2013.06.025

Johnson, C., Boles, H., Spencer, L., Poulet, L., Romeyn, M., Bunchek, J., et al. (2021). Supplemental food production with plants: a review of nasa research. *Front. Astronomy Space Sci.* 8. doi:10.3389/fspas.2021.734343

Jones, H. (2003). "Design rules for life support systems," in 33rd International Conference on Environmental Systems (ICES), Vancouver, B.C., Canada, 7-10 July 2003. Available at: https://ntrs.nasa.gov/citations/20040012725 (Accessed March 23, 2023).

Kaleta, A., and Górnicki, K. (2013). Criteria of determination of safe grain storage time - a review. *Adv. Agrophysical Res.*, 295–318.

Kanazawa, S., Ishikawa, Y., Tomita-Yokotani, K., Hashimoto, H., Kitaya, Y., Yamashita, M., et al. (2008). Space agriculture for habitation on Mars with hyper-thermophilic aerobic composting bacteria. *Adv. Space Res.* 41, 696–700. doi:10.1016/j.asr.2007.09.040

Kay, R. (1982). Dietary fiber. *J. Lipid Res.* 23, 221–242. doi:10.1016/S0022-2275(20)38151-7

Khan, M. A., Ngo, H. H., Guo, W. S., Liu, Y., Nghiem, L. D., Hai, F. I., et al. (2016). Optimization of process parameters for production of volatile fatty acid, biohydrogen and methane from anaerobic digestion. *Bioresour. Technol.* 219, 738–748. doi:10.1016/j.biortech.2016.08.073

Knowledge4Policy (2021). Nutritional value of whole grains. Available at: https://knowledge4policy.ec.europa.eu/health-promotion-knowledge-gateway/whole-grain-nutritional-value-whole-2_en (Accessed March 23, 2023).

Kobayashi, M., and Kobayashi, M. (1995). "Waste remediation and treatment using anoxygenic phototrophic bacteria," in *Anoxygenic photosynthetic bacteria advances in photosynthesis and respiration*. Editors R. E. Blankenship, M. T. Madigan, and C. E. Bauer (Dordrecht: Springer Netherlands), 1269–1282. doi:10.1007/0-306-47954-0_62

Lasseur, C., Brunet, J., De Weever, H., Dixon, M., Dussap, G., Godia, F., et al. (2010). MELiSSA: the European project of closed life support system. *Gravitational Space Res.* 23. http://citeseerx.ist.psu.edu/viewdoc/download?doi=10.1.1.464.3630andrep=rep1andtype=pdf

Lasseur, Ch., Verstraete, W., Gros, J. B., Dubertret, G., and Rogalla, F. (1996). Melissa: a potential experiment for a precursor mission to the moon. *Adv. Space Res.* 18, 111–117. doi:10.1016/0273-1177(96)00097-X

Lauwers, J., Appels, L., Thompson, I. P., Degrève, J., Van Impe, J. F., and Dewil, R. (2013). Mathematical modelling of anaerobic digestion of biomass and waste: power and limitations. *Prog. Energy Combust. Sci.* 39, 383–402. doi:10.1016/j.pecs.2013.03.003

Li, Y. Y., Sasaki, H., Yamashita, K., Seki, K., and Kamigochi, I. (2002). High-rate methane fermentation of lipid-rich food wastes by a high-solids co-digestion process. *Water Sci. Technol.* 45, 143–150. doi:10.2166/wst.2002.0420

Liebetrau, J., Weinrich, S., Sträuber, H., and Kretzschmar, J. (2017). "Anaerobic fermentation of organic material: biological processes and their control parameters," in *Encyclopedia of sustainability science and Technology*. Editor R. A. Meyers (New York, NY: Springer), 1–30. doi:10.1007/978-1-4939-2493-6_962-1

Lim, S.-J., Kim, B. J., Jeong, C.-M., Choi, J., Ahn, Y. H., and Chang, H. N. (2008). Anaerobic organic acid production of food waste in once-a-day feeding and drawing-off bioreactor. *Bioresour. Technol.* 99, 7866–7874. doi:10.1016/j.biortech.2007.06.028

Loader, C., Garland, J., Raychaudhuri, S., and Wheeler, R. (1997). A simple mass balance model of nitrogen flow in a bioregenerative life support system. *Life support & biosphere Sci. Int. J. earth space* 4, 31–41.

Luther, A., Beyaert, A., Brutsaert, M., Lasseur, C., Rebeyre, P., and Clauwaert, P. (2018). "Bio-electrochemical oxidation for CO_2 recovery in regenerative life support systems," in 42nd COSPAR Scientific Assembly Abstracts (COSPAR (Committee on Space Research)), California, USA, July 2018. Available at: http://hdl.handle.net/1854/LU-8573095 (Accessed March 23, 2023).

Macelroy, R. D., and Averner, M. M. (1978). Space ecosynthesis: an approach to the design of closed ecosystems for use in space. Available at: https://ntrs.nasa.gov/citations/19780018797 (Accessed March 23, 2023).

Mackie, R. I., White, B. A., and Bryant, M. P. (1991). Lipid metabolism in anaerobic ecosystems. *Crit. Rev. Microbiol.* 17, 449–479. doi:10.3109/10408419109115208

Maclean, H., Dochain, D., Waters, G., Dixon, M., Chaerle, L., and Van Der Straeten, D. (2010). "Identification of simple mass balance models for plant growth - towards food production on manned space missions," in Proceedings IFAC-CAB 2010 Conference, Leuven, Belgium, July 2010 (International Federation of Automatic Control), 7–9. 335–340. Available at: https://dial.uclouvain.be/pr/boreal/object/boreal:87876 (Accessed March 23, 2023).

Mastroleo, F. (2009). Molecular characterization of the life support bacterium Rhodospirillum rubrum S1H cultivated under space related environmental conditions. Université de Mons-Hainaut, Mons, Belgium. Available at: https://researchportal.sckcen.be/files/4517866/Molecular_characterization_of_the_life_support_bacterium_Rhodospirillum_rubrum_S1H_cultivated_under_space_related_environmental_conditions_thesis.Felice.20.01.09.BIS.without.pdf (Accessed March 23, 2023).

Mastroleo, F., Moussalli, C., Raeymaekers, L., Smolders, C., Leysen, L., Coninx, I., et al. (2020). "Investigating volatile fatty acids conversion to CO_2 by the MELiSSA bacterium Rhodospirillum rubrum," in MELiSSA Conference 2020, France, November 2020, 3–5. online.

MedlinePlus, (2023). Urine 24-hour volume. Available at: https://medlineplus.gov/ency/article/003425.htm (Accessed March 23, 2023).

MELiSSA Foundation (2023). Melissa space research program. Available at: https://www.melissafoundation.org/page/melissa-project (Accessed March 23, 2023).

MELiSSA (1989). Modelling. MELiSSA technical note 4. Available at: https://www.melissafoundation.org/download/609 (Accessed March 23, 2023).

Michel, N., De Wever, H., Dotremont, C., and Van Hoof, V. (2005). Engineering of the waste compartment. MELiSSA technical note 71.9.4. ECo process assistance. VITO Available at: https://www.melissafoundation.org/download/327 (Accessed March 23, 2023).

Molders, K., Quinet, M., Decat, J., Secco, B., Dulière, E., Pieters, S., et al. (2012). Selection and hydroponic growth of potato cultivars for bioregenerative life support systems. *Adv. Space Res.* 50, 156–165. doi:10.1016/j.asr.2012.03.025

Moore, K. J., and Hatfield, R. D. (1994). "Carbohydrates and forage quality," in *Forage quality, evaluation, and utilization* (New Jersey, United States: John Wiley & Sons, Ltd), 229–280. doi:10.2134/1994.foragequality.c6

Muys, M., Sui, Y., Schwaiger, B., Lesueur, C., Vandenheuvel, D., Vermeir, P., et al. (2019). High variability in nutritional value and safety of commercially available Chlorella and Spirulina biomass indicates the need for smart production strategies. *Bioresour. Technol.* 275, 247–257. doi:10.1016/j.biortech.2018.12.059

Nelson, G. J., Vijapur, S. H., Hall, T. D., Brown, B. R., Peña-Duarte, A., and Cabrera, C. R. (2020). Electrochemistry for space life support. *Electrochem. Soc. Interface* 29, 47–52. doi:10.1149/2.F06201IF

Nelson, M., Pechurkin, N. S., Allen, J. P., Somova, L. A., and Gitelson, J. I. (2010). Closed ecological systems, space life support and biospherics. *Environ. Biotechnol.*, 517–565. doi:10.1007/978-1-60327-140-0_11

Nicolau, E., Rodríguez-Martínez, J. A., Fonseca, J., Richardson, T.-M. J., Flynn, M., Griebenow, K., et al. (2010). Bioelectrochemical oxidation of urea with urease and platinized boron doped diamond electrodes for water recycling in space applications. *ECS Trans.* 33, 1853–1859. doi:10.1149/1.3484676

Page, V., and Feller, U. (2013). Selection and hydroponic growth of bread wheat cultivars for bioregenerative life support systems. *Adv. Space Res.* 52, 536–546. doi:10.1016/j.asr.2013.03.027

Pannico, A., Cimini, G., Quadri, C., Paradiso, R., Bucchieri, L., Rouphael, Y., et al. (2022). A plant characterization unit for closed life support: hardware and control design for atmospheric systems. *Front. Astron. Space Sci.* 9, 820752. doi:10.3389/fspas.2022.820752

Paradiso, R., Micco, V., Buonomo, R., Aronne, G., Barbieri, G., and De Pascale, S. (2013). Soilless cultivation of soybean for bioregenerative life-support systems: a literature review and the experience of the MELiSSA project - food characterisation phase I. *Plant Biol. Stuttg. Ger.* 16, 69–78. doi:10.1111/plb.12056

Peiro, E., Pannico, A., Colleoni, S., Bucchieri, L., Rouphael, Y., De Pascale, S., et al. (2020). Air distribution in a fully-closed higher plant growth chamber impacts crop performance of hydroponically-grown lettuce. *Front. Plant Sci.* 11, 537. doi:10.3389/fpls.2020.00537

Pilo Teniente, S. (2015). *Simulation of the gas phase integration between compartments CIVa and CV of the MELiSSA Pilot Plant*. Barcelona, Spain: Universitat Politècnica de Catalunya. Available at: https://upcommons.upc.edu/handle/2117/86047 (Accessed March 23, 2023).

Poughon, L., Creuly, C., Farges, B., Dussap, C.-G., Schiettecatte, W., Jovetic, S., et al. (2013). Test of an anaerobic prototype reactor coupled with a filtration unit for production of VFAs. *Bioresour. Technol.* 145, 240–247. doi:10.1016/j.biortech.2012.12.052

Poughon, L., Creuly, C., Godia, F., Leys, N., and Dussap, C.-G. (2021). Photobioreactor Limnospira indica growth model: application from the MELiSSA plant pilot scale to ISS flight experiment. *Front. Astronomy Space Sci.* 8. doi:10.3389/fspas.2021.700277

Poughon, L., Dussap, C. G., Cornet, J. F., and Gros, J. B. (1994). Melissa: behavior of the ecosystem under different light radiant energy inputs. *Warrendale, PA SAE Int.*, 941347. doi:10.4271/941347

Poughon, L. (2007a). Dynamic modelling of a coupled MELiSSA crew - compartment C4a with Matlab-Simulink. MELiSSA Technical Note 83.1. Laboratoire de Génie Chimique et Biochimique Available at: https://www.melissafoundation.org/download/199 (Accessed March 23, 2023).

Poughon, L., Farges, B., Dussap, C. G., Godia, F., and Lasseur, C. (2009). Simulation of the MELiSSA closed loop system as a tool to define its integration strategy. *Adv. Space Res.* 44, 1392–1403. doi:10.1016/j.asr.2009.07.021

Poughon, L., Gros, J. B., and Dussap, C. G. (2000). "MELISSA loop: first estimate of flow rates and concentrations through the loop," in 30th International Conference on Environmental Systems (ICES), Toulouse, France, 10-13 July 2000 (SAE Technical Paper Series) (Warrendale, PA: SAE International).

Poughon, L., Laroche, C., Creuly, C., Dussap, C.-G., Paille, C., Lasseur, C., et al. (2020). Limnospira indica PCC8005 growth in photobioreactor: model and simulation of the ISS and ground experiments. *Life Sci. Space Res.* 25, 53–65. doi:10.1016/j.lssr.2020.03.002

Poughon, L. (2007b). MELiSSA loop mass balance modelling with MatLab/simulink. MELiSSA Technical Note 79.2. Laboratoire de Génie Chimique et Biochimique Available at: https://www.melissafoundation.org/download/197 (Accessed March 23, 2023).

Poughon, L. (1994a). MELiSSA simulation and modelling. Spirulina modelling. Variable global stoichiometric equation of Spirulina platensis in different light conditions. Effects of light on diet composition. Best conditions to insure maximal mass recycling. MELiSSA Technical Note 17.3. Laboratoire de Génie Chimique et Biochimique Available at: https://www.melissafoundation.org/download/572 (Accessed March 23, 2023).

Poughon, L. (1994b). MELiSSA simulation and modelling. Study of partial conversion. The stoichiometric assumptions: origin and effects. The main consequences of the partial conversion of components. MELiSSA Technical Note 17.2. Laboratoire de Génie Chimique et Biochimique Available at: https://www.melissafoundation.org/download/571 (Accessed March 23, 2023).

Poulet, L., Dussap, C.-G., and Fontaine, J.-P. (2018). A physical modeling approach for higher plant growth in reduced gravity environments. *Astrobiology* 18, 1093–1100. doi:10.1089/ast.2017.1804

Poulet, L., Dussap, C.-G., and Fontaine, J-P. (2020). Development of a mechanistic model of leaf surface gas exchange coupling mass and energy balances for life-support systems applications. *Acta Astronaut.* 175, 517–530. doi:10.1016/j.actaastro.2020.03.048

Putnam, D. F. (1971). Composition and concentrative properties of human urine. Available at: https://ntrs.nasa.gov/citations/19710023044 (Accessed March 23, 2023).

Ramsay, I. R., and Pullammanappallil, P. C. (2001). Protein degradation during anaerobic wastewater treatment: derivation of stoichiometry. *Biodegradation* 12, 247–257. doi:10.1023/A:1013116728817

Rose, C., Parker, A., Jefferson, B., and Cartmell, E. (2015). The characterization of feces and urine: a review of the literature to inform advanced treatment Technology. *Crit. Rev. Environ. Sci. Technol.* 45, 1827–1879. doi:10.1080/10643389.2014.1000761

Sachdeva, N., Poughon, L., Gerbi, O., Dussap, C.-G., Lasseur, C., Leroy, B., et al. (2021). Ground demonstration of the use of Limnospira indica for air revitalization in a bioregenerative life-support system setup: effect of non-nitrified urine–derived nitrogen sources. *Front. Astronomy Space Sci.* 8. doi:10.3389/fspas.2021.700270

Shin, H.-S., Youn, J.-H., and Kim, S.-H. (2004). Hydrogen production from food waste in anaerobic mesophilic and thermophilic acidogenesis. *Int. J. Hydrogen Energy* 29, 1355–1363. doi:10.1016/j.ijhydene.2003.09.011

Stasiak, M., Gidzinski, D., Jordan, M., and Dixon, M. (2012). Crop selection for advanced life support systems in the ESA MELiSSA program: durum wheat (Triticum turgidum var durum). *Adv. Space Res.* 49, 1684–1690. doi:10.1016/j.asr.2012.03.001

Tepari, E. A. (2019). Evaluation of biohydrogen production from Co-fermentation of carbohydrates and proteins. Available at: https://ir.lib.uwo.ca/etd/6566.

Teuling, E., Wierenga, P. A., Schrama, J. W., and Gruppen, H. (2017). Comparison of protein extracts from various unicellular green sources. *J. Agric. Food Chem.* 65, 7989–8002. doi:10.1021/acs.jafc.7b01788

Thiron, B. (2020). *Global control of a life support system: flow control and optimisation*. Stockholm, Sweden: KTH School of Electrical Engineering and Computer Science. Available at: http://urn.kb.se/resolve?urn=urn:nbn:se:kth:diva-278509 (Accessed March 23, 2023).

Tikhomirov, A. A., Ushakova, S. A., Velichko, V. V., Tikhomirova, N. A., Kudenko, Yu. A., Gribovskaya, I. V., et al. (2011). Assessment of the possibility of establishing material cycling in an experimental model of the bio-technical life support system with plant and human wastes included in mass exchange. *Acta Astronaut.* 68, 1548–1554. doi:10.1016/j.actaastro.2010.10.005

Tranquille, N., and Emeis, J. J. (1996). Rhodospirillum rubrum food acceptability study for MELiSSA. MELiSSA Technical Note 30.1. TNO Prevention and Health Available at: https://www.melissafoundation.org/download/554 (Accessed March 23, 2023).

Tusé, D., and Miller, M. W. (1984). Single-cell protein: current status and future prospects. *C R C Crit. Rev. Food Sci. Nutr.* 19, 273–325. doi:10.1080/10408398409527379

U.S. Food & Drug Administration (2017). Nutrition information for raw vegetables. Available at: https://www.fda.gov/food/food-labeling-nutrition/nutrition-information-raw-vegetables (Accessed March 23, 2023).

Usherwood, N., and Segars, W. (2001). Nitrogen interactions with phosphorus and potassium for optimum crop yield, nitrogen use effectiveness, and environmental stewardship. *TheScientificWorldJournal* 1, 57–60. Suppl 2. doi:10.1100/tsw.2001.97

Vermeulen, A. C. J., Papic, A., and Brazier, F. (2018a). "Modeling and simulating the MELiSSA loop to understand the effects of system interaction on survivability during long-duration interstellar missions: an agent-based approach," in AgroSpace-MELiSSA Conference, Rome, Italy, May 16–18, 2018. doi:10.5281/zenodo.7791088

Vermeulen, A. C. J., Sirenko, M., Papic, A., Kiem, J., Theys, A., and Brazier, F. (2018b). "Evolving asteroid Starships: a bio-inspired approach for interstellar space systems," in Proceedings of the 69th International Astronautical Congress (IAC), Bremen, Germany, October 1–5, 2018.

Vermeulen, A. C., Papic, A., Kiem, J., Hallak, D., and Brazier, F. (2019). "Modeling and simulating a regenerative life support system to understand the effects of system interaction on survivability during deep space missions: an agent-based approach," in Proceedings of the 70th International Astronautical Congress (IAC), Washington DC, October 21–25, 2019.

Vermeulen, A. C. J., Hubers, C., de Vries, L., and Brazier, F. (2020a). What horticulture and space exploration can learn from each other: the Mission to Mars initiative in the Netherlands. *Acta Astronaut.* 177, 421–424. doi:10.1016/j.actaastro.2020.05.015

Vermeulen, A. C. J., Papic, A., Kiem, J., Hallak, D., and Brazier, F. (2020b). "Exploring the impact of irregular metabolic efficiencies and the space environment on the survivability of a regenerative life support system through agent-based modeling," in MELiSSA Conference 2020, November 3–5, 2020, online. doi:10.5281/zenodo.7791110

Vijapur, S. H., Hall, T. D., Snyder, S., Inman, M., Taylor, E. J., and Skinn, B. (2017). Electrochemical peroxide generation. *ECS Trans.* 77, 947–962. doi:10.1149/07711.0947ecst

Volk, T., and Rummel, J. D. (1987). Mass balances for a biological life support system simulation model. *Adv. Space Res.* 7, 141–148. doi:10.1016/0273-1177(87)90045-7

Vrati, S. (1984). Single cell protein production by photosynthetic bacteria grown on the clarified effluents of biogas plant. *Appl. Microbiol. Biotechnol.* 19, 199–202. doi:10.1007/BF00256454

Waters, G. C. R., Dixon, M. A., Masot, A., Albiol, J., and Godia, F. (2004). "Static mass balance studies of the MELiSSA pilot plant: integration of a higher plant chamber," in 34th International Conference on Environmental Systems (ICES), Colorado Springs, CO, 19-22 July 2004 (SAE Technical Paper Series) (Warrendale, PA: SAE International).

WebMD (2021). Are there health benefits of durum wheat? Available at: https://www.webmd.com/diet/are-there-health-benefits-of-durum-wheat (Accessed March 23, 2023).

Weng, C., and Jeris, J. S. (1976). Biochemical mechanisms in the methane fermentation of glutamic and oleic acids. *Water Res.* 10, 9–18. doi:10.1016/0043-1354(76)90151-2

Yin, J., Yu, X., Wang, K., and Shen, D. (2016). Acidogenic fermentation of the main substrates of food waste to produce volatile fatty acids. *Int. J. Hydrogen Energy* 41, 21713–21720. doi:10.1016/j.ijhydene.2016.07.094

Zambelli, A., León, A., and Garcés, R. (2015). "Mutagenesis in sunflower," in *Sunflower*. Editors Sunflower, E. Martínez-Force, N. T. Dunford, and J. J. Salas (Urbana, Illinois: AOCS Press), 27–52. doi:10.1016/B978-1-893997-94-3.50008-8

Zhang, D., Clauwaert, P., Luther, A., López Barreiro, D., Prins, W., Brilman, D. W. F. et al. (2018). Sub- and supercritical water oxidation of anaerobic fermentation sludge for carbon and nitrogen recovery in a regenerative life support system. *Waste Manag.* 77, 268–275. doi:10.1016/j.wasman.2018.04.008

Zhang, D., Luther, A., Clauwaert, P., and Ronsse, F. (2019). Mild temperature hydrothermal oxidation of anaerobic fermentation filtrate for carbon and nitrogen recovery in a regenerative life support system. *J. Supercrit. Fluids* 145, 39–47. doi:10.1016/j.supflu.2018.11.022

frontiers | Frontiers in Astronomy and Space Sciences

TYPE Original Research
PUBLISHED 18 September 2023
DOI 10.3389/fspas.2023.1197402

Check for updates

OPEN ACCESS

EDITED BY
Luigi Gennaro Izzo,
University of Naples Federico II, Italy

REVIEWED BY
Jan Hendrik Bredehöft,
University of Bremen, Germany
Sarah Milliken,
University of Greenwich, United Kingdom

*CORRESPONDENCE
Yoshiaki Kitaya,
kitaya@omu.ac.jp

RECEIVED 31 March 2023
ACCEPTED 28 August 2023
PUBLISHED 18 September 2023

CITATION
Kitaya Y, Kawamoto T, Endo R and Shibuya T (2023), Effect of fish density on biological production in aquaponics combining lettuce hydroponics and loach aquaculture for controlled ecological life support systems in space. *Front. Astron. Space Sci.* 10:1197402. doi: 10.3389/fspas.2023.1197402

COPYRIGHT
© 2023 Kitaya, Kawamoto, Endo and Shibuya. This is an open-access article distributed under the terms of the Creative Commons Attribution License (CC BY). The use, distribution or reproduction in other forums is permitted, provided the original author(s) and the copyright owner(s) are credited and that the original publication in this journal is cited, in accordance with accepted academic practice. No use, distribution or reproduction is permitted which does not comply with these terms.

Effect of fish density on biological production in aquaponics combining lettuce hydroponics and loach aquaculture for controlled ecological life support systems in space

Yoshiaki Kitaya[1]*, Takashige Kawamoto[2], Ryosuke Endo[2] and Toshio Shibuya[2]

[1]Organization for Research Promotion, Osaka Metropolitan University, Osaka, Japan, [2]Graduate School of Agriculture, Osaka Metropolitan University, Osaka, Japan

There is a need to develop production technology that effectively uses limited water and other resources to create a stable food supply in space. Aquaponics, which combine hydroponics and aquaculture, is expected to be an efficient system for producing crops and animal proteins. This system sustains the reuse of water and balances nutrient elements between both cultures using dissolved elements in fish excrement for plant growth. To evaluate the effect of fish density on biological production and nitrogen usage efficiency in aquaponics combining lettuce hydroponics and loach aquaculture, we investigated the growth performance of lettuce plants and loach fish. We focused on the balance of nutrient elements, especially nitrogen flow in the system. As a result, we found that lettuce grew in aquaponics with a half-strength standard solution with an optimal combination of the number of plants and fish as well as hydroponics with a standard solution. Increasing the density of loach fish and lettuce plants can increase the total biological production of fish and plants. However, it will be important to control both fish and plant densities to increase nitrogen recovery in aquaponics with a high fish density.

KEYWORDS

aquaculture, CELSS, hydroponics, plant production, space farm

1 Introduction

Plant production in space has become a growing concern as the possibility of long-term manned space flights and human habitation on the moon increases. The feasibility of such missions depends heavily on the availability of crops grown in Controlled Ecological Life Support Systems (CELSS) or space farms. These crops will provide food, CO_2/O_2 conversion, and water purification for the crew. For long-term manned space missions and human habitation in space, space food and nutrition systems should be based on space farming, with scheduled crop production that yields high volumes and has a rapid turnover rate. The development of production technology that optimizes the use of limited water resources to create a stable food supply is also crucial for success in space. Although plant materials are an important source of nutrients, they alone are insufficient to meet the needs

necessary for maintaining human health. Essential amino acids, which cannot be synthesized in the human body, are critical for maintaining physique and longevity. Richter et al. (2016) pointed out that obtaining complete nutrition from a purely plant-based diet (vegan diet) is impossible or difficult without considering the proper amounts and combinations. They reported that the most important missing nutrient is vitamin B_{12}, and other potentially deficient nutrients include protein, essential amino acids, long-chain n-3 polyunsaturated fatty acids, other vitamins (riboflavin, vitamin D), and minerals (calcium, iron, iodine, zinc, selenium). Therefore, animal proteins must be consumed to obtain certain vitamins and amino acids necessary for human health.

Aquaponics, a biological production system that combines hydroponics and aquaculture, can provide a stable supply of plant and animal ingredients while effectively using limited water resources. In this system, nutrients dissolved in fish excretion are recycled and used to promote plant growth. Using material reuse, aquaponics reduces waste and creates a sustainable production model. Aquaponics is an efficient system for water and nutrient use (e.g., Al-Hafedh et al., 2008; Wongkiew et al., 2017). By sharing water between hydroponics and aquaculture systems, plants can use the nutrient-rich components derived from fish excrement to grow. This allows for food production while simultaneously recycling nutrients and converting waste into valuable resources.

The nitrogen balance has been the main focus of aquaponics research on Earth (e.g., Hu et al., 2015), due to its importance for plant growth (Xu et al., 2012) and the availability, concentration, and accumulation of nitrogen compounds (Goddek et al., 2016). As a biological production system combining hydroponics and aquaculture, a thorough understanding of nitrogen balance is necessary to increase system productivity. Aquaponics can produce animal protein and semi-complete nutritional food crops that are the ingredients providing the best balance of human daily nutritional requirements, as demonstrated by Islam et al. (2022) with high-nutritional sweet potato plants (Kitaya et al., 2021) and tilapia fish. Garlic plants and tilapia fish have also been successfully grown in aquaponics, promoting biosynthesis of the medicinally important metabolite 'ajoene' in garlic plants compared to no fish (Naznin et al., 2015).

Most studies on aquaponics conducted on Earth have used tilapia and catfish in aquaculture due to their high growth rates and edibility (e.g., Graber and Junge, 2009; Nuwansi et al., 2016). However, their heads, internal organs, and bones are inedible, which is a disadvantage. In contrast, loach has a 100% edible portion and high nutritional value, as recognized by the Japan Ministry of Education, Culture, Sports, Science and Technology (2015). Loach is also a traditional Japanese ingredient. Additionally, loaches are capable of breathing through their intestines, making them resistant to dissolved oxygen deficiency. Thus, loach was selected as the fish species to be cultured in this study.

For the perspective of aquaponics in bio-regenerative life support systems (BLSS) in space, Przybyla (2021) and Brown et al. (2021) reviewed the possibility of space aquaculture. They also emphasized the importance of a closed aquaponic system for water and material recycling as well as a balanced nutritional intake (proteins, lipids, and carbohydrates) in a long-term human stay in space.

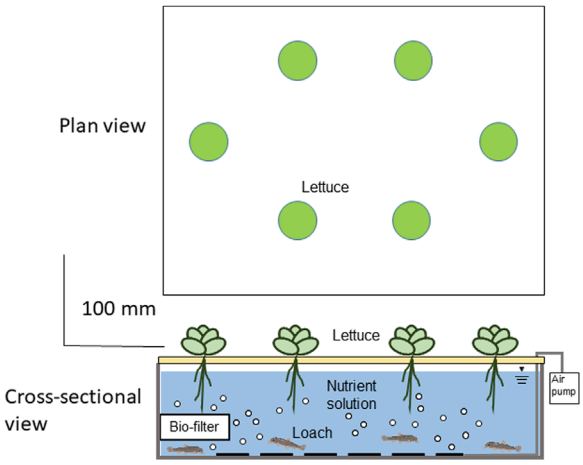

FIGURE 1
A schematic diagram of the aquaponics experiment combining lettuce hydroponics and loach aquaculture.

Many studies have investigated aquaponic culture with various plant types on Earth. In this study, lettuce was selected as the food plant to be cultured, as it is a common vegetable in plant factory culture and has a wealth of physiological and ecological data on environmental responses. We are assessing the effectiveness of fish excreta-derived components as fertilizers for plant growth in aquaponics, using a combination of loach aquaculture and lettuce hydroponics for integration into CELSS in space. We are particularly examining the nitrogen compound flow within the system, as it is an essential element for plants and is abundant in fish excreta while also being harmful to fish.

This study examined the impact of fish density on the biological production rate by manipulating fish density on Earth. Furthermore, the nitrogen balance was analyzed.

2 Materials and methods

2.1 General matters

Lettuce (*Lactuca sativa* L., 'crunch') and loach (*Misgurnus anguillicaudatus*) were cultured for 21 days on Earth. Each culture container in six test groups described later was filled with 12 L of water and stocked with loaches (initial average weight 2.9 g/fish) in the rootzone of lettuce plants in each container. The number of loaches per container ranged from 6 to 30, depending on the density. Twenty-one-day-old lettuce seedlings (fresh weight of 2.8 ± 0.2 g/plant) were planted in the holes, spaced 5 cm apart in a grid pattern (Figure 1).

Six lettuce plants were grown in each test group under controlled environmental conditions, with a temperature of 25°C, relative humidity of 70%, a CO_2 concentration of 700 μmol mol^{-1}, a photosynthetic photon flux density of 200 μmol m^{-2} s^{-1}, and a light period of 16 h d^{-1}. The light source used was LEDs (LDL-B20T 50/08/10-KOD, Sanwa Seimitsu Co., Ltd.). The nutrient solution was made from dechlorinated tap water. Continuous aeration

TABLE 1 Component of the fish feed.

Component	Content(5)
Protein	43
Lipid	7
Crude Fiber	3
Ash	20
Phosphorus	1.7
Moisture	10

TABLE 2 Concentrations of chemical fertilizer elements.

Elements	Concentration (mg L^{-1})
Anmonium-N	12
Nitrate-N	117
P_2O_5	60
K_2O	203
CaO	115
MgO	30
MnO	0.75
B_2O_3	0.75
Fe	1.35
Cu	0.015
Zn	0.045
Mo	0.015

(3.5 L min^{-1}) was provided to the nutrient solution. Loaches were fed once a day, five times a week, with commercially available goldfish feed (Sakihikari, Kyorin Co., Ltd.) equivalent to 1% of their body weight (about 0.03 g/fish) for 2 weeks before starting the experiment. The component of fish feed used are shown in Table 1.

Prior to the experiment, a biofilter consisting of non-woven fabric as a carrier for microorganisms was placed in the loach culture tank for a period of 3 weeks to facilitate the colonization of nitrite and nitrate bacteria.

Due to the inadequacy of certain fertilizer components required for lettuce growth from loach excrement alone in our preliminary experiment, we supplemented with a chemical nutrient solution. The additional medium used was a half-strength OAT House A-formula solution (OAT Agrio Co., Ltd.). The electrical conductivity of the culture medium was adjusted to about 1.2 dS m^{-1}. The pH in the solution was adjusted to about 6.0. The chemical composition of the half-strength nutrient solution is shown in Table 2.

Fresh weight measurements of lettuce and loach, along with ammonium nitrogen, nitrite nitrogen, nitrate-nitrogen concentration, pH, and electrical conductivity of the nutrient solution, were conducted weekly. On the final day of the experiment, the dry weight and nitrogen content of lettuce and loach were determined. To measure the dry weight, the harvested lettuce and loach were dried for approximately 7 days in a constant temperature drying oven at 80°C.

For solution analysis, the ammonium nitrogen concentration was determined using a spectrophotometer (AT-2000, Central Kagaku Co., Ltd., Japan), nitrite nitrogen concentration was measured using a simple reflection photometer (RQ flux plus 10, Kanto Kagaku Co., Ltd., Japan), and nitrate-nitrogen concentration was measured using a compact nitrate ion meter (LAQUAtwin NO3-11C, Horiba, Co., Ltd., Japan). The pH was measured using a compact pH meter (LAQUAtwin pH-33B, Horiba, Co., Ltd. Japan).

To analyze the nitrogen content of loach and lettuce, three individuals of loach and the edible parts (leaves and stems) of six individuals of lettuce from each group were powdered. The nitrogen content was measured using the heated persulfate decomposition method and an absorption photometer (DR-3900, DKK-Toa Co., Ltd., Japan).

The relative growth rate (RGR), a growth index for lettuce and loach, was calculated using Eq. 1. Additionally, the nitrogen usage efficiency (NUE), which represents the ratio of the accumulated nitrogen in lettuce and loach to the input nitrogen, was calculated using Eq. 2.

$$RGR = \frac{InW_2 - InW_1}{t_2 - t_1} \quad (1)$$

$$NUE = \frac{N_{plant} + N_{fish}}{N_{input}} \quad (2)$$

In Eq. 1, W_1 represents the dry weight (g) of plants and fish at time t_1, and W_2 represents the dry weight at time t_2, where t_1 and t_2 represent the times of transplanting and harvesting (in days). W_1 was calculated from the actual measured fresh weight of each individual at t_1 by using the Dry weight/Fresh weight ratio calculated from sample individuals previously obtained. In Eq. 2, N_{input} represents the amount of nitrogen (g) contained in the applied chemical fertilizer and feed, N_{plant} represents the amount of nitrogen (g) contained in lettuce, and N_{fish} represents the amount of nitrogen (g) contained in loach.

2.2 Test groups

Six test groups were established, comprising five aquaponic groups and one hydroponic group. Additionally, to determine the quantity of dissolved nitrogen released from 20 loaches, a test group was established where only loaches were cultured in the same hydroponic solution in a tank of the same size. Each aquaponic group consisted of 6 plants and 6, 12, 18, 24, and 30 loach fish (Table 1). Each individual loach was fed 0.06 g d^{-1}. A commercial feed for goldfish (Sakihikari, Kyorin Co., Ltd.) was fed twice a day with an interval of more than 3 h during the experimental period.

2.3 Nitrogen contents

The nitrogen content (g) of each component in the system was calculated using the following procedure: The amount of nitrogen contained in the nutrient solution of each test group was

calculated based on the nutrient solution composition specified by the manufacturer. The amount of nitrogen contained in the feed provided to the fish was calculated by multiplying the nitrogen content (g g^{-1}) contained in the feed by the total feed amount (g). No leftover feed remained during the experiment. The amount of nitrogen contained in the excretion from loaches was calculated as the amount of nitrogen derived from loach emissions, which was determined by measuring the total amount (g) of dissolved nitrogen components discharged by 20 loaches over 21 days in the test group where only loaches were cultured.

2.4 Statistical analysis

Significant differences were tested using the Tukey–Kramer method and expressed as the presence or absence of significant differences at a level of $p < 0.05$.

3 Results and discussion

3.1 Nitrogen compound concentration in the solution

As the fish density increased, so did the amount of feed and input nitrogen. This caused an increase in the amount of excrement and an accompanying increase in ammonium nitrogen concentration in the solution, as shown in Figure 2. Nitrite nitrogen concentrations also increased with increasing fish density, but remained at low levels. The nitrate-nitrogen concentration reached its maximum at a fish density of 1.5 fish L^{-1}. The hydroponic group, which had a fish density of 0 fish L^{-1}, had lower ammonium nitrogen and nitrite nitrogen concentrations than the aquaponic groups. The increase in nitrite nitrogen concentration and decrease in nitrate-nitrogen concentration at high loach densities may be due to the denitrification of nitrate. The insufficient water circulation in the nutrient solution tank may have led to a local micro-partial anaerobic environment, but further details are unknown since the distribution of dissolved oxygen, especially in the biofilter, was not measured in this experiment.

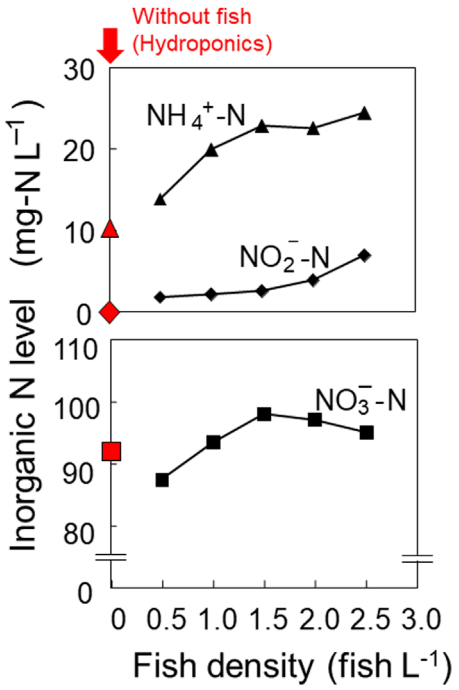

FIGURE 2
Concentrations of ammonium nitrogen, nitrite nitrogen, and nitrate nitrogen in the solution for each fish density during the experimental period.

3.2 Growth performance

On the final day of the experiment, lettuce plants showed no visible differences among the test groups (Figure 3). There was no significant difference ($p < 0.05$) in the lettuce biomass in the aquaponic and hydroponic groups (Table 3). Similarly, the RGR of lettuce plants did not change with increasing fish density (Figure 4), and there was no significant difference in the RGR of lettuce plants

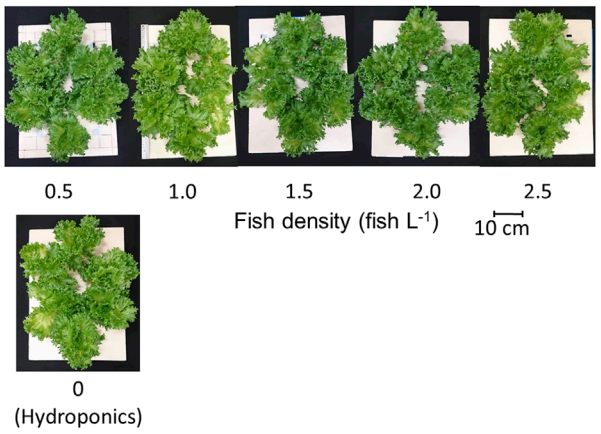

FIGURE 3
Photos of 6 lettuce plants grown for 21 days in each test group.

TABLE 3 Fresh weights of lettuce plants and loach fish as affected by fish density.

Density(fish L^{-1})	Lettuce (g/plant)		Loach (g/fish)
	leaves and stems	Roots	
0.5	82.6 ± 8.0*	6.4 ± 0.6	3.9 ± 0.3
1.0	99.6 ± 7.6	7.7 ± 0.7	3.8 ± 0.3
1.5	75.4 ± 3.3	7.3 ± 0.5	3.8 ± 0.2
2.0	79.7 ± 9.0	11.2 ± 1.0	3.6 ± 0.3
2.5	58.8 ± 3.4	7.3 ± 0.9	3.7 ± 0.2
$0_{(Hydroponics)}$	93.7 ± 7.5	7.5 ± 0.6	
ANOVA (p)	0.111	0.095	0.089

*Standard error.

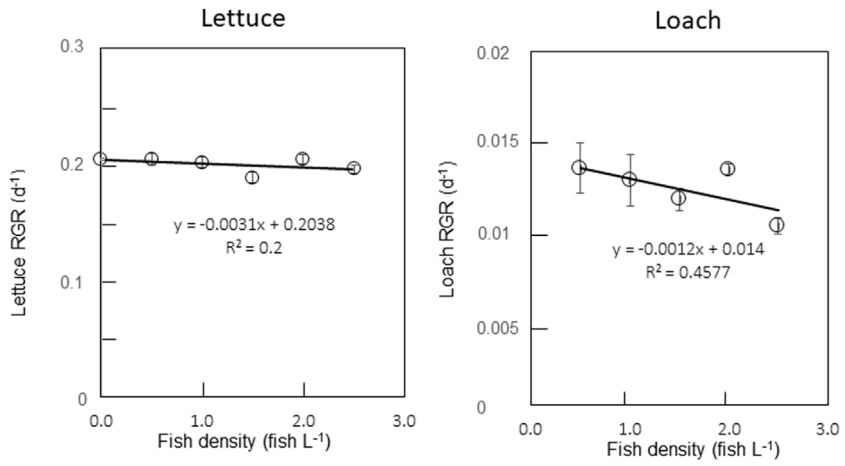

FIGURE 4
Effects of fish density on relativegrowth rates (RGRs) of lettuce plants and loach fish Error bars indicate standard errors.

in the test groups. It has been reported that lettuce growth can be inhibited by the accumulation of nitrite in solution (Hoque et al., 2007). However, in this experiment, the nitrite level did not inhibit lettuce growth.

On the last day of the experiment, the fresh weight of loach fish did not show any significant differences but tended to decrease with increasing fish density (Table 3). The RGR of loach also tended to decrease with increasing fish density (Figure 4). The increase in nitrite and ammonium ions in the culture solution (Figure 2) seemed to cause a slight decrease in the RGRs of loach, whereas there were no significant differences among the test groups. The accumulation of nitrite ions and ammonium ions inhibited loach growth, but the effect was not significant.

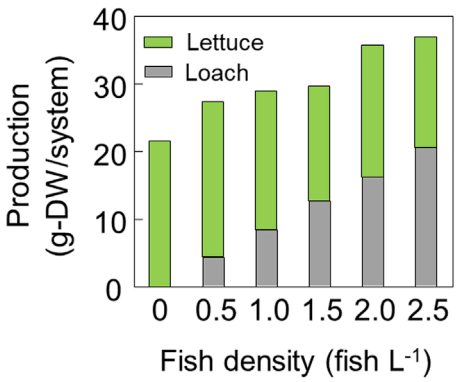

FIGURE 5
Dry mass production of lettuce plants and loach fish in the system as affected by fish density.

3.3 Biological production

The dry weight of the loach in each group is shown in Figure 5, which reveals an increase in loach production with increasing fish density. However, the growth rate of the loach tended to decrease as the fish density increased. Despite this, the loach population increased with the fish density, leading to an overall increase in production. In contrast, the RGR of lettuce was consistent across all fish densities, and the lettuce production was not affected by the fish density (Figure 5). Therefore, the total production of both lettuce and loach tended to increase as the fish density increased (Figure 5).

3.4 Nitrogen usage efficiency

Contents of nitrogen accumulated during the experimental period in lettuce plants and loach fish as affected by fish density are shown in Figure 6. The nitrogen contents in lettuce plants and loach fish tended to decrease with increasing fish density. These tendencies are partly due to the difference in the accumulated amount of biomass, but investigation of the reason requires more detailed analysis such as the type of nitrogen compounds.

As shown in Figure 7, the NUE of lettuce decreased with increased fish density. This can be attributed to the increase in input feed and nitrogen with increasing fish density, which led to the accumulation of unused nitrogen in the nutrient solution. Despite the constant RGR of lettuce, the increase in fish density did not result in a proportional increase in nitrogen uptake by lettuce, causing a decrease in NUE. In contrast, the NUE of loaches remained constant as the amount of food ingested by loaches did not change with increasing fish density. The total NUE of loach and lettuce decreased with increasing fish density, except for the 0.5 fish L^{-1} group, where there was a one-to-one ratio of lettuce

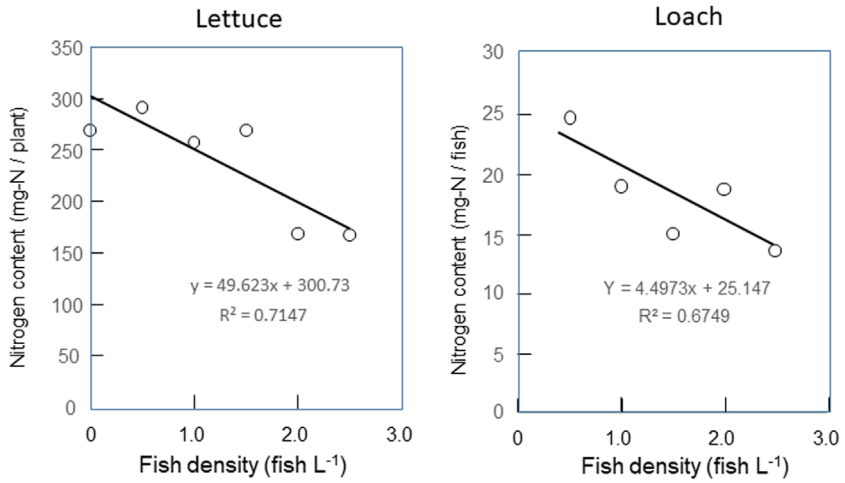

FIGURE 6
Effects of fish density on contents of nitrogen accumulated during the experimental period in lettuce plants and loach fish.

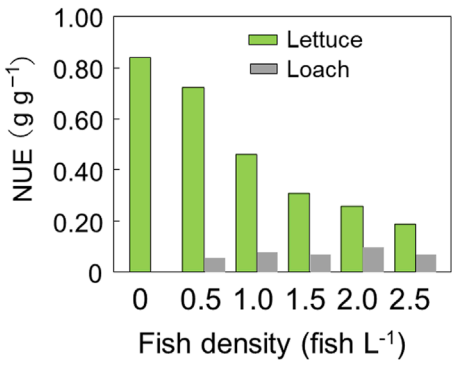

FIGURE 7
Nitrogen usage efficiency of lettuce leaves and stems and loach fish as affected by fish density.

plant to loach fish, and the efficiency was almost similar to that of hydroponics.

In the nitrogen balance, approximately 70% of the nitrogen from the feed was used by growing lettuce plants, while around 25% of the nitrogen from the feed was accumulated in loach fish. In all aquaponic groups, the end-of-experiment dissolved component was less than 5% of the supply, indicating that nitrogen was fully used in the entire system. The results in this study confirmed the facts of the usefulness of aquaponics from the viewpoint of the availability, concentration, and accumulation of nitrogen compounds (Goddek et al., 2016). However, as excessive nitrogen supply can decrease usage efficiency, further investigations are needed to determine how an increased nitrogen supply in an aquaponic system could affect the system's NUE. In addition, to find the optimal balance between plants and fish for efficiently accumulating nitrogen as a food source, a more detailed analysis, such as the type of nitrogen compounds in plants and fish is required.

In the long-term operation of aquaponics, it is also necessary to manage the mineral components other than the nitrogen compounds so that they are neither excessive nor deficient. For example, Lantovololona and Adavelo (2020) reported successful aquaponics that combined loach and lettuce, but the possibility of potassium deficiency for the lettuce growth.

In this study, we did not monitor the microbial communities. The monitoring and regulation of microbes will be important, especially for stable and safe production in the long term.

4 Conclusion

In this study, lettuce plants showed no difference in growth when a portion of the chemical fertilizer was replaced with the excretory component of loach fish. This suggests that loach excreta can be used to partially supplement chemical fertilizer. Aquaponics shows promise in reducing the environmental impact of aquaculture by enabling the simultaneous production of plants and fish, reducing the need for chemical fertilizers in lettuce hydroponics, and purifying aquaculture water.

It is essential to increase plant nitrogen absorption, for example, by increasing planting density, particularly to reduce unused nitrogen and improve nitrogen recovery in food production. Future studies should examine not only nitrogen but also other nutritional elements to model the optimal combination of loach, lettuce, and feed supply.

Due to the recent global population growth, there are concerns about ensuring a stable food supply and conserving water resources on Earth. The spin-off technology of aquaponic development in CELSS can provide valuable knowledge to meet the urgent need for developing production technology that uses water and

other resources efficiently to create a stable food supply on Earth.

Data availability statement

The raw data supporting the conclusion of this article will be made available by the authors, without undue reservation.

Ethics statement

The manuscript presents research on animals that do not require ethical approval for their study.

Author contributions

YK contributed to conception and design of the study and wrote the first draft of the manuscript. TK mainly conducted the experiment with support of TS and RE. All authors contributed to the article and approved the submitted version.

Conflict of interest

The authors declare that the research was conducted in the absence of any commercial or financial relationships that could be construed as a potential conflict of interest.

Publisher's note

All claims expressed in this article are solely those of the authors and do not necessarily represent those of their affiliated organizations, or those of the publisher, the editors and the reviewers. Any product that may be evaluated in this article, or claim that may be made by its manufacturer, is not guaranteed or endorsed by the publisher.

References

Al-Hafedh, Y., Alam, A., and Beltagi, M. S. (2008). Food production and water conservation in a recirculating aquaponic system in Saudi arabia at different ratios of fish feed to plants. *J. World Aquac. Soc.* 39 (4), 510–520. doi:10.1111/j.1749-7345.2008.00181.x

Brown, L., Peick, J., Pickett, M., Fanara, T., Gilchrist, S., Smiley, A., et al. (2021). Aquatic invertebrate protein sources for long-duration space travel. *Life Sci. Space Res.* 28, 1–10. doi:10.1016/j.lssr.2020.10.002

Goddek, S., Espinal, C. A., Delaide, B., Jijakli, M. H., Schmautz, Z., Wuertz, S., et al. (2016). Navigating towards decoupled aquaponic systems: A system dynamics design approach. *Water* 8, 303. doi:10.3390/w8070303

Graber, A., and Junge, R. (2009). Aquaponic systems: nutrient recycling from fish wastewater by vegetable production. *Desalination* 246, 147–156. doi:10.1016/j.desal.2008.03.048

Hoque, M. M., Ajwa, H. A., and Smith, R. (2007). Nitrite and ammonium toxicity on lettuce grown under hydroponics. *Commun. Soil Sci. Plant Analysis* 39, 207–216. doi:10.1080/00103620701759194

Hu, Z., Lee, J. W., Chandran, K., Kim, S., Brotto, A. C., and Khanal, S. K. (2015). Effect of plant species on nitrogen recovery in aquaponics. *Bioresour. Technol.* 188, 92–98. doi:10.1016/j.biortech.2015.01.013

Islam, A. F. M. S., Hirai, H., and Kitaya, Y. (2022). An aquaponic system with hydroponic culture of sweet potato and tilapia culture. *J. Agric. Ecol. Res. Int.* 23 (6), 62–72. doi:10.9734/jaeri/2022/v23i6499

Japan Ministry of Education, Culture, Sports, Science and Technology (2015). *Standard tables of food composition in Japan, 2020*. 8th Edn. Available at: https://www.mext.go.jp/a_menu/syokuhinseibun/mext_01110.html.

Kitaya, Y., Higashi, K., Shibuya, T., and Endo, R. (2021). Fundamental study on plant-based regenerative life-support systems with sweetpotato culture in space. *Trans. JSASS Aerosp. Tech. Jpn.* 19 (6), 889–891. doi:10.2322/tastj.19.889

Lantovololona, F. M. S., and Adavelo, J. M., 2021, Crop production in a loach (Misgurnus anguillicandatus) – lettuce (Lactuca saliva) raft aquaponics system, Proceedings of the the 2020 Global Conference on Aquaculture, Shanghai, China, 22–25. September 2021.

Naznin, M. T., Kitaya, Y., Shibuya, T., Hirai, H., Endo, R., and Lefsrud, M. (2015). Integrated culture of garlic and tilapia fish -source of protein and medicinal compound ajoene. *ActaHortic* 1098, 95–101. doi:10.17660/actahortic.2015.1098.9

Nuwansi, K. K. T., Verma, A. K., Prakash, C., Tiwari, V. K., Chandrakant, M. H., Shete, A. P., et al. (2016). Effect of water flow rate on polyculture of koi carp (*Cyprinus carpio* var. koi) and goldfish (*Carassius auratus*) with water spinach (*Ipomoea aquatica*) in recirculating aquaponic system. *Aquac. Int.* 24, 385–393. doi:10.1007/s10499-015-9932-5

Przybyla, C. (2021). Space aquaculture: prospects for raising aquatic vertebrates in a bioregenerative life-support system on a lunar base. *Front. Astronomy Space Sci.* 8, 1–16. doi:10.3389/fspas.2021.699097

Richter, M., Boeing, H., Grünewald-Funk, D., Heseker, H., Kroke, A., Leschik-Bonnet, E., et al. (2016). Vegan det - position of the German nutrition society (DGE). *Ernaehrungs Umsch. Int.* 63 (04), 92–102. doi:10.4455/eu.2016.021

Wongkiew, S., Hu, Z., Chandran, K., Lee, J. W., and Khanal, S. K. (2017). Nitrogen transformations in aquaponic systems: A review. *Aquac. Eng.* 76, 9–19. doi:10.1016/j.aquaeng.2017.01.004

Xu, G., Fan, X., and Miller, A. J. (2012). Plant nitrogen assimilation and use efficiency. *Annu. Rev. Plant Biol.* 63, 153–182. doi:10.1146/annurev-arplant-042811-105532

frontiers | Frontiers in Astronomy and Space Sciences

TYPE Original Research
PUBLISHED 21 September 2023
DOI 10.3389/fspas.2023.1229022

Check for updates

OPEN ACCESS

EDITED BY
Cyprien Verseux,
University of Bremen, Germany

REVIEWED BY
Thierry Dufour,
Université Paris-Sorbonne, France
Adriana Blachowicz,
NASA Jet Propulsion Laboratory (JPL),
United States

*CORRESPONDENCE
Laurence Lemelle,
laurence.lemelle@ens-lyon.fr
Christophe Place,
christophe.place@ens-lyon.fr

RECEIVED 25 May 2023
ACCEPTED 01 September 2023
PUBLISHED 21 September 2023

CITATION
Lemelle L, Mottin E, Le Tourneau D, Rouquette S, Campagnolo L, Thévenot C, Maillet A, Barde S, Garre E, Teisseire J, Fontelaye C, Jousseaume V, Pudda C, Constantin O, Marcoux P, Nonglaton G and Place C (2023), Surface contamination rates at different spatial scales in the Columbus module (ISS) during the MATISS campaigns. *Front. Astron. Space Sci.* 10:1229022. doi: 10.3389/fspas.2023.1229022

COPYRIGHT
© 2023 Lemelle, Mottin, Le Tourneau, Rouquette, Campagnolo, Thévenot, Maillet, Barde, Garre, Teisseire, Fontelaye, Jousseaume, Pudda, Constantin, Marcoux, Nonglaton and Place. This is an open-access article distributed under the terms of the Creative Commons Attribution License (CC BY). The use, distribution or reproduction in other forums is permitted, provided the original author(s) and the copyright owner(s) are credited and that the original publication in this journal is cited, in accordance with accepted academic practice. No use, distribution or reproduction is permitted which does not comply with these terms.

Surface contamination rates at different spatial scales in the Columbus module (ISS) during the MATISS campaigns

Laurence Lemelle[1]*, Eléonore Mottin[1], Denis Le Tourneau[2], Sébastien Rouquette[3], Lucie Campagnolo[4], Cécile Thévenot[4], Alain Maillet[4], Sébastien Barde[3], Emmanuel Garre[5], Jérémie Teisseire[5], Caroline Fontelaye[6], Vincent Jousseaume[6], Catherine Pudda[6], Olivier Constantin[6], Pierre Marcoux[6], Guillaume Nonglaton[6] and Christophe Place[2]*

[1]University Lyon, ENS de Lyon, University Claude Bernard, CNRS, Laboratoire de Géologie de Lyon-Terre Planètes et Environnement, Lyon, France, [2]University Lyon, ENS de Lyon, CNRS, Laboratoire de Physique, Lyon, France, [3]CNES, Paris, France, [4]MEDES-IMPS for CADMOS, Toulouse, France, [5]Surface du Verre et Interface, UMR CNRS/Saint-Gobain, Aubervilliers, France, [6]Univ. Grenoble Alpes, CEA, LETI, Grenoble, France

Future long-duration human spaceflights require developments to limit biocontamination of surface habitats. The three MATISS (Microbial Aerosol Tethering on Innovative Surfaces in the International Space Station) campaigns exposed surface treatments over several months in the ISS. To this end, eight sample holders designed were mounted with lamella-bearing FDTS ((1*H*, 1*H*, 2*H*, 2*H*)-perfluorodecyltrichlorosilane), SiOCH, and parylene hydrophobic coatings, at two different locations, for several months, during three distinct periods from 2016 to 2020. Tile scanning optical microscopy (×3 and ×30 magnifications) detected several thousand particles, indicating a relatively clean environment (a few particles per mm^2). In previous studies, exposure rates were analyzed for all the coarse and fine particles detected on the largest total area of the integrated FDTS area exposed in the ISS (several cm^2). Here, the contamination rates observed for a smaller constant area unit (the 0.66-cm^2 window area of the holder) were statistically analyzed. Therefore, a statistical difference in rate distributions between RGSH (Return Grid Sensor House) and EDR (European Drawer Rack) and between FDTS and either SiOCH or parylene was shown for the coarse particles but not for the fine particles. The contamination rates were found to be low, confirming the efficiency of the long-term air purification system. The rates tend to vary with the astronaut occupancy rates. Surfaces of spacecraft for long-duration exploration left unmanned during dormancy periods can be considered safe from biocontamination.

KEYWORDS

life support, biomaterials, space applications, space habitation, earth applications, astrobiology, surface biocontamination

1 Introduction

International space agencies are diligently striving to enhance manned spaceflight capabilities for prolonged durations, encompassing missions to diverse destinations, including low Earth orbit (LEO), cis-lunar space, the lunar surface, and ultimately Mars (James et al., 2007; Ott and Pierson, 2014; ISECG, 2018; Salmela et al., 2020). However, the potential biocontamination of enclosed habitats by the microflora carried by the crew presents a significant and unavoidable concern (Yamaguchi et al., 2014; Santomartino et al., 2020). The extended periods of isolation and dependence on closed-loop life support systems (Baranov et al., 2006) in manned stations further amplify this risk. The presence of biocontamination in the cabin not only poses threats to the health of astronauts but also entails potential damage to critical equipment (Ichijo et al., 2016; Farkas and Farkas, 2021). Over time, microorganisms have the capacity to develop resistance, mutate, and increase their virulence, thus transforming benign microbes into pathogenic agents due to the immune system disruptions experienced in space (Jorgensen et al., 1997; Wilson et al., 2007; Wilson et al., 2008; Tirumalai et al., 2017; Zea et al., 2017; Huang et al., 2018; Mukhopadhyay and Bagh, 2020; Fajardo-Cavazos and Nicholson, 2021). Consequently, it is imperative to effectively mitigate these risks (Siegel et al., 2007).

The transmission of pathogens through the air and water present on spacecraft is a critical concern (Novikova, 2004; Novikova et al., 2006; Ichijo et al., 2013; Lang et al., 2017; Acres et al., 2021). To ensure safety, filtration systems play a vital role in purifying these elements and undergo regular monitoring (Ott et al., 2004; Smirnov et al., 2004; Balistreri et al., 2013). Surfaces within the spacecraft harbor a diverse range of microorganisms that can act as sources of infection and contribute to pathogen transmission (Otter et al., 2011; Weber et al., 2013; Otter et al., 2016; Zea et al., 2018; Vaishampayan and Grohmann, 2019; Zea et al., 2020). The formation of biofilms on solid surfaces gives rise to a resilient microbial community capable of withstanding changes in the environment and the effects of antimicrobial agents (Pierson, 2001; Buchovec et al., 2020). As a result, biofilms are strongly associated with the persistence of chronic bacterial infections in humans.

Manual disinfection of surfaces on the International Space Station (ISS) poses challenges for astronauts, particularly when dealing with hard-to-reach areas, due to its labor-intensive and time-consuming nature. Furthermore, in long-duration exploration scenarios where spacecraft may remain unoccupied and unsterilized during dormant periods, the necessity for autonomous microbial monitoring and control systems becomes evident (Sethi and Manik, 2018; Ichijo et al., 2020; Mahnert et al., 2021). Implementing new solutions during the design phase of space modules has proven effective in mitigating the risks of surface biocontamination. Therefore, it is of utmost importance to prioritize the development of durable materials and equipment that limit the microbial growth and prevent its dissemination, thereby ensuring the future success of spacecraft missions (Bauer, 2020; Lin et al., 2020). Selection of materials that are unsuitable for microbial colonization and growth is a promising approach.

There are numerous strategies to limit surface biocontamination, including surfaces that passively repel microorganisms and facilitate their elimination through air purification systems. They constitute a viable option, provided certain constraints are met. These surfaces should be nanoparticle-free, have firmly anchored coatings, should be synthesized using solvent-free automated techniques, and should be compatible with various materials, including glass slides. In microgravity, microorganisms are primarily transported through droplets in non-turbulent laminar flows without thermal convection. Hydrophobic coatings act as a first line of defense by reducing the contact area between the surface and hydrophilic drops, rather than directly reducing adhesion

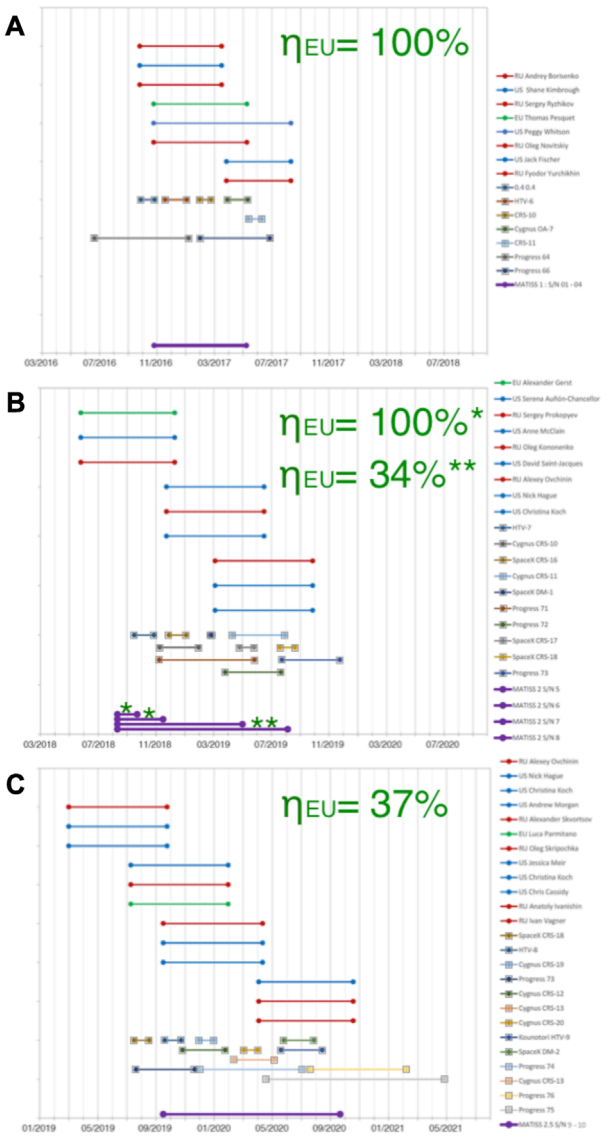

FIGURE 1
Timelines of the MATISS campaigns. **(A)** Dates of MATISS-1. Exposure dates of the holders (bottom, violet). Dates of the visiting vehicles (middle, one color per vehicle, squared tops for line). Dates of each astronaut in the ISS during the campaign (top, blue for the US astronauts, red for the Russian astronauts, and green for the EU astronauts, circled tops for line). The occupancy rate of the EU astronauts ($\sim\eta_{EU}$) during each campaign is reported in green. **(B)** Same for MATISS-2. **(C)** Same for MATISS-2.5.

forces (Glavan et al., 2013; Grinenval et al., 2014; Sadri et al., 2018; Sala de Medeiros et al., 2019). Numerous studies support the effectiveness of hydrophobic coatings in this regard (Moazzam et al., 2016; Chen et al., 2018; Jiang et al., 2020; Kefallinou et al., 2020; Lee et al., 2020; Wang et al., 2020; Li et al., 2021; Mandal et al., 2022).

The MATISS (Microbial Aerosol Tethering on Innovative Surfaces, in the International Space Station) experiment was conducted to explore the application of hydrophobic coatings, commonly used in various industries, for reducing surface biocontamination in spacecraft (Lemelle et al., 2020). In this experiment, surfaces within the Columbus module of the International Space Station were exposed for extended periods using a specially designed holder. This holder ensured the safe exposure of glass surfaces to astronauts and allowed for easy sealing within the station. Upon return to the laboratory, the sealed holder enabled the imaging of particles present on the exposed surfaces. The MATISS experiment was replicated three times between 2016 and 2020, involving the exposure of different surfaces for various durations. For example, the MATISS-1 campaign exposed surfaces for approximately 6 months starting in November 2016, the MATISS-2 campaign involved exposures of approximately 1, 3, and 12 months starting in August 2018, and the MATISS-2.5 campaign lasted for approximately 12 months starting in September 2019 (Figure 1).

In order to limit surface biocontamination, the MATISS experiment was carried out to assess the potential of a particular hydrophobic coating (FDTS) in reducing the biocontamination of surfaces on the ISS (Lemelle et al., 2020; 2022). In these previous studies, we analyzed systematically all the particles that could be detected on the largest area possible and considered them as one set to get average exposure rate values. Here, we analyze more extensively the exposure rates for centimeter-sized sub-unit of surfaces. Sub-sets of rates were newly compiled to evaluate the biocontamination variation between different Columbus positions, different types of hydrophobic coatings, and different time periods. Analyses were performed to display the diversity and variability of the sources and pathways of surface biocontamination observed during extended periods on the ISS.

2 Materials and methods

2.1 Hydrophobic surfaces: coatings and patterning

2.1.1 CEA hydrophobic coatings on silica surfaces

For this study, we selected chemical vapor deposition processes, all carried out in a vacuum on a glass lamella, to limit the use of potentially toxic organic solvents and to provide an excellent intra- and inter-lot reproducibility (Figure 2A).

SiOCH films of 1 µm thickness were deposited using Octamethylcyclotetrasiloxane (OMCTS) as the precursor under vacuum conditions at 2 Torr and 100°C. The water contact angle on SiOCH films was approximately 105 ± 2°. A 1-µm-thick layer of parylene was deposited using the SCS Labcoter® 2 (PDS 2010) Vapor Deposition System with parylene C as the precursor. The

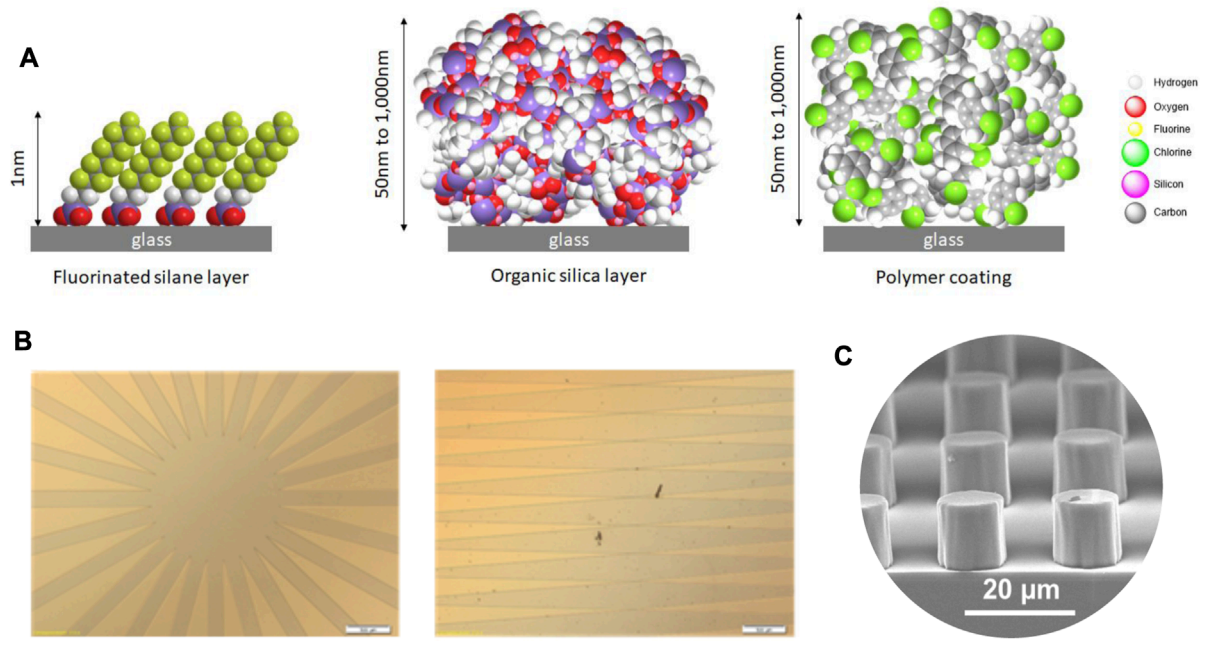

FIGURE 2
Hydrophobic surfaces exposed in the MATISS campaigns. **(A)** Atomic diagram of the molecules constituting the three uniform layers of nanometric thickness and different chemical compositions: fluorinated silane (FDTS, on the left), organic silica (SiOCH, in the middle), and parylene C polymer (on the right). **(B)** Optical images of the masks from which radial and mirror symmetric patterns of FDTS layers have been prepared. **(C)** Patterned layers of micrometric SiO_2 dots.

water contact angle on the parylene layers was approximately 87 ± 4°. The protocols are described in Lemelle et al. (2020).

The process of FDTS coating based on (1*H*, 1*H*, 2*H*, 2*H*)-perfluorodecyltrichlorosilane (FDTS) (ABCR, 97%) was described in Lemelle et al. (2022). The FDTS patterning protocol was as follows: the glass slides were cleaned before they were coated with a positive AZ1512HS photoresist and baked at 100°C. The samples were exposed for 25 s under UV light through a mask with radial and mirror symmetric patterns (Figure 2B). The development of the photoresist was carried out in AZ developer diluted in water under gentle shaking. The hydrophobic FDTS layer was deposited using the MVD100 equipment following the same protocol mentioned previously. Lastly, the rest of the photoresist layer was washed in acetone and ethanol in an ultrasonic bath. The water contact angle on FDTS films was 110 ± 2°.

2.1.2 Saint Gobain superhydrophobic silica surfaces

Pure silica micropatterns at the surface of a silica lamella were fabricated based on the combination of sol–gel process and nanoimprint lithography. The silica pattern was designed during the photolithographic step and functionalized with a vapor-phase deposition of fluorosilane molecules to obtain superhydrophobic surfaces (Dubov et al., 2013). All the characteristic geometrical parameters of the square lattice of circular pillars of the pattern, the height of the pillars (in the range 10 ± 0.5 μm) and the period of grating of 20 mm as well as the pillar diameter, the inter-pillar distance, and the longest dimension evaluated by interference profilometry and SEM (Figure 2C) and the corresponding water contact angle of approximately 135°, were reported in Dubov et al. (2013).

2.2 Holder and dedicated optical microscopy

2.2.1 The MATISS holder

In practice, the MATISS holder (8.5 cm × 6 cm × 1.2 cm, Figure 3A) can be considered a vented aluminum container with a 2-mm-thick slit between a transparent polycarbonate lid and the glass surfaces, allowing a laminar airflow on the surface of the mounted glass lamellae. The transition from the "laboratory-confined" state to the "ISS-exposed" state of the glass surfaces was manually operated by removing Kapton tape that sealed the slit and reversely by repositioning the Kapton tape. The aluminum mounting base has two slots that can be plugged using

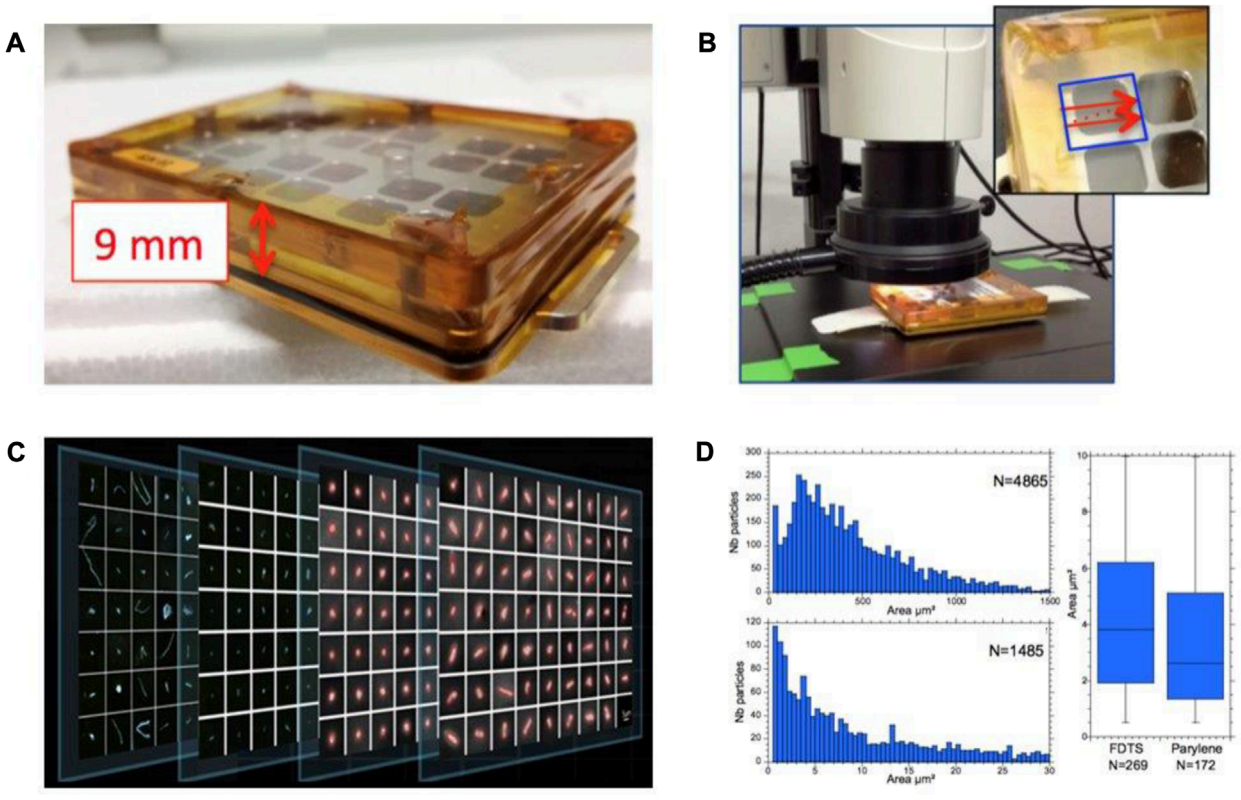

FIGURE 3
Optical microscopy and image analyses. **(A)** MATISS sample holder has lateral openings, here sealed with golden Kapton tape. **(B)** Holder was mounted on a scanning table. All the surface lamellae were imaged across the four windows of the holder (see inset and the blue frame) using a microscope. **(C)** Data treatment of each image at ×3 and ×30 magnifications generated crops for each particle. They are sorted and classified versus their X and Y coordinates and their area in the two sets of coarse (area > 50 μm^2) and fine (area < 50 μm^2) particles. **(D)** Particle size distributions are displayed as histograms, here all the coarse particles of MATISS-1 (top, left) and the fine particles (bottom, left), or as boxplots if the numbers are small (here FDTS and parylene coatings in a holder of MATISS-1).

TABLE 1 Coarse and fine particle rate values (particles.mm^{-2}.month^{-1}) measured on each window from the density (d in particles.mm^{-2}) during the three MATISS campaigns. Exposure location, exposure duration, types of coating [FDTS, SiOCH, and parylene (par.)], and nature of the lamella (glass or quartz) are reported.

Campaign		Location		Lamella		Total exposure time				Coarse particle		Fine particle	
Name	Year	Holder	Position	Support	Coating	Begin	End	N (Days)	N (months)	d	Rate	d	Rate
MATISS-1	2016/2017	H02	RGHS	Glass	FDTS	20/11/16	01/06/17	193	6	1.70	0.26	1.43	0.22
MATISS-1	2016/2017	H02	RGHS	Glass	FDTS	20/11/16	01/06/17	193	6	1.37	0.21	ND	ND
MATISS-1	2016/2017	H02	RGHS	Glass	FDTS	20/11/16	01/06/17	193	6	2.52	0.39	ND	ND
MATISS-1	2016/2017	H02	RGHS	Glass	FDTS	20/11/16	01/06/17	193	6	2.38	0.37	ND	ND
MATISS-1	2016/2017	H03	RGHS	Glass	FDTS	20/11/16	01/06/17	193	6	2.18	0.34	8.35	1.30
MATISS-1	2016/2017	H03	RGHS	Glass	FDTS	20/11/16	01/06/17	193	6	4.48	0.70	ND	ND
MATISS-1	2016/2017	H03	RGHS	Glass	FDTS	20/11/16	01/06/17	193	6	3.08	0.48	ND	ND
MATISS-1	2016/2017	H03	RGHS	Glass	FDTS	20/11/16	01/06/17	193	6	3.23	0.50	ND	ND
MATISS-1	2016/2017	H04	EDR	Glass	FDTS	20/11/16	01/06/17	193	6	1.73	0.27	2.65	0.41
MATISS-1	2016/2017	H04	EDR	Glass	FDTS	20/11/16	01/06/17	193	6	2.05	0.32	5.35	0.83
MATISS-1	2016/2017	H04	EDR	Glass	FDTS	20/11/16	01/06/17	193	6	2.73	0.42	ND	ND
MATISS-1	2016/2017	H04	EDR	Glass	FDTS	20/11/16	01/06/17	193	6	1.97	0.31	ND	ND
MATISS-1	2016/2017	H02	RGHS	Glass	SiOCH	20/11/16	01/06/17	193	6	2.33	0.36	ND	ND
MATISS-1	2016/2017	H02	RGHS	Glass	SiOCH	20/11/16	01/06/17	193	6	1.65	0.26	ND	ND
MATISS-1	2016/2017	H02	RGHS	Glass	SiOCH	20/11/16	01/06/17	193	6	0.75	0.12	ND	ND
MATISS-1	2016/2017	H02	RGHS	Glass	SiOCH	20/11/16	01/06/17	193	6	1.43	0.22	2.18	0.34
MATISS-1	2016/2017	H03	RGHS	Glass	SiOCH	20/11/16	01/06/17	193	6	1.80	0.28	1.07	0.17
MATISS-1	2016/2017	H03	RGHS	Glass	SiOCH	20/11/16	01/06/17	193	6	0.98	0.15	ND	ND
MATISS-1	2016/2017	H03	RGHS	Glass	SiOCH	20/11/16	01/06/17	193	6	0.92	0.14	ND	ND
MATISS-1	2016/2017	H03	RGHS	Glass	SiOCH	20/11/16	01/06/17	193	6	1.85	0.29	ND	ND
MATISS-1	2016/2017	H04	EDR	Glass	SiOCH	20/11/16	01/06/17	193	6	1.42	0.22	4.60	0.72
MATISS-1	2016/2017	H04	EDR	Glass	SiOCH	20/11/16	01/06/17	193	6	1.27	0.20	7.35	1.14
MATISS-1	2016/2017	H04	EDR	Glass	SiOCH	20/11/16	01/06/17	193	6	0.87	0.13	ND	ND
MATISS-1	2016/2017	H04	EDR	Glass	SiOCH	20/11/16	01/06/17	193	6	1.32	0.20	ND	ND
MATISS-1	2016/2017	H02	RGHS	Glass	Par.	20/11/16	01/06/17	193	6	1.42	0.22	ND	ND
MATISS-1	2016/2017	H02	RGHS	Glass	Par.	20/11/16	01/06/17	193	6	1.30	0.20	ND	ND
MATISS-1	2016/2017	H02	RGHS	Glass	Par.	20/11/16	01/06/17	193	6	1.48	0.23	ND	ND
MATISS-1	2016/2017	H02	RGHS	Glass	Par.	20/11/16	01/06/17	193	6	1.28	0.20	3.45	0.54
MATISS-1	2016/2017	H03	RGHS	Glass	Par.	20/11/16	01/06/17	193	6	1.92	0.30	5.98	0.93
MATISS-1	2016/2017	H03	RGHS	Glass	Par.	20/11/16	01/06/17	193	6	2.05	0.32	ND	ND
MATISS-1	2016/2017	H03	RGHS	Glass	Par.	20/11/16	01/06/17	193	6	1.37	0.21	ND	ND
MATISS-1	2016/2017	H03	RGHS	Glass	Par.	20/11/16	01/06/17	193	6	1.48	0.23	ND	ND
MATISS-1	2016/2017	H04	EDR	Glass	Par.	20/11/16	01/06/17	193	6	1.37	0.21	2.37	0.37
MATISS-1	2016/2017	H04	EDR	Glass	Par.	20/11/16	01/06/17	193	6	1.00	0.16	1.67	0.26
MATISS-1	2016/2017	H04	EDR	Glass	Par.	20/11/16	01/06/17	193	6	0.75	0.12	ND	ND
MATISS-1	2016/2017	H04	EDR	Glass	Par.	20/11/16	01/06/17	193	6	0.50	0.08	ND	ND
MATISS-2	2018	H05	RGHS	Glass	FDTS	23/08/18	03/10/18	41	1	0.47	0.34	2.25	1.65
MATISS-2	2018	H05	RGHS	Glass	FDTS	23/08/18	03/10/18	41	1	0.55	0.40	1.72	1.26

(Continued on the following page)

TABLE 1 (*Continued*) **Coarse and fine particle rate values (particles.mm^{-2}.month^{-1}) measured on each window from the density (d in particles.mm^{-2}) during the three MATISS campaigns. Exposure location, exposure duration, types of coating [FDTS, SiOCH, and parylene (par.)], and nature of the lamella (glass or quartz) are reported.**

Campaign		Location		Lamella		Total exposure time				Coarse particle		Fine particle	
Name	Year	Holder	Position	Support	Coating	Begin	End	N (Days)	N (months)	d	Rate	d	Rate
MATISS-2	2018	H05	RGHS	Glass	FDTS	23/08/18	03/10/18	41	1	0.67	0.49	1.82	1.33
MATISS-2	2018	H05	RGHS	Glass	FDTS	23/08/18	03/10/18	41	1	0.63	0.46	1.50	1.10
MATISS-2	2018	H06	RGHS	Glass	FDTS	23/08/18	26/11/18	95	3	0.75	0.24	2.47	0.78
MATISS-2	2018	H06	RGHS	Glass	FDTS	23/08/18	26/11/18	95	3	1.57	0.49	2.13	0.67
MATISS-2	2018	H06	RGHS	Glass	FDTS	23/08/18	26/11/18	95	3	1.48	0.47	6.60	2.08
MATISS-2	2018	H06	RGHS	Glass	FDTS	23/08/18	26/11/18	95	3	1.62	0.51	4.07	1.28
MATISS-2	2018	H08	RGHS	Glass	FDTS	23/08/18	12/08/19	354	12	3.33	0.28	2.05	0.17
MATISS-2	2018	H08	RGHS	Glass	FDTS	23/08/18	12/08/19	354	12	1.13	0.10	2.73	0.23
MATISS-2	2018	H08	RGHS	Glass	FDTS	23/08/18	12/08/19	354	12	2.12	0.18	7.15	0.61
MATISS-2	2018	H08	RGHS	Glass	FDTS	23/08/18	12/08/19	354	12	1.47	0.12	6.78	0.57
MATISS-2.5	2019/2020	H09	RGHS	Glass	FDTS	25/09/19	24/09/20	365	12	0.30	0.02	0.58	0.05
MATISS-2.5	2019/2020	H09	RGHS	Glass	FDTS	25/09/19	24/09/20	365	12	0.33	0.03	0.58	0.05
MATISS-2.5	2019/2020	H09	RGHS	Glass	FDTS	25/09/19	24/09/20	365	12	0.27	0.02	0.47	0.04
MATISS-2.5	2019/2020	H09	RGHS	Glass	FDTS	25/09/19	24/09/20	365	12	0.35	0.03	0.37	0.03
MATISS-2.5	2019/2020	H10	RGHS	Quartz	FDTS	25/09/19	24/09/20	365	12	0.65	0.05	1.62	0.13
MATISS-2.5	2019/2020	H10	RGHS	Quartz	FDTS	25/09/19	24/09/20	365	12	0.42	0.03	2.08	0.17
MATISS-2.5	2019/2020	H10	RGHS	Quartz	FDTS	25/09/19	24/09/20	365	12	0.28	0.02	1.07	0.09
MATISS-2.5	2019/2020	H10	RGHS	Quartz	FDTS	25/09/19	24/09/20	365	12	0.25	0.02	1.37	0.11

Velcro bands. Here, the measurement was sorted by the window area for the particles observed on the circa (8 × 8 mm^2) area (Table 1).

2.2.2 Optical microscopy and image analyses

The MATISS sample holders were placed on an X-Y table for imaging (Figure 3B). A tile scanning mode with a Leica Z16 ApoA MacroFluo optical microscope and a camera setup was used to capture images of the glass surface through the polycarbonate cover. Image processing techniques were applied to identify and measure the position and area of each particle where images were cropped and sorted into different area classes (Figure 3C).

Segmentation and refinement methods were used to analyze the particles in the images. Fine particles have an area < 50 µm^2, and coarse particles have an area > 50 µm^2. These processes were described in Lemelle et al. (2020). The statistic properties could then be studied for different data sets and classically plotted as distributions, for example, the distribution per area for the coarse (Figure 3D left, top) and fine (Figure 3D left, bottom) particles on all coatings of MATISS-1, or boxplots, such as the boxplot of the area of fine particles in a holder on a given coating (Figure 3D right).

In this study, each glass lamella was observed below four windows (8 × 8 mm^2), and the surface density for each window (in particles.mm^{-2}) was determined for both the fine and coarse particles to statistically investigate the surface contamination.

3 Results

Throughout the three MATISS campaigns, the holders were strategically positioned at two different locations within the Columbus module ("RGHS" for "Return Grid Sensor House" and "EDR" for "European Drawer Rack," Figure 4), mounted with different hydrophobic coatings, and exposed during different periods. While the coarse (area > 50 µm^2) and fine (area < 50 µm^2) particles detected on the RGHS location were initially pooled to be investigated. Here we compile and analyze the contamination at a finer grained scale, for the 56 probed windows versus the locations, periods, types of coating (Table 1).

3.1 Exposure at different periods

The MATISS experiments were conducted in triplicate from 2016 to 2020. Surfaces were exposed over several months: ~6 months from November 2016 for the MATISS-1 campaign; ~1, ~3, and ~12 months from August 2018 for the MATISS-2 campaign; and ~12 months from September 2019 for the MATISS-2.5

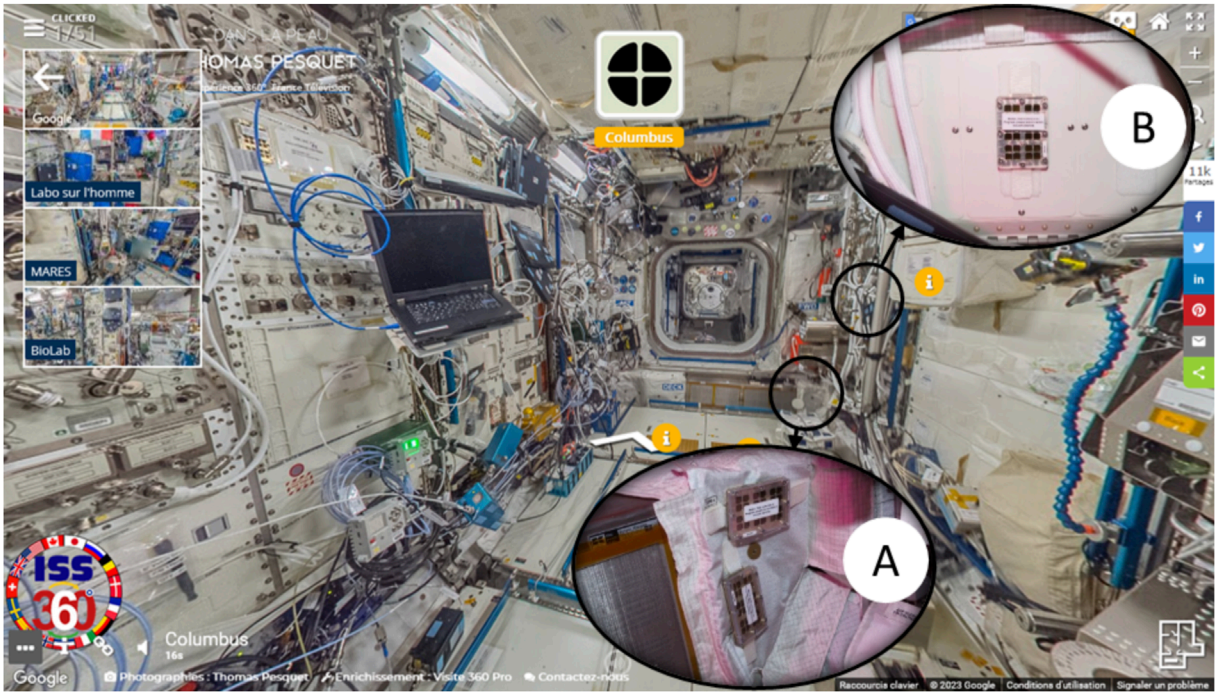

FIGURE 4
Photographs of the sample holders installed in the Columbus module. **(A)** Two holders installed near the Return Grid Sensor Housing (RGHS) and **(B)** one holder installed in front of the European Physiology Module's (EPM facility) front panel on the EDR front panel. Crops are photograph courtesy of NASA/ESA, which are permissible to use within the public domain superimposed on a Google Street View of the Columbus module.

campaign (Figure 1). The three average values of the contamination rates of the FDTS coatings exposed at the RGSH location previously compiled for each of the three MATISS campaigns (from November 2016 to 2020, Figure 1) were shown to be similar in the MATISS-1 and MATISS-2 campaigns whereas notably lower in the MATISS-2.5 campaign for both coarse and fine particles (Lemelle et al., 2022).

Statistical differences between the distributions of the rates compiled per window for all types of coatings, exposure times, and locations in the MATISS-2.5 campaign and the rates in MATISS-1 and 2 campaigns (Table 1; Figure 5A) were examined by unpaired Student's *t*-test. The values remain very significantly different for both the coarse and fine particles (p-values < 10^{-3}). The average rate of coarse particles in the MATISS-1 and MATISS-2 campaigns (0.30 ± 0.09 particles.mm^{-2}.month^{-1} for N = 24) is higher than that in MATISS-2.5 (0.23 ± 0.07 particles.mm^{-2}.month^{-1}, mean ± SD for N = 12). The average rate of fine particles in the MATISS-1 and MATISS-2 campaigns (0.79 ± 0.40 particles.mm^{-2}.month^{-1} for N = 24) is higher than that in MATISS-2.5 (0.08 ± 0.04 particles.mm^{-2}.month^{-1} for N = 8).

3.2 Exposure rates at RGHS and EPM

During the MATISS-1 campaigns, holders were installed simultaneously in two specific locations on the Columbus module for approximately 6 months starting from November 2016 (Figure 1). The first location was in close proximity to the return grid, where the majority of the cabin air in Columbus was extracted at a rate of 400 m^3/h and reintroduced into the adjacent module. Two holders were positioned near the hatch (Figure 4). The crew's activities in this area were limited to manual filter maintenance or cleaning tasks. Throughout the monthly exposure periods, particles were continuously transported by the airflow. The air velocity near the holders was modeled to be 0.21 m/s (approximately 40 ft/min). The second location was situated in front of the EPM (European Physiology Module) rack on the EDR, located in the central section of the Columbus cabin (Figure 4). The primary source of the airflow in this area was an air outlet positioned approximately 1 m above the exposure area. This outlet expelled 55 m^3/h of air, but the flow was directed toward the center of the cabin rather than the surface of the holder.

We examine the contamination rate values in the RGSH and EDR locations after exposure over 6 months during the MATISS-1 campaign (Table 1; Figure 5B). The statistical difference in coarse particle rate distributions between RGSH and EDR was examined by unpaired Student's *t*-test and found to be significantly different (p-values < 0.03) contrary to that of the fine particle rates (p = 0.43). The average rate distribution of coarse particles in the RGSH location (0.30 ± 0.09 particles.mm^{-2}.month^{-1} for N = 24) is higher than that in EDR (0.23 ± 0.07 particles.mm^{-2}.month^{-1}, mean ± SD for N = 12). The average rate distribution of the fine particles (0.63 ± 0.33 particles.mm^{-2}.month^{-1}, mean ± SD for N = 12) is higher than that of the coarse particles.

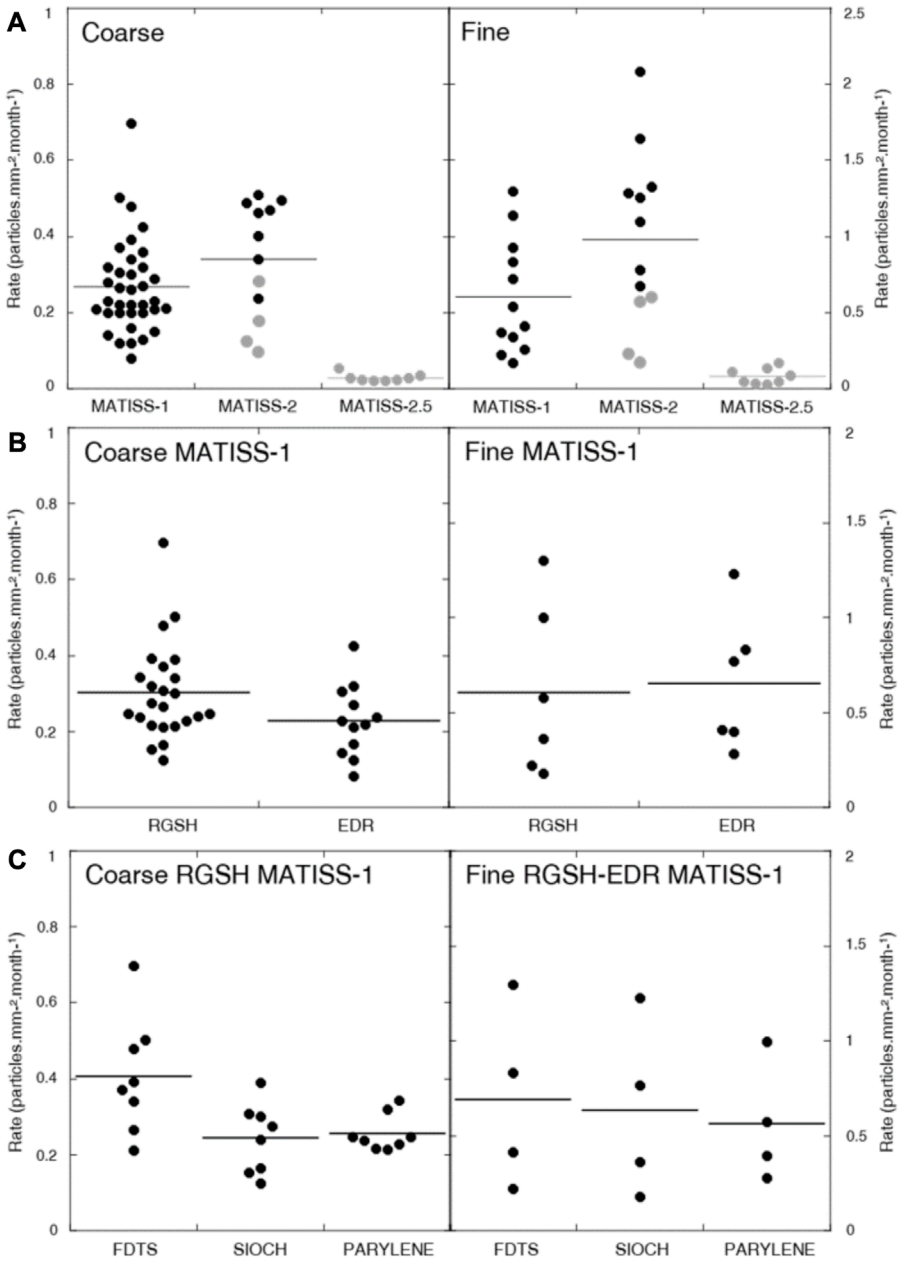

FIGURE 5
Surface contamination rates. **(A)** Coarse particle rates (left) and fine particle rates (right) versus the different MATISS campaigns versus the occupancy rate value (100% in black; approximately 35% in gray). **(B)** Coarse particle rates (left) and fine particle rates (right) in the MATISS-1 campaign versus the different locations. **(C)** Coarse particle rates (left) and fine particle rates (right) in the MATISS-1 campaign and RGSH location versus the different coatings. The mean values are shown as horizontal lines. All data are tabulated in Table 1.

3.3 Exposure rates on different hydrophobic coatings

The biocontamination was, therefore, probed from the MATISS-1 campaigns in the RGHS location versus the three types of hydrophobic coatings (FDTS, SiOCH, and parylene). The contours of the fine particles, observed on the Saint Gobain superhydrophobic surfaces, could not be sorted with the same data treatment. The pillars of the textured surface show brighter contrasts on their edge, impeding and altering a systematic and exhaustive image processing. Therefore, the particle's area and the fine and coarse particle sets herein sorted are difficult to compare to those observed on the hydrophobic coatings. Similarly, the FDTS-patterned surfaces displayed numerous particles, among which coarse particles were identified as default products of the process. For higher hydrophobicity (FDTS > SiOCH > parylene), the coating should favor adhesion of the coarse hydrophobic particles. Conversely, it hinders more the fine particles, that are brought to the surface with their own hydrous sphere or through water droplet deposition.

Given the significant difference in the contamination rates in the RGSH and EDR locations for the coarse particles, these rates were not pooled compared to the fine particles. Statistical differences between the distributions of the rates compiled per window on the FDTS and either on SiOCH or parylene (Table 1; Figure 5C) were examined by unpaired Student's *t*-test. The rates on FDTS are found to be significantly higher for the coarse particles (*p*-values = 0.01), which is less clear for the fine particle rates (p = 0.35). The average rate of coarse particles on FDTS (0.40 ± 0.11 particles.mm^{-2}.month^{-1}, mean ± SD for N = 8) is higher than that on both the SiOCH (0.24 ± 0.03 particles.mm^{-2}.month^{-1}, mean ± SD for N = 8) and parylene (0.25 ± 0.04 particles.mm^{-2}.month^{-1}, mean ± SD for N = 8). The average rate value for the fine particles is 0.63 ± 0.33 particles.mm^{-2}.month^{-1}, mean ± SD for N = 12.

4 Discussion and conclusion

The significant difference among the tested distributions of rates is particularly evident when comparing the various campaigns. As previously proposed, these rates can be presented in regard of the two range values of the occupancy rates of the Columbus module for each campaign, η_{EU} (%). The occupancy rate is estimated as the fraction of time an EU astronaut (green line in Figure 1) is present in the ISS during the holder's exposure (violet line in Figure 1). Values reported in Figure 1 were evaluated considering only the occupancy periods of the European astronauts who are the module's main occupants. The values were found to be 100% for MATISS-1 and some of the holders of MATISS-2 and approximately 35% for MATISS-2.5 and one holder of MATISS-2 (Lemelle et al., 2022). These findings support the conclusion drawn for the sets of all the particles of each campaign, suggesting that contamination rate differences are associated with ISS activity, likely influenced by astronaut occupancy (Lemelle et al., 2022). During periods of high occupancy in MATISS-1 and MATISS-2 (in black in Figure 5A), there is a noticeable increase in coarse and fine particle contamination levels. In contrast, when the occupancy is low (approximately 35%, in gray in Figure 5A), contamination remains relatively low in both MATISS-2 and MATISS-2.5. To some extent, the rates appear to be lower in MATISS-2.5, which may be correlated with an even lower activity of the astronauts during the COVID period. MATISS-2.5 may be close to the lower contamination rates that can be detected with our experimental setup.

Occupancy integrates multi-parameters from various sources and routes of surface contamination by fine and coarse particles over long periods of exposure. During these periods, both the sources and modes of contamination can change and evolve. In long-duration space missions, the astronaut microbiome evolves (Voorhies et al., 2019), and these changes differ among the crew members (Morrison et al., 2021). Despite the dynamic nature of the individual crew members' microbiome composition and diversity, a delayed process of microbial homogenization between the crew and habitat surfaces is expected (Mahnert et al., 2021). The crew's microbiome effectively contaminates abiotic surfaces in a confined cabin. The specific pathways of contamination, like through aerosols or shed skin fragments, and the amount of contamination can vary based on the number of astronauts, types, and intensity of activities carried out by the crew members.

The tested distributions show a difference near the RGSH and EDR positions regarding coarse particles. No such distinction is observed for fine particles despite contamination rates being twice higher. The surface contamination by the coarse particles, even if cumulated over more than 6 months, is not averaged at the scale of the Columbus modulus. The involvement of astronauts in activities near RGSH and EDR likely contributes to the local contamination by the coarse particles, and this factor should not be underestimated. Conversely, surface contamination by fine particles is spatially uniform, emphasizing that coatings are relevant at the first order to limit the rate of fine particle contamination. For fine particles, a noticeable property of rate distribution is the much higher relative error value (~50%) than the coarse particle rates (~30%). This may be interpreted by a spatial homogeneity higher for the coarse than the fine particles at the scale of the holders, likely displaying different advection and deposition modes.

A difference between the rates of FDTS and other coatings among the tested distributions is only observed for coarse particles and is somewhat uncertain, primarily due to over-sampling. Additional investigations such as the fraction of thinner particles (Lemelle et al., 2020), kinetics, or spatial distribution analysis at the window scale are needed to determine the potential benefits of hydrophobic coatings in reducing biocontamination on surfaces within the ISS (Lemelle et al., 2022). The substantial relative error for each coating type indicates a high level of heterogeneity at the holder and possibly lamella scales, suggesting the presence of a surface depot resulting from an irregular and heterogeneous aerosol pathway.

In this study, the comprehensive analysis conducted at a fine-grain scale offers an approach to investigate the sources and pathways of contamination in the Columbus module over extended periods. The findings confirm that, regardless of the parameters considered, the contamination rate per window area is low, indicating the effectiveness of the long-term air purification system. Moreover, it is observed that higher contamination rates occur during periods when astronaut occupancy increases. Although there may be temporary variations linked to specific activities, especially for coarse particles, this trend suggests that surface contamination over periods exceeding 6 months can be approximated by a constant rate directly proportional to the number of astronauts present. Consequently, unmanned spacecraft during dormant periods, as expected in long-duration exploration, are likely to exhibit significantly lower levels of surface contamination (Ott, 2016; LaPelusa et al., 2021; Bijlani et al., 2021).

Data availability statement

The original contributions presented in the study are included in the article; further inquiries can be directed to the corresponding authors.

Author contributions

LL, CP, LC, AM, and SB designed the MATISS-1 project; LL, CP, and SR designed the MATISS-2 project; LL, CP, GN, and SR designed the MATISS-2.5 project; DL and EM machined the sample holder

and carried out the microscopy imaging; GN, CF, VJ, CaP, OC, JT, and EG prepared the surfaces; PM carried out the microbiological investigations; LC, CT, AM, and SB managed the qualification for spaceflight of the MATISS-1 experiment and the communication with the astronauts; CT and SR managed the qualification for spaceflight of the MATISS-2 and MATISS-2.5 experiments and the communication with the astronauts; LL, CP, and GN wrote the paper. All authors contributed to the article and approved the submitted version.

Funding

The CNES, the French space agency, provided financial support for the MATISS hardware design and for the MATISS experiments.

Acknowledgments

The authors thank the NASA and ESA astronauts that were involved in the MATISS experiments. The authors also acknowledge the contribution of SFR BioSciences (UMS3444/CNRS, US8/Inserm, ENS de Lyon, UCBL) PLATIM facility. CEA-Leti acknowledges the support of the Agence Nationale de la Recherche through the LabEx ARCANE program (ANR-11-LABX-0003-01) and the Graduate School on Chemistry, Biology and Health of Université Grenoble Alpes CBH-EUR-GS (ANR-17-EURE-0003). Anne-Dominique Malinge and Philippe Boulez contributed to the final integration of the MATISS experiments.

Conflict of interest

The authors declare that the research was conducted in the absence of any commercial or financial relationships that could be construed as a potential conflict of interest.

Publisher's note

All claims expressed in this article are solely those of the authors and do not necessarily represent those of their affiliated organizations, or those of the publisher, the editors, and the reviewers. Any product that may be evaluated in this article, or claim that may be made by its manufacturer, is not guaranteed or endorsed by the publisher.

References

Acres, J. M., Youngapelian, M. J., and Nadeau, J. (2021). The influence of spaceflight and simulated microgravity on bacterial motility and chemotaxis. *npj Microgravity* 7, 7–11. doi:10.1038/s41526-021-00135-x

Balistreri, S. F., Steele, J. W., Caron, M. E., and Laliberte, Y. J. (2013). International space station common cabin air assembly condensing heat exchanger hydrophilic coating operation, recovery, and lessons learned. NASA Technical Report JSC-CN-27469. Available at: https://ntrs.nasa.gov/archive/nasa/casi.ntrs.nasa.gov/20130000766.pdf.

Baranov, V. M., Polikarpov, N. A., Novikova, N. D., Deshevaia, E. A., Poddubko, S. V., Svistunova, I., et al. (2006). Main results of the biorisk experiment on the international space station. *Aviakosm. Ekol. Med.* 40 (3–9), 3–9. PMID: 17193961.

Bauer, J. (2020). Microgravity and cell adherence. *Int. J. Mol. Sci.* 21, 2214. doi:10.3390/ijms21062214

Bijlani, S., Stephens, E., Singh, N. K., Venkateswaran, K., and Wang, C. C. C. (2021). Advances in space microbiology. *iScience* 24, 102395. doi:10.1016/j.isci.2021.102395

Buchovec, I., Gricajeva, A., Kalėdienė, L., and Vitta, P. (2020). Antimicrobial photoinactivation approach based on natural agents for control of bacteria biofilms in spacecraft. *Int. J. Mol. Sci.* 21, 6932. doi:10.3390/ijms21186932

Chen, Y., Lu, W., Guo, Y., Zhu, Y., Lu, H., and Wu, Y. (2018). Superhydrophobic coatings on gelatin-based films: fabrication, characterization and cytotoxicity studies. *RSC Adv.* 8, 23712–23719. doi:10.1039/C8RA04066D

Dubov, A. L., Perez-Toralla, K., Letailleur, A., Barthel, E., and Teisseire, J. (2013). Superhydrophobic silica surfaces: fabrication and stability. *J. Micromech. Microeng.* 23, 125013. doi:10.1088/0960-1317/23/12/125013

Fajardo-Cavazos, P., and Nicholson, W. L. (2021). Mechanotransduction in prokaryotes: A possible mechanism of spaceflight adaptation. *Life* 11, 33. doi:10.3390/life11010033

Farkas, Á., and Farkas, G. (2021). Effects of spaceflight on human skin. *Ski. Pharmacol. Physiol.* 34, 239–245. doi:10.1159/000515963

Glavan, A. C., Martinez, R. V., Maxwell, E. J., Subramaniam, A. B., Nunes, R. M. D., Soh, S., et al. (2013). Rapid fabrication of pressure-driven open-channel microfluidic devices in omniphobic RF paper. *Lab. Chip* 13, 2922–2930. doi:10.1039/C3LC50371B

Grinenval, E., Nonglaton, G., and Vinet, F. (2014). Spatially controlled immobilisation of biomolecules: A complete approach in green chemistry. *Appl. Surf. Sci.* 289, 571–580. doi:10.1016/j.apsusc.2013.11.046

Huang, B., Li, D. G., Huang, Y., and Liu, C. T. (2018). Effects of spaceflight and simulated microgravity on microbial growth and secondary metabolism. *Mil. Med. Res.* 5, 18. doi:10.1186/s40779-018-0162-9

Ichijo, T., Yamaguchi, N., Tanigaki, F., Shirakawa, M., and Nasu, M. (2016). Four-year bacterial monitoring in the international space station-Japanese experiment module "kibo" with culture-independent approach. *npj Microgravity* 2, 16007. doi:10.1038/npjmgrav.2016.7

Ichijo, T., Hieda, H., Ishihara, R., Yamaguchi, N., and Nasu, M. (2013). Bacterial monitoring with adhesive sheet in the international space station-"Kibo", the Japanese experiment module. *Microbes Environ.* 28, 264–268. doi:10.1264/jsme2.me12184

Ichijo, T., Shimazu, T., and Nasu, M. (2020). Microbial monitoring in the international space station and its application on earth. *Bio. Pharm. Bul.* 43, 254–257. doi:10.1248/bpb.b19-00912

International Space Exploration Coordination Group (2018). The global exploration roadmap. ISECG Technical Report. Available at: https://www.globalspaceexploration.org/wordpress/wp-content/isecg/GER_2018_small_mobile.pdf.

James, J. T., Parmet, A. J., and Pierson, D. L. (2007). Aerospace toxicology and microbiology. Available at: https://ntrs.nasa.gov/citations/20070032022.

Jiang, R., Hao, L., Song, L., Tian, L., Fan, Y., Zhao, J., et al. (2020). Lotus-leaf-inspired hierarchical structured surface with non-fouling and mechanical bactericidal performances. *Chem. Eng. J.* 398, 125609. doi:10.1016/j.cej.2020.125609

Jorgensen, J. H., Skweres, J. A., Mishra, S. K., McElmeel, M. L., Maher, L. A., Mulder, R., et al. (1997). Development of an antimicrobial susceptibility testing method suitable for performance during space flight. *J. Clin. Microbiol.* 35, 2093–2097. doi:10.1128/jcm.35.8.2093-2097.1997

Kefallinou, D., Ellinas, K., Speliotis, T., Stamatakis, K., Gogolides, E., and Tserepi, A. (2020). Optimization of antibacterial properties of "hybrid" metal-sputtered superhydrophobic surfaces. *Coatings* 10, 25. doi:10.3390/coatings10010025

Lang, J. M., Coil, D. A., Neches, R. Y., Brown, W. E., Cavalier, D., Severance, M., et al. (2017). A microbial survey of the international space station (ISS). *PeerJ* 5, e4029. doi:10.7717/peerj.4029

LaPelusa, M., Donoviel, D., Branzini, S. E., Carlson, P. E., Culler, S., Cheema, A. K., et al. (2021). Microbiome for mars: surveying microbiome connections to healthcare with implications for long-duration human spaceflight, virtual workshop july 13 2020. *Microbiome* 9, 2. doi:10.1186/s40168-020-00951-5

Lee, Y., Chung, Y. W., Park, J., Park, K., Seo, Y., Hong, S. N., et al. (2020). Lubricant-infused directly engraved nano-microstructures for mechanically durable endoscope lens with anti-biofouling and anti-fogging properties. *Sci. Rep.* 10, 17454. doi:10.1038/s41598-020-74517-8

Lemelle, L., Campagnolo, L., Mottin, E., Le Tourneau, D., Garre, E., Marcoux, P., et al. (2020). Towards a passive limitation of particle surface contamination in the Columbus module (ISS) during the MATISS experiment of the Proxima Mission. *npj Microgravity* 6, 29–37. doi:10.1038/s41526-020-00120-w

Lemelle, L., Rouquette, S., Mottin, E., Le Tourneau, D., Marcoux, P. R., Thévenot, C., et al. (2022). Passive limitation of surface contamination by perFluoroDecylTrichloroSilane coatings in the ISS during the MATISS experiments. *npj Microgravity* 8, 31–38. doi:10.1038/s41526-022-00218-3

Li, J., Yuan, T., Zhou, C., Chen, B., Shuai, Y., Wu, D., et al. (2021). Facile Li-Al layered double hydroxide films on Al alloy for enhanced hydrophobicity, anti-biofouling and anti-corrosion performance. *J. Mater. Sci. Technol.* 79, 230–242. doi:10.1016/j.jmst.2020.10.072

Lin, X., Zhang, K., Wei, D., Tian, Y., Gao, Y., Chen, Z., et al. (2020). The impact of spaceflight and simulated microgravity on cell adhesion. *Int. J. Mol. Sci.* 21, 3031. doi:10.3390/ijms21093031

Mahnert, A., Verseux, C., Schwendner, P., Koskinen, K., Kumpitsch, C., Blohs, M., et al. (2021). Microbiome dynamics during the HI-SEAS IV mission, and implications for future crewed missions beyond Earth. *Microbiome* 9, 27. doi:10.1186/s40168-020-00959-x

Mandal, P., Ivvala, J., Arora, H. S., Ghosh, S. K., and Grewal, H. S. (2022). Bioinspired micro/nano structured aluminum with multifaceted applications. *Colloids Surf. B Biointerfaces* 211, 112311. doi:10.1016/j.colsurfb.2021.112311

Moazzam, P., Razmjou, A., Golabi, M., Shokri, D., and Landarani-Isfahani, A. (2016). Investigating the BSA protein adsorption and bacterial adhesion of Al-alloy surfaces after creating a hierarchical (micro/nano) superhydrophobic structure. *J. Biomed. Mater. Res.* 104, 2220–2233. doi:10.1002/jbm.a.35751

Morrison, M. D., Thissen, J. B., Karouia, F., Mehta, S., Urbaniak, C., Venkateswaran, K., et al. (2021). Investigation of spaceflight induced changes to astronaut microbiomes. *Front. Microbiol.* 12, 659179. doi:10.3389/fmicb.2021.659179

Mukhopadhyay, S., and Bagh, S. (2020). A microgravity responsive synthetic genetic device in Escherichia coli. *Biosens. Bioelectron.* 167, 112462. doi:10.1016/j.bios.2020.112462

Novikova, N., De Boever, P., Poddubko, S., Deshevaya, E., Polikarpov, N., Rakova, N., et al. (2006). Survey of environmental biocontamination on board the international space station. *Res. Microbiol.* 157, 5–12. doi:10.1016/j.resmic.2005.07.010

Novikova, N. D. (2004). Review of the knowledge of microbial contamination of the Russian manned spacecraft. *Microb. Ecol.* 47, 127–132. doi:10.1007/s00248-003-1055-2

Ott, C. M., Bruce, R. J., and Pierson, D. L. (2004). Microbial characterization of free floating condensate aboard the Mir Space Station. *Microb. Ecol.* 47, 133–136. doi:10.1007/s00248-003-1038-3

Ott, C. M., Pierson, D. L., Shirakawa, M., Tanigaki, F., Hida, M., Yamazaki, T., et al. (2014). Space habitation and microbiology: status and roadmap of space agencies. *Microb. Environ.* 29, 239–242. doi:10.1264/jsme2.ME2903rh

Ott, C. M. (2016). Risk of adverse health effects due to host-microorganism interactions. Available at: https://ntrs.nasa.gov/search.jsp?R=20170001973.

Otter, J. A., Donskey, C., Yezli, S., Douthwaite, S., Goldenberg, S. D., and Weber, D. J. (2016). Transmission of sars and mers coronaviruses and influenza virus in healthcare settings: the possible role of dry surface contamination. *J. Hosp. Infect.* 92, 235–250. doi:10.1016/j.jhin.2015.08.027

Otter, J. A., Yezli, S., and French, G. L. (2011). The role played by contaminated surfaces in the transmission of nosocomial pathogens. *Infect. Control. Hosp. Epidemiol.* 32, 687–699. doi:10.1086/660363

Pierson, D. L. (2001). Microbial contamination of spacecraft. *Space Biol. Bull.* 14, 1–6. Available at: https://ntrs.nasa.gov/citations/20100036603.

Sadri, B., Goswami, D., Sala de Medeiros, M., Pal, A., Castro, B., Kuang, S., et al. (2018). Wearable and implantable epidermal paper-based electronics. *ACS Appl. Mater. Interfaces* 10, 31061–31068. doi:10.1021/acsami.8b11020

Sala de Medeiros, M., Chanci, D., Moreno, C., Goswami, D., and Martinez, R. V. (2019). Waterproof, breathable, and antibacterial self-powered e-textiles based on omniphobic triboelectric nanogenerators. *Adv. Funct. Mater.* 29, 1904350. doi:10.1002/adfm.201904350

Salmela, A., Kulmala, I., Karvinen, A., Taillebot, V., Weiss, P., Gobert, T., et al. (2020). Measurement and simulation of biocontamination in an enclosed habitat. *Aerosol. Sci. Eng.* 4, 101–110. doi:10.1007/s41810-020-00057-3

Santomartino, R., Waajen, A. C., de Wit, W., Nicholson, N., Parmitano, L., Loudon, C. M., et al. (2020). No effect of microgravity and simulated mars gravity on final bacterial cell concentrations on the international space station: applications to space bioproduction. *Front. Microbiol.* 11, 579156. doi:10.3389/fmicb.2020.579156

Sethi, S. K., and Manik, G. (2018). Recent progress in super hydrophobic/hydrophilic self-cleaning surfaces for various industrial applications: A review. *Polym. Plast. Technol. Eng.* 57, 1932–1952. doi:10.1080/03602559.2018.1447128

Siegel, J. D., Rhinehart, E., Jackson, M., and Chiarello, L. (2007). Guideline for isolation precautions: preventing transmission of infectious agents in health care settings. *Am. J. Infect. Control* 35, S65–S164. doi:10.1016/j.ajic.2007.10.007

Smirnov, E. M., Ivanov, N. G., Telnov, D. S., Son, C. H., and Aksamentov, V. K. (2004). Computational fluid dynamics study of air flow characteristics in the columbus module, *SAE Technical Paper* 01–2500. doi:10.4271/2004-01-2500

Tirumalai, M. R., Karouia, F., Tran, Q., Stepanov, V. G., Bruce, R. J., Ott, C. M., et al. (2017). The adaptation of escherichia coli cells grown in simulated microgravity for an extended period is both phenotypic and genomic. *npj Microgravity* 3, 15–19. doi:10.1038/s41526-017-0020-1

Vaishampayan, A., and Grohmann, E. (2019). Multi-resistant biofilm-forming pathogens on the international space station. *J. Biosci.* 44, 125. doi:10.1007/s12038-019-9929-8

Voorhies, A. A., Mark Ott, C., Mehta, S., Pierson, D. L., Crucian, B. E., Feiveson, A., et al. (2019). Study of the impact of long-duration space missions at the International Space Station on the astronaut microbiome. *Sci. Rep.* 9, 9911. doi:10.1038/s41598-019-46303-8

Wang, T., Huang, L., Liu, Y., Li, X., Liu, C., Handschuh-Wang, S., et al. (2020). Robust biomimetic hierarchical diamond architecture with a self-cleaning, antibacterial, and antibiofouling surface. *ACS Appl. Mater. Interfaces* 12, 24432–24441. doi:10.1021/acsami.0c02460

Weber, D., Anderson, D., and Rutala, W. (2013). The role of the surface environment in healthcare-associated infections. *Curr. Opin. Infect. Dis.* 26, 338–344. doi:10.1097/QCO.0b013e3283630f04

Wilson, J. W., Ott, C. M., Bentrup, K. H., Ramamurthy, R., Quick, L., Porwollik, S., et al. (2007). Space flight alters bacterial gene expression and virulence and reveals a role for global regulator Hfq. *Proc. Nat. Acad. Sci.* 104, 16299–16304. doi:10.1073/pnas.0707155104

Wilson, J. W., Ott, C. M., Quick, L., Davis, R., Bentrup, K. H., Crabbé, A., et al. (2008). Media ion composition controls regulatory and virulence response of Salmonella in spaceflight. *PLoS One* 3, e3923. doi:10.1371/journal.pone.0003923

Yamaguchi, N., Roberts, M., Castro, S., Oubre, C., Makimura, K., Leys, N., et al. (2014). Microbial monitoring of crewed habitats in space—current status and future perspectives. *Microbes Environ.* 29, 250–260. doi:10.1264/jsme2.ME14031

Zea, L., Larsen, M., Estante, F., Qvortrup, K., Moeller, R., Dias de Oliveira, S., et al. (2017). Phenotypic changes exhibited by *E. coli* cultured in space. *Front. Microbiol.* 8, 1598. doi:10.3389/fmicb.2017.01598

Zea, L., McLean, R. J. C., Rook, T. A., Angle, G., Carter, D. L., Delegard, A., et al. (2020). Potential biofilm control strategies for extended spaceflight missions. *Biofilm* 2, 100026. doi:10.1016/j.bioflm.2020.100026

Zea, L., Nisar, Z., Rubin, P., Cortesão, M., Luo, J., McBride, S. A., et al. (2018). Design of a spaceflight biofilm experiment. *Acta Astronaut.* 148, 294–300. doi:10.1016/j.actaastro.2018.04.039

frontiers | Frontiers in Astronomy and Space Sciences

TYPE Mini Review
PUBLISHED 22 September 2023
DOI 10.3389/fspas.2023.1180522

Check for updates

OPEN ACCESS

EDITED BY
Cyprien Verseux,
University of Bremen, Germany

REVIEWED BY
Marco Pane,
Probiotical SpA, Italy
Kirsi Lehto,
University of Turku, Finland

*CORRESPONDENCE
Joel Doré,
joel.dore@inrae.fr

RECEIVED 06 March 2023
ACCEPTED 11 September 2023
PUBLISHED 22 September 2023

CITATION
Doré J and Ortega Ugalde S (2023), Human-microbes symbiosis in health and disease, on earth and beyond planetary boundaries.
Front. Astron. Space Sci. 10:1180522.
doi: 10.3389/fspas.2023.1180522

COPYRIGHT
© 2023 Doré and Ortega Ugalde. This is an open-access article distributed under the terms of the Creative Commons Attribution License (CC BY). The use, distribution or reproduction in other forums is permitted, provided the original author(s) and the copyright owner(s) are credited and that the original publication in this journal is cited, in accordance with accepted academic practice. No use, distribution or reproduction is permitted which does not comply with these terms.

Human-microbes symbiosis in health and disease, on earth and beyond planetary boundaries

Joel Doré[1]* and Sandra Ortega Ugalde[2]

[1]Université Paris-Saclay, INRAE, AgroParisTech, MICALIS, MetaGenoPolis, Jouy-en-Josas, France,
[2]Directorate of Technology, Engineering and Quality, European Space Agency, Noordwijk, Netherlands

Humans are microbial, ecosystems and symbioses. The relationship that humans have with their microbiomes is an essential element to maintaining health and wellbeing. Recent changes in lifestyles may have fostered an alteration of this symbiosis, which is frequently associated with chronic disorders. Here, we will review the state of the art on the central role of human-microbes symbiosis in health and disease, highlighting the innovations expected from the emerging knowledge on host-microbes symbiosis, for diagnosis, preventive nutrition, and a medicine of the 'microbial human'. Since microbiome science also impacts several sustainable development goals of the Planetary Boundaries Initiative, we will also explore how microbiome science could help to provide sustainability tools and strategies aligned with the life support systems sought by the Micro-Ecological Life Support Systems Alternative (MELiSSA) Project lead by the European Space Agency (ESA).

KEYWORDS

MELiSSA (Micro-Ecological Life Support System Alternative), microbiome, symbiosis, life support system, health and disease

1 Introduction

The microbiota is the complex and dynamic community of microbes with which humans interact on a constant basis. Human-associated microbes are present on the skin and at every mucosal interface of the human body, but the highest densities are found in the large intestine. It is estimated that in the human body there are overall 50 trillion bacteria as well as a multitude of archaea, phages, fungi, and yeasts.

These microbes exert several functions that pertain to four essential domains of regulation, acting not only as endocrine and metabolic, immuno-inflammatory and neuro-vegetative regulators, but also as antimicrobial protectors.

These functions are expressed at 3 key interfaces: 1) food-microbes, 2) microbes-microbes, and 3) microbes-human cells. It is hypothesized that they can provide protective benefits to the human host by preventing infections as well as the onset and progression of a large array of chronic conditions that have increased in incidence. These chronic conditions are seen today by the World Health Organization (WHO) as an epidemic, considering they represent a major public health burden: obesity, inflammatory diseases, liver conditions, some cancers, neuro-degenerative and neuro-psychiatric disorders (Malard et al., 2021a).

1.1 Features of a health-associated microbiota

Although the establishment of a concise definition of the 'normal' microbiota has remained challenging, the identification of structural and functional alterations of the gut microbiota has been evaluated in numerous clinical conditions, aiming to document a plausible link. Molecular characterization of the human intestinal microbiota has gone through a technical revolution with the application of high throughput sequencing that has given insights into inter-individual similarities and differences in microbiota in health and disease. Analyzing hundreds of individual microbiota profiles revealed that healthy individuals share a core microbiota. It gathers a rather small number of bacterial species that are present in every healthy individual (Tap et al., 2009; Qin et al., 2010). Interestingly, this core microbiome is less than 20 species out of the average 300 species of each dominant intestinal microbiome. In addition, the microbiota appears remarkably stable over time for each person, except in early life or at old age, as well as upon intake of therapeutic treatments or drastic changes in life habits or nutrition (Falony et al., 2016; Zhernakova et al., 2016).

This indicates that it would be possible to point at bacterial species that are consistently associated with dietary recommendations known to be beneficial - or conversely detrimental - for human health.

Table 1 summarizes the two sets of bacterial taxa proposed based on studies of volunteers of the UK-Twin cohort. Due to functional redundancy, diverse microbial species will often contribute to similar functions irrespective of their taxonomic assignment, hence a normal/health-associated microbiota may be better specified on a functional standpoint rather than in terms of composition. Indeed, a series of metabolites derived from microbiome metabolism have gained interest as they are associated with health or risk/disease as shown on Table 2 (Martinez et al., 2017).

In addition, early shotgun metagenomics-based microbiome studies highlighted two unexpected elements of stratification of the microbiota with health relevance.

Firstly, microbiome richness was recognized as a stratifier. Microbiomes show a broad heterogeneity in health and disease. In some studies, a separate fraction of the population shows a low richness microbiome, and this may even be a predictive feature in several contexts. For example, a low richness microbiome will predict.

- Non-response to calory restriction in obesity (Cotillard et al., 2013)
- Severity/progression in acute liver conditions (Qin et al., 2014; Sole et al., 2018)
- Non-response to cancer immunotherapies and a lesser progression-free survival in melanoma (Gopalakrishnan et al., 2018) and lung cancer (Routy et al., 2018)
- Reduced survival rate following hematopoietic stem cell transplantation (HSCT) in blood cancer therapy (Taur et al., 2014)
- A lesser global survival of patients receiving HSCT during blood-cancer therapy (Peled et al., 2020)
- A higher mortality from acute graft *versus* host disease during blood-cancer therapy (Taur et al., 2014; Jenq et al., 2015)

TABLE 1 Bacterial taxa associated to a healthy or unhealthy diet (Asnicar et al., 2021). Taxa are ranked from the most to the least prevalent [%]. When the genome does not correspond to a cultured strain, a Co-Abundant Genes-cluster (CAG) is indicated.

Bacterial taxa associated to healthy diet	Bacterial taxa associated to unhealthy diet
Faecalibacterium prausnitzii [99.5]	*Ruthenibacterium lactatiformans* [99.1]
Eubacterium eligens [92.5]	*Flavonifractor plautii* [92.9]
Oscillibacter sp 57.20 [89.3]	*Clostridium leptum* [91.7]
Romboutsia ilealis [82.9]	*Escherichia coli* [67.1]
Haemophilus parainfluenzae [54.6]	*Collinsella intestinalis* [66.5]
Firmicutes bacterium CAG 95 [51.3]	*Clostridium* sp CAG 58 [64.3]
Oscillate sp PC13 [50.0]	*Eggerthella lenta* [61.7]
Veillonella dispar [46.8]	*Anaerotruncus colihominis* [50.5]
Roseburia sp CAG 182 [41.3]	*Clostridium boltae* [50.1]
Veillonella atypica [40.5]	*Clostridium spiriforme* [43.7]
Clostridium sp CAG 167 [40.1]	*Ruminococcus gnavus* [43.3]
Veillonella infantium [38.5]	*Clostridium innocuum* [41.2]
Bifidobacterium animalis [38.2]	*Blautia hydrogenotrophica* [28.6]
Prevotella copri [36.0]	*Clostridium symbiosum* [27.6]
Firmicutes bacterium CAG 170 [34.3]	*Clostridium boltae* CAG 59 [26.7]

[%] when referring to prevalence means [% microbiomes with taxon in dominance].

Secondly, four ecological configurations which stratify the human population have been described and are also known as enterotypes (Arumugam et al., 2011; Costea et al., 2017a). One combines the genus *Bacteroides* as dominant taxon and a low richness. This enterotype (B2) is associated with the highest prevalence of altered metabolic and inflammatory markers conferring a higher suspicion of cardiometabolic risk for this segment of the population (Vieira-Silva et al., 2020).

1.2 Altered host-microbes symbiosis

Host-microbes symbiosis guarantees maintenance of health and wellbeing, yet for more than half a century our inner microbial inhabitants and symbiosis have received little consideration. Today, the epidemiological evidence is that an uncontrolled increase in the incidence of so-called non-transmissible chronic diseases (Bach, 2002) is characterized by an alteration in the homeostasis of the host-microbes symbiosis. Host-microbe symbiosis is affected by every life event, from birth to nutrition, lifestyles, exposure to ubiquitous chemicals in the environment, food, and medical therapies. Individual and societal changes of these parameters may have contributed to the alteration of the microbiota that is documented in many chronic diseases (Blottière and Doré, 2016). But beyond the mere alteration of the microbiota, chronic diseases are typically characterized by the concomitant alteration of host parameters such as intestinal permeability, inflammatory tone, and oxidative stress. In addition, not only physiological, but also psychological stress will impact

TABLE 2 Microbiome-derived features and metabolites that may be associated with health or risk/disease (Martinez et al., 2017).

Features associated to health	Features associated to risk/disease
Short chain fatty acids, specifically butyrate	Short chain fatty acids
B-complex vitamins, vitamin K and folate	Ammonia
Fecal secondary bile acids, deoxycholic acid and lithocholic acid	Lipopolysaccharide (endotoxin)
Gamma Amino Butyric Acid (precursor of serotonin)	Fecal primary and secondary bile acids
Methane	Trimethylamine (precursor of Trimethylamine N-oxide (TMAO))
Indole-propionic acid (tryptophan metabolite)	Hydrogen sulfide
Polysaccharide A (PSA)	Indoxyl-sulfate
N-acyl amides (human signal molecules mimics)	p-cresyl-sulfate
Indoles	Indoles
Branched-chain amino-acids, arginine, glutamine, histidine	Phenols
Phenolic compounds and conjugated linoleic acids (anti-inflammatory metabolites)	Phenolic acids

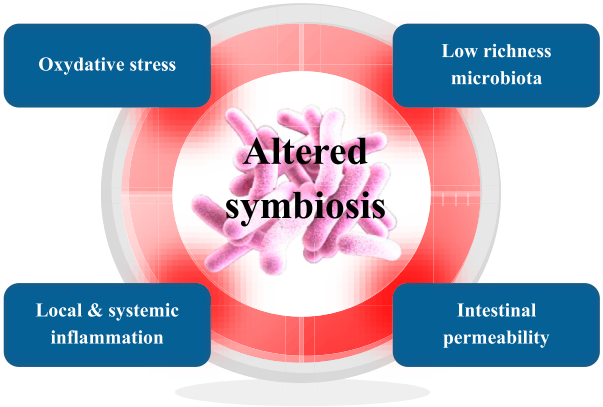

FIGURE 1
Overall concept of host-microbes symbiosis with interacting features such as microbiome richness and composition, intestinal permeability, inflammatory tone, and oxidative stress signals. These features can be triggers of a vicious circle that upon initiation can lead to 'critical transition' towards an alternative stable state of pre-disease or disease (Van de Guchte et al., 2018).

host parameters at the intestinal level, specifically permeability and inflammation via cortisol (Madison and Kiecolt-Glaser, 2019; Ilchmann-Diounou and Menard, 2020; Varanoske et al., 2022). For the past 30 years, microbiota alteration observed in chronic diseases has been documented and recognized as 'dysbiosis'. A major paradigm shift is now leading to dysbiosis being recognized as a disruption of host-microbes symbiosis. The microbiome is in constant functional interaction with several features of the human host, such that any alteration of the microbiome will affect the host and conversely. As described earlier, the main host features that will determine the overall configuration of the symbiosis landscape are gut permeability, inflammation, and oxidative stress (van de Guchte et al., 2018; van de Guchte et al., 2020). Figure 1 illustrates the overall concept of these interacting features of symbiosis. Beyond simple bidirectional host-microbes interactions, recent research shows that alteration of these features can lead to positive feedbacks establishing a vicious circle whereby the whole system can enter alternative stable states sustained by circular causalities (Scheffer et al., 2001; Kéfi et al., 2014; van de Guchte et al., 2018; van de Guchte et al., 2020). This may lead to a loss of the healthy microbiome functions explained above (direct anti-microbial protection as well as endocrino-metabolic, immuno-inflammatory and neuro-vegetative regulation). For example, the ecological perturbation of the microbiome due to a course of antibiotic will induce a loss of the barrier function, which may cause nosocomial infection with *Clostridioides difficile*, or a proliferation of the previously subdominant pathogen (Ramirez et al., 2020; Raplee et al., 2021).

Early evidence of causality was recently provided by the demonstration that symbiosis, reconstructed by microbiota transfer from patients to initially germ-free or microbiome depleted animals, can mimic the diseased phenotype or at least be accompanied by a metabolic, inflammatory, or infectious risk. Examples that support this evidence were documented in obesity (Ridaura et al., 2013), Crohn's disease (Schaubeck et al., 2016), severe alcoholic hepatitis (Llopis et al., 2016), or depression (Kelly et al., 2016), and autism (Sharon et al., 2019). Similarly, Fecal Microbiota Transfer (FMT), now recognized by regulatory agencies for the treatment of recurrent *C. difficile* infection, is being tested in various clinical settings with the primary incidence of restoring symbiotic homeostasis and reducing symptoms of the clinical condition. This approach has restored insulin sensitivity in diabetic subjects (Vrieze et al., 2012) or soothed the inflammatory context in ulcerative colitis (Paramsothy et al., 2017; Costello et al., 2019). It was also demonstrated to impact severe hepatic conditions (Philips et al., 2017) as well as autism (Kang et al., 2017; Kang et al., 2019) and Graft *versus* Host Disease (Biliński et al., 2022).

1.3 Factors impacting the microbiome

Rather than a sole alteration of the microbiome, the common thread in numerous chronic conditions is an altered host-microbes symbiosis which is known to be under the influence of numerous intrinsic and environmental factors.

Among the intrinsic host factors, genetics, ethnic origin, age (but mainly in early life and old age) and sex will potentially play pivotal roles (Zhernakova et al., 2016). In addition, the overall health state is also associated with alterations of the microbiome where gut transit state is a key player. This intrinsic factor has a marked influence on the microbiome that 'proxis', such as 'time since previous stool passage' or the score on the Bristol stool scale at the moment of fecal sample collection, are highly associated with microbiome variations. Among the key features to consider, microbiome gene richness and its enterotype are also highly relevant.

Aside from intrinsic factors, modulators of the microbiome arise from elements of environmental exposure where both medical treatments and diet will rank highest (Falony et al., 2016;

Asnicar et al., 2021). Antibiotics, transit modulators, proton pump inhibitors, biological immunomodulators and psychotics can have a significant impact on the microbiome. Among dietary factors, plant-based food is most beneficially impactful and both quantity and diversity will matter greatly. Dietary fibers and associated polyphenols are seen as the active ingredients and their diversity in molecular types will matter, as it will mobilize a range of enzymatic competences among microbes that are rather specialized in their substrate range and glycohydrolytic activities (Ranaivo et al., 2022).

2 Innovative strategies

Microbiome science has reached a point of maturity, impacting preventive nutrition and medicine via monitoring and diagnostic innovations as well as translational therapeutic developments (Wilkinson et al., 2021).

2.1 Diagnostics and predictive models

Despite the recognition of the importance of host-microbes symbiosis in a large array of immune-mediated clinical conditions microbiome configuration and host related symptoms have never been combined in the context of innovative diagnostic models. The two most obvious parameters that could be combined immediately are immune status and microbiome profile. The former is commonly assessed by Medical Biology Laboratories (blood cell counts, CRP, calprotectin) and the latter is today amenable to standardized assessment. As recently tested in the context of pediatric ulcerative colitis, mapping the symbiosis status based on a combination of a microbiome parameter and a measure of inflammatory tone, not only allows to position each patient distant from healthy controls, but it also allows to anticipate the potential for each patient to enter remission during a 1-year clinical management under standard care with immuno-suppressants and/or corticoids (van de Guchte et al., 2021). Nevertheless, the relevance of such novel approaches will require qualification and verification of the biomarker's associations, and in turn the evaluation of their potential to assist the decision process of healthcare professionals, with ensuing benefits for the patient. Aside from Standard Operating Procedures and reference materials that are available for Medical Biology Laboratories to implement these assessments, the complete pipeline will have to be in place for medical doctors to prescribe, obtain and use these new predictors for their clinical value to be evaluated in diverse clinical indications.

Statistical approaches that can generate predictive models linking microbiome features with relevant metadata are captured under the term Machine Learning (ML). Among ML approaches, supervised ML refers to algorithms that take a set of features and the target values to predict, while unsupervised ML algorithms take as input a set of features and identify any structure within them. ML methods applied to microbiome data, which often suffers from high-dimensionality, sparsity, and compositionality issues, require specific caution in their application and associated data management. ML models are already trained towards the identification of microbiome signatures with diagnostic or predictive value in various disease conditions (Boolchandani et al., 2019; Aryal et al., 2020; Bezek et al., 2020; Fernández-Edreira et al., 2021; Marcos-Zambrano et al., 2021; Liñares-Blanco et al., 2022).

2.2 Prevention and therapy

Similarly, for preventive or therapeutic reasons, it seems appropriate to develop and validate innovative strategies that will ensure a more efficient preservation and/or restoration of symbiosis by targeting at the same time host and microbiome parameters. This is a paradigm shift from former strategies whereby single bioactives (pre-, pro- or post biotics) were used with the aim to provide and complement a given lost function. Combining bioactives targeting several of the triggers mentioned above could improve the potential to act on feed-back loops and break vicious circles that would otherwise remain unaffected or strongly resilient when tackling only one of many triggers. Although not yet implemented in the clinic, a recent publication showed in a mouse model that three food-grade bioactives targeting microbiota, gut permeability, inflammation, and oxidative stress could correct impaired behavior (anxiety and depression) to the same extent as an antidepressant (Faucher et al., 2022). Following the same rationale, we have also described how host-microbes systems modeling suggests that combining immunosuppressant and FMT would likely increase the potential to set in remission infants with pediatric ulcerative colitis (Paramsothy et al., 2017; Costello et al., 2019; van de Guchte et al., 2021). Strong expectations can also be put in other severe conditions such as autism or life-threatening liver cirrhosis (Kang et al., 2017; Philips et al., 2017; Kang et al., 2019). Finally, with the aim to increase the rate of response to a very effective therapeutic approach in a cancer treatment for which the microbiome dictates the status of non-responder in more than half of the patients, a clinical trial combining FMT and immunotherapy has been initiated (NCT04988841). Such innovative strategies would apply equally to prevention in the general population as to therapies in chronic diseases. These innovative therapies should also be accompanied by hygiene and dietary recommendations ensuring a quality of life in nutritional and psychological terms to strengthen the subsequent maintenance of symbiosis.

3 Application for space-travel conditions

As stated in previous sections, several intrinsic and extrinsic aspects directly affect the human gut microbiome and spaceflight is certainly a factor playing a pivotal role. Astronauts endure several physiological and psychological changes while in space due to the exposure to "the space exposome" which gathers galactic cosmic radiation, altered gravity, confinement, nutrient supply, sleep deprivation and alteration of the circadian rhythms, (Crucian et al., 2018). Even though some of the side effects have been extensively documented such as: fluid redistribution, cognitive impairment and decline, bone loss, muscle atrophy, *etc.*, the taxonomic and functional evolution of the astronaut gut microbiome and its impact on the overall astronaut health has drawn little attention (Cucinotta et al., 2014; Grimm et al., 2016; Demontis et al., 2017; Tanaka et al., 2017; Crucian et al., 2018;

Jillings et al., 2020). However, deeper understanding on these areas is essential if we want to succeed in our objective of long-duration human space exploration beyond Low Earth Orbit (LEO).

To date, only a few studies have been devoted to monitoring the evolution of the gut microbiome of human space travelers and these studies have a limited sample size and diversity (Brown et al., 1976; Taylor et al., 1997; Ritchie et al., 2015; Casero et al., 2017; Turroni et al., 2017; Hao et al., 2018; Alauzet et al., 2019; Garrett-Bakelman et al., 2019; Jiang et al., 2019; Voorhies et al., 2019; Avila-Herrera et al., 2020; Liu et al., 2020; Urbaniak et al., 2020; Brereton et al., 2021; Chen et al., 2021; Morrison et al., 2021). Hence, they should be interpreted with caution and future studies of astronauts that include a larger number and diversity of individuals is required to determine the global patterns of microbiome evolution to spaceflight to enable the development of predictive models. Nevertheless, preliminary results from real space missions, such as the Astronauts' Microbiome Project and the Twins Study, showed that microbiome richness composition remains substantially unchanged with progressive convergence in the microbiota composition among the crew members (Garrett-Bakelman et al., 2019; Voorhies et al., 2019). Overall abundance of the genera *Lactobacillus* and *Bifidobacterium* decreased which could contribute to alterations in the host immune functions. In addition, intestinal permeability of the host could be compromised due to the described combination of increased proportions of genera associated with chronic intestinal inflammation and decreased abundance of those with anti-inflammatory properties, represented by *Parasutterella* and *Akkermansia,* respectively. However, this dysbiosis was transient and reversible upon return to Earth which indicates a resilience of the microbial ecosystem of the gastrointestinal tract. In this respect, a direct association with this observed dysbiosis and the specific microsystem the crew is exposed to inside the spacecraft can be drawn. The habitable environments of spacecrafts are strictly sanitized and controlled by the Environmental Control and Life Support System (ECLSS) which up to date is mainly devoted to the physical and chemical purification and recycling of the air and water and it is highly dependent on continuous resupply of these and other crew consumables from Earth. In addition, these crew consumables, i.e., oxygen, water, food, hygienic material, *etc.*, are also subjected to strict sanitation controls and transported in sterile packaging from Earth. Hence, due to these stringent hygienic and sterile conditions imposed in the habitable areas of the spacecraft, the crew is exposed to a completely novel and specific microsystem which is not a reflection of the habitable areas humans experience while on Earth and may contribute to the transient dysbiosis observed in the recent astronaut microbiome studies.

However, this situation will change with the integration of regenerative LSS in human exploration missions foreseen by space agencies where sustained human presence on Martian floor is targeted. Whereas during voyage, ECLSS will remain based only (or mostly) on physico-chemical recycling processes due to the intrinsic mass of the cycle components as well as the inherent mass, volume and energy requirements of the system, upon arrival on martial soil, the regenerative ECLSS could become the unlocking key to meeting human needs, as local resources and materials could be harnessed and transformed by the system itself into suitable inputs (Verseux et al., 2016). Regenerative LSS development has been supported by International Space Agencies, where the European Space Agency (ESA) was a pioneer by the implementation of the MELiSSA (Micro-Ecological Life-Support Systems Alternative) project in 1989 (Lasseur et al., 2010). Ground-based analog space simulations have recently analyzed the impact on the subjects' health upon integration of regenerative LSS in the loop (Hao et al., 2018; Chen et al., 2021). This resulted in higher microbiome diversity and richness levels of bacteria associated with not only anti-inflammatory properties but also with increased ability to metabolize dietary polysaccharides highlighting its beneficial impact on the maintenance of a healthy gut microbiota among the crewmembers (Yilmaz et al., 2011; Field et al., 2014; Bowers et al., 2017; Kuehnast et al., 2022). Microbiome science has made useful progress that could support overtime monitoring of the microbiome during space travel. Highly standardized methods have been published (Costea et al., 2017b) and a complete value-chain involving medical biology laboratories is emerging delivering

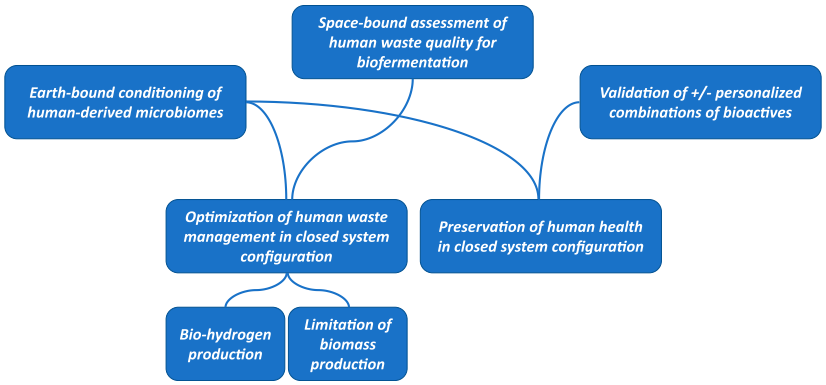

FIGURE 2
Outline of specific objectives that would benefit from the development of predictive modeling tools towards circularization of processes in a closed system configuration. Both optimization of waste management and preservation of human health are indicated as outcomes. Currently available procedures for the conditioning of human intestinal contents in a way that will preserve the integrity of the complex microbiome as a full ecosystem would allow both earth-bound and space-bound applications.

microbiome information to assist clinicians in their decision-making process. Moreover, strategies for the mitigation of alterations of host-microbes symbiosis for astronauts could benefit from recent evidence, provided in clinical trials, that proper conditioning of human stool collected before any stress can be used for near complete reconstruction of post-stress altered microbiome using an autologous procedure (Malard et al., 2021b). Finally, microbiome assessment and management could serve specific goals such as optimizing sustainability of waste fermentation or promoting health benefits of FMT. Ecological modeling of complex intestinal ecosystems management is already underway (Ianiro et al., 2022; Schmidt et al., 2022) and further efforts towards metabolic modeling could be most instrumental as shown in a few pioneering examples: i) butyrate production by the intestinal microbiota (Muñoz-Tamayo et al., 2011); ii) orientation towards primary (detrimental) or secondary (beneficial) bile acids (Kastl et al., 2022); or iii) modulation of immune-inflammatory context and/or gut-brain signaling by the modulation of tryptophan metabolism (Xue et al., 2022). In a recent review, the importance of establishment of a microbiome baseline determination and pre-flight preparations is highlighted (Kuehnast et al., 2022). The settlement of a previous knowledge on the healthy and diverse baseline microbiome and its taxonomic and/or functional fingerprint for each space traveler is suggested and a detailed protocol to conduct this baseline determination is provided. Implementation of this methodology would enable the identification of perturbations in the microbiome and if combined with meticulous metadata recording of the crew's daily operations (i.e., exercise diary, food intake and composition, health parameters, *etc.*) statistical correlations could be established (Yilmaz et al., 2011; Field et al., 2014; Bowers et al., 2017).

Based on ongoing efforts, a roadmap for the development of predictive modelling can be suggested. This roadmap could become the baseline for future activities within the frame of the MELiSSA Project lead by ESA. Figure 2 highlights the specific objectives suggested above and for which predictive modeling would be most appropriate.

Author contributions

All authors listed have made a substantial, direct, and intellectual contribution to the work and approved it for publication.

Funding

This publication work was supported in part by the European Commission in the context of ERC-2017-AdG No. 788191, Horizon 2020 research and innovation programme under grant agreement No. 964590, and in the context of MetaGenoPolis grant ANR-11-DPBS-0001.

Conflict of interest

The authors declare that the research was conducted in the absence of any commercial or financial relationships that could be construed as a potential conflict of interest.

Publisher's note

All claims expressed in this article are solely those of the authors and do not necessarily represent those of their affiliated organizations, or those of the publisher, the editors and the reviewers. Any product that may be evaluated in this article, or claim that may be made by its manufacturer, is not guaranteed or endorsed by the publisher.

References

Alauzet, C., Cunat, L., Wack, M., Lozniewski, A., Busby, H., Agrinier, N., et al. (2019). Hypergravity disrupts murine intestinal microbiota. *Sci. Rep.* 9, 9410. doi:10.1038/s41598-019-45153-8

Arumugam, M., Raes, J., Pelletier, E., Paslier, D., Yamada, T., Mende, D. R., et al. (2011). Enterotypes of the human gut microbiome. *Nature* 473, 174–180. doi:10.1038/nature09944

Aryal, S., Alimadadi, A., Manandhar, I., Joe, B., and Cheng, X. (2020). Machine learning strategy for gut microbiome-based diagnostic screening of cardiovascular disease. *Hypertension* 76, 1555–1562. doi:10.1161/HYPERTENSIONAHA.120.15885

Asnicar, F., Berry, S. E., Valdes, A. M., Nguyen, L. H., Piccinno, G., Drew, D. A., et al. (2021). Microbiome connections with host metabolism and habitual diet from 1,098 deeply phenotyped individuals. *Nat. Med.* 27, 321–332. doi:10.1038/s41591-020-01183-8

Avila-Herrera, A., Thissen, J., Urbaniak, C., Be, N. A., Smith, D. J., Karouia, F., et al. (2020). Crewmember microbiome may influence microbial composition of ISS habitable surfaces. *PLoS One* 15, e0231838. doi:10.1371/journal.pone.0231838

Bach, J. F. (2002). The effect of infections on susceptibility to autoimmune and allergic diseases. *N. Engl. J. Med.* 347, 911–920. doi:10.1056/NEJMra020100

Bezek, K., Petelin, A., Pražnikar, J., Nova, E., Redondo, N., Marcos, A., et al. (2020). Obesity measures and dietary parameters as predictors of gut microbiota phyla in healthy individuals. *Nutrients* 12, 2695. doi:10.3390/nu12092695

Biliński, J., Jasiński, M., and Basak, G. W. (2022). The role of fecal microbiota transplantation in the treatment of acute graft-versus-host disease. *Biomedicines* 10, 837. doi:10.3390/biomedicines10040837

Blottière, H. M., and Doré, J. (2016). Impact des nouveaux outils de métagénomique sur notre connaissance du microbiote intestinal et de son rôle en santé humaine. *Medecine/Sciences* 32, 944–951. doi:10.1051/medsci/20163211009

Boolchandani, M., D'Souza, A. W., and Dantas, G. (2019). Sequencing-based methods and resources to study antimicrobial resistance. *Nat. Rev. Genet.* 20, 356–370. doi:10.1038/s41576-019-0108-4

Bowers, R. M., Kyrpides, N. C., Stepanauskas, R., Harmon-Smith, M., Doud, D., Reddy, T. B. K., et al. (2017). Minimum information about a single amplified genome (MISAG) and a metagenome-assembled genome (MIMAG) of bacteria and archaea. *Nat. Biotechnol.* 35, 725–731. doi:10.1038/nbt.3893

Brereton, N. J. B., Pitre, F. E., and Gonzalez, E. (2021). Reanalysis of the Mars500 experiment reveals common gut microbiome alterations in astronauts induced by long-duration confinement. *Comput. Struct. Biotechnol. J.* 19, 2223–2235. doi:10.1016/j.csbj.2021.03.040

Brown, L. R., Fromme, W. J., Handler, S. F., Wheatcroft, M. G., and Johnston, D. A. (1976). Effect of Skylab missions on clinical and microbiologic aspects of oral health. *J. Am. Dent. Assoc.* 93, 357–363. doi:10.14219/jada.archive.1976.0502

Casero, D., Gill, K., Sridharan, V., Koturbash, I., Nelson, G., Hauer-Jensen, M., et al. (2017). Space-type radiation induces multimodal responses in the mouse gut microbiome and metabolome. *Microbiome* 5, 105. doi:10.1186/s40168-017-0325-z

Chen, Y., Xu, C., Zhong, C., Lyu, Z., Liu, J., Chen, Z., et al. (2021). Temporal characteristics of the oropharyngeal and nasal microbiota structure in crewmembers stayed 180 Days in the controlled ecological life support system. *Front. Microbiol.* 11, 617696. doi:10.3389/fmicb.2020.617696

Costea, P. I., Hildebrand, F., Manimozhiyan, A., Bäckhed, F., Blaser, M. J., Bushman, F. D., et al. (2017a). Enterotypes in the landscape of gut microbial community composition. *Nat. Microbiol.* 3, 8–16. doi:10.1038/s41564-017-0072-8

Costea, P. I., Zeller, G., Sunagawa, S., Pelletier, E., Alberti, A., Levenez, F., et al. (2017b). Towards standards for human fecal sample processing in metagenomic studies. *Nat. Biotechnol.* 35, 1069–1076. doi:10.1038/nbt.3960

Costello, S. P., Hughes, P. A., Waters, O., Bryant, R. V., Vincent, A. D., Blatchford, P., et al. (2019). Effect of fecal microbiota transplantation on 8-week remission in patients with ulcerative colitis: A randomized clinical trial. *JAMA* 32, 156–164. doi:10.1001/jama.2018.20046

Cotillard, A., Kennedy, S. P., Kong, L. C., Prifti, E., Pons, N., le Chatelier, E., et al. (2013). Dietary intervention impact on gut microbial gene richness. *Nature* 500, 585–588. doi:10.1038/nature12480

Crucian, B. E., Choukèr, A., Simpson, R. J., Mehta, S., Marshall, G., Smith, S. M., et al. (2018). Immune system dysregulation during spaceflight: potential countermeasures for deep space exploration missions. *Front. Immunol.* 9, 1437. doi:10.3389/fimmu.2018.01437

Cucinotta, F. A., Alp, M., Sulzman, F. M., and Wang, M. (2014). Space radiation risks to the central nervous system. *Life Sci. Space Res. (Amst)* 2, 54–69. doi:10.1016/j.lssr.2014.06.003

Demontis, G. C., Germani, M. M., Caiani, E. G., Barravecchia, I., Passino, C., and Angeloni, D. (2017). Human pathophysiological adaptations to the space environment. *Front. Physiol.* 8, 547. doi:10.3389/fphys.2017.00547

Falony, G., Joossens, M., Vieira-Silva, S., Wang, J., Darzi, Y., Faust, K., et al. (2016). Population-level analysis of gut microbiome variation. *Science* 352, 560–564. doi:10.1126/science.aad3503

Faucher, P., Dries, A., Mousset, P. Y., Leboyer, M., Dore, J., and Beracochea, D. (2022). Synergistic effects of Lacticaseibacillus rhamnosus GG, glutamine, and curcumin on chronic unpredictable mild stress-induced depression in a mouse model. *Benef. Microbes* 13, 253–264. doi:10.3920/BM2021.0188

Fernández-Edreira, D., Liñares-Blanco, J., and Fernandez-Lozano, C. (2021). Machine Learning analysis of the human infant gut microbiome identifies influential species in type 1 diabetes. *Expert Syst. Appl.* 185, 115648. doi:10.1016/j.eswa.2021.115648

Field, D., Sterk, P., Kottmann, R., De Smet, J. W., Amaral-Zettler, L., Cochrane, G., et al. (2014). Genomic standards consortium projects. *Stand Genomic Sci.* 9, 599–601. doi:10.4056/sigs.5559680

Garrett-Bakelman, F. E., Darshi, M., Green, S. J., Gur, R. C., Lin, L., Macias, B. R., et al. (2019). The nasa twins study: A multidimensional analysis of a year-long human spaceflight. *Science* 364, eaau8650. doi:10.1126/science.aau8650

Gopalakrishnan, V., Spencer, C. N., Nezi, L., Reuben, A., Andrews, M. C., Karpinets, T. V., et al. (2018). Gut microbiome modulates response to anti-PD-1 immunotherapy in melanoma patients. *Science* 359, 97–103. doi:10.1126/science.aan4236

Grimm, D., Grosse, J., Wehland, M., Mann, V., Reseland, J. E., Sundaresan, A., et al. (2016). The impact of microgravity on bone in humans. *Bone* 87, 44–56. doi:10.1016/j.bone.2015.12.057

Hao, Z., Li, L., Fu, Y., and Liu, H. (2018). The influence of bioregenerative life-support system dietary structure and lifestyle on the gut microbiota: A 105-day ground-based space simulation in lunar palace 1. *Environ. Microbiol.* 20, 3643–3656. doi:10.1111/1462-2920.14358

Ianiro, G., Punčochář, M., Karcher, N., Porcari, S., Armanini, F., Asnicar, F., et al. (2022). Variability of strain engraftment and predictability of microbiome composition after fecal microbiota transplantation across different diseases. *Nat. Med.* 28, 1913–1923. doi:10.1038/s41591-022-01964-3

Ilchmann-Diounou, H., and Menard, S. (2020). Psychological stress, intestinal barrier dysfunctions, and autoimmune disorders: an overview. *Front. Immunol.* 11, 1823. doi:10.3389/fimmu.2020.01823

Jenq, R. R., Taur, Y., Devlin, S. M., Ponce, D. M., Goldberg, J. D., Ahr, K. F., et al. (2015). Intestinal blautia is associated with reduced death from graft-versus-host disease. *Biol. Blood Marrow Transplant.* 21, 1373–1383. doi:10.1016/j.bbmt.2015.04.016

Jiang, P., Green, S. J., Chlipala, G. E., Turek, F. W., and Vitaterna, M. H. (2019). Reproducible changes in the gut microbiome suggest a shift in microbial and host metabolism during spaceflight. *Microbiome* 7, 113. doi:10.1186/s40168-019-0724-4

Jillings, S., van Ombergen, A., Tomilovskaya, E., Rumshiskaya, A., Litvinova, L., Nosikova, I., et al. (2020). Macro- and microstructural changes in cosmonauts' brains after long-duration spaceflight. *Sci. Adv.* 6, eaaz9488. doi:10.1126/sciadv.aaz9488

Kang, D. W., Adams, J. B., Coleman, D. M., Pollard, E. L., Maldonado, J., McDonough-Means, S., et al. (2019). Long-term benefit of Microbiota Transfer Therapy on autism symptoms and gut microbiota. *Sci. Rep.* 9, 5821. doi:10.1038/s41598-019-42183-0

Kang, D. W., Adams, J. B., Gregory, A. C., Borody, T., Chittick, L., Fasano, A., et al. (2017). Microbiota transfer therapy alters gut ecosystem and improves gastrointestinal and autism symptoms: an open-label study. *Microbiome* 5, 10. doi:10.1186/s40168-016-0225-7

Kastl, A., Zong, W., Gershuni, V. M., Friedman, E. S., Tanes, C., Boateng, A., et al. (2022). Dietary fiber-based regulation of bile salt hydrolase activity in the gut microbiota and its relevance to human disease. *Gut Microbes* 14, 2083417. doi:10.1080/19490976.2022.2083417

Kéfi, S., Guttal, V., Brock, W. A., Carpenter, S. R., Ellison, A. M., Livina, V. N., et al. (2014). Early warning signals of ecological transitions: methods for spatial patterns. *PLoS One* 9, e92097. doi:10.1371/journal.pone.0092097

Kelly, J. R., Borre, Y., O' Brien, C., Patterson, E., el Aidy, S., Deane, J., et al. (2016). Transferring the blues: depression-associated gut microbiota induces neurobehavioural changes in the rat. *J. Psychiatr. Res.* 82, 109–118. doi:10.1016/j.jpsychires.2016.07.019

Kuehnast, T., Abbott, C., Pausan, M. R., Pearce, D. A., Moissl-Eichinger, C., and Mahnert, A. (2022). The crewed journey to Mars and its implications for the human microbiome. *Microbiome* 10, 26. doi:10.1186/s40168-021-01222-7

Lasseur, C., Brunet, J., de Weever, H., Dixon, M., Dussap, G., Godia, F., et al. (2010). MELiSSA: the European project of closed life support system. *Gravit. Space Res.* 23, 3–12. Grand challenges in space synthetic biology. Available at: https://www.researchgate.net/publication/285646885_Grand_challenges_in_space_synthetic_biology (Accessed September 15, 2023).

Liñares-Blanco, J., Fernandez-Lozano, C., Seoane, J. A., and López-Campos, G. (2022). Machine learning based microbiome signature to predict inflammatory bowel disease subtypes. *Front. Microbiol.* 13, 872671. doi:10.3389/fmicb.2022.872671

Liu, Z., Luo, G., Du, R., Sun, W., Li, J., Lan, H., et al. (2020). Effects of spaceflight on the composition and function of the human gut microbiota. *Gut Microbes* 11, 807–819. doi:10.1080/19490976.2019.1710091

Llopis, M., Cassard, A. M., Wrzosek, L., Boschat, L., Bruneau, A., Ferrere, G., et al. (2016). Intestinal microbiota contributes to individual susceptibility to alcoholic liver disease. *Gut* 65, 830–839. doi:10.1136/gutjnl-2015-310585

Madison, A., and Kiecolt-Glaser, J. K. (2019). Stress, depression, diet, and the gut microbiota: human–bacteria interactions at the core of psychoneuroimmunology and nutrition. *Curr. Opin. Behav. Sci.* 28, 105–110. doi:10.1016/j.cobeha.2019.01.011

Malard, F., Dore, J., Gaugler, B., and Mohty, M. (2021a). Introduction to host microbiome symbiosis in health and disease. *Mucosal Immunol.* 14, 547–554. doi:10.1038/s41385-020-00365-4

Malard, F., Vekhoff, A., Lapusan, S., Isnard, F., D'incan-Corda, E., Rey, J., et al. (2021b). Gut microbiota diversity after autologous fecal microbiota transfer in acute myeloid leukemia patients. *Nat. Commun.* 12, 3084. doi:10.1038/s41467-021-23376-6

Marcos-Zambrano, L. J., Karaduzovic-Hadziabdic, K., Loncar Turukalo, T., Przymus, P., Trajkovik, V., Aasmets, O., et al. (2021). Applications of machine learning in human microbiome studies: A review on feature selection, biomarker identification, disease prediction and treatment. *Front. Microbiol.* 12, 634511. doi:10.3389/fmicb.2021.634511

Martinez, K. B., Leone, V., and Chang, E. B. (2017). Microbial metabolites in health and disease: navigating the unknown in search of function. *J. Biol. Chem.* 292, 8553–8559. doi:10.1074/jbc.R116.752899

Morrison, M. D., Thissen, J. B., Karouia, F., Mehta, S., Urbaniak, C., Venkateswaran, K., et al. (2021). Investigation of spaceflight induced changes to astronaut microbiomes. *Front. Microbiol.* 12, 659179. doi:10.3389/fmicb.2021.659179

Muñoz-Tamayo, R., Laroche, B., Walter, É., Doré, J., Duncan, S. H., Flint, H. J., et al. (2011). Kinetic modelling of lactate utilization and butyrate production by key human colonic bacterial species. *FEMS Microbiol. Ecol.* 76, 615–624. doi:10.1111/j.1574-6941.2011.01085.x

Paramsothy, S., Kamm, M. A., Kaakoush, N. O., Walsh, A. J., van den Bogaerde, J., Samuel, D., et al. (2017). Multidonor intensive faecal microbiota transplantation for active ulcerative colitis: A randomised placebo-controlled trial. *Lancet* 389, 1218–1228. doi:10.1016/S0140-6736(17)30182-4

Peled, J. U., Gomes, A. L. C., Devlin, S. M., Littmann, E. R., Taur, Y., Sung, A. D., et al. (2020). Microbiota as predictor of mortality in allogeneic hematopoietic-cell transplantation. *N. Engl. J. Med.* 382, 822–834. doi:10.1056/NEJMoa1900623

Philips, C. A., Pande, A., Shasthry, S. M., Jamwal, K. D., Khillan, V., Chandel, S. S., et al. (2017). Healthy donor fecal microbiota transplantation in steroid-ineligible severe alcoholic hepatitis: A pilot study. *Clin. Gastroenterology Hepatology* 15, 600–602. doi:10.1016/j.cgh.2016.10.029

Qin, J., Li, R., Raes, J., Arumugam, M., Burgdorf, K. S., Manichanh, C., et al. (2010). A human gut microbial gene catalogue established by metagenomic sequencing. *Nature* 464, 59–65. doi:10.1038/nature08821

Qin, N., Yang, F., Li, A., Prifti, E., Chen, Y., Shao, L., et al. (2014). Alterations of the human gut microbiome in liver cirrhosis. *Nature* 513, 59–64. doi:10.1038/nature13568

Ramirez, J., Guarner, F., Bustos Fernandez, L., Maruy, A., Sdepanian, V. L., and Cohen, H. (2020). Antibiotics as major disruptors of gut microbiota. *Front. Cell. Infect. Microbiol.* 10, 572912. doi:10.3389/fcimb.2020.572912

Ranaivo, H., Thirion, F., Béra-Maillet, C., Guilly, S., Simon, C., Sothier, M., et al. (2022). Increasing the diversity of dietary fibers in a daily-consumed bread modifies gut microbiota and metabolic profile in subjects at cardiometabolic risk. *Gut Microbes* 14, 2044722. doi:10.1080/19490976.2022.2044722

Raplee, I., Walker, L., Xu, L., Surathu, A., Chockalingam, A., Stewart, S., et al. (2021). Emergence of nosocomial associated opportunistic pathogens in the gut microbiome after antibiotic treatment. *Antimicrob. Resist Infect. Control* 10, 36. doi:10.1186/s13756-021-00903-0

Ridaura, V. K., Faith, J. J., Rey, F. E., Cheng, J., Duncan, A. E., Kau, A. L., et al. (2013). Gut microbiota from twins discordant for obesity modulate metabolism in mice. *Science* 341, 1241214. doi:10.1126/science.1241214

Ritchie, L. E., Taddeo, S. S., Weeks, B. R., Lima, F., Bloomfield, S. A., Azcarate-Peril, M. A., et al. (2015). Space environmental factor impacts upon murine colon microbiota and mucosal homeostasis. *PLoS One* 10, e0125792. doi:10.1371/journal.pone.0125792

Routy, B., le Chatelier, E., Derosa, L., Duong, C. P. M., Alou, M. T., Daillère, R., et al. (2018). Gut microbiome influences efficacy of PD-1–based immunotherapy against epithelial tumors. *Science* 359, 91–97. doi:10.1126/science.aan3706

Schaubeck, M., Clavel, T., Calasan, J., Lagkouvardos, I., Haange, S. B., Jehmlich, N., et al. (2016). Dysbiotic gut microbiota causes transmissible Crohn's disease-like ileitis independent of failure in antimicrobial defence. *Gut* 65, 225–237. doi:10.1136/gutjnl-2015-309333

Scheffer, M., Carpenter, S., Foley, J. A., Folke, C., and Walker, B. (2001). Catastrophic shifts in ecosystems. *Nature* 413, 591–596. doi:10.1038/35098000

Schmidt, T. S. B., Li, S. S., Maistrenko, O. M., Akanni, W., Coelho, L. P., Dolai, S., et al. (2022). Drivers and determinants of strain dynamics following fecal microbiota transplantation. *Nat. Med.* 28, 1902–1912. doi:10.1038/s41591-022-01913-0

Sharon, G., Cruz, N. J., Kang, D. W., Gandal, M. J., Wang, B., Kim, Y. M., et al. (2019). Human gut microbiota from autism spectrum disorder promote behavioral symptoms in mice. *Cell.* 177, 1600–1618.e17. doi:10.1016/j.cell.2019.05.004

Sole, C., Llopis, M., Solà, E., da Silva, K., Guilly, S., Le-Chatelier, E., et al. (2018). Gut microbiome is profoundly altered in acute-on-chronic liver failure as evaluated by quantitative metagenomics. Relationship with liver cirrhosis severity. *J. Hepatol.* 68, S11–S12. doi:10.1016/S0168-8278(18)30240-X

Tanaka, K., Nishimura, N., and Kawai, Y. (2017). Adaptation to microgravity, deconditioning, and countermeasures. *J. Physiological Sci.* 67, 271–281. doi:10.1007/s12576-016-0514-8

Tap, J., Mondot, S., Levenez, F., Pelletier, E., Caron, C., Furet, J. P., et al. (2009). Towards the human intestinal microbiota phylogenetic core. *Environ. Microbiol.* 11, 2574–2584. doi:10.1111/j.1462-2920.2009.01982.x

Taur, Y., Jenq, R. R., Perales, M. A., Littmann, E. R., Morjaria, S., Ling, L., et al. (2014). The effects of intestinal tract bacterial diversity on mortality following allogeneic hematopoietic stem cell transplantation. *Blood* 124, 1174–1182. doi:10.1182/blood-2014-02-554725

Taylor, G. R., Graves, R. C., and Brockett, R. M. (1997). *Skylab environmental and crew microbiology studies. NASA SP-3777*. Washington, DC: NASA, Sci and Tech Inf Office, 53–63.

Turroni, S., Rampelli, S., Biagi, E., Consolandi, C., Severgnini, M., Peano, C., et al. (2017). Temporal dynamics of the gut microbiota in people sharing a confined environment, a 520-day ground-based space simulation, MARS500. *Microbiome* 5, 39. doi:10.1186/s40168-017-0256-8

Urbaniak, C., Lorenzi, H., Thissen, J., Jaing, C., Crucian, B., Sams, C., et al. (2020). The influence of spaceflight on the astronaut salivary microbiome and the search for a microbiome biomarker for viral reactivation. *Microbiome* 8, 56. doi:10.1186/s40168-020-00830-z

van de Guchte, M., Blottière, H. M., and Doré, J. (2018). Humans as holobionts: implications for prevention and therapy. *Microbiome* 6, 81. doi:10.1186/s40168-018-0466-8

van de Guchte, M., Burz, S. D., Cadiou, J., Wu, J., Mondot, S., Blottière, H. M., et al. (2020). Alternative stable states in the intestinal ecosystem: proof of concept in a rat model and a perspective of therapeutic implications. *Microbiome* 8, 153. doi:10.1186/s40168-020-00933-7

van de Guchte, M., Mondot, S., and Doré, J. (2021). Dynamic properties of the intestinal ecosystem call for combination therapies, targeting inflammation and microbiota, in ulcerative colitis. *Ulcerative Colitis. Gastroenterol.* 161, 1969–1981.e12. doi:10.1053/j.gastro.2021.08.057

Varanoske, A. N., McClung, H. L., Sepowitz, J. J., Halagarda, C. J., Farina, E. K., Berryman, C. E., et al. (2022). Stress and the gut-brain axis: cognitive performance, mood state, and biomarkers of blood-brain barrier and intestinal permeability following severe physical and psychological stress. *Brain Behav. Immun.* 101, 383–393. doi:10.1016/j.bbi.2022.02.002

Verseux, C., Baqué, M., Lehto, K., De Vera, J. P. P., Rothschild, L. J., and Billi, D. (2016). Sustainable life support on Mars - the potential roles of cyanobacteria. *Int. J. Astrobiol.* 15, 65–92. doi:10.1017/S147355041500021X

Vieira-Silva, S., Falony, G., Belda, E., Nielsen, T., Aron-Wisnewsky, J., Chakaroun, R., et al. (2020). Statin therapy is associated with lower prevalence of gut microbiota dysbiosis. *Nature* 581, 310–315. doi:10.1038/s41586-020-2269-x

Voorhies, A. A., Mark Ott, C., Mehta, S., Pierson, D. L., Crucian, B. E., Feiveson, A., et al. (2019). Study of the impact of long-duration space missions at the International Space Station on the astronaut microbiome. *Sci. Rep.* 9, 9911. doi:10.1038/s41598-019-46303-8

Vrieze, A., van Nood, E., Holleman, F., Salojärvi, J., Kootte, R. S., Bartelsman, J. F. W. M., et al. (2012). Transfer of intestinal microbiota from lean donors increases insulin sensitivity in individuals with metabolic syndrome. *Gastroenterology* 143, 913–916.e7. doi:10.1053/j.gastro.2012.06.031

Wilkinson, J. E., Franzosa, E. A., Everett, C., Li, C., Bae, S., Berzansky, I., et al. (2021). A framework for microbiome science in public health. *Nat. Med.* 27, 766–774. doi:10.1038/s41591-021-01258-0

Xue, H., Chen, X., Yu, C., Deng, Y., Zhang, Y., Chen, S., et al. (2022). Gut microbially produced indole-3-propionic acid inhibits atherosclerosis by promoting reverse cholesterol transport and its deficiency is causally related to atherosclerotic cardiovascular disease. *Circ. Res.* 131, 404–420. doi:10.1161/CIRCRESAHA.122.321253

Yilmaz, P., Kottmann, R., Field, D., Knight, R., Cole, J. R., Amaral-Zettler, L., et al. (2011). Minimum information about a marker gene sequence (MIMARKS) and minimum information about any (x) sequence (MIxS) specifications. *Nat. Biotechnol.* 29, 415–420. doi:10.1038/nbt.1823

Zhernakova, A., Kurilshikov, A., Bonder, M. J., Tigchelaar, E. F., Schirmer, M., Vatanen, T., et al. (2016). Population-based metagenomics analysis reveals markers for gut microbiome composition and diversity. *Science* 352, 565–569. doi:10.1126/science.aad3369

frontiers | Frontiers in Astronomy and Space Sciences

TYPE Original Research
PUBLISHED 13 December 2023
DOI 10.3389/fspas.2023.1229043

Check for updates

OPEN ACCESS

EDITED BY
Luigi Gennaro Izzo,
University of Naples Federico II, Italy

REVIEWED BY
Marwen Moussa,
AgroParisTech Institut des Sciences et Industries du Vivant et de L'environnement, France
Alessio Papini,
University of Florence, Italy

*CORRESPONDENCE
Estelle Couallier,
estelle.couallier@univ-nantes.fr

RECEIVED 25 May 2023
ACCEPTED 10 November 2023
PUBLISHED 13 December 2023

CITATION
Tallec J, Vandermies M, Coene C, Lamaze-Lefebvre B, Demey D, Frappart M and Couallier E (2023), Implementation of an automated process for *Limnospira indica* harvesting and culture medium recycling for space applications.
Front. Astron. Space Sci. 10:1229043.
doi: 10.3389/fspas.2023.1229043

COPYRIGHT
© 2023 Tallec, Vandermies, Coene, Lamaze-Lefebvre, Demey, Frappart and Couallier. This is an open-access article distributed under the terms of the Creative Commons Attribution License (CC BY). The use, distribution or reproduction in other forums is permitted, provided the original author(s) and the copyright owner(s) are credited and that the original publication in this journal is cited, in accordance with accepted academic practice. No use, distribution or reproduction is permitted which does not comply with these terms.

Implementation of an automated process for *Limnospira indica* harvesting and culture medium recycling for space applications

Jordan Tallec[1,2,3], Marie Vandermies[4], Céline Coene[5], Brigitte Lamaze-Lefebvre[6], Dries Demey[5], Matthieu Frappart[1] and Estelle Couallier[1]*

[1]CNRS, ONIRIS, Laboratoire de Génie des Procédés, Environnement et Agroalimentaire, GEPEA, Nantes Université, Saint Nazaire, France, [2]Capacités SAS, Nantes, France, [3]CNRS, AlgoSolis, Université de Nantes, Saint-Nazaire, France, [4]GlaxoSmithKline Biologicals, Rixensart, Belgium, [5]Redwire Space NV, Kruibeke, Belgium, [6]ATG Europe for ESA-European Space Agency, Noordwijk, Netherlands

Future long-term space exploration missions require the implementation of circular life support systems for the supply of water, oxygen and food from mission wastes. Therefore, separation systems dealing with multi-phasic streams need to be addressed. The BioHarvest (BHV) study focused on solid/liquid separation in space with the aim to demonstrate the continuous separation and harvesting of the cyanobacterium *Limnospira indica* from its culture broth under axenic conditions. The cyanobacterium biomass is intended to be used for further food processing while the broth free of organic matter and resupplied with nutrients should be directly recycled into the photobioreactor (PBR). In this study, an automated breadboard model based on a two-step process was built. First, a Biomass Harvesting Unit (BHU) separates the biomass produced in the PBR from the culture medium with dead-end filtration. Second, the Medium Filtration Unit (MFU) further treats the culture medium to retain the dissolved organic compounds using crossflow filtration. The performances of BHU and MHU met the requirements in batch mode and in short continuous mode: the BHU was able to retain all the biomass and the MFU could retain more than 90% of organic matter while being permeable to nutrients. The productivity of the MFU was also very good, with a high permeation flux allowing treating the targeted 80 L of culture per day. However, continuous operation of the BHV technology could not be achieved in the long term due to biomass accumulation as a sticky cake with a high specific resistance on the BHU filter, despite backwashing cycles and intense vibrations. Future work shall therefore focus on this critical step, to improve process performance by preventing fouling of the filter sheets.

KEYWORDS

regenerative life support, solid-liquid separation, filtration technology, harvesting of microalgae, biomass for food

1 Introduction

Future long-term space exploration missions require the implementation of circular life support systems for the supply of water, oxygen and food from mission wastes. MELiSSA

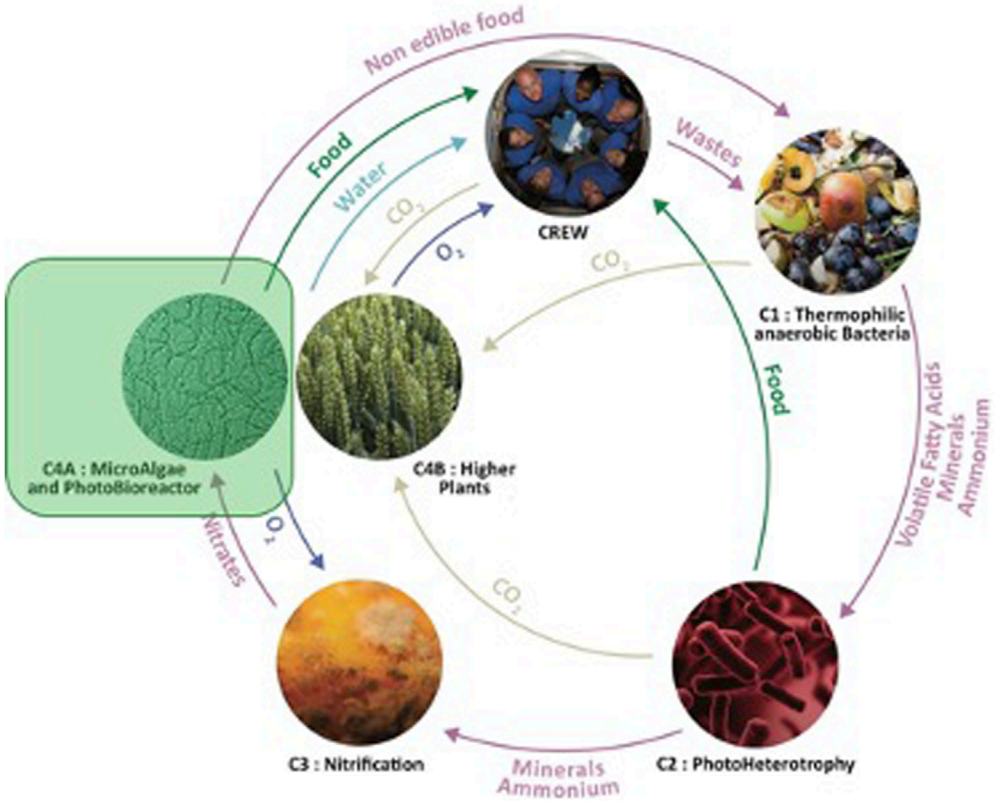

FIGURE 1
Diagram of the MELiSSA Loop with the compartment C4A highlighted in green.

(Micro-Ecological Life Support System Alternative) is the European project of circular life support systems led by the European Space Agency (ESA) since 1987. The MELiSSA loop as depicted in Figure 1 is composed of five interlinked compartments. The compartment C4A is responsible for air revitalization and edible biomass production. It relies on a photobioreactor growing the cyanobacterium *Limnospira indica*. Besides its high radiation resistance, this microorganism shows a high nutritional quality and therapeutic value which are beneficial in space but also on Earth. Microalgae and cyanobacteria have lately gained interest worldwide due to their extensive application potential on Earth in various fields such as renewable energy, pharmaceutical, construction, food and feed industries.

The BioHarvest (BHV) project aimed to study solid/liquid separation in space dedicated to the Solid Loop of the compartment C4A. The objective was to demonstrate the separation and harvesting of the cyanobacterium *Limnospira indica* from axenic cultures in photobioreactors under space compatible conditions. After separation using the BioHarvest technology, the biomass (i.e., the solid outlet stream) is intended to be used for further food processing while the culture broth (i.e., the liquid outlet stream) resupplied with nutrients shall be suitable for reinjection into the photobioreactor (PBR) where *the strain* is cultivated.

Starting with a literature review of the potential separation principles and associated technologies, a trade-off based on the requirements of the harvested product and the space constraints were performed. In the last 6–7 years, the following dewatering/harvesting techniques have been mainly studied to enhance the harvesting of microalgae.

Considering the processes based on density difference, centrifugation remains the reference (faster, more effective, and useable on most microalgae strains). However, less energy consuming methods were also investigated. Settling or flotation are exploited after the addition of classical inorganic salts, or more original coagulating agents such as cellulose nanocrystals for the recovery of *Nannochloropsis oculata* (Verfaillie et al., 2020) or cooking oil-surfactant emulsion for harvesting *Chlorella vulgaris* with high pH (Potocar et al., 2020). The addition of microspheres has been investigated for the enhancement of Ballasted Dissolved Air Flotation (DAF) on *Scenedesmus obliquus*, *Chlorella vulgaris* and *Arthrospira maxima* with up to 95% coagulant reduction and 99% cells separation (Ometto et al., 2014). Depraetere et al. (2015) could also achieve separation by spontaneous settling of *Arthrospira platensis* by enrichment in carbohydrates in nitrogen starved culture conditions. Spirulina settling through flocculation has been implemented in the form of bioflocculation using fungi biomass (with efficiencies ranging from 90% to 100% after pH adjustment) (Nazari et al., 2021), autoflocculation (pH-induced flocculation) in salt-rich culture medium (Formosa-Dague et al., 2018), and using a combination of salts and extra-polymeric substances such

as polysaccharides in the medium (Rashid et al., 2019). For these techniques, even if efficiency and low energy are widely recognized, the presence of additives contaminating the biomass and hindering culture medium recycling are a brake on the development for certain applications (Singh and Patidar, 2018).

Membrane processes based on steric separation by crossflow filtration (Rossignol et al., 1999) or by shear-enhanced (dynamic) filtration (Frappart et al., 2011) have been studied for many years and show very good performances, sometimes in combination with a preliminary coagulation (Zhao et al., 2020a). Here, ensuring sufficient water recovery and a final high biomass concentration (up to 180 g/L for combined sedimentation and dynamic filtration (Hapońska et al., 2018)) are the key points. The main limitations lie in the possible membrane fouling reducing the process performances (productivity and selectivity) and the energy consumption (due to pumping in this pressure-driven process). The most innovative studies of the recent years rely on membrane design: a membrane with a wave pattern structure allowed to accumulate biomass in the hollows of the structure and maintain membrane zones devoid of fouling layers to promote permeation (Zhao et al., 2020b), and another membrane was highly negatively charged to prevent fouling by microalgae cells (Huang et al., 2020). Human urine has been employed as a forward osmosis solution exploited first as a nutrient source for cultivation of *Chlorella vulgaris* and then for biomass dewatering and concentration, but the concentration factor remains low (Volpin et al., 2019). For the dewatering/harvesting of *Arthrospira* species at industrial scale, sieving is the reference as the cells are large (Belay, 1997) and it was shown that centrifugation was less efficient (GEPEA and Algosolis expertise). In a MELiSSA context, microfiltration and ultrafiltration with organic and mineral membranes were studied by Rossi and others (Rossi et al., 2004; Rossi et al., 2005; Rossi et al., 2008). Among the selection of membranes, the ones related to ultrafiltration (40–50 kDa) showed the best performances in terms of permeation fluxes (~40–50 L/h/m^2 for organic membranes; ~30–40 L/h/m^2 for inorganic membranes). The authors also highlighted the major role of exopolysaccharides in the fouling phenomenon.

Most of microalgae harvesting studies were conducted for terrestrial applications, where specific aspects of the space environment such as the operability under microgravity were not approached. Furthermore, these studies lack information regarding the quality and composition of the solid and liquid fractions recovered from the separation process. The BioHarvest study aimed to partly fill this gap by studying solid/liquid separation in space compatible conditions. Focusing on the C4A compartment of the MELiSSA loop, the objective of BioHarvest was more specifically to demonstrate the separation and harvesting of the cyanobacterium *Limnospira indica* from axenic cultures in photobioreactors under space conditions. To this end, a BioHarvest automated breadboard model (BBM) attached to a photobioreactor was developed to separate the cyanobacterium biomass from its culture broth. The BBM was designed to operate under microgravity and axenic conditions, in order to deliver edible biomass of 4%–8% suspended matter and recycle more than 90% of the culture medium back to the photobioreactor. The maximal limit of biomass concentration in the liquid outflow was 0.01 g/L. The target was to achieve a continuous life test period of at least 40 days.

The final selection of the technologies composing the BBM was conducted according to the trade-off methodology ALiSSE (Advanced Life Support System Evaluator). ALiSSE is a decision tool dedicated to life support system comparison and evaluation. This methodology is based on multiple criteria: mass, energy and power, efficiency, risk to humans, reliability, crew time, sustainability, and life cycle cost.

Based on the literature review, the requirements and the ALiSSE criteria, two steps were selected and introduced in the BHV as distinct units. Firstly, the Biomass Harvesting Unit (BHU) consists of the dead-end filtration of the culture on a vibrating stainless steel medium, inspired by the usual sieving, able to recover the biomass in a continuous way and release a maximum of water. Secondly, the Medium Filtration Unit (MFU) based on ultrafiltration removes organic matter (polysaccharides) from broth before culture medium recycling and ensures sterility of medium in case of punctual contamination. The design of the harvesting process is detailed in the following paragraphs and the performances are demonstrated.

2 Materials and methods

2.1 Breadboard configuration

The BioHarvest demonstration unit was made of three subsystems (see Figure 2). 1- the photobioreactor (PBR) to cultivate *Limnospira indica* in a dedicated culture medium. It possessed its own control system and electronics. 2- the biomass harvesting unit (BHU) to collect *Limnospira indica* and evacuate it into a drain, while the clarified culture medium is sent to filtrate tank 3- the medium filtration unit (MFU) dedicated to the filtrate purification by ultrafiltration, i.e., the concentration of extracellular organic matter and potential cell fragments in the retentate and the recovery of the culture medium in the permeate to be recycled into the PBR. The nutrient content in the permeate was verified for culture medium adjustment by addition of nutrients if needed. The steps 2 and 3 were automated using a control system and electronics (CSE) unit giving access to the measured and calculated values (e.g., temperature, pressure, liquid level, weight, operation time, mass balance, flow rates). A loop allowed an automated cleaning in place while the PBR was sterilized using chemicals and steam.

2.1.1 Photobioreactor

The cultivation of *Limnospira indica* was ensured in HECTOR (see Figures 3A, B), an airlift photobioreactor with a useful capacity of 170 L and a culture thickness of 6 cm. It was equipped with a LED lighting system, pH, temperature and dissolved oxygen probes connected to its own control system. The control software (C-BIO2) recorded each minute the monitored parameters (pH, temperature, dissolved oxygen, light intensity) and controlled the fixed parameters (pH, temperature, light intensity). In this way, automatic regulation of the culture conditions was ensured according to the setpoints fixed by the operator (i.e., for temperature, pH, and light intensity). Temperature regulation was performed by circulation of industrial water in the internal heat exchanger. Regulation of pH was performed by injections of CO_2 from a gas bottle into the gas inlet line. The target was to produce 80 ± 10 L/day

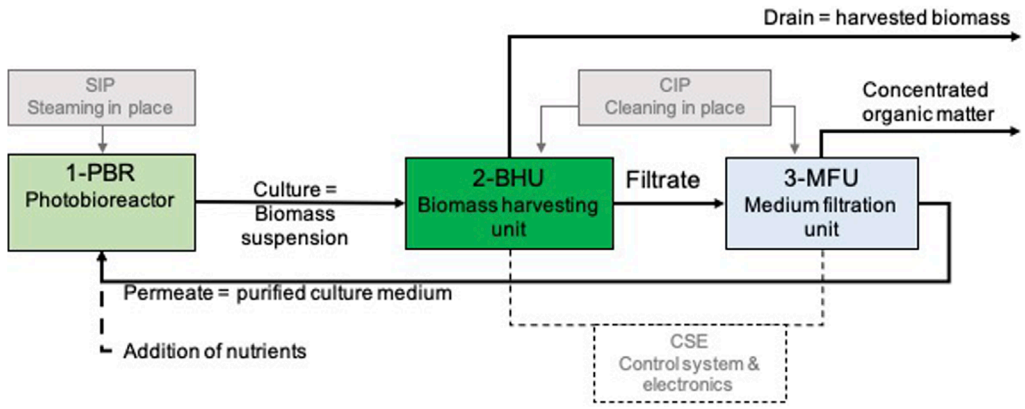

FIGURE 2
Overview of the BioHarvest sub-systems.

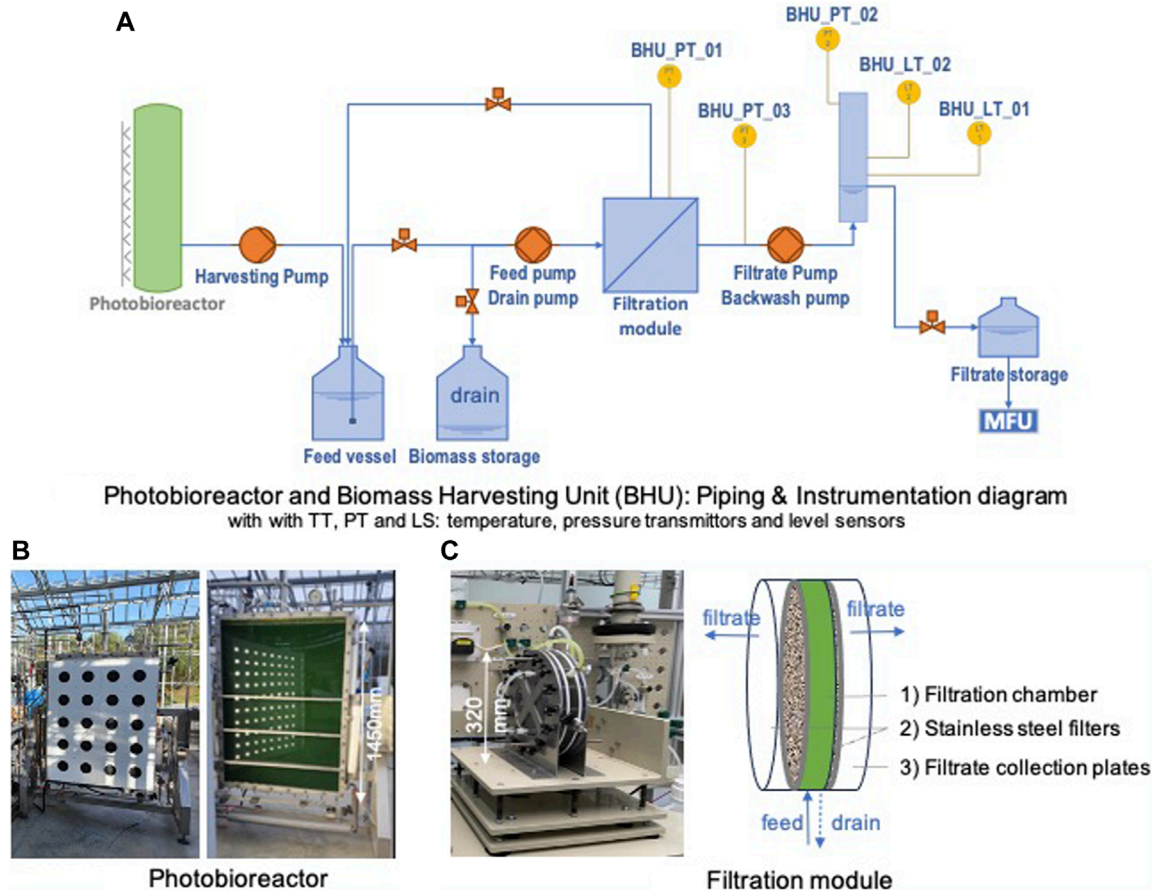

FIGURE 3
HECTOR photobioreactor and Biomass Harvest Unit system (BHU) with detailed filtration module.

of culture with 2 g/L of suspended matter (SM) corresponding to biomass.

2.1.2 BHU: biomass harvest unit

The dead-end filtration module [see Figures 3A, C)] was made of 1) a central filtration chamber (0.79 L) to collect the harvested biomass before draining, with 2) on both sides two stainless steel non woven filters (effective filtration area of 0.025 m^2 each) and 3) at the external sides two polycarbonate filtrate collection plates from which the filtrate was evacuated. Two nonwoven filters were tested, made of a stainless-steel mesh with pore distributions around 5 and 10 µm (Bekaert).

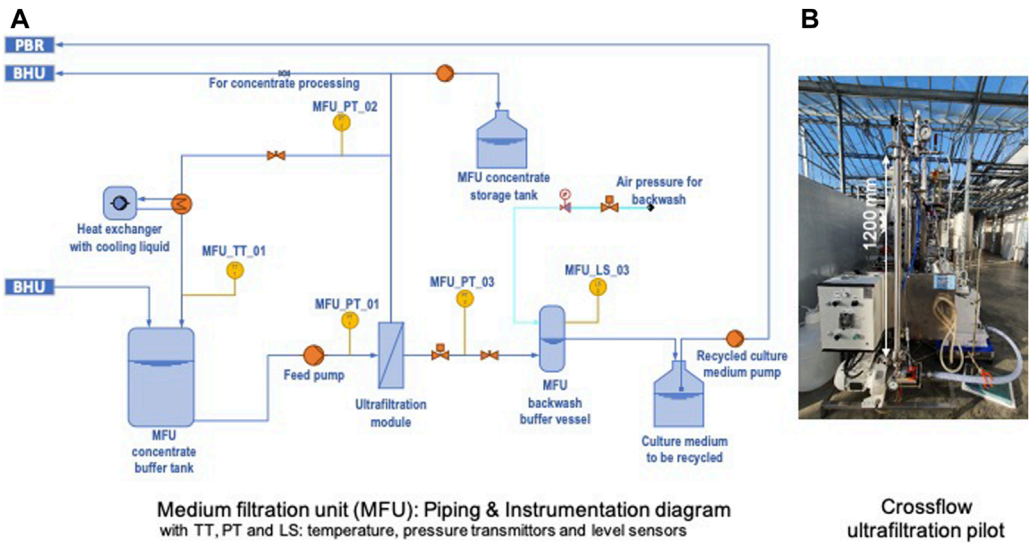

FIGURE 4
Medium filtration unit system (MFU).

The biomass suspension was pumped from the PBR into the central filtration chamber. The filtrate was directed to a buffer volume, from which it could be injected to the MFU or used for backwash. Based on a timer or on observed pressure acting on the CSE, the BHU was drained of the harvested biomass before being submitted to a backwash using the filtrate coming from the buffer volume. The target was to recover at least 90% of the culture medium and to harvest the biomass with a SM (suspended matter) of 4%–8%.

2.1.3 MFU: medium filtration unit

The crossflow pilot XLAB 5 (PALL) was equipped with an INSIDE CéRAM™ membrane from Tami industries (ref. MTB200511U015) containing an active layer in zirconium dioxide with a 15 kDa cut-off to limit the fouling by polysaccharides (see Figure 4). This ultrafiltration ceramic membrane measured 1,178 mm long and 20 mm in diameter, with 5 channels of 6 mm hydraulic diameter, for a total membrane area of 0.13 m^2. The temperature was regulated using a heat exchanger. The pure water flux with the clean membrane was 120 L/h/m^2 at 0.8 bar, 30°C. The filtration unit was designed to allow a crossflow velocity higher than 2 m/s. At the outlet of this unit, concentrated organic "waste" was collected, while a buffer vessel was foreseen collecting the permeate. The target volume reduction rate (VRR) for the crossflow filtration step was 15, with a continuous extraction of the permeate. Like the BHU, drainage and backwash were applied based on a timer or on observed pressure.

The pure continuous mode experiments were limited by the productivity of the BHU. Therefore, a fed-batch mode was deployed: 1- filtration of 20 L of filtrate for VRR between 1 and 2.4; 2- a new volume of filtrate (15 L) was added in the feed tank to reach experimentally a VRR = 10. The limited volume of filtrate produced by BHU, the size of the feed tank (20 L) and the dead volume of MFU also limited the VRR.

2.2 Online measurements and control

The control logic was divided into control loops (master control, BHU control, MFU control, cleaning). The master control loop was the general start and stop of the whole BBM. The automated operation of BHU control relied on the succession of sequences of filtration, draining (i.e., collecting the harvested algae), and backwash. The transition from filtration to draining and backwash was time-based or triggered by the pressure buildup in the filtration module. The same principle was applied to the MFU. In addition, the cleaning loop allowed to initiate a chemical cleaning to restore the BHU/MFU performance in case the backwash was not sufficient to counteract pressure buildup. Daily nominal operation (i.e., filtration) was foreseen during about 16 h, the remaining hours being dedicated to draining, backwashing and cleaning.

2.3 Offline measurements

To monitor the culture in the photobioreactor, the suspended matter concentration corresponding to the biomass (SM), the pigments concentration and the inorganic composition of the medium was measured during culture. To monitor the performance of the BHU, the suspended matter but also the dry matter concentration was measured in the filtrate and the drain. To monitor the performance of the MFU, the organic carbon concentration was measured in the permeate and the retentate. The biomass concentration (in grams of suspended matter per liter of culture) was obtained by filtering a known volume of culture on 0.7 µm cellulose filter, drying and weighing, while the dry matter concentration was obtained by direct drying and weighing of the samples. Chlorophyll a (Chl-a) and carotenoids were determined by an extraction with methanol then using a UV-Vis spectrophotometer according to Ritchie (2006) and Strickland and Parsons (1968). Dissolved inorganic and organic carbon concentrations were measured

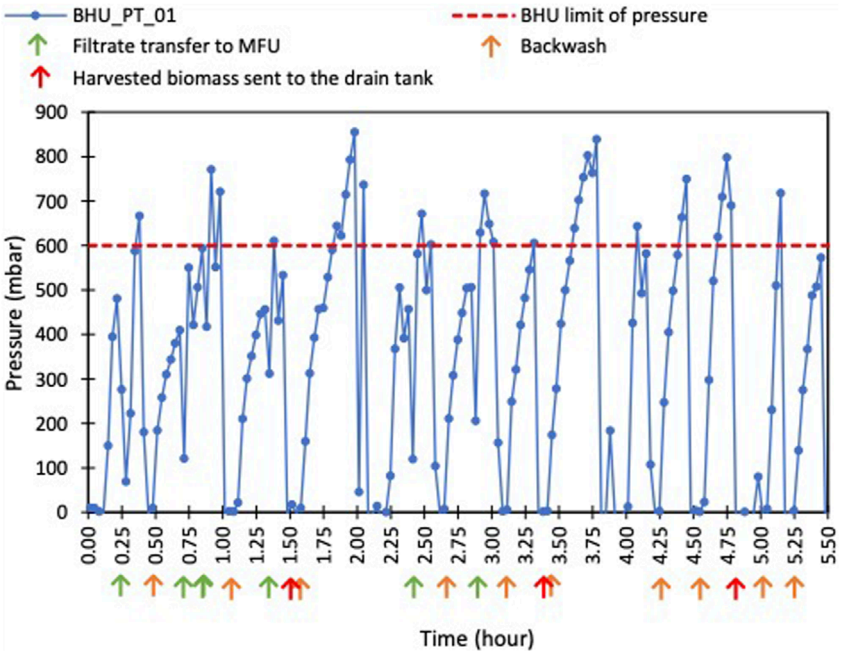

FIGURE 5
Continuous filtration of suspended matter (no vibration during filtration, only during backwash; drain cycle after 3 backwashes).

with a TOC-meter (Shimadzu TOC 5000) on filtered culture at 0.7 µm (Minisart, Sartorius tedium, Germany). Anions and cations concentrations were measured using an anionic chromatograph (Dionex) and cationic chromatograph (Dionex) respectively (DX-120 ion chromatograph).

3 Results and discussion

The performances of the biomass harvesting in BHU and the culture medium purification in MFU were first evaluated separately in batch mode. Then the continuous mode including several cycles of filtration, drainage and backwash was deepened.

3.1 Validation of the BHV performances in batch mode

3.1.1 Biomass harvest unit (BHU)

The aim of the BHU step is to separate the biomass from the culture medium. Two mesh filters (5 and 10 µm) were used to filtrate a microalgae suspension of 0.71 ± 0.04 g_{SM}/L. The pilot unit was used here at a controlled filtration flux to match with the flow target corresponding to the filtration of half the photobioreactor per day (3.33 L/h = 80 L/day). The filtration was very efficient because, with both meshes, no microalgae cells were found into the filtrate and the dry matter retention rate was 94 ± 1%. The suspended matter into the filtrate (50 mg/L) corresponded to the released organic matter, probably the polysaccharides described in the literature.

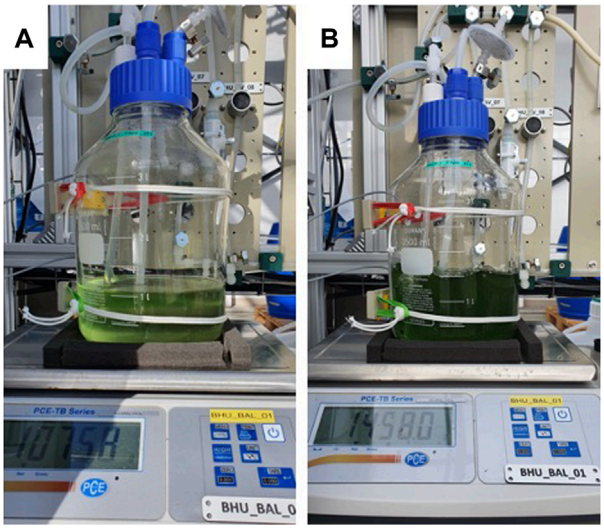

FIGURE 6
Impact of the vibrations during backwash/drain on the recovery of biomass in the BHU hydraulic circuit **(A)**: no vibration: clear solution; **(B)** presence of vibration: more suspended matter recovered.

3.1.2 Medium filtration unit (MFU)

The aim of the MFU unit is to purify the BHU filtrate from the organic compounds to avoid culture drifts when the medium is recycled. Based on literature (Hadj-Romdhane et al., 2013), a cut-off of 15 kDa, a transmembrane pressure (PTM) of 0.8 bar and a tangential speed of 2.3 m/s were used. The filtrate used to test MFU

TABLE 1 Repartition of the biomass (suspended matter) and the culture medium (liquid phase) after 6 h of filtration in BHU.

	V (L)	%v. liquid	Suspended matter concentration (g/L)	Mass of suspended matter (g)	%w. Suspended matter
Drain	5.8	32.8	2.8	16.5	71.2
Filtrate	10.5	59.5	0.06	0.6	2.7
Cake	0.04	0.2	75.0	3.1	13.4
BHU	1.3	7.4	2.3	2.9	12.6

came from a culture maintained in batch mode for a longer period and contained 182 mg/L of organic carbon. In terms of productivity, the initial permeate flux (at VRR = 1) was 62.8 L/h/m^2, 52% of the water flux. This flux was sufficient to ensure the treatment of more than 190 L/day of filtrate. In terms of selectivity, at VRR = 1, the membrane was able to decrease the organic carbon concentration from 182 mg C/L in the feed to 53 mg C/L in the permeate with a retention rate of 71%.

The batch tests demonstrated that the selected conditions allowed to fulfill the requirements: a full retention of the biomass by BHU and a strong reduction of organic matter by MFU. Consequently, the continuous mode was carried out to evaluate the performances of several cycle sequences.

3.2 Continuous mode: separation performance on biomass harvesting unit (BHU)

During this sequence the main objectives were to separate the biomass from the culture medium, to achieve a biomass concentration between 40 and 80 g_{SM}/L in the drain tank and to maintain the productivity and selectivity performances with backwash and draining to allow a continuous production. The culture concentration varied during the tests between 1.5 and 2 g_{SM}/L, so that the target concentration of biomass into the drain corresponded to a concentration factor ranging from 25 to 55.

3.2.1 Filtration cycle

An example of continuous filtration of biomass in BHU is depicted in Figure 5, where the pressure in the filtration chamber versus the filtration time is presented. The BHU worked as expected during the first 3.5 h. The pressure in the filter chamber increased during filtration because of the accumulation of the biomass on the filter. This is normal for dead-end filtration. At the same time, a quantity of filtrate was generated and transferred to the MFU (green arrow when 500 mL of filtrate was transferred). When the limit of pressure was reached (600 mbar in this test), a backwash cycle was automatically initiated to remove the cake from the mesh (orange arrow). To facilitate the unclogging effect of the backwash, the filter was equipped with a vibration system which was activated during backwash cycle allowing more suspended matter recovery (Figure 6). The activation of the drain cycle was fixed after 3 backwashes cycles (red arrow). The filter kept during several hours good performances concerning the separation of the suspended matter (cells) from the medium. After 6 h, only 3% of the suspended matter from all the culture treated passed through the filter.

The concentrated biomass was distributed between different compartments: 1) inside BHU hydraulic circuit, 2) as a filtration cake deposited on the filter and 3) inside the drain tank. This distribution changed during the filtration and depended on the number of drain cycles that occurred. After 6 h of filtration, as expected, most of the suspended matter (71%) was recovered in the drain tank (Table 1). However, a concentration between 40 and 80 g/L was expected in the drain (concentrated harvested biomass) but it reached only 2.8 g/L. This can be explained by the fact that the biomass was not maintained in suspension, despite vibrations. Indeed, a sticky cake of biomass was formed on the filter within a concentration of 75 g_{SM}/L. The adhesion of the cake to the filter limited the collection of the biomass in the drain tank. The accumulation of matter on the filter induced an increasing pressure in the filtration chamber. This rise initiated the backwash cycle and the drain cycle. After 3.5 h, the mesh was partially clogged and a new increase of pressure in the filter house appeared directly and started new backwashes and drain cycles (Figure 5, orange and red dots) that promoted the dilution of the drain tank. When the clogging appeared, it became difficult to generate filtrate for MFU because the produced filtrate was used for the repeated backwashing (no green dots anymore).

3.2.2 Improvement of BHU operation

In order to improve this harvesting phase, three enhancements were combined during the filtration cycle and compared to the initial conditions (case A): introduction of vibrations during the filtration cycle and not only during the backwash cycle, as well as the reduction of the maximum pressure in the filter chamber before a backwash cycle (case B); case B with the reduction of the mesh cut-off from 10 to 5 µm (case C). In Figure 7, the required time to produce 500 mL of filtrate is followed in the different conditions, versus the volume of filtrate sent to MFU. In case B, the filtrate recovery was twice higher than in initial conditions (case A) before a drastic increase in the time required to send the 500 mL of to MFU, because of the necessary backwash. Reducing the membrane cut-off from 10 to 5 µm (case C) allowed producing 17 L of filtrate before clogging. The optimization of the procedure allowed to multiply the volume of recovered filtrate by 5.7 times. However, clogging was still present, limiting the operation.

A second approach was to add an internal recirculation diaphragm pump to the BHU filter chamber. The aim was to create a low shear at the filter surface and to prevent biomass accumulation. This solution led to cellular deterioration, allowing a portion of the

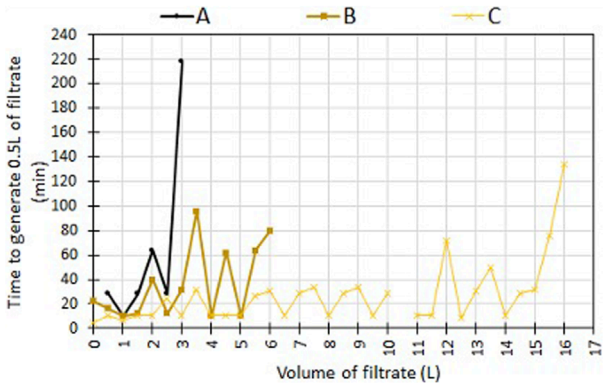

FIGURE 7
Time required to recover Vf = 500 mL of filtrate versus the total volume of filtrate sent to MFU. Comparison of solution for BHU improvement: **(A)** initial conditions (10 µm; no vibration; maximum pressure before backwash at 600 mbar): only 6 mL × 500 mL of filtrate recovered; **(B)** vibration during filtration phase + reduction of maximum pressure before backwash to 500 mbar: 12 mL × 500 mL of filtrate recovered; **(C)**: vibration during filtration phase + reduction of maximum pressure before backwash to 500 mbar + membrane cut-off at 5 µm: 34 mL × 500 mL of filtrate recovered.

biomass passing through the filter, which impacted the retention quality. Thus this solution was not retained.

3.2.3 Analysis of the characteristics of the biomass accumulated on the filter (cake resistance)

During dead-end filtration, there is an accumulation of the biomass on the filter, generating a cake. Using classical equations of the dead-end filtration, it is possible to calculate the cake specific resistance which is a useful parameter to estimate the filterability of the product.

This calculation was performed:

- using the results of the batch tests,
- using the results obtained at constant flow in specific periods on the BHU
- using the results of the complementary tests.

At constant flow, Eq. (1) can be used to calculate the cake specific resistance:

$$\Delta p = \frac{\eta . R_s}{S} . Q + \frac{\eta . r_c . C . Q^2}{S^2} . t \quad (1)$$

Where t is the time (s), V the filtrated volume (m^3), Q the flow ($m^3.s^{-1}$), η the dynamic viscosity of filtrate (Pa.s), S the filter area (m^2), Δp the pressure (Pa), C the dry matter concentration ($kg.m^{-3}$), R_s the clean filter resistance (m^{-1}) and r_c the cake resistance ($m.kg^{-1}$).

During the batch tests, the mean cake resistance estimated with the last 0.5 L filtrated using Eq. 1 was: 10^{14} m kg^{-1}. It is a bit high for dead-end filtration, that is why the addition of vibration was decided to facilitate the cake disruption and removal even during the filtration phase.

The results obtained with the C configuration (vibration during filtration phase + reduction of maximum pressure before backwash at 500 mbar + membrane cut-off at 5 µm) between 17 h and 29 h were analyzed. In Figure 8, the evolution of the pressure versus time for the different filtration cycles (1–11) are drawn. Three main phases can be observed. The first phase during the first 10 min (0.20 h) and below 30 mbar, filtrations were similar, the pressure was low, a slow fouling occurred. The second phase occurred between 0.2 and 0.3–0.4 h, until 450 mbar with a strong rise of the pressure meaning a strong clogging of the filter. During the third phase, above 0.3–0.4 h and 450 mbar, the cake was built with biomass accumulation above the filter leading to a bundle of lines for the different cycles.

The resistance of the clean filter was low (2.9×10^{10} m^{-1}). In the first phase, the accumulation of material led to an apparent specific resistance of initial cake equal to 5×10^{13} m kg^{-1}. In the second phase, the total resistance of the filter reached 7.5×10^{12} m^{-1} at 450 mbar by deposit of biomass and/or organic material in the filter. In the third phase, the biomass accumulated on the filter formed a more compact cake with a specific resistance reaching 4.1×10^{14} m kg^{-1}. That means that the cake is denser than in the batch tests. No strong modification of the slope is observed when the vibrations start at 200 mbar.

According to literature (SUEZ, 2023), a r_c between 10^{14} and 10^{15} m kg^{-1} is too high for a classical press filter and a specific resistance lower than 10^{12} m kg^{-1} should be reached. Some adjuvants like diatomite can be used to reduce and obtain a very low specific resistance near 10^{10} m kg^{-1} to facilitate juice clarification, for example, but this kind of additive does not fit to the initial space requirements.

These results confirm that the reduction of the pressure to 500 mbar for the realization of the backwash seems beneficial because from 450 mbar, one can observe the compaction of the cake which will undeniably reduce the productivity of this harvesting phase. In addition, finding a strategy to limit or even mechanically eliminate the cake is most likely the next step. Indeed, preliminary tests at lab scale with mechanical agitation inside the filtration chamber reduced the specific resistance of the cake to the interval 1.7×10^{13}–2.7×10^{13} $m.kg^{-1}$.

First results demonstrated that BHU was efficient for the separation but needed adjustments to fully meet the expected performances, notably the increase of harvested biomass concentration. The accumulation of suspended matter on the filter surface and its limitation and/or removing is a key point. The interaction between specific *Limnospira* properties and morphology and filter characteristics needs to be further investigated. The adhesion of the biomass to the filter could be mitigated by the integration of spacers, or by the modification of the design of the filtration cell or filter material. The cake could also be removed by the addition of a mechanical action. Some of these solutions are currently studied at laboratory scale and seem promising but will require further investigations.

3.3 Culture medium recycling by MFU

3.3.1 Selectivity of MFU

The main objective of the MFU step is to treat the filtrate from BHU to recover a purified culture medium in the permeate that

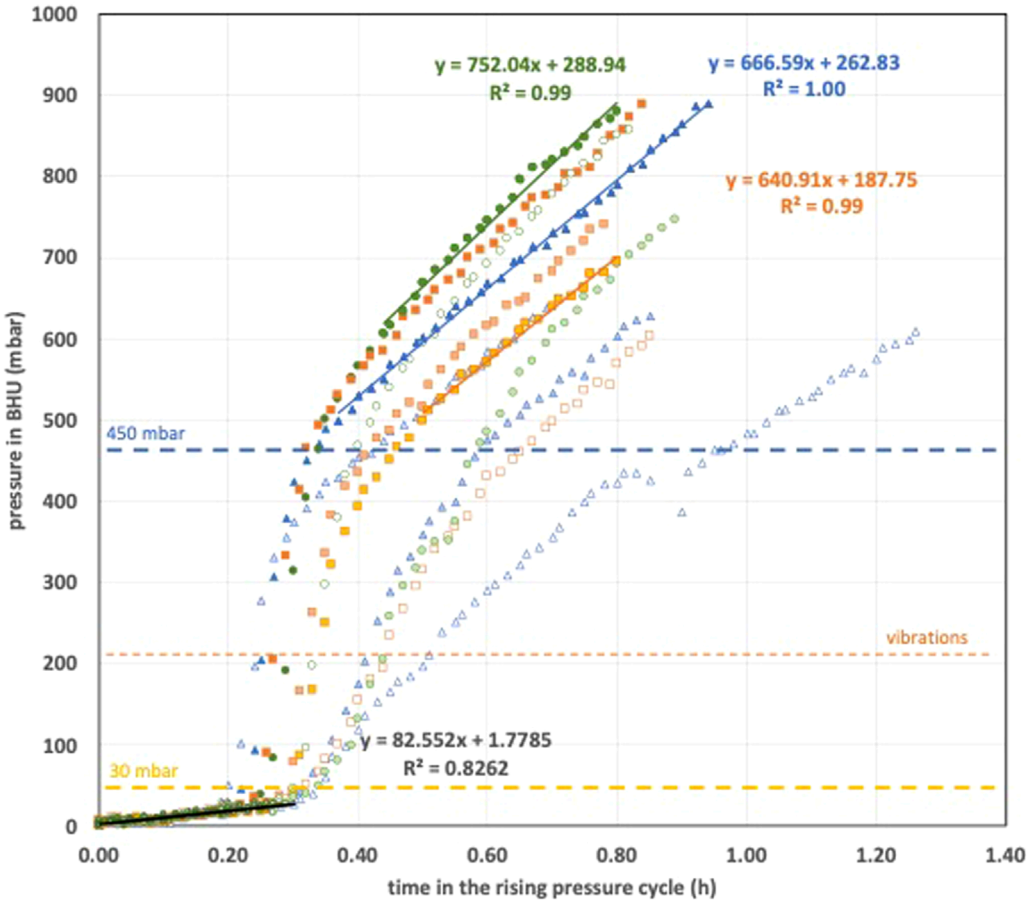

FIGURE 8
Filtration of algal suspension in pilot scale BHU at constant flow (3.3 L/h); triangles, squares and circles corresponding respectively to cycles 1–4, 5–8, and 9–11.

can be recycled to the culture, and concentrate organic components using a 15 kDa ceramic membrane (Hadj-Romdhane et al., 2013). Depraetere et al. (2015) have already shown the negative effect of the accumulation of organic materials on further dewatering if the culture medium is not treated. Figure 9 shows the mass balance of the organic carbon and the concentration of the organic carbon in the permeate and the retentate respectively, during the ultrafiltration of 20 L + 15 L of filtrate to a volume reduction ratio (VRR) of 10. The total quantity of carbon that has been introduced in the MFU pilot is equal to the sum of carbon in the permeate and retentate, within the analysis variability. A small difference can be noted at VRR = 3.5 because the corresponding addition of filtrate in the MFU feed led to experimental variations on concentration and volume measurements. The mass balance shows that the organic matter accumulation on the membrane is negligible. The results show that a small quantity of organic carbon went through the membrane. The concentration in the permeate stayed relatively constant, confirming the results obtained during batch tests. The majority of the organic carbon was retained in the retentate (Figure 9) with a rejection rate between 93% and 96%. At the same time, the rejection rate of inorganic carbon remained low, less than 4%. At a VRR of 10, 17%–20% of the initial organic carbon was in the permeate.

The concentration of organic carbon in the permeate was maintained between 45 and 50 mg C/L. With the increase of VRR, the concentration reached nearly 1,600 mg C/L at VRR 10, and compared with the initial concentration after BHU system which is between 160 and 182 mg C/L, it confirms an almost total retention of organic carbon with the 15 kDa membrane, as expected (Hadj-Romdhane et al., 2013).

3.3.2 Productivity of MFU

In Figure 10, the productivity of MFU is analyzed through the permeate flux (A) and the volume distribution (B). The initial permeation flux during the ultrafiltration of the BHU filtrate through the 15 kDa mineral membrane was 60 ± 1 L/h.m^2 (Figure 10A). During the concentration, the flux of permeate decreased slightly. At VRR = 4 and 10, the permeate flux was respectively 59 ± 3 L/h.m^2 and 48 L/h.m^2. The variation of the flux due to the culture conditions (initial concentration of organic matter, age of the microalgae culture) was limited. 5 h were required to treat the 35 L of initial filtrate.

At the end of operation (Figure 10B), at VRR 10, 90% of the filtrate was recovered into the permeate and 83% of initial organic carbon (even the eventual residue of biomass issued from BHU) was

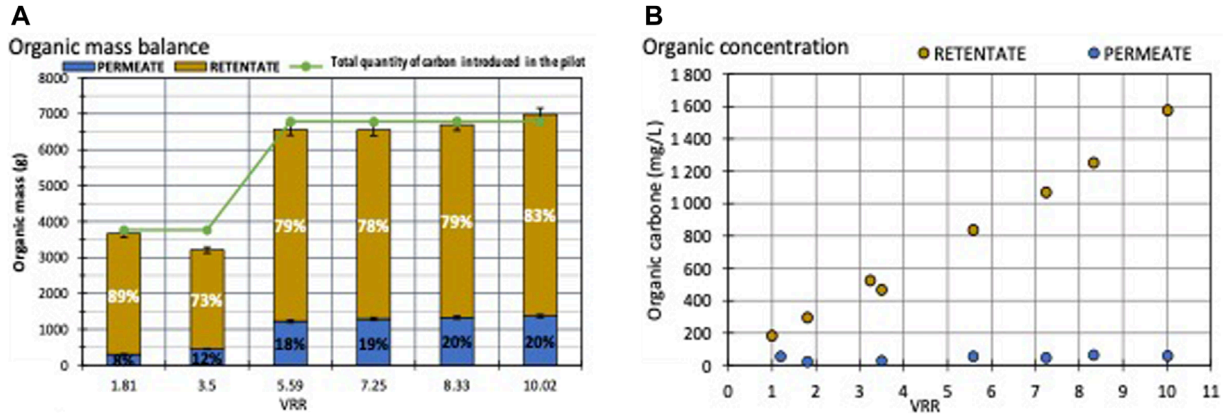

FIGURE 9
MFU selectivity: organic carbon mass balance **(A)** and evolution of the organic carbon concentration in the retentate and permeate **(B)** during the ultrafiltration of filtrate in MFU (15 kDa–T = 30°C–PTM = 0.8 bar–v = 2.3 m/s).

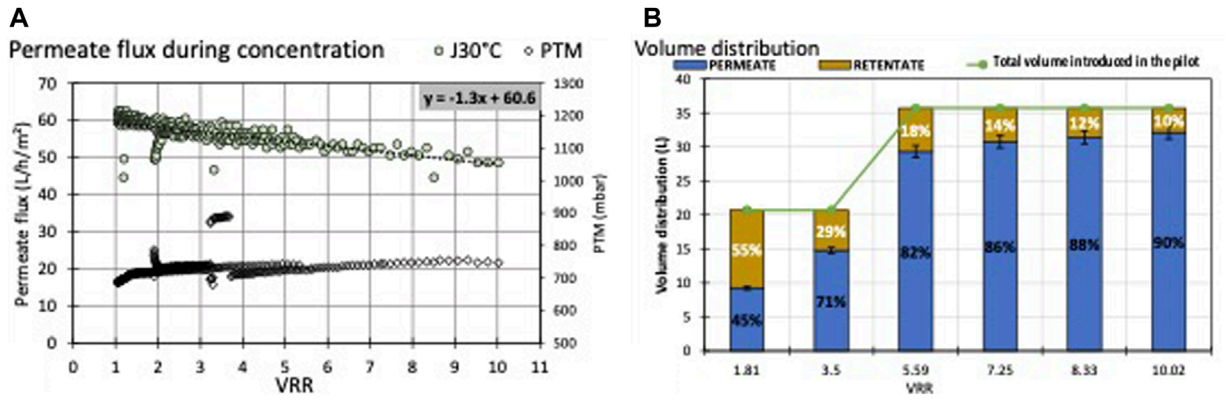

FIGURE 10
MFU productivity: permeate flux **(A)** and Volume distribution **(B)** during MFU (15 kDa–T = 30°C–PTM = 0.8 bar–v = 2.3 m/s).

concentrated in 10% of the initial volume. The high performances of the MFU were in accordance with the expectations relying of the former studies (Rossi et al., 2008; Hadj-Romdhane et al., 2013).

A scale up for the treatment of 80 L/day of filtrate from BHU (half of the photobioreactor to respect the dilution rate of the culture) can be done. If the flux remains stable, 12 h will theoretically be necessary to reach a VRR = 15 corresponding to the production of 75 L of recycled culture medium. This range of time shows that the chosen membrane surface of 0.13 m^2 is appropriate to achieve this objective during the day, including the cleaning operations.

Finally, the selected BHU dead-end filtration process with adaptations such as vibrations and mechanical cake removal will be well adapted to the harvesting of *Limnospira indica*, and the coupling with MFU ultrafiltration will allow a high quality water recovery, which is very interesting for space applications. However, BHU would not be adapted to strains like *Nannochloropsis oculate, Chlamydomonas reinhardtii or Chlorella vulgaris* also studied for space applications, because those microalgae would not be retained by the filter due to their smaller size. Another process satisfying ALiSSE criteria should be developed, for example, micro or ultrafiltration, with related questions among which the limited suspended matter concentration that could be reached, the potential fouling or a potential higher retention of nutrients.

4 Conclusion

The BioHarvest (BHV) project aimed to study solid/liquid separation in space dedicated to the Solid Loop of the compartment C4A of the MELiSSA program. The objective was to perform the harvesting of the cyanobacterium *Limnospira indica* from axenic cultures in photobioreactors under space conditions. The BioHarvest demonstration unit was made of three subsystems: a PBR to produce the biomass, the BHU based on dead-end filtration to harvest the biomass and clarify the culture medium and MFU based on ultrafiltration to purify the culture medium before recycling. The capacity of BHU to separate the biomass from the culture medium was demonstrated. Only 3% of the suspended matter went through the filter. However, the biomass accumulation on the mesh filter directly impacted the volume distribution and

the suspended matter concentration in the harvesting tank. Several enhancements were obtained based on the selection of the mesh cut-off, the introduction of vibrations and pressure regulation. However, complementary methods to mitigate the cake accumulation are still needed.

With regards to the performance of MFU in fed-batch mode, the demonstration test showed that the selectivity of the filter met the expectations: the system allowed to decrease the concentration of organic components by a factor 4. Likewise, the productivity of the filter membrane was within the expected range. By extrapolating the test results, the MFU as designed in the breadboard can indeed theoretically support a daily harvesting target of 80 L/day. However, as the MFU is dependent from BHU, its performance could not be fully evaluated.

From this study, it appears that the most critical step is the accumulation of the biomass as a cake on the filter of the BHU, limiting the whole process productivity. In future works, the physicochemical properties of the concentrated biomass and their evolution during the process (rheology, adhesion properties) shall be deepened to better understand the paste behavior and select the best BHU modifications. The selection of a new mesh to limit the adhesion and a mechanical cake removal may be the most promising enhancements among several possibilities.

Data availability statement

The datasets presented in this article are not readily available because the analyzed datasets for this study are available upon request to interested researchers, on condition of a prior agreement from ESA. Requests to access the datasets should be directed to EC, estelle.couallier@univ-nantes.fr.

Author contributions

JT was involved in the conception of the work, the building of the units, the acquisition, analysis and interpretation of the data and the drafting of the paper. MV participated to the conception of the work, the building of the units, the acquisition, analysis and interpretation of the data. CC participated in the drafting and reviewing of the paper. BL-L participated to the conception of the work, bringing her knowledge of the MELiSSA pilot plant, former works and space constraints. DD was involved in the conception of the work, the building of the units, the acquisition, analysis and interpretation of the data and the drafting of the paper. MF participated to the conception of the work, the building of the units and the data analysis and the drafting of the paper. EC was involved in the conception of the work, the building of the units, the acquisition, analysis and interpretation of the data, the drafting, reviewing and submission of the paper. All authors contributed to the article and approved the submitted version.

Funding

The BioHarvest study was performed in the frame of the ESA Contract No. 4000132825/20/NL/KML.

Acknowledgments

The pilots were built by the Redwire Space NV and GEPEA Capacités teams. The experiments were performed at the Algosolis Plateform, with the help of Emmanuel Dechandol for the installation.

Conflict of interest

Author MV was employed by GlaxoSmithKline Biologicals. Authors CC and DD were employed by Redwire Space NV.

The remaining authors declare that the research was conducted in the absence of any commercial or financial relationships that could be construed as a potential conflict of interest.

Publisher's note

All claims expressed in this article are solely those of the authors and do not necessarily represent those of their affiliated organizations, or those of the publisher, the editors and the reviewers. Any product that may be evaluated in this article, or claim that may be made by its manufacturer, is not guaranteed or endorsed by the publisher.

References

Belay, A. (1997). *Spirulina platensis (Arthrospira), physiology, cell biology and biotechnology*. London, UK: A. Vonshak, 131.

Depraetere, O., Pierre, G., Noppe, W., Vandamme, D., Foubert, I., Michaud, P., et al. (2015). Influence of culture medium recycling on the performance of Arthrospira platensis cultures. *Algal Res.* 10, 48–54. doi:10.1016/j.algal.2015.04.014

Formosa-Dague, C., Gernigon, V., Castelain, M., Daboussi, F., and Guiraud, P. (2018). Towards a better understanding of the flocculation/flotation mechanism of the marine microalgae Phaeodactylum tricornutum under increased pH using atomic force microscopy. *Algal Res.* 33, 369–378. doi:10.1016/j.algal.2018.06.010

Frappart, M., Masse, A., Jaffrin, M. Y., Pruvost, J., and Jaouen, P. (2011). Influence of hydrodynamics in tangential and dynamic ultrafiltration systems for microalgae separation. *Desalination* 265, 279–283. doi:10.1016/j.desal.2010.07.061

Hadj-Romdhane, F., Zheng, X., Jaouen, P., Pruvost, J., Grizeau, D., Croué, J. P., et al. (2013). The culture of Chlorella vulgaris in a recycled supernatant: effects on biomass production and medium quality. *Bioresour. Technol.* 132, 285–292. doi:10.1016/j.biortech.2013.01.025

Hapońska, M., Clavero, E., Salvadó, J., Farriol, X., and Torras, C. (2018). Pilot scale dewatering of Chlorella sorokiniana and Dunaliella tertiolecta by sedimentation followed by dynamic filtration. *Algal Res.* 33, 118–124. doi:10.1016/j.algal.2018.05.007

Huang, R., Liu, Z., Yan, B., Li, Y., Li, H., Liu, D., et al. (2020). Layer-by-layer assembly of high negatively charged polycarbonate membranes with robust antifouling property for microalgae harvesting. *J. Membr. Sci.* 595, 117488. doi:10.1016/j.memsci.2019.117488

Nazari, M. T., Rigueto, C. V. T., Rempel, A., and Colla, L. M. (2021). Harvesting of Spirulina platensis using an eco-friendly fungal bioflocculant produced from agro-industrial by-products. *Bioresour. Technol.* 322, 124525. doi:10.1016/j.biortech.2020.124525

Ometto, F., Pozza, C., Whitton, R., Smyth, B., Torres, A. G., Henderson, R. K., et al. (2014). The impacts of replacing air bubbles with microspheres for the clarification of algae from low cell-density culture. *Water Res.* 53, 168–179. doi:10.1016/j.watres.2014.01.012

Potocar, T., Leite, L. de S., Daniel, L. A., Pivokonsky, M., Matoulkova, D., and Branyik, T. (2020). Cooking oil-surfactant emulsion in water for harvesting Chlorella vulgaris by sedimentation or flotation. *Bioresour. Technol.* 311, 123508. doi:10.1016/j.biortech.2020.123508

Rashid, N., Nayak, M., Lee, B., and Chang, Y.-K. (2019). Efficient microalgae harvesting mediated by polysaccharides interaction with residual calcium and phosphate in the growth medium. *J. Clean. Prod.* 234, 150–156. doi:10.1016/j.jclepro.2019.06.154

Ritchie, R. J. (2006). Consistent sets of spectrophotometric chlorophyll equations for acetone, methanol and ethanol solvents. *Photosynth Res.* 89, 27–41. doi:10.1007/s11120-006-9065-9

Rossi, N., Derouiniotchaplain, M., Jaouen, P., Legentilhomme, P., and Petit, I. (2008). Arthrospira platensis harvesting with membranes: fouling phenomenon with limiting and critical flux. *Bioresour. Technol.* 99, 6162–6167. doi:10.1016/j.biortech.2007.12.023

Rossi, N., Jaouen, P., Legentilhomme, P., and Petit, I. (2004). Harvesting of cyanobacterium Arthrospira platensis using organic filtration membranes. *Food Bioprod. Process.* 82, 244–250. doi:10.1205/fbio.82.3.244.44177

Rossi, N., Petit, I., Jaouen, P., Legentilhomme, P., and Derouiniot, M. (2005). Harvesting of cyanobacterium*Arthrospira platensis*using inorganic filtration membranes. *Sep. Sci. Technol.* 40, 3033–3050. doi:10.1080/01496390500385046

Rossignol, N., Vandanjon, L., Jaouen, P., and Quemeneur, F. (1999). Membrane technology for the continuous separation microalgae/culture medium: compared performances of cross-flow microfiltration and ultrafiltration. *Aquac. Eng.* 20, 191–208. doi:10.1016/s0144-8609(99)00018-7

Singh, G., and Patidar, S. K. (2018). Microalgae harvesting techniques: a review. *J. Environ. Manag.* 217, 499–508. doi:10.1016/j.jenvman.2018.04.010

Strickland, J. D. H., and Parsons, T. R. (1968). *A practical handbook of seawater analysis*. Ottawa, Canada: Fisheries Research Board of Canada.

SUEZ (2023). *Collective work suez water handbook*. https://www.suezwaterhandbook.Fr/.

Verfaillie, A., Blockx, J., Praveenkumar, R., Thielemans, W., and Muylaert, K. (2020). Harvesting of marine microalgae using cationic cellulose nanocrystals. *Carbohydr. Polym.* 240, 116165. doi:10.1016/j.carbpol.2020.116165

Volpin, F., Yu, H., Cho, J., Lee, C., Phuntsho, S., Ghaffour, N., et al. (2019). Human urine as a forward osmosis draw solution for the application of microalgae dewatering. *J. Hazard. Mater.* 378, 120724. doi:10.1016/j.jhazmat.2019.06.001

Zhao, Z., Ilyas, A., Muylaert, K., and Vankelecom, I. F. J. (2020b). Optimization of patterned polysulfone membranes for microalgae harvesting. *Bioresour. Technol.* 309, 123367. doi:10.1016/j.biortech.2020.123367

Zhao, Z., Li, Y., Muylaert, K., and Vankelecom, I. F. J. (2020a). Synergy between membrane filtration and flocculation for harvesting microalgae. *Sep. Purif. Technol.* 240, 116603. doi:10.1016/j.seppur.2020.116603

Frontiers in
Astronomy and Space Sciences

Explores planetary science and extragalactic astronomy in all wavelengths

Advances the understanding of our universe - from planetary science to extragalactic astronomy, to high-energy and astroparticle physics.

Discover the latest Research Topics

See more →

Frontiers

Avenue du Tribunal-Fédéral 34
1005 Lausanne, Switzerland
frontiersin.org

Contact us

+41 (0)21 510 17 00
frontiersin.org/about/contact